by Stéphane Reboulet[1], Miguel Company[2], Thierry Adatte[3], Roque Aguado[4†], François Baudin[5], Jean-François Deconinck[6], Stan Duxbury[7], Ginés de Gea[8], Jacek Grabowski[9], Bruno Granier[10], Daria Ivanova[11], Nico M.M. Janssen[12], Jaap Klein[13], Iskra Lakova[11], Melanie G. Leng[14], Damian G. Lodowski[9], Mathieu Martinez[15], Emanuela Mattioli[1], John M. McArthur[16], Davide Olivero[1], Daniela Reháková[17], and José María Tavera[2]*

The Global Boundary Stratotype Section and Point (GSSP) for the base of the Valanginian Stage, the Vergol section (Montbrun-les-Bains, Drôme, SE France) and its Standard Auxiliary Boundary Stratotype (SABS), Cañada Luenga section (Cehegín, SE Spain)

[1] Université Claude Bernard Lyon 1, ENSL, CNRS, LGL-TPE, F-69622, Villeurbanne, France; *Corresponding author, *E-mail: stephane.reboulet @univ-lyon1.fr*
[2] Departamento de Estratigrafía y Paleontología, Universidad de Granada, E-18002 Granada, Spain
[3] ISTE, Geopolis, CH-1015 Lausanne, Switzerland
[4] Departamento de Geología, CEACTEMA, Universidad de Jaén, E-23700 Linares, Spain
[†]Deceased February 23, 2023
[5] Institut des Sciences de la Terre de Paris, Sorbonne Université, France
[6] Université Bourgogne Europe, UMR CNRS 6282 Biogéosciences, 6 Bd Gabriel, 21000 Dijon, France
[7] Church Lane, Chester, UK
[8] Departamento de Geología, CEACTEMA, Universidad de Jaén, E-23071 Jaén, Spain
[9] Polish Geological Institute, National Research Institute, ul. Rakowiecka 4, 00-975 Warsaw, Poland
[10] Muséum d'histoire naturelle (MHN), Route de Malagnou 1, 1208 Genève, Switzerland; Association Carnets de Géologie, 2 impasse Charles Martel, F-29217 Plougonvelin, France
[11] Geological Institute, Bulgarian Academy of Sciences, 1113 Sofia, Bulgaria
[12] TNO, Geological Survey, Utrecht, The Netherlands
[13] 429 Chemin du Thuve, 04700 Oraison, France
[14] NEIF, British Geological Survey, Keyworth, Nottingham NG12 5GG, UK
[15] Géosciences Rennes, Bâtiment 15 OSUR, Université de Rennes 1, 35042 Rennes, France
[16] Earth Sciences, University College London, Gower Street, London WC1E 6BT, UK
[17] Department of Paleontology, Faculty of Sciences, Comenius University, Ilkovičova 6, 842 15 Bratislava, Slovakia

(Received: March 23, 2025; Revised accepted: August 1, 2025; Online published: September 15, 2025)

https://doi.org/10.18814/epiiugs/2025/025028

Following votes by the Valanginian Working Group, the International Subcommission on Cretaceous Stratigraphy and the International Commission on Stratigraphy, the Executive Committee of the International Union of Geological Sciences unanimously approved in December 2024 the Global Stratotype Section and Point (GSSP) for the Valanginian Stage (Cretaceous System). The base of the Valanginian Stage is defined at the base of limestone bed VGL-B136 of the Vergol section (Montbrun-les-Bains, SE France), and correlated by the First Occurrence of the ammonite species *Hoedemaekeria* (nov. gen.) *pertransiens*. Other fossil groups such as calpionellids and calcareous nannofossils are used to characterize the Berriasian/Valanginian boundary. A calibration to the carbon and strontium isotope stratigraphy is also proposed. The age model based on astrochronology allows to date the base of the Valanginian Stage at 137.05 Ma (± 0.2 Ma). Palaeomagnetic investigations reveal that the section is remagnetized and therefore no palaeomagnetic stratigraphy is available. However, an integrated stratigraphy provides an accurate correlation with the Cañada Luenga section (Cehegín, SE Spain), proposed as Standard Auxiliary Boundary Stratotype (SABS), that is characterized by magnetic chrons calibrated by several biostratigraphic scales. The base of the Valanginian Stage falls in the lowermost part of magnetic Chron M14r.

Introduction

Since the recognition of the Valanginian carbon isotopic anomaly (Weissert, 1989) and its definition as the Weissert Oceanic Anoxic

Event (Erba et al., 2004), a renewed interest for the Valanginian Stage is witnessed by the increasing number of papers (see Ogg et al., 2012; Gale et al., 2020, and references therein). In this context, it has become urgent to formally define the Global Boundary Stratotype Section and Point (GSSP) of this stage. A first attempt was made during the Second International Symposium on Cretaceous Stage boundaries at the 1995 Brussels meeting (Bulot et al., 1996). The former Valanginian Working Group (VWG) provisionally recommended that a calpionellid should be used as a primary marker. The group noted that some French and Spanish sites were under consideration as boundary stratotype sections, but no section was recommended. However, a year before the meeting, Blanc et al. (1994) had proposed the Montbrun-les-Bains section (Drôme, France), better known as Vergol, as a candidate for the Valanginian GSSP, using an ammonite as the primary marker for the base of the stage. Later, the Cañada Luenga section (Cehegin, Spain) was proposed as an alternative GSSP (Aguado et al., 2000). In the 2010s decade, two research teams worked on these French (mainly on ammonites and calcareous nannofossils; Kenjo, 2014; Kenjo et al., 2021) and Spanish (mainly on ammonites; Company and Tavera, 2015) sections.

After two decades of relative inactivity, the VWG needed to be reconstituted. Miguel Company (Granada University, Spain) and Stéphane Reboulet (Lyon University, France) accepted to be the new chairs of the current VWG (since 2016). The list of members also had to be updated with respect to the works published on the Valanginian; 27 active specialists of main fields of stratigraphy agreed to collaborate (see https://cretaceous.stratigraphy.org/wgs/valanginian).

The first goal was to extend the work on both candidate sections, applying an integrated stratigraphic approach in order to fulfill the requirements for a GSSP. On the basis of preliminary studies undertaken during 2021 and 2022, two informal proposals were produced by Company et al. (2023; Cañada Luenga) and Reboulet et al. (2023; Vergol), and submitted to the current VWG in early 2023. The group approved the First Occurrence (FO) of the ammonite species *Hoedemaekeria* (nov. gen.) *pertransiens* (new combination for "*Thurmanniceras*" *pertransiens*; see Appendix 1, Taxonomic note) as the primary marker and the Vergol section was selected as candidate for the GSSP. According to this result, a single formal proposal on the Valanginian GSSP was written by Reboulet and Company (reporters) et al. (2024), including the Cañada Luenga section as a candidate for the Standard Auxiliary Boundary Stratotype (SABS). As approved by the International Commission on Stratigraphy (ICS; Head et al., 2023), the SABS provides a complementary expression of the boundary interval without designating a specific point. This formal proposal was submitted to successive votes of the Subcommission on Cretaceous Stratigraphy and the International Commission on Stratigraphy, being finally unanimously approved by the Executive Committee of the International Union of Geological Sciences.

The Valanginian Stage and Its Definition

Historical Background

The term Valanginian was coined by Desor (1854) to refer to the beds outcropping in the Neuchâtel region (Switzerland), between the "calcaires compactes et blancs" of the Jurassic and the "Marnes d'Hauterive", and which corresponded to the "Néocomien inférieur" of Campiche (1853). This vague definition was later detailed by Desor and Gressly (1859), who included in this stage, from top to bottom: "la limonite ou calcaire ferrugineux", "le calcaire compact ou marbre bâtard", and "les marnes et brèches marneuses grises et bitumineuses".

As this historic area is located in a shallow-marine environment, some lithological units are thin, condensed, laterally discontinuous or generally poor in ammonites. Consequently, French workers undertook studies in the Vocontian basin (SE France) where the successions are well-characterized by ammonites. This step corresponds to the transition from a lithostratigraphic approach to a biostratigraphic one. Several authors (Lory, 1860-64; Coquand, 1863, 1866; Coquand and Boutin, 1869) soon established the correlation of the Valanginian with the pelagic sediments of the lowermost Cretaceous in SE France, specifically with the succession formed by the "Calcaires de Berrias à *Terebratula diphyoides*" and the "Marnes à *Belemnites latus* et ammonites pyriteuses", although shortly after, Coquand (1871) would propose the Berriasian for the Berrias limestones. This separation was subsequently adopted by most authors (Kilian, 1887, 1889, 1896; Renevier, 1897; Lory, 1898; Paquier, 1900). However, Kilian (1907, 1910), probably to reaffirm his position in the dispute with Toucas (cf. discussion in Hoedemaeker, 1995) over the Jurassic/Cretaceous boundary, proposed eliminating the Berriasian and replacing it with the *Hoplites Boissieri* Zone (= Infravalanginian) as the lowest zone of the Valanginian. It was with Mazenot (1939) that the Berriasian recovered its independence, ratified at the Lyon Colloquium of 1963.

The boundary between the Berriasian and the Valanginian was historically placed between the Berrias limestones and the marls with pyritized ammonites, that is, between the *Ammonites boissieri* and *Ammonites roubaudianus* zones since they were introduced by Kilian (1889). This scheme was slightly modified by Mazenot (1939), who distinguished, in the upper part of the *Berriasella boissieri* Zone, a level (Horizon de Beaucels = "Horizon supérieur" of Mazenot 1939 = "Horizon 3" of Kilian) with a clearly Berriasian fauna but containing some elements with Valanginian affinities (*Kilianella* aff. *pexiptycha* and *Thurmannites* aff. *pertransiens*). This horizon was later transferred to the base of the Valanginian (Barbier and Thieuloy, 1965) and then integrated in the new *Thurmanniceras pertransiens* Subzone (of the former *Kilianella roubaudi* Zone) by Le Hégarat and Remane (1968). Finally, Busnardo and Thieuloy (1979) would propose the *Thurmanniceras otopeta* Zone for the Beaucels Horizon. According to this interpretation, the Berriasian/Valanginian (B/V) boundary was placed between the *Berriasella calisto* Subzone (introduced by Le Hégarat and Remane, 1968) in the uppermost part of the Berriasian and the *T. otopeta* Zone at the base of the Valanginian.

This solution, provisionally recommended by the Cretaceous Subcommission at Copenhagen (Birkelund et al., 1984), was accepted by most authors (Company, 1982, 1987; Company and Tavera, 1982; Rawson, 1983; Tavera, 1985; Bulot, 1990; Ettachfini, 1991). However, it should be noted that Hoedemaeker (1982, 1983, 1984, 1987) suggested an alternative to this zonal scheme. He moved the B/V boundary to the base of his *Tirnovella alpillensis* Subzone, a stratigraphic interval, nearly correlatable with the *B. calisto* Subzone, and in which, according to his observations, typically Berriasian species coexisted with others belonging to genera traditionally considered as characteristic of the

Valanginian. This option was rejected by most Cretaceous biostratigraphic workers.

During the Second International Symposium on Cretaceous Stage boundaries (Brussels, 1995), the former Valanginian Working Group (VWG, Bulot et al., 1996) provisionally recommended placing the base of the Valanginian at the base of the Calpionellid Zone E, which corresponded almost exactly to the base of the *Thurmanniceras pertransiens* ammonite Zone. Indeed, in their study of the Montbrun-les-Bains section (Vergol), Blanc et al. (1994) observed that the First Occurrences (FOs) of *Calpionellites darderi* (index species of Zone E) and *Hoedemaekeria pertransiens* are almost synchronous (see also Blanc, 1996). They proposed Vergol as a candidate section for the Valanginian GSSP and to put the golden spike at the base of bed 210 in which they recorded the FO of *H. pertransiens*. Thus, they confirmed the suggestion of Bulot et al. (1993) and Bulot and Thieuloy (1995) to define the base of the Valanginian Stage using an ammonite as primary marker, namely the first appearance of *H. pertransiens*. However, the provisional recommendation of the VWG (Bulot et al., 1996) was to place the boundary at the base of *Calpionellites* Zone E (FO of *C. darderi* in bed 209, Blanc et al., 1994). In their report, the former VWG only emphasized the broader geographic distribution of the calpionellid index species (recorded from Mexico to Turkey; see below), with respect to distribution of the ammonite *H. pertransiens*. However, in a more informal way, the choice of a calpionellid marker was also motivated by disagreements on the taxonomy of some ammonites (cf. identifications) that led to some discrepancies in their stratigraphic interpretations and correlations problems. In the last decade, most of these palaeontological issues have been solved because of huge improvements in systematic studies and the biostratigraphy of the upper Berriasian–lower Valanginian interval, mainly made by Company and Tavera (2015) and Kenjo et al. (2021; see also Kenjo, 2014). On the basis of their work on the Vergol section, these latter authors proposed the first appearance of *H. pertransiens* to define the base of the Valanginian. Consequently, this option corresponds to the historical concept of the (base of the) stage as the base of its former lowest zone, *Hoplites* (*Kilianella*) *roubaudiana* Zone sensu Kilian, matching approximatively with the base of *H. pertransiens* Zone. Kenjo et al. (2021, p. 22–24) discussed the choice of the primary marker and also compared the French candidate section for the Valanginian GSSP with the Cañada Luenga section (Cehegín, SE Spain) that was proposed as a possible boundary stratotype by Aguado et al. (2000), who defined the base of the Valanginian by the FO of *C. darderi*.

Primary Marker

Even though all species are biogeographically limited, the Valanginian Working Group (VWG) preferred to use, as a primary marker, a unique event such as the first appearance of a fossil species to define the B/V boundary. This allows an unequivocal determination of age, contrary to chemical and physical events that are repetitive (Remane et al., 1996, p. 79), and used here as secondary markers of the Valanginian base. Other reasons can be evoked to justify this approach. Concerning the C-isotope trends, the B/V boundary as observed in the Vergol and Cañada Luenga sections (see below) is not characterized by major changes. Minor variations are not easy to record (cf. sample step) and recognize in some other sections (more particularly when they are condensed), and should be interpreted carefully. For the strontium isotope stratigraphy, the construction of $^{87}Sr/^{86}Sr$ curves of Early Cretaceous time is mainly based on data coming from SE France and SE Spain (see below) and thus, for the moment, has not been widely applied elsewhere. The geomagnetic reversal is a worldwide event and practically instantaneous at the geological time scale. However, the identification of magnetozones requires to be anchored to a solid biostratigraphic framework for any given section in order to reduce errors and improve accuracy for a nonambiguous correlation to the reference geomagnetic polarity time scale (Ogg, 2020). Futhermore, specific environmental and sedimentary conditions are required for recording a complete and exploitable magnetic signature, as evoked in the current work (cf. the Vergol section) for the Vocontian basin (see chemical remagnetization, Katz et al., 1998, 2000). In cyclo-astrochonology, the 405-kyr eccentricity cycle is classically used as a geochronometer for the Mesozoic (Martinez et al., 2015, and references therein) and the record of a series of these cycles throughout a section allows to give an age model for the studied interval, and also reinforce correlations, as proposed in the current work for the Vergol and Cañada Luenga successions (see below). However, this approach is not really relevant in order to characterize a surface as the B/V boundary.

Concerning the choice of the primary marker, three biostratigraphic fossil groups were recognized by the former VWG (Bulot et al., 1996): ammonites, calpionellids, and calcareous nannofossils. The current VWG discussed the advantages and drawbacks of four taxa: *Hoedemaekeria pertransiens* (index species of the first ammonite Valanginian zone), *Neocomites premolicus* (index species of the first ammonite subzone), *Calpionellites darderi* (index species of the first calpionellid Valanginian zone), and *Calcicalathina oblongata* (index species of the first nannofossil Valanginian zone). In order to define the base of the Valanginian, the first appearance of *H. pertransiens* was selected as the primary marker according to the following points, including both conceptual and pragmatic approaches. At Vergol, the First Occurrence (FO) of this ammonite marker is recorded in bed VGL-B136. To characterize the B/V boundary, the FO of *N. premolicus*, *C. darderi* and *C. oblongata* are considered as secondary markers, as well as chemical and physical events as evoked previously, allowing an integrated stratigraphy for a global correlation (see below).

The following points refer to the conceptual approach. The index species, *Hoedemaekeria pertransiens*, has been historically attributed, since its definition (Sayn, 1907), to the genus *Thurmanniceras* Cossmann (1901) or to its objective synonyms *Thurmannia* Hyatt (1900; non Heer, 1852) and *Thurmannites* Kilian and Reboul (1914). The type species of the genus *Thurmanniceras* (*Ammonites Thurmanni* Pictet and Campiche, 1860) is based on poorly preserved and difficult to interpret type material. However, this has not prevented the assignment to the genus of more than forty species with very diverse phylogenetic origins and palaeogeographic and stratigraphic distributions, turning it into a paradigmatic catch-all taxon. This has led many authors to question the attribution of *pertransiens* (and other closely related species such as *otopeta* and *gratianopolitensis*) to the genus *Thurmanniceras* since the 1980s (Hoedemaeker, 1982; Gayte, 1984, Bulot, 1995). This is the reason why, pending a thorough revision, the generic name of these species appears between inverted commas in the most recent literature (Company and Tavera, 2013, 2015; Kenjo, 2014; Kenjo et al.,

2021; Reboulet et al., 2022), including the latest versions of the standard Mediterranean ammonite zonation (Reboulet et al., 2014, 2018; Szives et al., 2024).

In the framework of an integrated stratigraphy made on some Moroccan sections (Reboulet et al., 2022), new and well-preserved neocomitids, sampled on the B/V boundary interval, allowed the completion of Spanish (Company, 1987; Aguado et al., 2000; Company and Tavera, 2015) and French (Kenjo, 2014; Kenjo et al., 2021) faunal data. Our preliminary results (this work) allow us to consider that the species *otopeta*, *pertransiens* and *gratianopolitensis* should be grouped into a new genus, different from *Thurmanniceras* Cossmann, which would be restricted to the type species *Thurmanniceras thurmanni*. This new genus, *Hoedemaekeria*, is formally introduced here (see Appendix 1, Taxonomic note).

Hoedemaekeria pertransiens is common, well preserved and shows a continuous range at Vergol section (Kenjo et al., 2021 and references therein; see below). According to these authors, and considering a global approach (see below), this species is common in basin facies, rarer to absent in shelf facies. It has a short stratigraphic range (restricted to the *H. pertransiens* Zone). This point is relevant, more particularly in situations where the stratigraphic record of the species is poor and not continuous (scarcity of the index species due to ecological factors, bad preservation conditions, etc.). In this case, the shorter the stratigraphic distribution, the closer we are to characterizing the base of the stage. *Hoedemaekeria pertransiens* has a large palaeogeographic distribution and it is relatively well represented in the Mediterranean Province of the Mediterranean–Caucasian Subrealm (Tethyan Realm; Company, 1987; Bulot, 1995; Klein, 2005; Kenjo, 2014; Kenjo et al., 2021). A recent record of *H. pertransiens* in Mexico (Ovando-Figueroa et al., 2024a) shows the great potential of this species in the Tethyan Realm (see below; for the palaeobiogeographical attribution of Mexico during the Early Cretaceous, see Ovando-Figueroa et al., 2024b). It can be considered that the relatively wider distribution of *C. darderi* than *H. pertransiens* does not represent a significant advantage. Indeed, this calpionellid species is not recognized in some biogeographic domains (Boreal Realm and Eastern Tethys) and thus the characterization of the boundary will be also impossible on large parts of some continents (using a single marker). Microfossils have a potential of correlation higher than macrofossils when dating boreholes. For the Berriasian and Valanginian stages, the inter-calibrations "macro/microfossils" (outcrops and boreholes) are very often based on the association "ammonites and calcareous nannofossils" (see below). Indeed, calcareous nannofossils such as *C. oblongata* represent a powerful proxy for borehole dating. Finally, it was noted that microfossils can be more easily affected by reworking, and thus one has to be very cautious with their use because reworked material can remain well preserved in some cases. Even though the FO of a taxon is not affected by reworking, this process modifies the range of species and thus, in some situations, it will be more difficult to pinpoint the "true" FO. In any case, the ranges (and FOs) of both these valuable biostratigraphic markers, i.e., *C. darderi* and *C. oblongata*, are very well calibrated to the primary marker *H. pertransiens* at the Vergol section, allowing a large inter-regional correlation, from platform to basin environments, based on outcrops and boreholes (see below).

According to a pragmatic approach, it can be noted that ammonites (such as *H. pertransiens*) can be often directly and easily identified in the field. This should not be the first criterion for choosing a marker, but we have to facilitate the application and the deployment of the selected solution by the widest number of researchers, including those working in developing countries. Moreover, the community of Cretaceous ammonite workers is relatively well represented in different countries enabling the expertise of a specialist to be deployed in different areas, as shown by a regular and substantial activity of the IUGS Kilian group (Hoedemaeker et al. 2003; Reboulet et al., 2006, 2009, 2011, 2014, 2018; Szives et al., 2024).

A detailed discussion about the choice of the primary marker (and the section) for the Valanginian GSSP was proposed by Kenjo et al. (2021, p. 22–24), in particular: "The base of Phanerozoic stages is often defined by biologic markers (GSSP table of ICS, http://www.stratigraphy.org/index.php/ics-gssps) that are ammonites for all stages of the Jurassic System (ratified GSSPs or proposals in progress for other stages). Indeed, for this period and also for Cretaceous, studies on ammonites generally provide the highest biostratigraphical resolution of stages to establish their subdivision and define their base …. a priority is given here to ammonite biostratigraphic data in order to make a good and workable correspondence in the subdivision of the Valanginian Stage (ammonite (sub-)zones) and the definition of its base...".

The Vergol Section (SE France): the Valanginian GSSP

Location and Geological Setting

The site is located in the Montbrun-les-Bains commune in the department of Drôme (France), about 50 km east of Orange and 40 km west of Sisteron (Fig. 1A, B). GPS coordinates are: 44°12'11.5"N, 5°25'04.1"E (WGS84 reference frame; https://www.google.com/maps). It appears on the Séderon sheet of the "Carte géologique de la France" at the 1/50,000 scale (Flandrin et al., 1964) and on the topographic sheet, scale 1/25,000, Banon Sault, n° IGN 3240 OT.

The Vergol section was palaeogeographically located in the central part of the epicontinental Vocontian basin (SE France), at a palaeolatitude of approximately 30°N (Savostin et al., 1986; Gréselle and Pittet, 2010; Fig. 2). This basin was surrounded by carbonate platforms (Cotillon et al., 1980; Gréselle and Pittet, 2010), such as the Jura platform to the north, and the Provence platform to the south. The Vocontian basin belonged to the passive margin of the European Tethys and it was infilled by a sequence of sediments which were deposited in a hemipelagic environment (Gréselle et al., 2011; Martinez et al., 2013).

Access and Protection

At Vergol, three successive sites of observations were selected to provide a continuous log from the upper Berriasian (*Tirnovella alpillensis* Zone) to the middle part of the lower Valanginian (*Hoedemaekeria pertransiens* Zone and *Neocomites neocomiensiformis* Zone p.p.). Two long exposures are located along the road D159 where the lithological succession is easily and continuously followed. An intermediate exposure occurs along (and on the sides of) the small creek orthogonal to the road. Due to the large area of exposure, most of the beds can be easily observed on many sites (Fig. 3). Thus, the exposure conditions

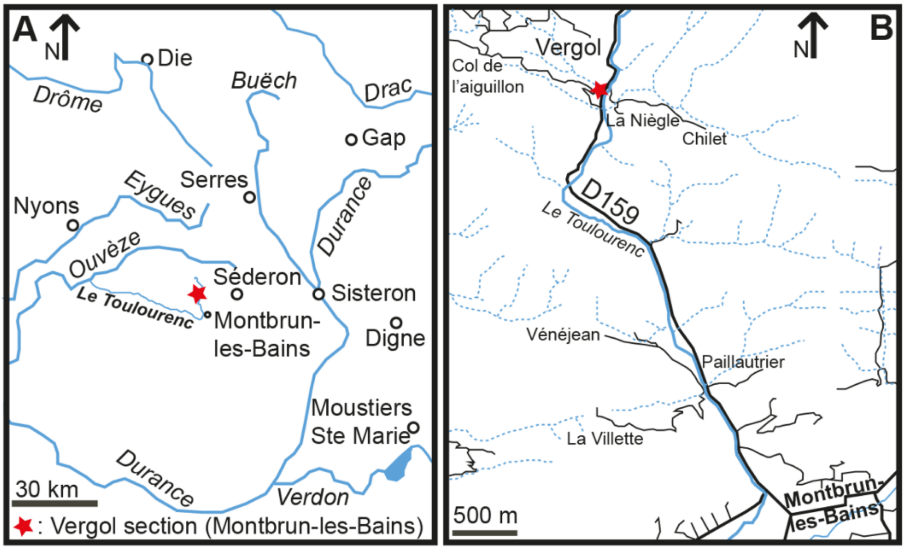

Figure 1. Location of the Vergol section (Montbrun-les-Bains, Drôme, France). A, general geographic map modified from Kenjo et al. (2021). B, detailed location map modified from https://www.geoportail.gouv.fr/carte. Red star: Vergol section, GPS coordinates are 44°12'11.5"N 5°25'04.1"E (WGS84 reference frame; https://www.google.com/maps).

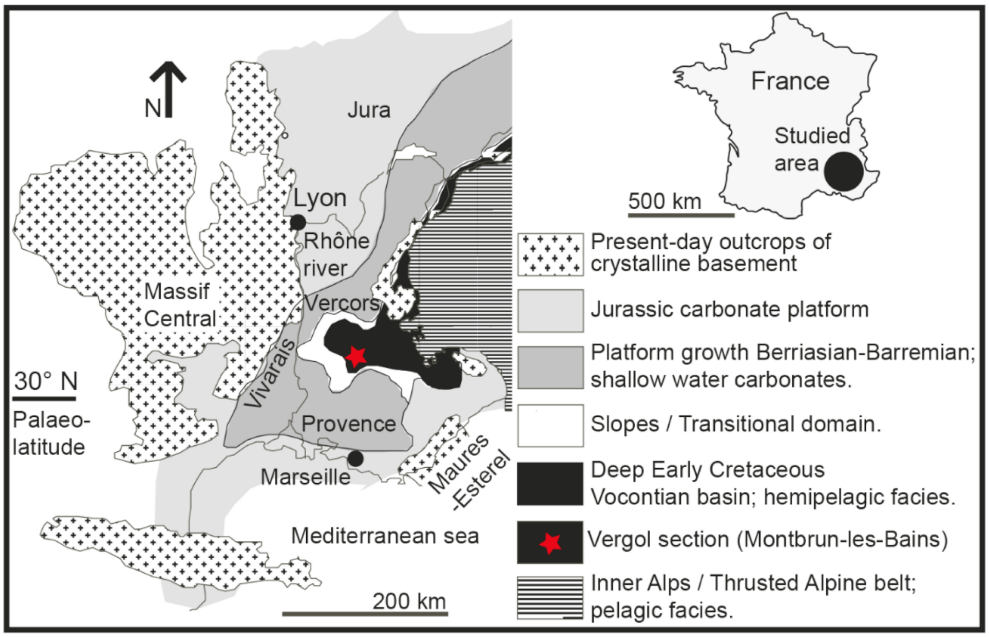

Figure 2. Palaeogeographic map of the Vocontian basin (SE France, Lower Cretaceous) modified from Ferry (1991). Red star: Vergol section.

of the Vergol section are highly suitable for accurate observations and high-resolution sampling. The corresponding sites of observations are indicated alongside the section (Fig. 4).

Most of the succession is exposed along the road and a large surface area of outcrop (including the interval boundary) is located in Parcel 218 (of the land register) that belongs to the municipality of Montbrun-les-Bains. Taking into account that this area is public property, the section is fully and permanently accessible.

The whole section is included in the "Parc Naturel Régional des Baronnies Provençales". The scientific committee (SC) of the park (S. Reboulet is one of the SC members), in collaboration with the Montbrun-les-Bains municipality and the Drôme Department, has a project for the development and protection of the Vergol site.

General Description of the Section

The interval of the Vergol section which embraces the Berriasian/Valanginian (B/V) boundary is 53.12 m thick from bed VGL-B95 to bed VGL-V43. The cumulative thicknesses are indicated along the section (in metres, measured from the base of the section; Fig. 4). It was extensively described by Kenjo (2014) and Kenjo et al. (2021) and the bed numbering system used here is based on their work. Those authors proposed a correlation with the Vergol section sensu Blanc et al. (1994) and Blanc (1996). Above bed VGL-V43, there is a synsedimentary disturbance (12 m thick); this slump is located in the *N. neocomiensiformis* Zone, around 34 m above the (B/V) boundary.

The Vergol section is an expanded succession deposited in a hemi-

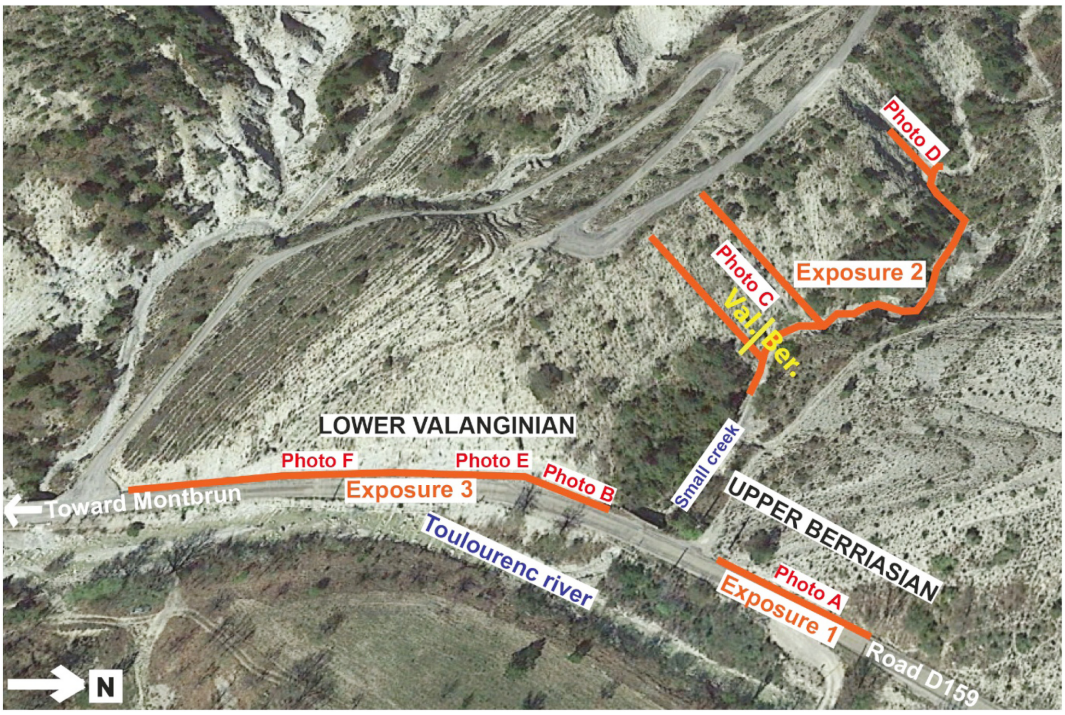

Figure 3. Access and exposure of the Vergol section. Sites of observations (see orange lines); location map modified from Google Earth (https://earth.google.com/); the location of photos (A to F) illustrated in Fig. 5 is indicated here.

pelagic environment of the Vocontian basin, that is optimal for a continuous sedimentary record (see astrochronology, Martinez et al., 2013, 2015). The studied interval (VGL-B95 to VGL-V43) is composed of marl–limestone alternations (Figs. 4 and 5). This interval does not show any evidence of sedimentary hiatuses such as hardgrounds, phosphate nodules or glauconitic intervals, which are observed in more proximal sections located on the surrounding platforms (Gréselle and Pittet, 2010). Only three very small layers (millimetric to centimetric in thickness), interpreted as turbidites, are recorded but these are located approximatively 9 metres below and 8 metres above the B/V boundary. The succession is characterized by an absence of tectonic disturbance. Metamorphism and (strong) diagenetic alteration can be excluded. According to Gréselle et al. (2011) "the long-distance correlation of the marl–limestone alternations in the Vocontian basin shows that they have a primary origin, and demonstrates that they cannot result from a diagenetic redistribution of carbonates" (see also Cotillon et al., 1980).

The base of the studied interval (upper Berriasian) is characterized by thick limestone beds (such as VGL-B100 and VGL-B101, Fig. 5A) alternating with thin marl layers. Limestone beds become thinner stratigraphically upwards while marl layers are thicker. The uppermost Berriasian is characterized by a limestone-dominated interval of 11 limestone beds (calcareous bundle VGL-B119 to VGL-B129; Fig. 5C, D) named the "Otopeta bundle" that is located just below the B/V boundary. Around this boundary and in the lowermost Valanginian (Fig. 5B, E), the limestone beds tend to be thinner while marlstones are thicker, even if the marl layers remain generally thinner than limestones. From bed VGL-V30 to bed VGL-V43 (Fig. 5F), marl layers become generally thicker than limestones. According to the Dunham's (1962) classification, the fine-grained limestones are mudstones or wackestone.

The studied succession is very expanded and has a very good sedimentary record; the rate of sedimentation is around 23 m/Myr (see below).

Sequence Stratigraphy

The hierarchy of cycles used here matches with the cyclostratigraphic framework of Gréselle and Pittet (2010; see also Gréselle, 2007; Gréselle et al., 2011) who worked on a large transect from proximal (Jura and Provence platforms) to distal (Vocontian basin) palaeoenvironments (Fig. 2).

As reported on the Vergol section, these authors (op. cit.) recognized four orders of depositional cycles (a to d, see Fig. 6) allowing them to propose an orbital control for the formation of lithological cycles that can be defined as depositional sequences sensu Strasser et al. (1999): (a) Elementary sequences are defined in the basin (deep environment). They correspond to 20 kyr precession cycles (a single limestone–marl couplet, sometimes doubled); (b) Small-scale sequences are the smallest order of sequences recognized in the platform, margin and basin. These sequences correspond to 100 kyr short-term eccentricity cycles (composed of 4, 5 or 6 repetitively stacked elementary couplets characterized by an increasing thickness of the limestone beds and higher carbonate content towards the top of the sequence); (c) Medium-scale sequences are defined on the platform and margins by discontinuity surfaces (cf. changes in facies evolution). In the basin, medium-scale sequences are made of four small-scale sequences; thus, they match to 400 kyr long-term eccentricity cycles (Ber 13, Ber 14, Ber 15, Val 1, Val 2). Medium-scale sequences are often characterized by a strong asymmetry in carbonate content (thicker and harder limestone beds related to higher carbonate contents at the top of sequences); (d) Large-scale sequences are here formed by two medium-scale sequences. These sequences are bounded by major facies changes and discontinuities in sedimentation on the platform areas (SB C or Be8, SB D or Va1, SB E or Va2).

Gréselle and Pittet (2010) proposed a reconstruction of sea-level

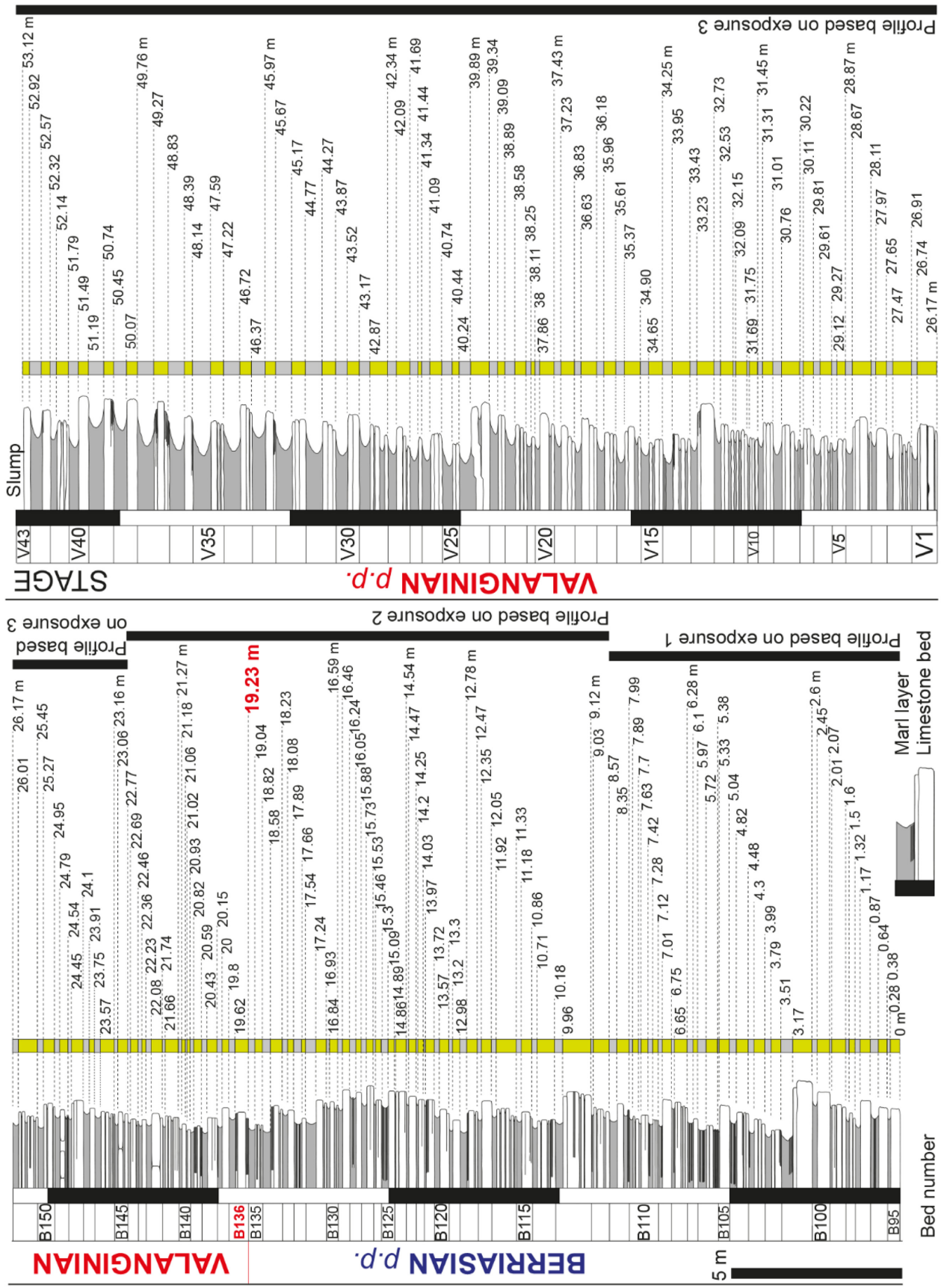

Figure 4. Section modified from Kenjo et al. (2021) with indications of cumulative thicknesses (in metres, measured from the base of the section) and stratigraphic intervals of three sites of observations where the profile was drawn; the three exposures are located in Fig. 3. The numbering system is based on the limestone–marl couplets; more explanations in Kenjo et al. (2021, figure caption 1).

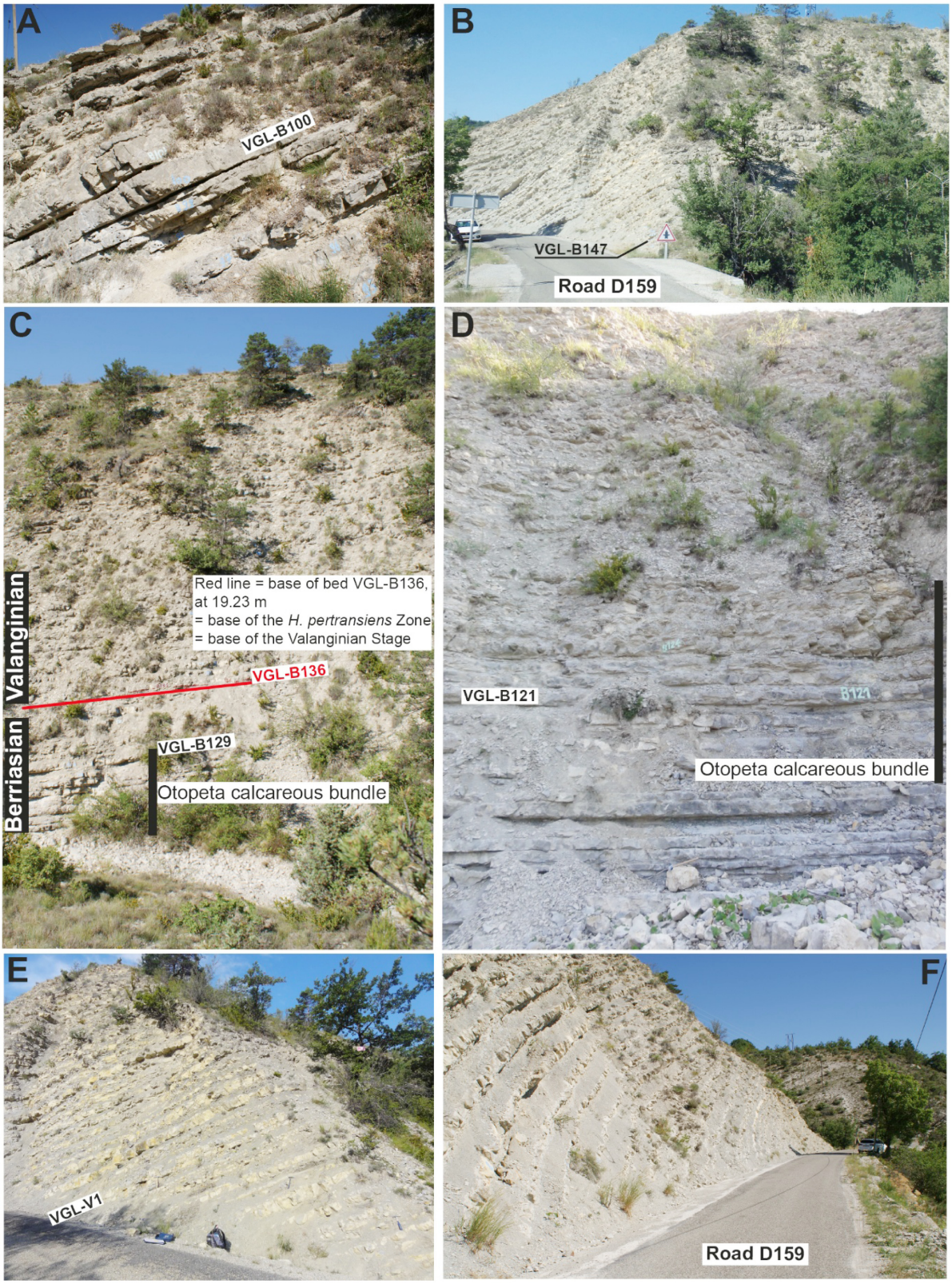

Figure 5. Photos showing some exposures of the Vergol section. Letters A to F are located in Fig. 3; explanations see text (photos Reboulet).

fluctuations using the identified small, medium and large-scale sequences as well as depositional geometries. Medium- and long-term curves are reported with a strong asymmetric sea-level oscillation (Fig. 6). Their shape could be interpreted as a rapid transgressive phase and a much slower regression (if no sedimentation rate change is identified in a sequence). It can be noted that the boundary level (VGL-B136) occurred during a sea-level highstand.

Medium-scale and large-scale sequences can be correlated from the

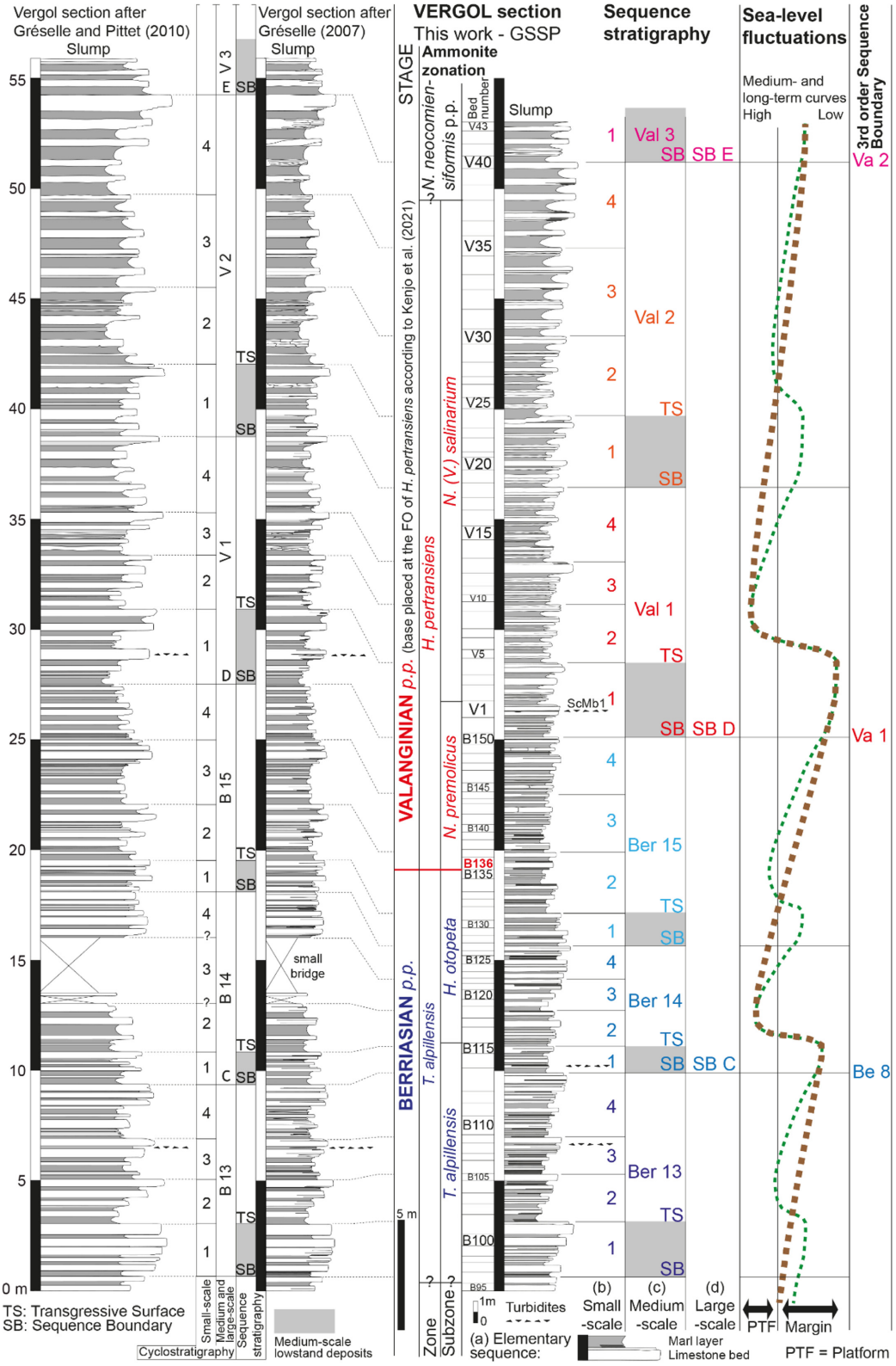

Figure 6. Sequence stratigraphy of the Vergol section. The current profile (lithology and ammonite zonation modified from Kenjo et al., 2021) is correlated with those proposed by Gréselle (2007, fig. 3.45a) and Gréselle and Pittet (2010, fig. 11). The sequence stratigraphy (a to d) is established according to Gréselle (2007), Gréselle and Pittet (2010), and Gréselle et al. (2011): (a) Elementary sequences (20 kyr precession cycles), (b) Small-scale sequences (100 kyr short-term eccentricity cycles), (c) Medium-scale sequences (400 kyr long-term eccentricity cycles), and (d) Large-scale sequences; more explanations see text. Sea-level fluctuations (peri-Vocontian area) modified from Gréselle and Pittet (2010, fig. 17). 3rd order Sequence Boundary (Be8, Va1, Va2) according to Haq et al. (1987) and Hardenbol et al. (1998). Three turbidites are recorded: in layers VGL-B108, VGL-V1 (see Gréselle, 2007; the latter corresponds to the ScMb1 surface from Blanc, 1996, p. 85), and VGL-B114 (this work)

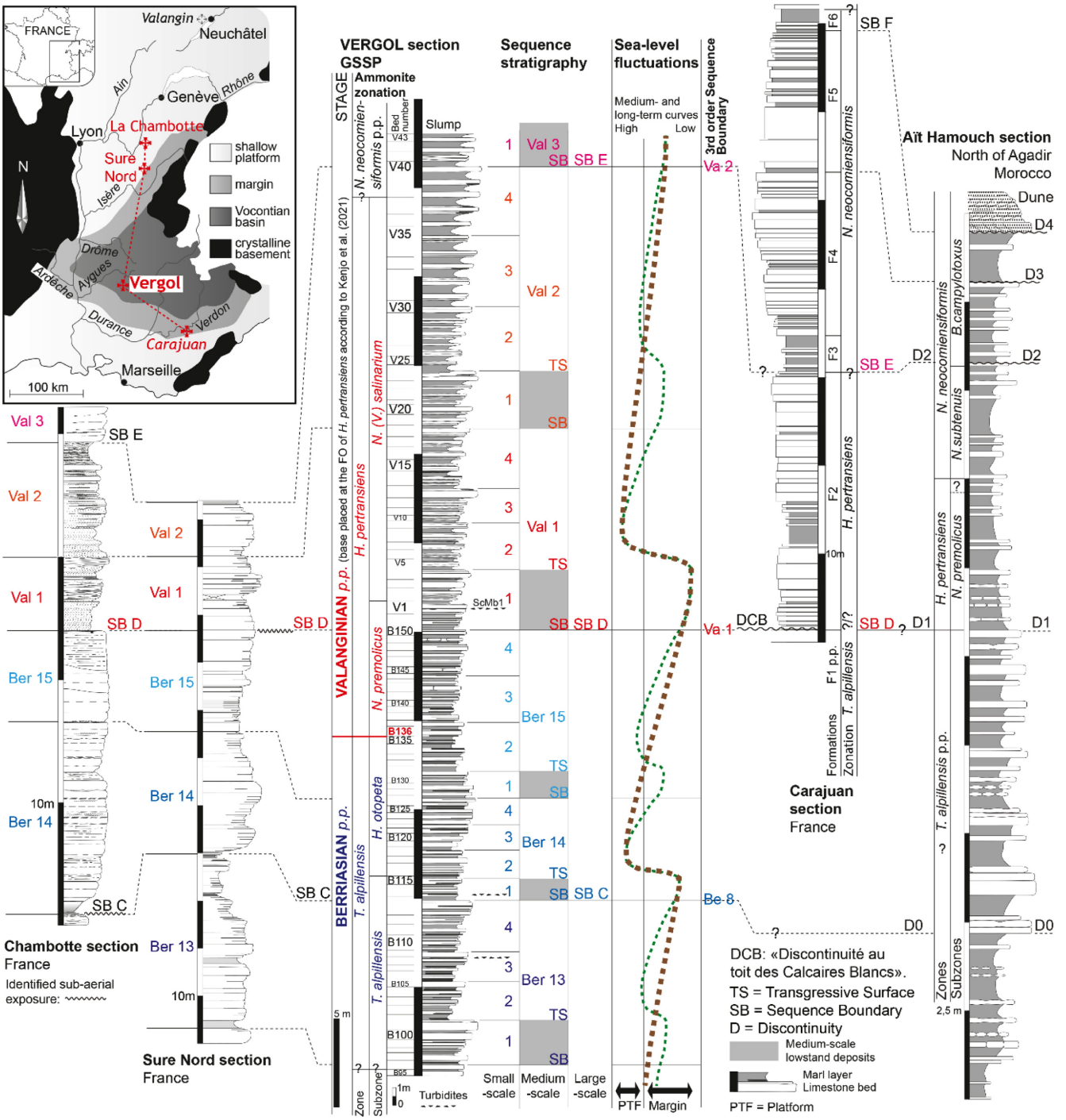

Figure 7. Correlation transect France (Vocontian basin and surrounding platforms)-Morocco. Interpretations based on Gréselle (2007), Gréselle and Pittet (2010), Gréselle et al. (2011), Kenjo et al. (2021) and Reboulet et al. (2022). For further explanations on the Vergol section, see Fig. 6 and its caption. The Chambotte (distal part of the Jura-Dauphinois carbonate platform, SE France) and the Sure Nord (Chartreuse margin, SE France) sections modified from Gréselle and Pittet (2010). The Carajuan section (distal margin of the Provence Platform, SE France) modified from Gréselle and Pittet (2010), and Reboulet et al. (2022). Aït Hamouch section (Essaouira-Agadir basin (EAB), Morocco) from Reboulet et al. (2022). Location of French sections on the inset map modified from Gréselle et al. (2011).

Jura-Dauphinois to Provence platforms, *via* the Vocontian basin (Fig. 7). According to Gréselle and Pittet (2010), "each section was interpreted in terms of sequence stratigraphy based on the stratigraphic evolution of the depositional environments, on the observation of remarkable surfaces and on the geometries of the sedimentary bodies". Reliable biostratigraphic data allowed correlations of the Vergol section with the Aït Hamouch section located in the Essaouira-Agadir basin (EAB, Morocco; Fig. 7; Reboulet et al., 2022). Consequently, the major sequence boundaries Be8, Va1 and Va2 were recognized in the northern and southern margin of the Mesozoic Tethys Ocean.

Biostratigraphy

A taxonomic index is provided in Appendix 2.

Ammonites

A total of 1023 ammonites, sampled in limestone beds, were identified. Data are provided by Kenjo (2014) and Kenjo et al. (2021; 855 specimens) and the unpublished work of Jaap Klein (168 specimens; Fig. 8). Most of them are stored either in the "Collections de géologie" of the "Université Claude Bernard" (Lyon, France; collection of Kenjo and Reboulet) or in the Klein's collection, Numbers RGM 778277-778431, in the Naturalis Biodiversity Center, Leiden, The Netherlands. The ammonite study made by J. Klein was restricted to the interval VGL-B121 up to VGL-V19; phylloceratids, lytoceratids and *Neolissoceras grasianum* were not sampled.

Dissolution of shells is usual, and ammonites are preserved as internal calcareous moulds. A huge systematic revision of all species was made during the PhD thesis of Kenjo (2014). Palaeontological comments (with photos of ammonites), information on stratigraphy and quantitative data were provided by Kenjo et al. (2021); a long list of references is available in their work. The ammonite fauna of the studied section (Fig. 8) is illustrated in Figs. 9 to 12. It consists of 20 (sub-)genera grouped into 7 families, using the suprageneric classification proposed by Klein (2005) and Klein et al. (2007, 2009; an appendix is given in Kenjo et al., 2021). The ammonite zonation is based on the recognition of successive faunal turnovers and by using interval zones of index species, defined by the first appearance, and characterized by their association (Kenjo et al., 2021). It corresponds to the standard zonation of the IUGS Kilian group (Reboulet et al., 2018; Szives et al., 2024).

Neocomitids are used to build the zonal scheme. The Berriasian interval is well characterized by the occurrences of *Tirnovella alpillensis*, and *Hoedemaekeria otopeta* that is relatively abundant in beds VGL-B127-B128-B129 (Fig. 8). The first occurrences (FO) of both these taxa allow to place the bases of the *T. alpillensis* Zone and *H. otopeta* Subzone, respectively. The lowest specimen of *T. alpillensis* has been found in VGL-B96 (Kenjo et al., 2021). As no sampling has been made below this layer, it cannot be excluded that the *T. alpillensis* Zone is partly represented in the studied interval (see question marks put at the base of the (Sub-)Zone, Fig. 8). Lithological correlations show that the bed VGL-B96 should correspond to bed COUR-96 of the Courchons section (Saint-André-les-Alpes, Alpes-de-Haute-Provence; Kenjo, 2014). In this last section, the FO of *T. alpillensis* is observed around one metre below (bed COUR-92), but this specimen was identified with doubt. The presence of other typical Berriasian taxa such as *Erdenella paquieri*, *Berriasella calisto* and *Fauriella boissieri* is significant in this interval. The base of the Valanginian is defined at the base of limestone bed VGL-B136 (at 19.23 m, measured from the base of the section) in which the FO of *Hoedemaekeria pertransiens* (primary marker) is recorded. The basal part of the lower Valanginian assemblage is also characterized by the occurrences of *Hoedemaekeria gratianopolitensis* and *Neocomites premolicus*. The FO of this latter species can be used to recognize the base of the Valanginian if *H. pertransiens* is rare or absent (see Ettachfini, 2004; Reboulet et al., 2022). In the upper part of the studied section, the FO of *Neocomites neocomiensiformis* indicates the base of the *N. neocomiensiformis* Zone. The lower Valanginian is characterized by *Sarasinella* (see discussion in Reboulet et al., 2022). *Kilianella* is also recorded in this substage, but the genus first occurs in the top part of the Berriasian.

Olcostephanids are mainly represented by rare *Spiticeras* and *Olcostephanus* that occur in the upper Berriasian and lower Valanginian intervals, respectively (Fig. 8).

Haploceratids, lytoceratids and phylloceratids are rare to common. The species belonging to these families are not really useful to characterize the Berriasian versus Valanginian ammonite assemblages, except *Neolissoceras* (*Vergoliceras*) *salinarium* that first occurs around the B/V boundary, and *Lytoceras honnoratianum* that seems restricted to the Berriasian interval in the Vergol section. The main discrepancy between J. Klein's unpublished results and those of Kenjo et al. (2021) concerns the stratigraphic range of *Neolissoceras* (*Vergoliceras*); this is related to different taxonomical concepts (cf. identifications). According to J. Klein, *Neolissoceras* (*Vergoliceras*) sp. ind. and *N.* (*V.*) *salinarium* first occur in the top part of the Berriasian *H. otopeta* Subzone (see the small dashed rectangle in Fig. 8) while Kenjo et al. (2021) observed these events in the basal part of the *H. pertransiens* Zone. During the last meeting of the Kilian Group (Warsaw, 2022), M. Company presented his joint work with S. Reboulet and made some proposals that were accepted (Szives et al., 2024). Among them, the *N.* (*V.*) *salinarium* Subzone was considered as the second subzone of the *H. pertransiens* Zone (see also Kenjo, 2014). This zonal scheme is adopted here, according to the ammonite ranges proposed by Kenjo et al. (2021).

Heteromorphs are represented by bochianitids, with *Bochianites neocomiensis* being rare but regularly found, and protancyloceratids, with *Leptoceras* and *Protancyloceras* that occur around the boundary interval. In layers VGL-B123-124, *Leptoceras* sp. ind. are relatively abundant. J. Klein also recorded this acme in the lower part of the *H. otopeta* Subzone in some sections of SE France such as Ginestous (see Janssen, 2021, figs. 6 and 7).

Belemnites

Comparable to other cephalopod groups (especially ammonites), belemnites occur either in abundance or can be virtually absent and everything in between. However, one important difference in the distribution of the belemnites compared to ammonites is their relative greater abundance in the marl layers as compared to limestone beds (see Janssen, 2021, for further explanation). Belemnites are stored in the Janssen's collection in the Naturalis Biodiversity Center, Leiden, The Netherlands. The collection numbers are: RGM288680–288700, RGM288822, RGM582032, RGM582071–582079, RGM582106–582131, RGM582230–582251, RGM582326–582324, RGM582380–582382, RGM582433–582437, RGM582607–582615, RGM614560–614593.

The upper Berriasian is characterized by taxa such as *Berriasibelus incertus*, *B.* aff. *exstinctorius*, *B. triquetrus, Castellanibelus* sp. E, *Gillieronibelus mayeri* and *Tithonobelus orbignyi*, of which most disappear in the uppermost Berriasian (Fig. 8). In addition, species that relate to *Duvalia* ex gr. *lata* (i.e. *Duvalia lata lata*, *D. lata constricta* and *Duvalia tornajoensis*) diminish significantly and occur less frequently, from the upper Berriasian into the lower Valanginian.

The B/V boundary does not coincide with a FO of any belemnite taxon. The first belemnites that indicate an early Valanginian age are from the

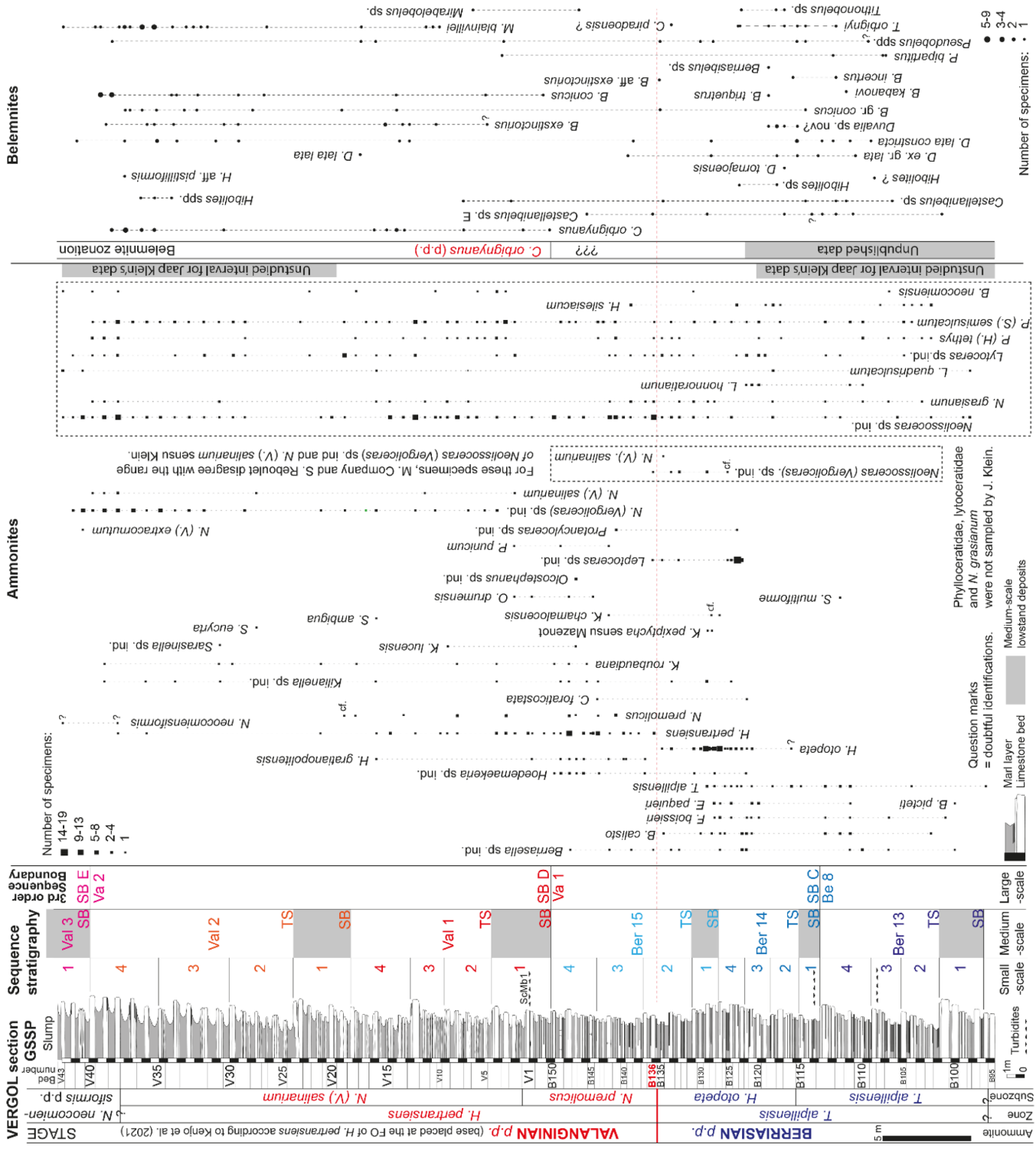

Figure 8. Ammonites and belemnites of the Vergol section, ranges and zonations. Concerning ammonites, the unpublished study made by J. Klein was restricted to the interval VGL-B121 up to VGL-V19. Klein's new data are included with Kenjo (2014) and Kenjo et al. (2021)'s data, except for the lower part of the range of Neolissoceras (Vergoliceras) sp. ind. and N. (V.) salinarium (cf. the small dashed rectangle); see explanation in the text. Phylloceratids, lytoceratids and Neolissoceras grasianum (grouped in the large dashed rectangle) were not sampled by J. Klein. Concerning belemnites, data are from Janssen (2021), updated by the author (this study) for the basal part of the section. For further explanations on the Vergol section, see Fig. 6 and its caption.

Castellanibelus orbignyanus Zone (FO of the index species in the marl layer VGL-B150, base of layer at 25.27 m; Fig. 8), as defined in Janssen (2021). Here, conventional Valanginian taxa first occur, such as *Castellanibelus orbignyanus*, *Berriasibelus conicus*, *Berriasibelus exstinctorius*, *Hibolites* aff. *pistilliformis* and *Mirabelobelus blainvillei*. Especially *Berriasibelus*, *Castellanibelus* and *Duvalia* ex gr. *lata* but also some

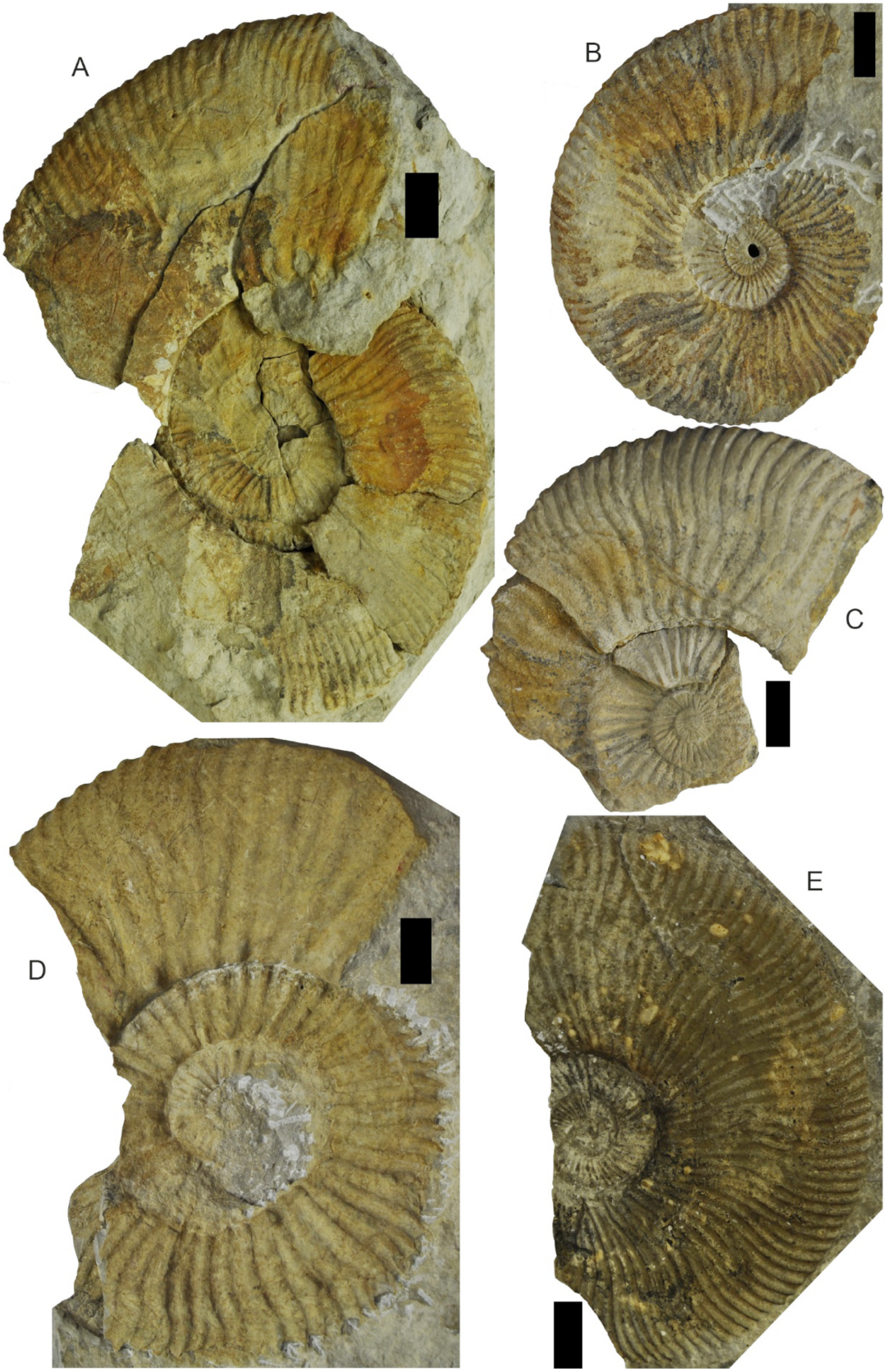

Figure 9. Ammonites (neocomitids) of the Vergol section (collection of Kenjo and Reboulet, UCBL-FSL, University of Lyon, France): A, Tirnovella alpillensis, UCBL-FSL 485397, VGL-B112, T. alpillensis (Sub-)Zone; B, Berriasella calisto, UCBL-FSL 485412, VGL-B113, T. alpillensis (Sub-)Zone; C, Fauriella boissieri, UCBL-FSL 485591, VGL-B125, T. alpillensis Zone, Hoedemaekeria otopeta Subzone; D, Erdenella paquieri, UCBL-FSL 485337, VGL-B121, T. alpillensis Zone, H. otopeta Subzone; E, T. alpillensis, UCBL-FSL 485603, VGL-B116, T. alpillensis Zone, H. otopeta Subzone. Scale bar = 1 cm.

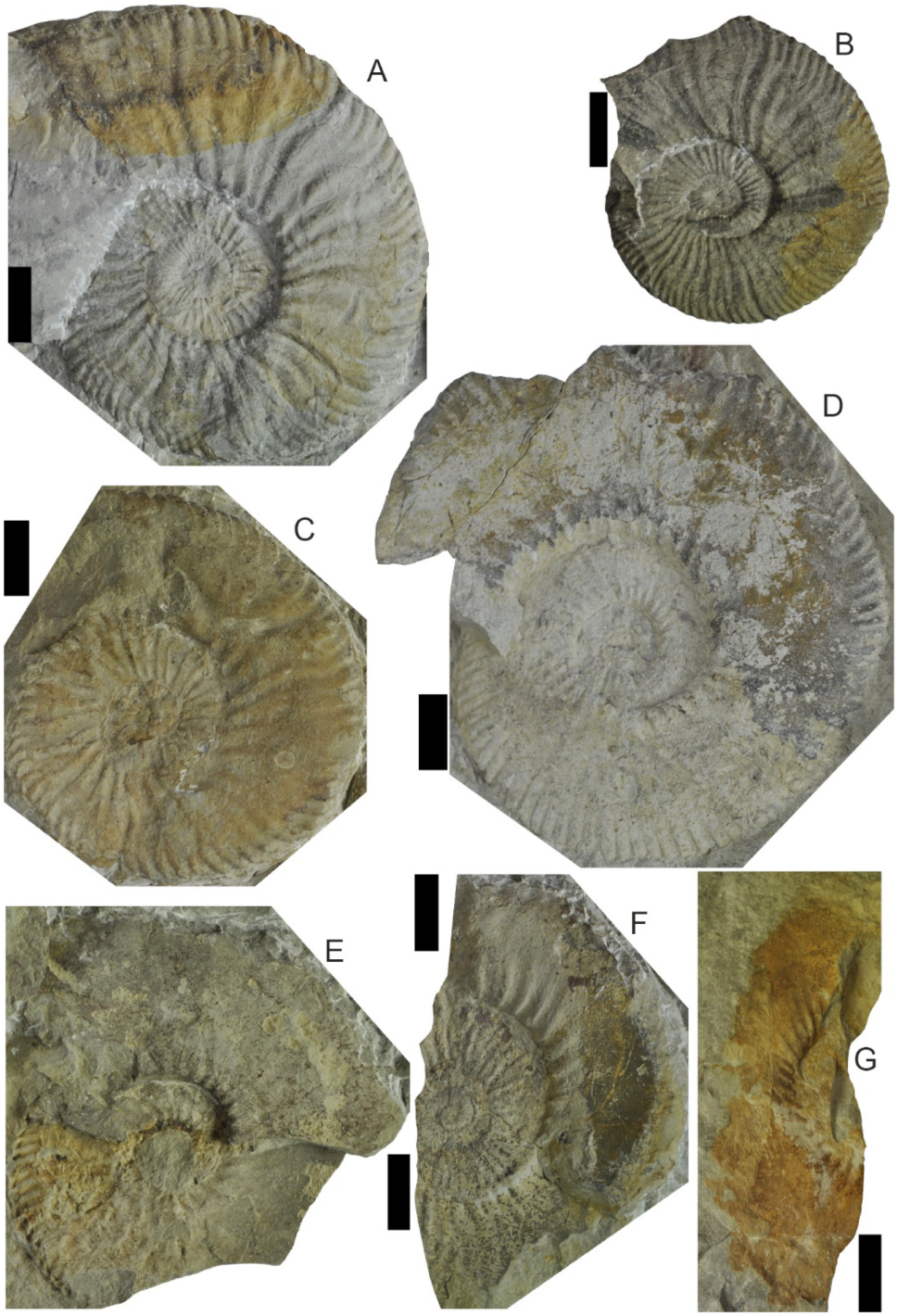

Figure 10. Ammonites (neocomitids) of the Vergol section (collection of Kenjo and Reboulet, UCBL-FSL, University of Lyon, France): A, Hoedemaekeria otopeta, UCBL-FSL 485350, VGL-B129, Tirnovella alpillensis Zone, H. otopeta Subzone; B, H. otopeta, UCBL-FSL 485345, VGL-B127, T. alpillensis Zone, H. otopeta Subzone; C, Hoedemaekeria pertransiens, UCBL-FSL 485376, VGLB148, H. pertransiens Zone, N. premolicus Subzone; D, H. pertransiens, UCBL-FSL 485546, VGL-V16, H. pertransiens Zone, N. (V.) salinarium Subzone; E, H. pertransiens, UCBL-FSL 485380, VGL-V22, H. pertransiens Zone, N. (V.) salinarium Subzone. F, H. pertransiens, UCBL-FSL 485377, VGL-V1b, H. pertransiens Zone, Neocomites premolicus Subzone; G, H. pertransiens, UCBL-FSL 485379, VGL-B136, H. pertransiens Zone, N. premolicus Subzone. Scale bar = 1 cm.

hibolitoid genera (*Mirabelobelus* and *Hibolites*) are common, though species abundances might fluctuate throughout the lower Valanginian and into the lowermost upper Valanginian (see Janssen and Clément, 2002).

Calpionellids

Sixty-six samples were collected in limestone beds from the Vergol section in order to use them for thin-sections production. They served

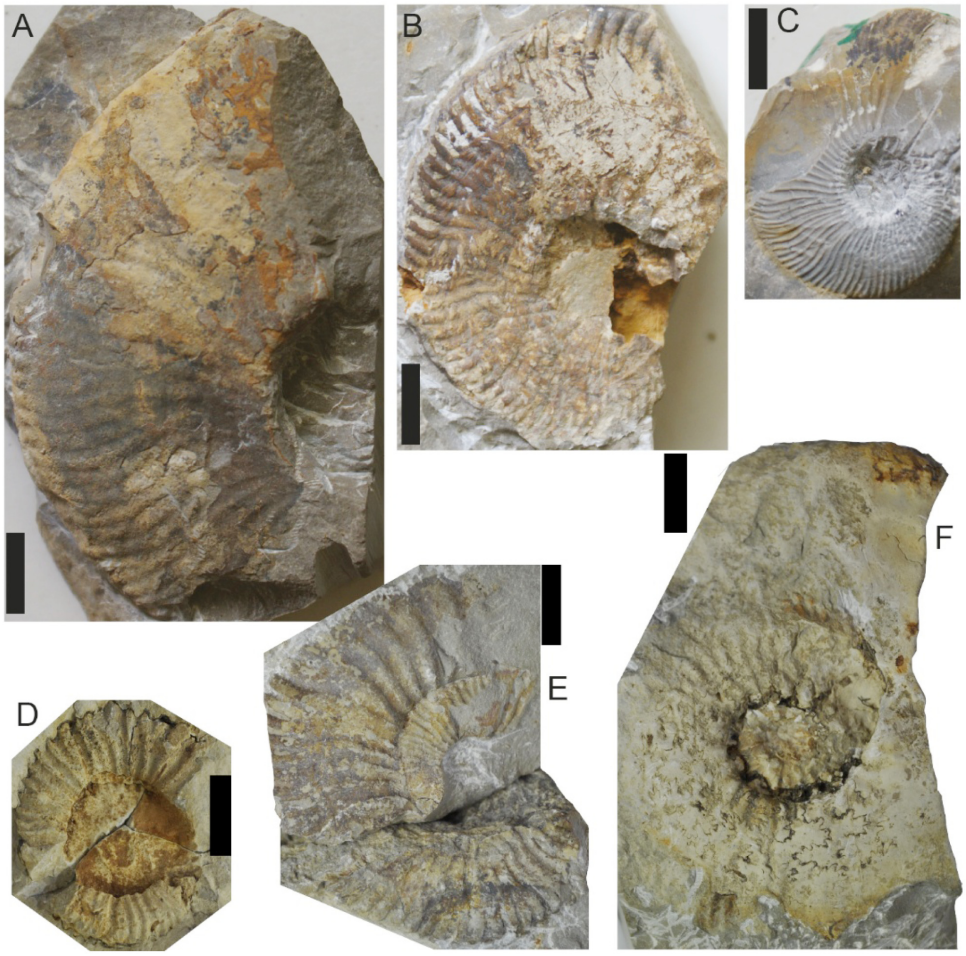

Figure 11. Ammonites (neocomitids) of the Vergol section (collection of Kenjo and Reboulet, UCBL-FSL, University of Lyon, France): A, Neocomites premolicus, UCBL-FSL 485388, VGL-V8, Hoedemaekeria pertransiens Zone, N. premolicus Subzone; B, Neocomites neocomiensiformis, UCBL-FSL 485389, VGL-V43, N. neocomiensiformis Zone; C, N. premolicus, UCBL-FSL 485387, VGL-B141, H. pertransiens Zone, N. premolicus Subzone; D, Kilianella lucensis, UCBL-FSL 485440, VGL-V9, H. pertransiens Zone, N. premolicus Subzone; E, Kilianella roubaudiana, UCBL-FSL 485439, VGL-V31, H. pertransiens Zone, N. (V.) salinarium Subzone; F, Sarasinella eucyrta, UCBL-FSL 485446, VGL-V28, H. pertransiens Zone, N. (V.) salinarium Subzone. Scale bar = 1 cm.

for documentation of succession of stratigraphically important calcareous microfossils (calpionellids and calcareous dinoflagellates) and for microfacies analyses. Thin sections are stored in Reháková's collection at the Department of Geology and Palaeontology, Faculty of Natural Sciences, Comenius University, Bratislava (Slovakia). Bio- and abiotic components, and biomarkers were studied under a LEICA DM 2500 microscope, equipped with an Axiocam ERc 5s camera, at the Department of Geology and Palaeontology, Comenius University in Bratislava. The standard calpionellid zonation of Remane et al. (1986) modified by Pop (1986) and the calcareous dinocyst zones sensu Reháková (2000a) modified on the basis of Ivanova and Kietzmann (2017) were applied. Microfacies were interpreted according to Dunham (1962). Standard microfacies types (SMFs) and facies zones (FZs) were defined as proposed by Wilson (1975) and modified by Flügel (2004). New data are presented here.

Calpionellids are not frequent in the Vergol section and become even rarer and less diverse from the onset of the *Praecalpionellites murgeanui* Subzone. The preservation of their loricae is very good in the lower part of the section where samples contain a calpionellid association of the *Calpionellopsis oblonga* Subzone. Higher in the section (Fig. 13), in the *P. murgeanui* Subzone as well as in the *Calpionellites* Zone (*Calpionellites darderi* and *Calpionellites major* Subzones), the abundance of calpionellids and their diversity decrease rapidly. The preservation of loricae in the last-mentioned subzones is variable. While loricae of *C. oblonga* are well preserved, loricae of *Praecalpionellites* and *Calpionellites* species, locally also remaniellids and tintinnopsellids, are much thinner and their collars are partially reduced and, in the case of the high portion of organic matter in matrix, calpionellid loricae show microbially induced dark linings. Nevertheless, their preservation is good enough for the identification on the species level and for the correlation on the (inter-)regional scale. In any case, a uniform preservation would not be expected under variable environmental conditions, as documented by Iskra Lakova who studied coeval calpionellid association in the Cañada Luenga section in which abundant and well-preserved calpionellids in the *Calpionellites* Zone are documented. Similar preservation was recorded in the Hlboč section in the Western Carpathians (Vašíček et al., 1994). Calpionellid assemblages of the Vergol section are illustrated in Figs. 14 and 15 (A–N).

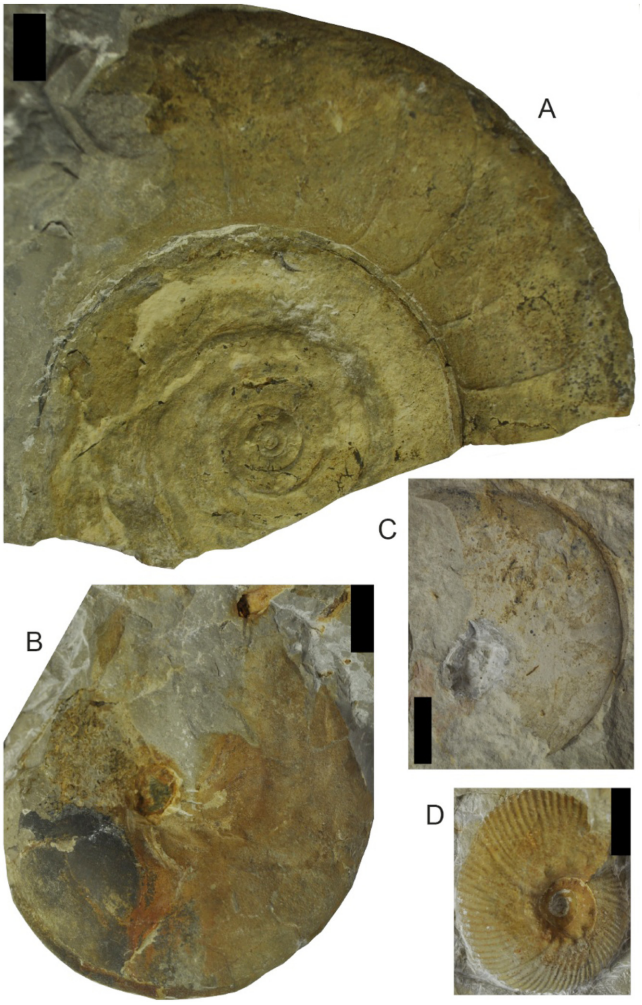

Figure 12. Ammonoids (olcostephanids, haploceratids, phylloceratids and lytoceratids) of the Vergol section (collection of Kenjo and Reboulet, UCBL-FSL, University of Lyon, France): A, Lytoceras honnoratianum, UCBL-FSL 485455, VGL-B121, Tirnovella alpillensis Zone, Hoedemaekeria otopeta Subzone; B, Ptychophylloceras (Semisulcatoceras) semisulcatum, UCBL-FSL 485458, VGL-V9, Hoedemaekeria pertransiens Zone, Neocomites premolicus Subzone; C, Neolissoceras (Vergoliceras) salinarium, UCBL-FSL 485463, VGL-V2, H. pertransiens Zone, N. (V.) salinarium Subzone; D, Spiticeras multiforme, UCBL-FSL 485476, VGL-B112, T. alpillensis (Sub-)Zone. Scale bar = 1 cm.

The *Calpionellopsis* Zone was introduced as the "D Zone" by Remane (in Le Hégarat and Remane, 1968) and later defined as the *Calpionellopsis* Standard Zone by Allemann et al. (1971). The FO of *Calpionellopsis simplex* defines the base of the zone and the FO of *C. darderi* its top. This zone is divided into the *C. simplex* (D1 Subzone of Remane, 1971; not identified in the Vergol section), *C. oblonga* and *P. murgeanui* subzones (Fig. 13).

The *Calpionellopsis oblonga* Subzone corresponds to the D2+D3 subzones of Remane (in Le Hégarat and Remane, 1968), named the *C. oblonga* Subzone by Remane et al. (1986). Pop (1986) restricted the subzone to the interval between the FO of *C. oblonga* at its base and the FO of *P. murgeanui* on the top of subzone. In the Vergol section, *C. oblonga* is common to frequent.

The *P. murgeanui* Subzone was defined and introduced by Pop (1986). Its base is defined by the FO of *P. murgeanui*. At Vergol, *P. murgeanui* is rare to common, accompanied by *Praecalpionellites sirniaensis* (scarce). *Calpionellopsis oblonga* becomes rare. Due to the rare occurrence and insufficient preservation of collars in the rare loricae resembling those of *Praecalpionellites* genus, species were sometimes identified with doubt (see question marks on Fig. 13). Therefore, it is not possible to strictly establish a boundary between the *C. oblonga* and *P. murgeanui* subzones. The first well-preserved loricae of *P. sirniaensis* and *P. murgeanui* were documented in limestone samples VGL-B114 and VGL-B117, respectively.

Allemann et al. (1971) designated Remane's (1971) E zone as the *Calpionellites* Standard Zone. Pop (1974) restricted the top of this zone to the LO of the genus *Calpionellites*. The lower boundary of the *Calpionellites* Zone was placed at the FO of *C. darderi*; at Vergol this matches in limestone bed VGL-B133 (base of layer at 17.89 m). Pop (1994) subdivided the *Calpionellites* Zone into the *C. darderi* and *C. major* subzones. Benzaggagh et al. (2012) introduced *Calpionellites-Oblonga* or E1 Subzone coinciding with the *C. darderi* Subzone. Benzaggagh (2020) proposed a new calpionellid (sub-)zonal scheme. It will have to be thoroughly checked to confirm its use for inter-regional correlation. The large palaeogeographic distribution of localities in which calpionellids were documented was shown by Wimbledon et al. (2020); the distribution of index species of *Calpionellites* standard Zone was summarized by Lakova and Petrova (2013) or Jiménez-López et al. (2021).

The *C. darderi* Subzone was first mentioned by Trejo (1980) but formally introduced by Pop (1994). In the Vergol section *C. darderi* is rare to common.

The *C. major* Subzone was established by Pop (1994). The lower boundary is defined by the FO of the index species (recorded in limestone bed VGL-B149) and its upper boundary by the LO of the genus *Calpionellites*. Benzaggagh et al. (2012) introduced *Calpionellites-Tintinnopsella* or E2 Subzone corresponding to the *C. major* Subzone.

Calcareous dinoflagellate cysts

Material and methods are indicated above in part "*Calpionellids*". New data are presented here.

Concerning calcareous dinoflagellates (phototropic algae producing cysts), it is important to emphasize that every new detailed study improves the understanding of the cyst successive distribution (Grabowski et al., 2016; Kowal-Kasprzyk, 2016; Ivanova and Kietzmann, 2017; Reháková, 2019; Molčan Matejová et al., 2022; Kietzmann et al., 2023) and helps to refine cyst zonations as proposed by Borza (1969), Lakova et al. (1999) and Reháková (2000b). In assemblages dominated by calpionellids, calcareous dinoflagellates are generally rare to scarce which can make their identification in thin-sections much more difficult.

Based on the combination of older and new data, upper Berriasian and lower Valanginian deposits generally contain cyst associations consisting of *Stomiosphaera wanneri*, *Cadosina minuta* (about this species, see Granier (2024) and note in the taxonomic index, Appendix 2), *Colomisphaera vogleri*, *Colomisphaera conferta*, *Colomisphaera heliosphaera*, *Colomisphaera lucida* and *Carpistomiosphaera valanginiana*. Apart from the last two mentioned cysts, all others, together with some of long-ranging species such as *Cadosina semiradiata semiradiata*, *Cadosina semiradiata fusca*, *Cadosina semiradi-*

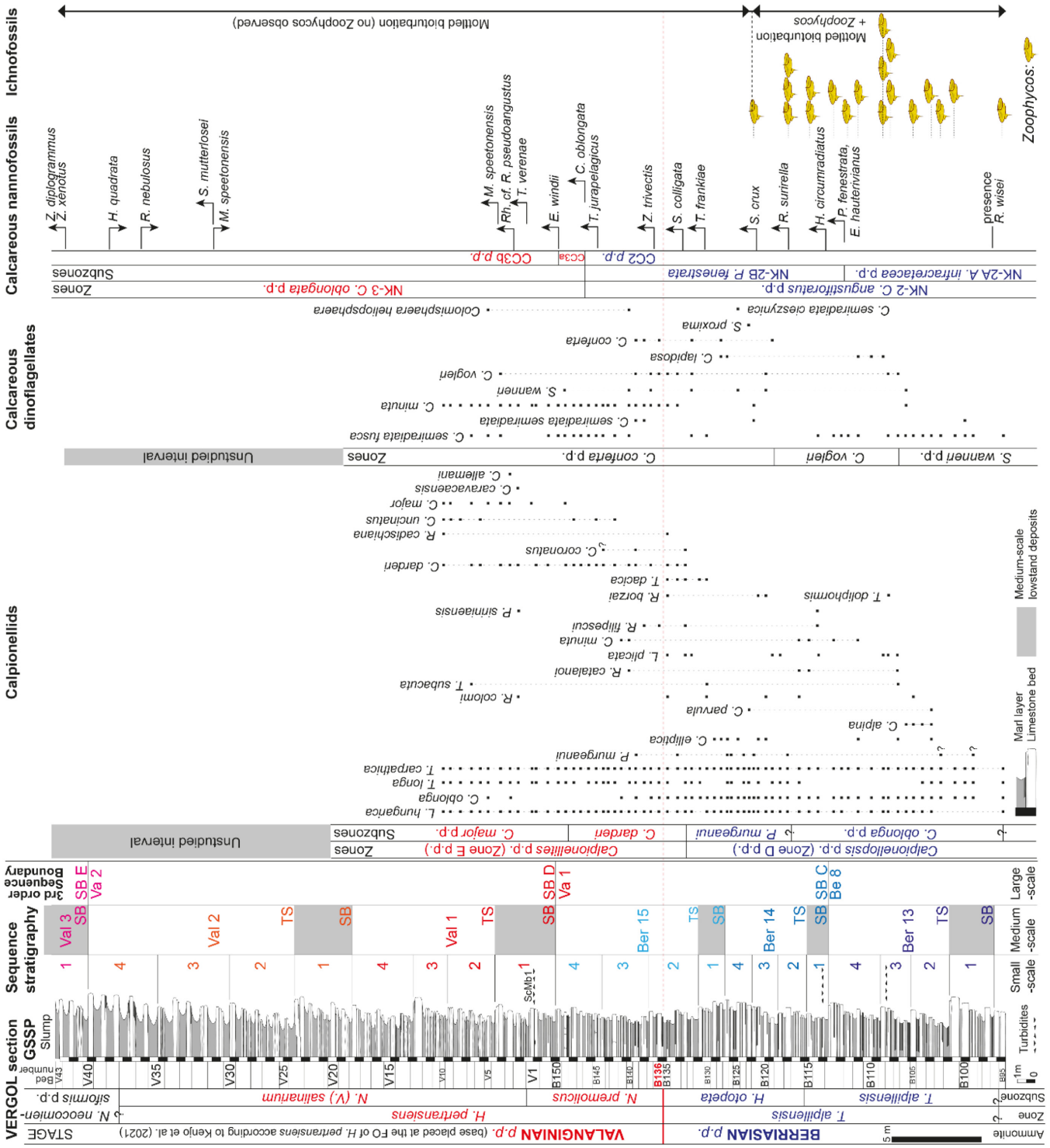

Figure 13. Calpionellids, calcareous dinoflagelletes, calcareous nannofossils (data modified from Kenjo et al., 2021) and ichnofossils of the Vergol section, ranges and zonations. For further explanations on the Vergol section, see Fig. 6 and its caption.

ata cieszynica, *Stomiosphaerina proxima* and *Colomisphaera lapidosa*, were documented in the Vergol section (Fig. 13). Here, most of the cysts mentioned above are rather rare to scarce; only *C. minuta,* which forms clusters of several cysts, is more frequent.

Thus, the *S. wannneri*, *C. vogleri* and *C. conferta* cyst zones (sensu Grabowski et al., 2016; Ivanova and Kietzmann, 2017; Kietzmann et al., 2023) have been recognized throughout the Vergol section. The lowermost part of the section has been tentatively assigned to the *S. wanneri* Zone. The base of the *C. vogleri* Zone is drawn at the FO of its index species in bed VGL-B106. The B/V boundary falls within the *C. conferta* Zone, the base of which is placed at the FO of the index species in bed VGL-B119 (base of layer at 12.98 m; Fig. 13). Calcareous dinoflagellate assemblages of the Vergol section are illustrated in Figs. 15 (O–T) and 16 (A–F).

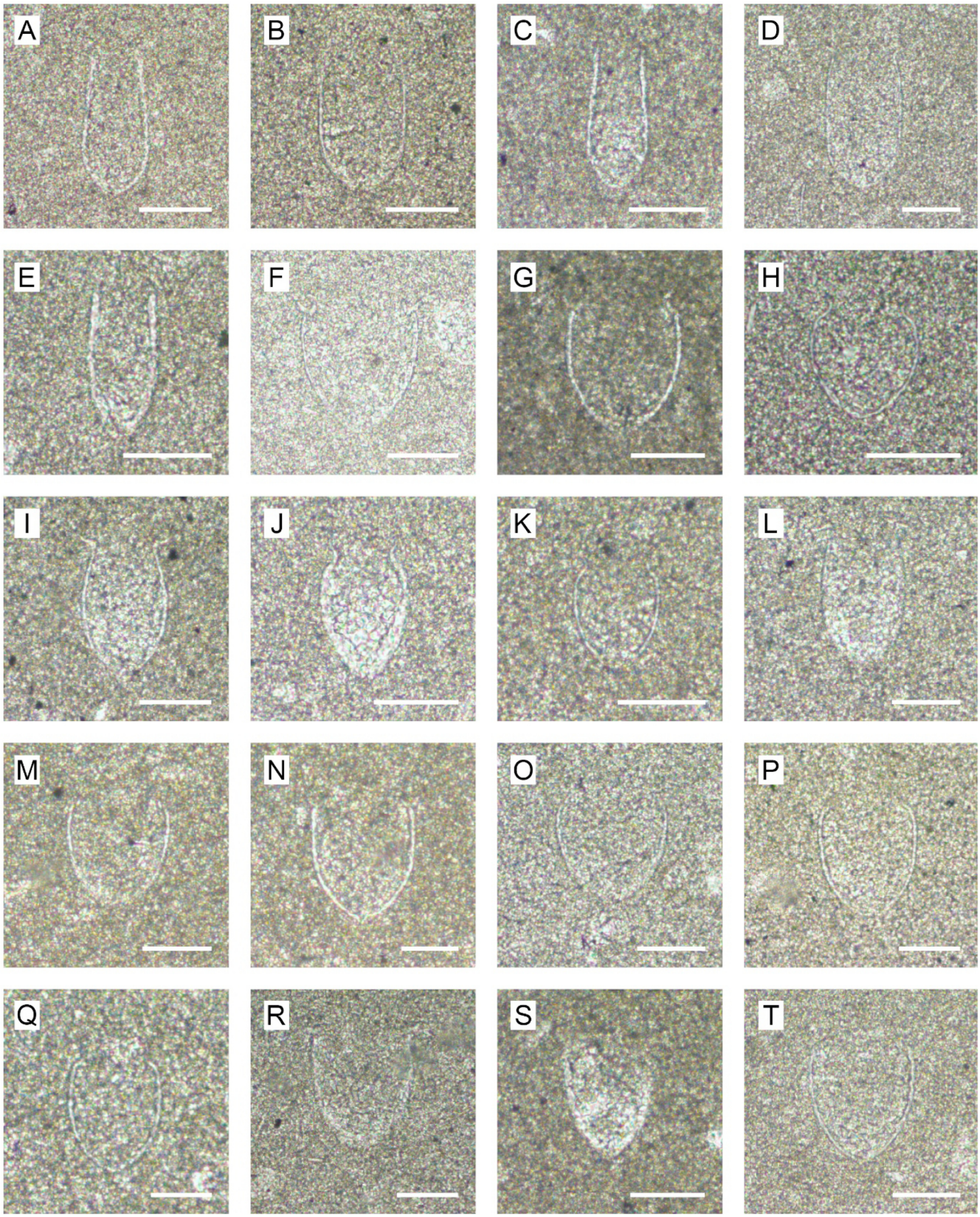

Figure 14. Calpionellids of the Vergol section (collection of Reháková, Comenius University, Bratislava, Slovakia): A, Calpionellopsis oblonga, VGL-B105; B, Praecalpionellites siriniaensis, VGL-B114; C, C. oblonga, VGL-B118; D, Tintinnopsella longa, VGL-B118; E, C. oblonga, VGL-B126; F, Remaniella filipescui, VGL-B127; G, Praecalpionellites murgeanui, VGL-B127; H, Lorenziella hungarica, VGL-B130; I, Tintinnopsella carpathica, VGL-B131; J, Lorenziella plicata, VGL-B132; K, L. plicata, VGL-B132; L, T. carpathica, with bacterially induced dark rim, VGL-B132; M, Calpionellites darderi, VGL-B133; N, R. filipescui, VGL-B133; O, C. darderi, VGL-B133; P, C. darderi, VGL-B133; Q, L. plicata, VGL-B135; R, Remaniella borzai, VGL-B135; S, Calpionellites uncinatus, VGL-B142; T, C. darderi, VGL-B144. Scale bar = 50 µm.

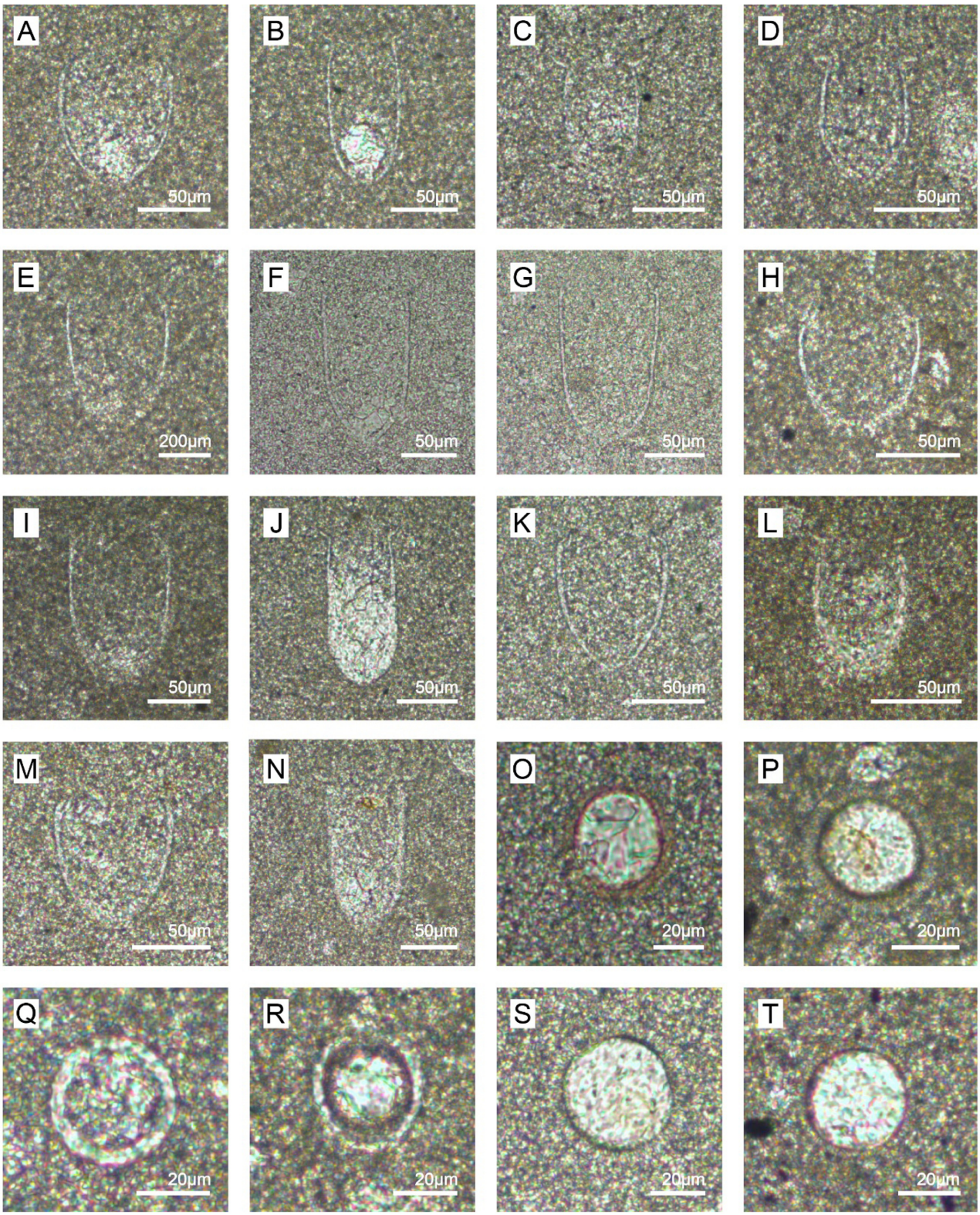

Figure 15. Calpionellids of the Vergol section (collection of Reháková, Comenius University, Bratislava, Slovakia): A, Calpionellites darderi, VGL-B144; B, Tintinnopsella longa, VGL-B148; C, Remaniella borzai, VGL-B120; D, Tintinnopsella doliphormis, VGL-B108; E, Calpionellites major, VGL V1B; F, Calpionellites caravacaensis, VGL V2; G, Praecalpionellites siriniaensis, VGL V2; H, C. darderi, VGL-V3; I, C. major, VLG-V3; J, T. longa, VGL-V5; K, Calpionellites coronatus, VGL-V9; L, Remaniella catalanoi, VGL-V10; M, C. darderi, VGL-V10; N, Remaniella cadischiana, VGL-V10. Scale bar = 50 µm, except for E scale bar = 200 µm. Calcareous dinoflagellates of the Vergol section (collection of Reháková, Comenius University, Bratislava, Slovakia): O, Cadosina semiradiata fusca, VGL-B130; P, Colomisphaera conferta, VGL-B132; Q, Stomiosphaera wanneri, VGL-B132; R, Stomiosphaerina proxima, VGL-B132; S, Colomisphaera vogleri, VGL-B134; T, C. vogleri, VGL-B136. Scale bar = 20 µm.

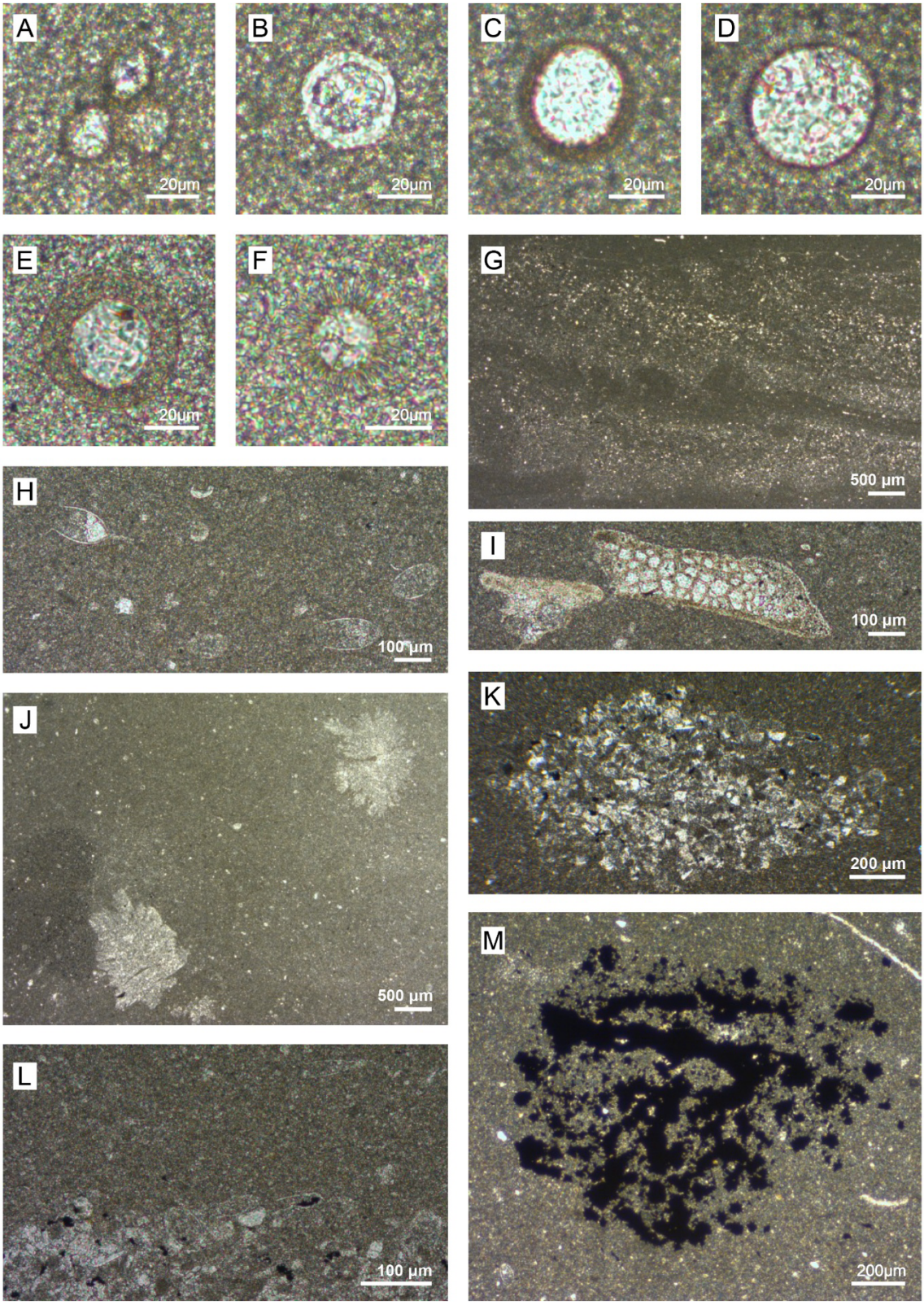

Figure 16. Calcareous dinoflagellates of the Vergol section (collection of Reháková, Comenius University, Bratislava, Slovakia): A, Cadosina minuta, VGL-B137; B, Stomiosphaera wanneri, VGL-B137; C, Cadosina semiradiata semiradiata, VGL-B138; D, Colomisphaera vogleri, VGL-B139; E, Cadosina semiradiata ciezsynica, VGL-B140; F, Colomisphaera heliosphaera, VGL-B140. Scale bar = 20 µm. Microfacies of the Vergol section (collection of Reháková, Comenius University, Bratislava, Slovakia): G, Matrix with marks of bioturbation, VGL-B132; H, microfacies with Tintinnopsella carpathica, VGL-B135; I, fragment of aptychus, VGL-B141; J, ? Sclerites of deep-water corals, VGL-V2; K, Patchy accumulation of bioclasts and silt admixure due to bioturbation, VGL-V7; L, Enlarged image of the burrowed matrix presented in image K, deformed lorica and Tintinnopsella subacuta in upper part of picture, VGL-V7; M, Pyrite accumulation, VGL-V10.

Organic-walled dinoflagellate cysts and other palynomorphs (miospores, acritarchs, scolecodonts, microforaminifera)

Twenty-five marl samples were prepared at the University of Bordeaux (France, Laurent Londeix) and a set of slides is stored in the collection of the Marine Palynology and Paleoceanography group, Utrecht University, The Netherlands, under code "000.000.017.384". An initial combined count of 500 specimens per sample, was made of all palynomorphs observed. The count of dinocysts, acritarchs, microforaminifera and scolecodonts (the marine sub-set) was then increased to 500 per sample, allowing better resolution. A fully quantitative palynofloral analysis of the upper Berriasian–lower Hauterivian interval from the Vocontian basin, including the Vergol section, was reported by Duxbury (2024; assemblages are illustrated in this work). This included some systematic revision of marine taxa and contributes to the current study on the B/V boundary.

Distribution chart: Some fluctuation in dinocyst species diversity was noted, and the overall trend was one of increasing diversity up-section, ranging from 32 dinocyst species in marl layer VGL-B97 to 60 species in marl layer VGL-V31 (see Figs. 17 and 18 for sampling levels). Many species are long-ranging, occurring throughout the studied interval, but others have their first occurrences (FO) and/or last occurrences (LO) within this range. As well as FO and LO, quantitative data allow the recognition of acmes and top and/or base common occurrences.

Absolute abundance occurrences of some more common dinocysts, including several long-ranging taxa, are shown in Fig. 17. They were selected as they demonstrate significant individual and relative changes in abundance up-section, which, if repeated in further studies, may be of fine-scale correlative value in the Vocontian basin. Counts of miospore taxa on which the Sporomorph EcoGroup (SEG) plot is based are also shown.

The effects of various palaeoenvironmental changes on dinocyst assemblages in the Vocontian basin are only partially understood (see Wilpshaar and Leereveld, 1994), and although assemblage fluctuations observed in the current study were often very marked with some apparently rapid, no detailed interpretation has been possible here. Possible causes of assemblage change due to various palaeoenvironmental factors were discussed by Pross and Brinkhuis (2005; surface water productivity and/or salinity and/or temperature, inshore/offshore trends), and the same would probably apply to the B/V boundary species.

One gross change in dinocyst assemblages recorded here was a significant up-section increase in the ceratioid taxon *Phoberocysta neocomica*, as low as marl layer VGL-V5 (*H. pertransiens* Zone), associated with increased numbers of a further ceratioid, *Pseudoceratium pelliferum*, although the last is common as low as marl layer VGL-B147 (*H. pertransiens* Zone, Fig. 17). Wilpshaar and Leereveld (1994) noted that high abundances of their *Muderongia* Group (including *Phoberocysta*) have been reported in sediments representing variable salinity conditions (e.g. Lister and Batten, 1988). It may be the case therefore that the studied section as low as marl layer VGL-V5 (and possibly as low as marl layer VGL-B147) was deposited in conditions of relatively reduced surface water salinity.

The large majority of observed miospore species have very long ranges - most range at least as low as the Middle Jurassic. Acritarchs (marine algae of uncertain affinity) and scolecodonts (jaws of polychaete annelids) are generally rare and appear to be of no stratigraphic value here (Fig. 17).

Microforaminiferal test linings were common to very abundant throughout the studied section. There was significant variation in numbers, however, with relative frequency dropping markedly at sea-level maxima and increasing particularly in later regressive phases, presumably demonstrating a preference for shallower settings.

Miospores formed consistently below 20% of the initial count and often below 10%. The quantitative counts per sample for all miospore, acritarch, microforaminifera and scolecodont species are shown in Fig. 17. Abbink's (1998) SEG model demonstrated palaeoecological changes, including sea-level fluctuations. His scheme was further summarised in Abbink et al. (2004). Abbink considered 6 SEGs (Fig. 18) to be important in interpreting his assemblages. Miospores recorded here have been similarly grouped, although because of the relatively low count of miospores, assemblage fluctuations may suggest only an approximation of palaeoenvironmental changes. Three SEG's, namely Coastal, Lowland and Upland were particularly prominent.

For reasons fully discussed in Abbink (1998) and pursued at Vergol by Duxbury (2024), the relationship between the coastal and lowland SEGs can be taken as a proxy for sea-level change. This is mainly because of the relative loss of lowland habitat during sea-level rise and the opposite effect during regressions. A prominent peak in the Coastal SEG and a marked reduction in the Lowland and Upland SEGs were seen here centred on marl sample VGL-B129 and close to peak marine influence in the medium-scale sequence Ber 14. These palynofloral occurrences are associated with other evidence within the *T. alpillensis* Zone (*H. otopeta* Subzone; Fig. 18), including a high in the long-term sea-level curve and a high in the marl $\delta^{13}C$ isotope curve, although the relationship between the palynofloral assemblage and $\delta^{13}C$ seems less straightforward.

A marked, stepped reduction in the Coastal SEG and an associated increase in Lowland and Upland taxa was recorded between marl layers VGL-B129 and B151, suggesting a lowstand event at the latter level, associated with both a low in the long-term and medium-term sea-level curves and a low in the $\delta^{13}C$ marl isotope curve, towards the top of the *N. premolicus* Subzone (*H. pertransiens* Zone; Fig. 18).

There was particularly close correspondence between the SEG plot, particularly the Coastal curve, and the $\delta^{13}C$ marl isotope curve between marl layers VGL-B129 and V31, interpreted as following the regressive/transgressive/regressive cycle indicated by the long-term sea-level curve (Fig. 18).

Palynological events and zonations in the Tethys: Several Tethyan palynofloral zonation schemes exist, with the most relevant to the current study being those of Habib (1975, 1977, 1978; Habib and Drugg, 1983), Monteil (1985, 1990, 1992b, 1993) and Leereveld (1997).

Although he used Monteil's (1993) data, Leereveld (1997) concluded that, "based on the selected dinocyst events the suite of zones cannot be recognised in SE Spain. In the Rio Argos succession, the position of the French middle Berriasian–Valanginian dinocyst zones can only be approximated, because of distinct differences in ranges of the diagnostic taxa". Leereveld (1997) extrapolated his zones with varying degrees of success, into Morocco, Libya, SE France, Switzerland, Romania and the North Atlantic. He recognized that the value of the regional dinocyst zonations is limited for interregional correlation. Leereveld

Figure 17. Palynomorphs of the Vergol section, organic-walled dinoflagellate cysts, miospores, acritarchs, microforaminifera and scolecodonts. Absolute abundance of main taxa. For further explanations on the Vergol section, see Fig. 6 and its caption.

(1997) listed several reasons for discrepancies between workers.

Because of difficulties reconciling these published schemes and the necessarily broad-brush approach to applying them here, a new zonation scheme was proposed in Duxbury (2024), based directly on first-hand observations at Vergol; for further details see Duxbury (2024, pp. 598–610). Zonation of the Vergol B/V boundary interval in terms

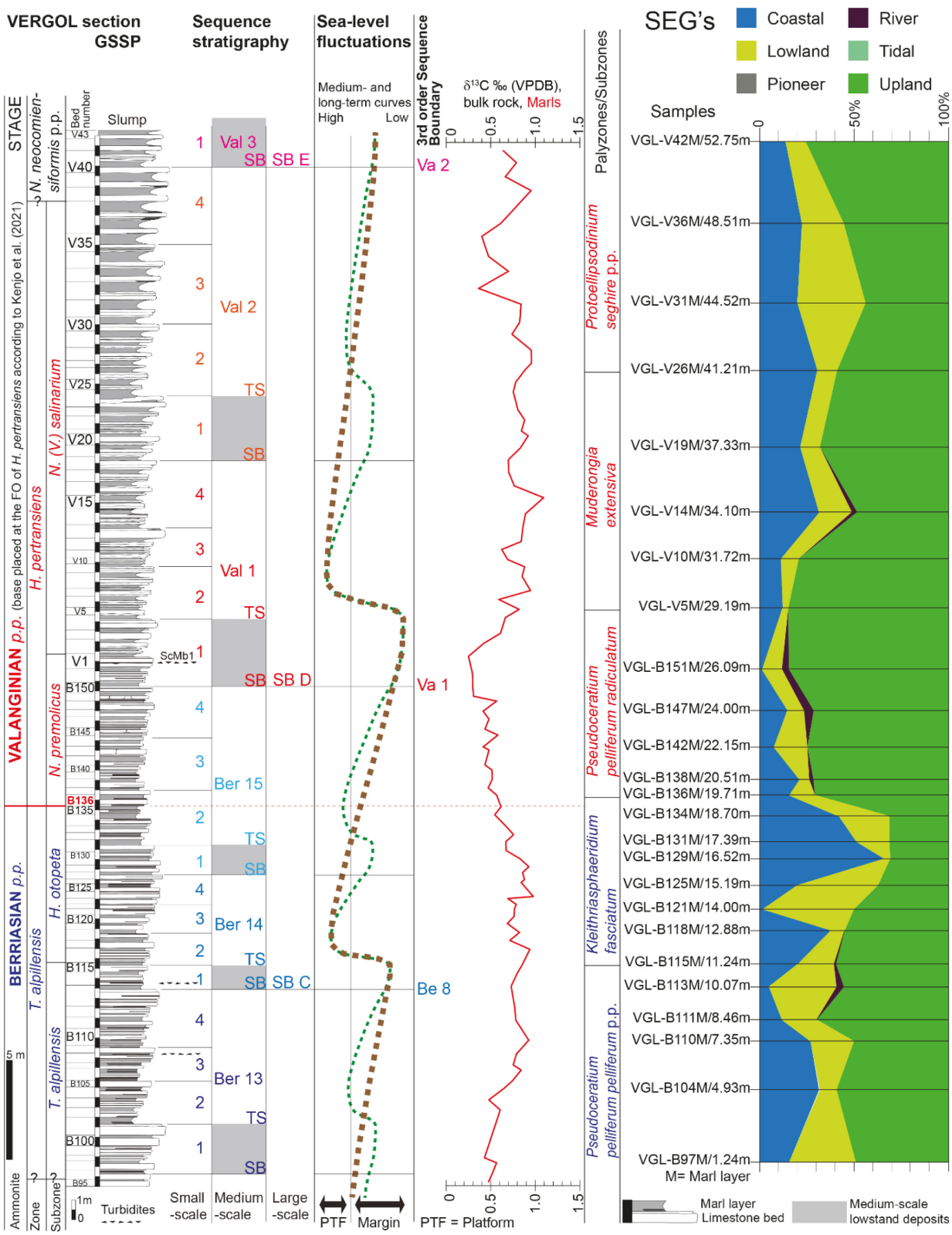

Figure 18. Sporomorph EcoGroups (SEG) plot (Abbink, 1998; Abbink et al., 2004) showing the relative percentages of miospore groupings, mainly represented by three communities: (1) Coastal, reflecting coastal communities: vegetation growing immediately along the coast, never submerged by the sea but under a constant influence of salt spray; (2) Lowland, reflecting lowland communities: vegetation on plains and/or in fresh water swamps; the plains may (periodically) be submerged by fresh water, resulting in the possible presence of "wetter" (marsh) and "drier" taxa in this group; there is no influence of (sea) salt, except, perhaps, under extreme circumstances; and (3) Upland, reflecting upland communities: vegetation on higher terrain well above groundwater level that is never submerged by water. For further discussion see Duxbury (2024). The carbon isotope curve is included to facilitate comparisons; comments are in the main text section "Carbon and oxygen isotope stratigraphy". For further explanations on the Vergol section, see Fig. 6 and its caption.

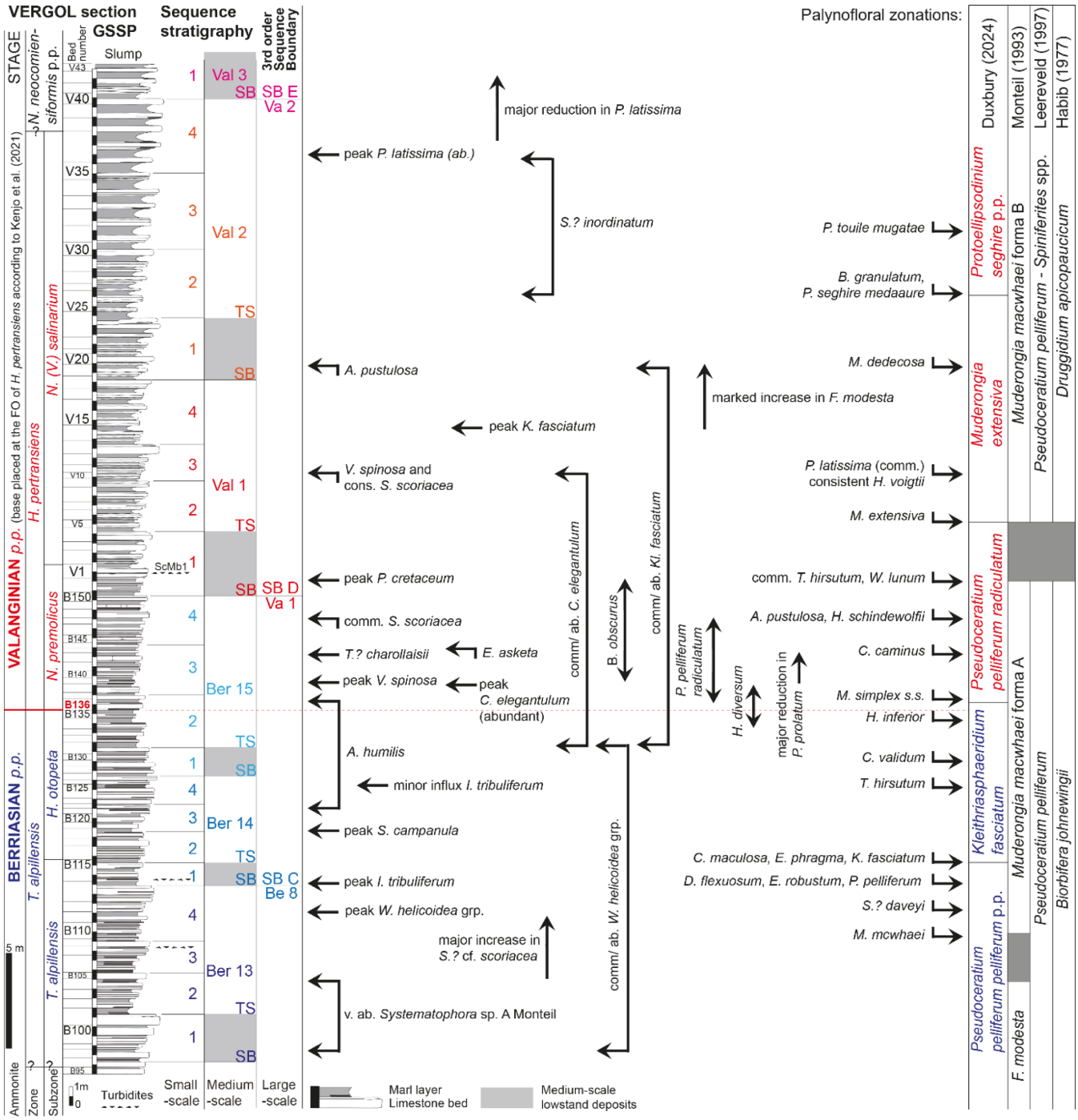

Figure 19. Palynological events of the Vergol section set against the palynofloral zonation schemes of Habib (1977), Monteil (1993), Leereveld (1997) and Duxbury (2024). For further explanations on the Vergol section, see Fig. 6 and its caption.

of the Duxbury (2024) scheme, compared to the schemes of Habib, Monteil and Leereveld, is presented in Fig. 19. A key marker in the Monteil's zonation, the FO of *Muderongia mcwhaei*, was noted in the Vergol section in marl layer VGL-B110 (base of layer at 7.28 m). The isolated occurrence of *Thalassiphora*? *charollaisii* in marl layer VGL-B142 (base of layer at 22.08 m) might be also of particular significance for regional value. Other palynofloral events may allow intra-regional correlation but this needs to be tested further.

Calcareous nannofossils

Ninety-two samples have been studied for calcareous nannofossils in the Vergol section. With respect to Kenjo et al. (2021), eleven additional layers have been studied in the current work. Samples were systematically taken from adjacent limestone–marl couplets with a closer spacing across the B/V boundary. Samples and calcareous nannofossil slides are labelled with a FSL number and curated at the "Collections de géologie" of the "Université Claude Bernard" (Lyon, France;

collection of Kenjo, Mattioli and Reboulet). In this work, taxonomy is based on Bralower et al. (1989), Aguado (1994), Bown et al. (1998), and Aguado et al. (2000). The zonation of calcareous nannofossils is established using interval zones, which are defined by the FO and LO of marker species. Although preservation is commonly poor to moderate with specimens severely overgrown, several bioevents are recorded across the stage boundary of the Vergol section. These events allow a precise boundary characterization at Vergol, as shown by Kenjo et al. (2021), although some of them might have a local extent. Only events useful in calcareous nannofossil zonations are discussed here (Fig. 13). The distribution chart of nannofossil taxa is given in Figure S1. Assemblages are illustrated in Fig. 20.

The presence of *Cretarhabdus angustiforatus* is observed from the basal interval of the section (marl layer VGL-B108). This event allows

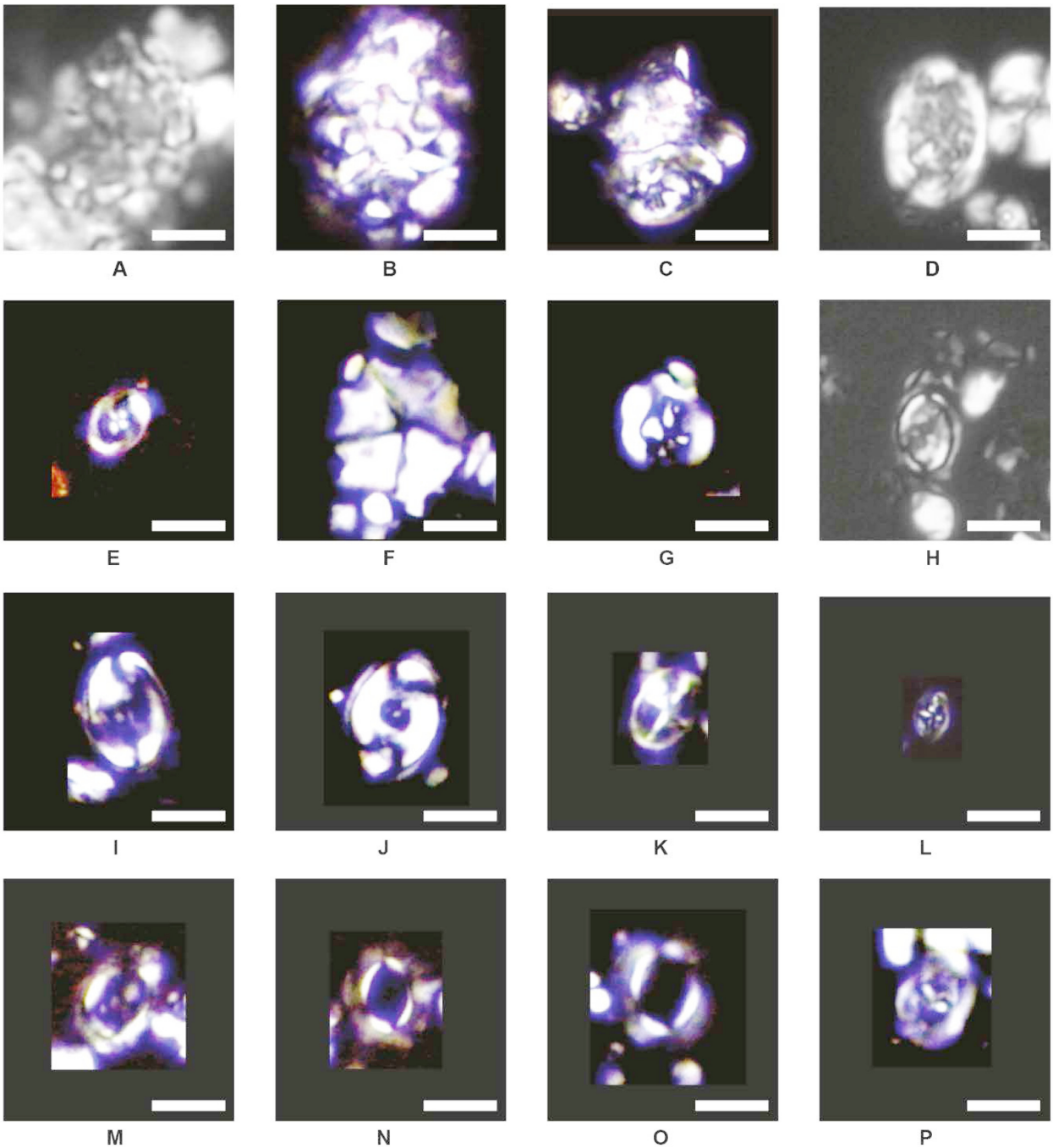

Figure 20. Micrographs of selected, stratigraphically relevant calcareous nannofossil species recorded at Vergol section (collection of Kenjo, Mattioli and Reboulet, UCBL-FSL, University of Lyon, France): A, Calcicalathina oblongata VGL-146M (M=marl layer), the earliest recorded specimen at Vergol; B, C. oblongata VGL-V3M. C, C. oblongata VGL-V3M; D, Large and overgrown Rhagodiscus asper VGL-V1b (closely resembling to Calcicalathina erbae Bergen, 1998 and Calcicalathina praeoblongata Aguado et al., 2000); E, Eiffellithus windii VGL-B151; F, Micrantholithus speetonensis VGL-V38M; G, Helenea quadrata VGL-V2cM; H, Percivalia fenestrata VGL-B112M; I, P. fenestrata VGL-B151M; J, Rhagodiscus nebulosus VGL-V2cM; K, Staurolithites crux VGL-V2c; L, Staurolithites mutterlosei VGL-V31M; M, Tubodiscus frankiae VGL-V2cM; N, T. frankiae VGL-V2cM; O, Tubodiscus jurapelagicus VGL-V3M; P, Zeugrhabdotus trivectis VGL-V3M. Scale bar = 5 µm.

the recognition of the *C. angustiforatus* Nannofossil Zone (NZ) (NK-2) that is subdivided into two nannofossil subzones (NSZ), namely *Assipetra infracretacea* (NK-2A) and *Percivalia fenestrata* (NK-2B). The top of *A. infracretacea* NSZ is placed at the base of the marl layer VGL-B112 because of the FO of *P. fenestrata*. Our record is consistent with that of Aguado et al. (2000) in SE Spain.

The FO of *Calcicalathina oblongata* (base of the NK-3 NZ) is recorded in the marl layer VGL-B146 (base of layer at 23.57 m) that corresponds to the lowermost part of *H. pertransiens* Zone. The FO of *C. oblongata* is also used to designate the base of CC3 NZ of Sissingh (1977). The CC3 NZ is subdivided into a and b, based on the FO of *Eiffellithus windii* that in the Vergol section occurs in the limestone bed VGB-150 (Fig. 13).

The recovery of the FO of *C. oblongata* in the lowermost part of *H. pertransiens* Zone is consistent with previous biostratigraphic data. In fact, Bown et al. (1998) in their synthesis of Tethyan nannofossil biostratigraphy also reported this event at the base of the *H. pertransiens* Zone. Duchamp-Alphonse et al. (2007) recorded consistently the FO of *C. oblongata* in the lowermost part of *H. pertransiens* Zone of the Angles section. Conversely, *C. oblongata* is recorded higher in the upper part of the *H. pertransiens* Zone in SE Spain (Aguado et al., 2000).

This discrepancy is probably related to the introduction of a new species (*C. praeoblongata*, Aguado et al., 2000), morphologically similar to *C. oblongata* but with primitive characters. These latter authors found *C. praeoblongata* in the lower part of the *T. alpillensis* Subzone in SE Spain (Cañada Luenga and Miravetes sections). The pictures of *C. praeoblongata* shown by Aguado et al. (2000, fig. 8, images 28–33), however, look like overgrown specimens of *Rhagodiscus asper*, and do not possess a central area structure rising from the wall (as is in the diagnosis of the genus *Calcicalathina*), but the insertions of the central area grid on the inner part of the wall are visible. Thus, the discrepant range of *C. oblongata* in SE France and SE Spain might be related to different taxonomic concepts.

Another relevant event is the FO of *Micrantholithus speetonensis* in the limestone bed VGL-V4 (Fig. 13). This species is considered as endemic of the Boreal Realm, where *C. oblongata* has not been recovered, and was used by Crux (1989) and Mutterlose (1991) to define a NZ typical of the lower Valanginian at high latitudes. In a single sample (marl layer VGB-B133), the occurrence of *Speetonia colligata* has been recorded. According to Perch-Nielsen (1985), in the North Sea the FO of *C. oblongata* can be substituted by the FO of *S. colligata*. The recovery of these two species in Vergol attests the relevance of the section for correlations between the Tethyan and Boreal realms.

Ichnofossils

Almost all the beds are characterized by very good exposures of both the sections and the upper surfaces. As a consequence, the easy and large observations allow an optimal analysis of the ichnoassemblages in every stratum. The density of the trace fossils has been evaluated following an abundance scale (see Olivero, 1996, p. 281). New data are presented here.

The trace-fossil association observed through the section covering the B/V boundary interval is characterized by a low diversity. Two kinds of ichnofossils are recognized: a mottled undefined bioturbation and *Zoophycos* (Fig. 13).

The mottled bioturbation is produced by abundant and undefined burrows, which lack of well-marked organization and are visible as complex spots of light and dark grey colour. These trace fossils are responsible for an early homogenization of the substrate and suggest well oxygenated conditions, slow, regular and constant sedimentation, and soup to soft-ground consistency (Olivero 1996). This dense bioturbation is observed throughout the section, but its intensity decreases in some beds, where *Zoophycos* is recorded.

Zoophycos is a deep complex burrow system, with one opening at the seafloor and produced by a deposit feeder (Olivero, 2003; Olivero and Gaillard, 2007). *Zoophycos* are only observed in limestone beds of the upper Berriasian. They are extremely abundant and dense in beds VGL-B109, B115 and especially B117. In this last case, the *Zoophycos* are the largest of the section, reaching 90 cm of width, with 3 to 5 superimposed whorls. The presence of *Zoophycos* suggests: (a) soft- to firm substrates, (b) low sedimentation rate, necessary to form the best sediment for the burrow development, (c) accumulation of huge quantities of organic matter promoted by the low sedimentation rates (Nasiri et al., 2020). The "ideal conditions" should correspond to irregular and fast supplies of carbonate-rich material alternating with periods of low or non-deposition (see Olivero, 1996). Concerning the sequence stratigraphy of the Vergol section, *Zoophycos* abundance increases in the calcareous bundles at the end of the small-scale sequences, and, for the medium-scale sequences, in or close to the maximum flooding intervals (Fig. 13). According to the previous remarks made on the "ideal conditions" for the installation and development of *Zoophycos* producers, these intervals could be characterized by a lower sedimentation rate. The greatest abundance of the ichnotaxa recorded in limestone bed VGL-B109 matches with a turbidite layer occurring just below. The turbidite may have supplied a high organic content inside the substrate, preserved owing to dysaerobic conditions, and trapped in the sediment because of high deposition rates. This organic matter was subsequently exploited by the *Zoophycos* organisms. Above the bed VGL-B123, *Zoophycos* completely disappear and are no longer observed.

Microfacies

Material and methods are indicated above in part "*Calpionellids*". New data are presented here.

Wackestone texture dominates in the biomicrite limestones of the Vergol section over the less-represented mudstone texture which locally occurs at the base of the upper Berriasian sequence (Ber 13, *T. alpillensis* (Sub-)Zone). All limestone beds have pyrite scattered in the matrix, in most of them patchy and nest-like accumulations of framboidal pyrite are documented (Figs. 16 G–M and Figure S2). In the basal part of the section, the presence of scattered organic matter in the limestone matrix varies, while towards to the top its presentation is rather continuous. Dissolved phosphate may have been fixed due to microbial activity which led to phosphatization of bioclasts. Bioclasts are represented by rather frequent radiolarians and sponge spicules, common fragments of thin-shelled ostracods and crinoids, rare fragments of aptychi, calcite-walled foraminifera, ophiurids, echinoids, globochaetes, bivalves, gastropods, ammonites, belemnites and scarse miliolid foraminifera, together with common to rare calpionellids and calcareous dinoflagellate cysts. It can be noted that the

presence and abundances of radiolarians regularly accompanied by sponge spicules coincided with sea-level maxima flooding phases (Figure S2). Laminae of redeposited older sediments (VGL-B132) are recorded close to a transgressive surface. Enhanced siliciclastics admixture (VGL-B136-140-141) are observed in the interval of the ongoing regression. Pseudomorphs after some of the sulfate minerals (VGL-V2) are documented in the maximum lowering of sea-level curve. The standard microfacies (SMF) 3 (sensu Flügel, 2004) prevailed in the Vergol section. This microfacies corresponds to the facies zone (FZ) 1 sensu Wilson (1975) and indicates a lower slope to basinal environment.

Chemical and Physical Stratigraphy

Carbon and oxygen isotope stratigraphy

Early Cretaceous trends of $\delta^{13}C$, $\delta^{18}O$, Mg/Ca in calcite were discussed using data obtained from belemnites from SE France (and Spain), including the Vergol section, by McArthur et al. (2007). Recently, limestones (103 beds) and marls (95 layers) were sampled for bulk-rock analysis. These new data are presented here.

The base of the Valanginian (bed VGL-B136) is not marked in either limestones or marls by any anomaly in the $CaCO_3$ percentage, nor in Mg/Ca, $\delta^{18}O$, or $\delta^{13}C$ values (Fig. 21).

At the base of the section, at bed VGL-B95, the percentage of $CaCO_3$ in limestones is around 98 ± 2% and in marls is around 80 ± 5%. The proportion of $CaCO_3$ in limestones declines uniformly up section to be 87 ± 4% in the upper part of the section above bed VGL-V35. In marls, the proportion of $CaCO_3$ is more variable than in limestones, fluctuating by around ± 15%. Berriasian marls contain around 80% $CaCO_3$ whilst Valanginian marls contain around 60%, with the transition occurring over the 8 metres of section upwards from VGL-B127.

Values of Mg/Ca in limestones are uniformly between 8 and 10 mmol/mol apart from minor excursions to values of about 14 in the vicinity of bed VGL-B120 (around 12.5 m) and bed VGL-V25 (around 40.5 m and 41.5 m). In contrast, values of Mg/Ca in marls locally jump to between 15 and 25 in the vicinity of layer VGL-B115 (between 10.5 m and 14 m) and are high (between 15 and 25) above layer VGL-V7 (i.e. above 30 m). A single marl sample, VGL-25 (arrowed on Fig. 21), has a value of 75 mmol/mol coincident with a minimum in the percentage of $CaCO_3$.

The stable isotope composition of oxygen shows a variability of around ± 0.15‰ in $\delta^{18}O$ in limestones and an overall apparent cyclicity with three minima and two maxima (Fig. 21). There is a broad match of maxima and minima to the position of sequence boundaries, with minima occurring around the "lowest" SB, SB D (Va1), and SB E (Va2) and with maxima broadly coinciding with SB C (Be8) and the SB above VGL-V18. The trend in $\delta^{18}O$ in the marls is more spikey but overall it parallels the trend in the limestones, but with a variable offset to more negative values; in layer VGL-B148 and below, the values in marls are about 0.3‰ lower than those in limestones and in layer VGL-B149 and above, the values in marls are about 0.8‰ lower than those in limestones. The change in the offset of $\delta^{18}O$ between marls and limestones is abrupt and occurs about 5.5 m above the B/V boundary.

In the lower part of the section, below VGL-V1, $\delta^{13}C$ in both marls and limestones shows a broad positive peak, with values for limestones being about 0.5‰ more positive than values in marls (Fig. 21). Above VGL-V5, the difference in $\delta^{13}C$ between marls and limestones essentially vanishes and both have values around 0.8‰ to the top of the section, albeit with some scatter and an interval of 0.6‰ between VGL-V31 and VGL-V37, where $\delta^{13}C$ in marls briefly dips to values less positive than in the limestones. The trend for limestones is confused by three values close to V10 that have ^{13}C values around 0.8‰ lower than values of other limestones, possibly owing to sampling an unusually high proportion of diagenetic cement.

As carbon stratigraphy is used here for global correlation (see below), further explanations are given on the choice of data presentation. The $\delta^{13}C$ curves are here presented separately for limestone and marl lithologies (Fig. 21). In sections elsewhere, a different isotopic composition for limestone and marl is documented for different time intervals and sedimentary basins (e.g., Beltran et al., 2007; Mercuzot et al., 2020). Such differences may be explained by a primary different composition of bulk carbonate analysed for $\delta^{13}C$, i.e. the microfossils versus allochthonous platform-derived carbonates (Beltran et al., 2007). Alternatively, a different diagenetic overprint may affect the $\delta^{13}C$ signal of the two lithologies. In fact, organic matter remineralisation may produce lower $\delta^{13}C$ values in early cements in marls compared to carbonate-rich facies (Irwin et al., 1977). This second hypothesis may apply to the Vergol section as marls are enriched in organic matter with respect to limestones (see below), and organic matter will have undergone early diagenesis.

Whatever the cause of any marl–limestone differences in isotopic composition, the $\delta^{13}C$ of both limestones and marls displays the same long-term trend at Vergol, such as (Fig. 21): an increase of values from low $\delta^{13}C$ (~0.9‰ in limestone; ~0.5‰ in marls) in the lower part of the *T. alpillensis* Zone; a short-lived plateau in values (~1.1‰ in limestone; ~0.8‰ in marls) in the upper part of *T. alpillensis* Zone; and then a general trend toward low $\delta^{13}C$ values occurring across the B/V boundary to reach a negative shift in the lower part of the *H. pertransiens* Zone (~0.5‰ in limestone; ~0.3‰ in marls).

Strontium isotope stratigraphy (SIS)

Sr-isotope stratigraphy (SIS) is a means of dating and correlating sediments using the $^{87}Sr/^{86}Sr$ of Sr in marine precipitates, such as biogenic apatite and carbonate: a synopsis of the method as applied to the Cretaceous is given in McArthur and Howarth (2025). When used to date sediment, the $^{87}Sr/^{86}Sr$ of a sample is matched to the same value on the reference curve for the Cretaceous (see fig. 1 in McArthur and Howarth, 2025). When used to correlate (see fig. 2 in McArthur and Howarth, 2025; see below), $^{87}Sr/^{86}Sr$ acts as a proxy fossil which has changed through time in a known way.

As the world's oceans today are homogenous in $^{87}Sr/^{86}Sr$ (for discussion, see McArthur et al., 2020), they are assumed to have always been homogenous, so SIS can be used worldwide for correlation and dating; that is, the method is synchronous worldwide and suffers no latitudinal or longitudinal restrictions on its application. It is also independent of taxa, being unaffected by "vital effects".

The rate at which $^{87}Sr/^{86}Sr$ was changing through the base of the Valanginian was 0.000036 per Myr. With the best modern instrumen-

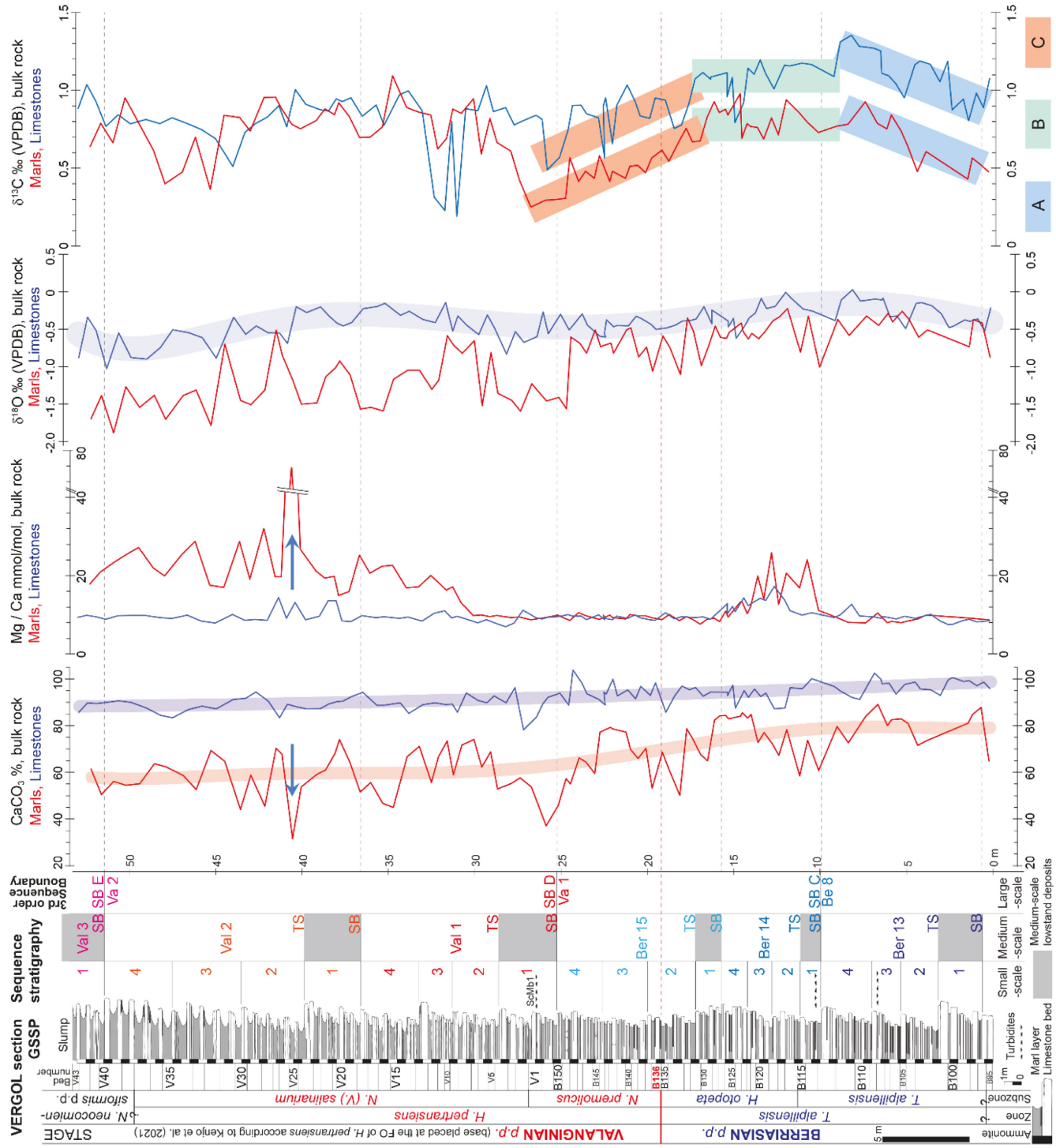

Figure 21. Chemical stratigraphy of the Vergol section: $CaCO_3$ percentage, Mg/Ca, oxygen ($\delta^{18}O$) and carbon ($\delta^{13}C$) isotopes; red and blue curves for samples coming from marls and limestones, respectively; rectangle A, general trend toward high $\delta^{13}C$ values; rectangle B, a short-lived plateau in $\delta^{13}C$ values; rectangle C, general trend toward low ^{13}C values. For further explanations on the Vergol section, see Fig. 6 and its caption.

tation, and replicate analysis to decrease the standard error of the mean, $^{87}Sr/^{86}Sr$ can be measured to ± 0.000004 between many laboratories, and ± 0.000001 in a few leading laboratories (McArthur et al., 2020, 2025; McArthur and Howarth, 2025), giving a potential age resolution around the B/V boundary of ≈ 0.12 to 0.03 Myrs.

The limitation on the method is that it requires well-preserved marine phases for analysis (francolite of fish teeth, calcitic fossils, early diagenetic calcite cements). Whilst such material is common across the GSSP, its presence is not guaranteed elsewhere – but then neither is the presence of fossils useful for correlation, nor a palaeomagnetic signal, guaranteed elsewhere. The method does allow for interpolation: should material for analysis not be available from a target hori-

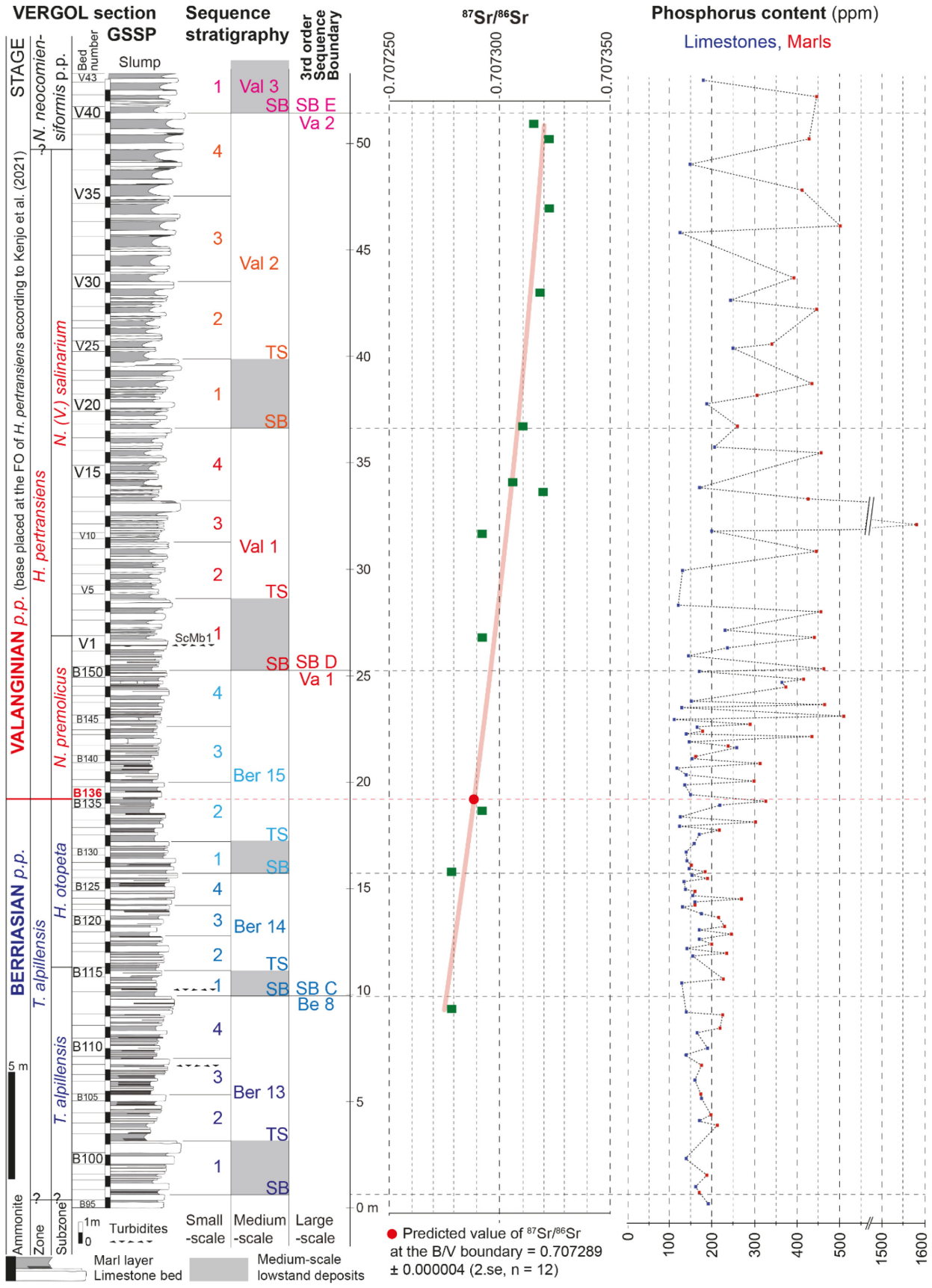

Figure 22. Chemical stratigraphy of the Vergol section: strontium isotopes ($^{87}Sr/^{86}Sr$) after McArthur et al. (2007), and McArthur and Howarth (2025); phosphorus content (red and blue dots for samples coming from marls and limestones, respectively). For further explanations on the Vergol section, see Fig. 6 and its caption.

zon one wishes to correlate to the GSSP, profiling $^{87}Sr/^{86}Sr$ either side of the target horizon will usually be possible, with interpolation to the target bed possible to determine its $^{87}Sr/^{86}Sr$.

Values of $^{87}Sr/^{86}Sr$ increase upsection and have been fitted in Fig. 22 with a second-order polynomial. The value of $^{87}Sr/^{86}Sr$ at the B/V boundary predicted by this polynomial is 0.707289 ± 0.000004 (2.se, $n = 12$). The boundary value given here (from McArthur and Howarth, 2025) is 0.000005 less than the value given for the B/V boundary ($^{87}Sr/^{86}Sr = 0.707294$) in McArthur et al. (2007, 2020) owing to new finds of ammonites in sections at Vergol (Kenjo et al., 2021) that lower the putative boundary position by 7 metres from that used by McArthur et al. (2007). For these latter authors, the base of Valanginian stage was placed at the base of their bed V14b (their fig. 3), that matches with the bed VGL-V1b herein. The current B/V boundary, defined at the base of bed VGL-B136 (at 19.23 m), corresponds to the layer W91 following the bed numbering used by McArthur et al. (2007, fig. 3).

Phosphorus contents

Total phosphorus content was measured on 110 whole-rock samples: 59 and 51 samples for limestone and marlstone, respectively. Phosphorus analyses were conducted at the Institute of Earth Sciences (University of Lausanne, Switzerland). Samples were analysed for total phosphorus analyses using the ascorbic acid method (Eaton et al., 1995), following the procedure outlined in Bodin et al. (2006). Phosphorus concentrations were measured in ppm using a UV/Vis photospectrometer (Perkin Elmer UV/Vis Photospectrometer Lambda 10, Perkin Elmer, Waltham, MA, USA; $\lambda = 865$ nm) with a mean precision of 5%. New data are presented here.

Total phosphorus contents range between 124 and 1581 ppm (Fig. 22). The marl layers are systematically more enriched compared to the limestone beds. Contents are low in the Berriasian and begin to increase approximately 2 m below the base of *H. pertransiens* Zone (B/V boundary) reaching maximum values in the Val 1 sequence (1581 ppm). Note that this general P increase is observed in both marl layers and limestone beds.

The increase in P contents characterizing the earliest Valanginian is widely observed in both platform and basinal environments (e.g., Montclus, Angles, La Chambotte, Morales et al., 2013; this work). These enhanced P fluxes coincide with higher detrital inputs, leading to a shift between photozoan and heterozoan carbonate production and ultimately to the demise of the carbonate platform during the Valanginian (Weissert event). In the western European domain (England, Germany, France and Switzerland), phosphorus is a good tracer of the phase of enhanced humidity leading strong weathering and subsequent increased fertilization, which reached a maximum in the earliest Valanginian.

Geochemically, the base of *H. pertransiens* Zone is consequently marked by important environmental, climatic and global changes, which are well expressed in the Vergol section.

Clay mineralogy

A total of 52 marl samples were analysed using X-Ray Diffraction (XRD). After moderate grinding in a mortar, powdered samples were decarbonated with a 0.2N HCl solution. The < 2 µm fraction (clay-sized particles) was extracted with a syringe after deflocculation and decantation of the suspension for 95 minutes following Stokes' law; this fraction was then centrifuged. Clay residue was then smeared on oriented glass slides and run in a Bruker D8 diffractometer with CuK_α radiations, a LynxEye detector and a Ni filter with a voltage of 40 kV and an intensity of 25 mA (Biogéosciences laboratory, Université Bourgogne Europe in Dijon, France). Goniometer scanning ranged from 2.5° to 28° for each analysis. Three runs were performed for each sample to discriminate the clay phases: (1) air-drying; (2) ethylene-glycol solvation at room temperature during 24 hours, and (3) heating at 490 °C during 2 hours, as recommended by Moore and Reynolds (1997). Clay minerals were identified using their main diffraction (d_{001}) peaks and by comparing the three diffractograms obtained. The relative proportions of the clay minerals are estimated using peak intensity ratios. The error margin of the method is approximately ± 5%. New data are presented here.

The clay mineral assemblages are dominantly composed of random illite-smectite mixed-layers (Interstratified Illite-Smectite Reichweite R0, I-S R0, 25 to 70%; it can be ascribed to smectite), illite (15 to 40%) and kaolinite (5 to 30%). Traces of chlorite never exceeding 10% also occur throughout the section. According to the clay mineralogy, it is possible to distinguish three stratigraphic intervals showing a characteristic mineralogical signature (Fig. 23).

The first interval corresponding to the lower part of the *H. otopeta* Subzone from 11.25 to 15.82 m, is mainly characterized by a high proportion of I-S R0 which gradually increases upwards from 40% to more than 70%. This increase in I-S occurs essentially at the expense of illite, while the low proportions of kaolinite (less than 12% in this interval) show minor variations.

By contrast, the second interval between 15.82 and 25.36 m, presents a marked decrease in the proportions of I-S R0 mainly balanced by an increase in the proportions of kaolinite and illite. The highest proportions of kaolinite (about 25%) occur just below the B/V boundary. Within this interval, the fluctuations of the relative proportions of clay minerals are important with, in particular, a new increase in the proportions of I-S R0 at the expense of illite and kaolinite within the *N. premolicus* Subzone.

The third interval from 25.36 m to 34,80 m, shows relatively weak fluctuations of clay assemblages, with relatively abundant illite (about 40%), average proportions of I-S R0 close to 35% and average proportions of kaolinite around 20%. This mineral is however relatively abundant at the base of this interval.

Numerous analyses of the clay fraction of Berriasian–Valanginian sediments deposited in the Vocontian basin have been carried out since the 1980s (Deconinck et al., 1985; Levert and Ferry, 1988; Morales et al., 2013; Charbonnier et al., 2020). All show that the assemblages consist of illite, I-S R0 sometimes called smectites, and kaolinite. The composition of clay assemblages of the Berriasian–Valanginian of Vergol is therefore consistent with previous analyses.

The influence of diagenesis on clay assemblages seems moderate. However, I-S are relatively rich in illite and do not expand up to 17 angstroms after glycol solvation, suggesting that an incipient illitisation of smectite occurred due to burial. However, the influence of diagenesis does not seem to have been sufficient to profoundly modify the initial detrital composition of the clay assemblages.

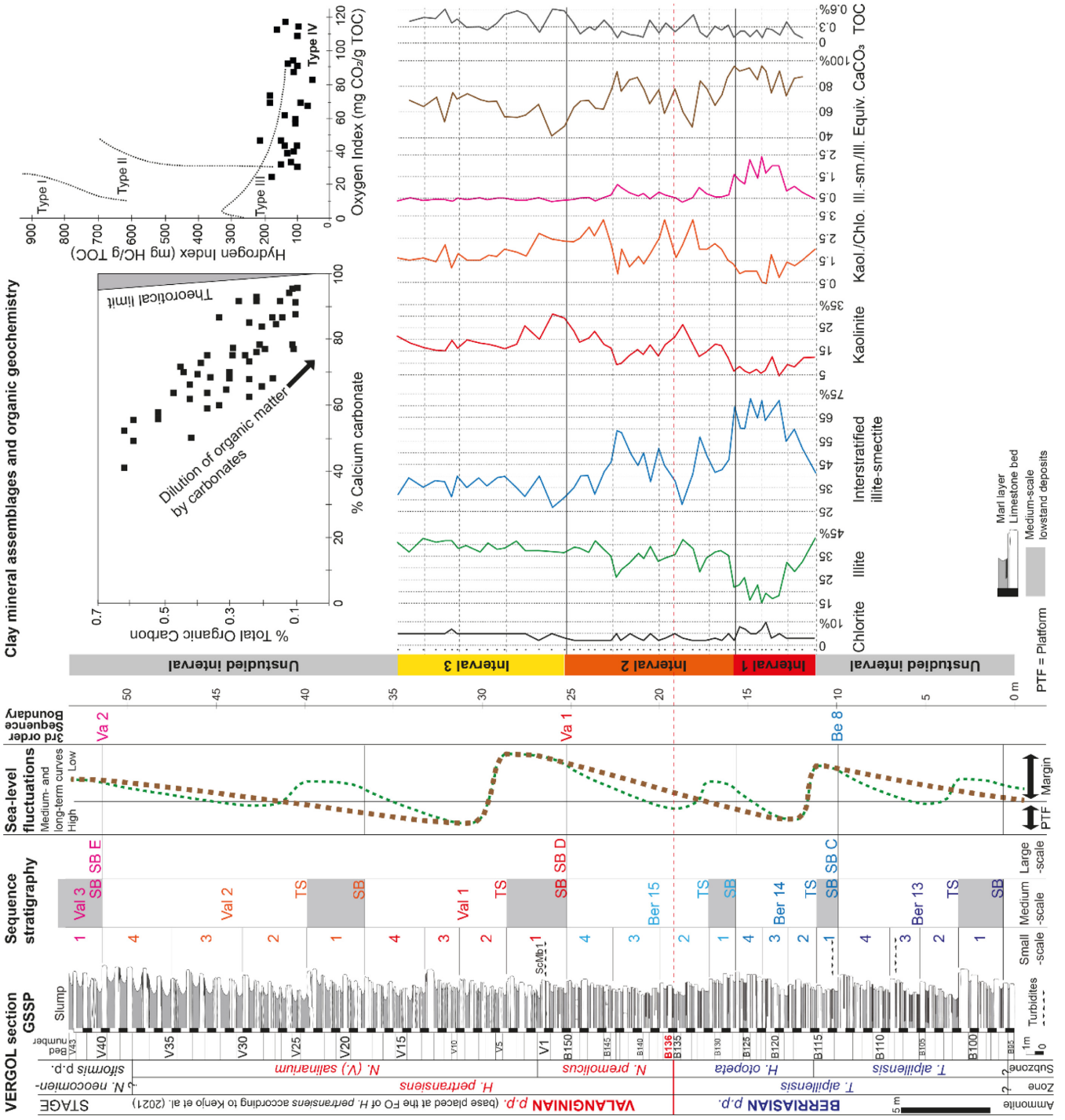

Figure 23. Clay mineral assemblages and organic geochemistry of the Vergol section. For further explanations on the Vergol section, see Fig. 6 and its caption.

The mineralogical change between the first and the second interval coincides with the Ber 15 sequence boundary (Fig. 23). The sea-level fall could be responsible for the significant increase in illite and kaolinite at the expense of smectites due to deeper erosion on continental areas. This change coincides with a decrease in $CaCO_3$ probably as a consequence of the dilution of the carbonate production by siliciclastic detrital particles. As stated above, on carbonate platforms, the end of the Berriasian is marked by the replacement of a photozoan carbonate production to an heterozoan one (Morales et al., 2013). This could be the consequence of a transition to a more regularly humid climate at the end of the Berriasian. This trend is also recorded in the Mid-Polish basin by the evolution of the relative proportions of palynomorphs (Kujau et al., 2013). It is also likely that the increase in kaolinite in the Vocontian basin results from a modification of the geometry of the carbonate platforms from a rimmed platform to a ramp. Indeed, a rimmed platform can play the role of a kaolinite trap while a ramp morphology facilitates the export of kaolinite into the basin (Godet et al., 2008).

The passage from the second to the third interval also coincides with

a sequence boundary (Va1). The mineralogical change is less marked, but the high proportions of kaolinite are consistent with an enhanced erosion and/or a more humid climate.

Organic geochemistry

A total of 50 marl samples were analyzed using a Rock-Eval©6 Turbo (Vinci Technologies) at ISTeP (Sorbonne University, Paris, France) for a quantitative and qualitative study of their organic matter and inorganic carbon content. The method, described in detail by Espitalié et al. (1985-86), Lafargue et al. (1998) and Behar et al. (2001), allows the determination of both total organic carbon (TOC) and total inorganic carbon (MinC) of the samples with an error of about ± 3%. A $CaCO_3$ equivalent can be calculated by assuming that all inorganic carbon is in the form of calcite (%$CaCO_3$ = %MinC × 8.33). The hydrogen index (HI) and oxygen index (OI) derived from the Rock-Eval method are correlated with the H/C and O/C atomic ratios, respectively, which allow the origin of the organic matter to be determined (Tissot and Welte, 1984). Tmax is defined as the pyrolysis temperature at which the maximum yield of hydrocarbons is produced by the kerogen (Espitalié et al., 1977), thus giving a quick estimate of the thermal maturity of the samples (Espitalié, 1986). New data are presented here.

The interpretable Tmax values range from 427 to 437°C with an average of 433°C. These values indicate that the organic matter did not experience high temperatures during burial. Such moderate thermal diagenesis allows the organic parameters (TOC, HI, OI) to be interpreted as a primary signal that may reflect environmental changes that occurred during deposition of the B/V boundary strata.

The carbonate content of the marl layers ranges from 41 to 96%, with an average value of about 73%, while the organic carbon content fluctuates between 0.1 and 0.63%, with an average of 0.3% TOC (Fig. 23). The negative relationship between $CaCO_3$ and TOC percentages most certainly reflects fluctuations in one of the three main sediment components, namely carbonate, organic matter and siliciclastic detrital input. According to Ricken (1993), an inverse relationship between $CaCO_3$ and TOC indicates that dilution by carbonate cycling input is the dominant controlling factor. The low organic matter content is here explained by a much higher carbonate flux than organic matter flux.

Based on HI and OI values, the organic matter preserved in these marl facies is related to Type IV, an oxidation-resistant organic fraction (Fig. 23). Geochemically, Type IV is a highly oxidized and altered organic residue whose origin is not easily determined by the thermal Rock-Eval method. However, it is highly probable that this organic residue consists of fragments of higher plants that are more resistant than planktonic organic matter. The low amount of organic matter, coupled with low HI values and high OI values, argues for deposition in fully oxic waters (Tyson, 1995). Berriasian–Valanginian strata certainly represent conditions of low organic productivity and poor preservation of organic matter.

Although organic carbon contents are very low, the highest contents seem to coincide with periods of low sea-level in the basal part of the Valanginian. This is consistent with an oxidation-resistant organic matter fraction, the origin of which is probably associated with continental inputs rather than indigenous marine production.

The evolution of the carbonate contents of the marl layers does not show a clear relationship with the interpretation of sea-level variations.

Cyclostratigraphy and astrochronology

Gamma-Ray Total Count (GRTC) was measured at Vergol every 20 cm from beds VGL-B127 to VGL-V42. This represents a total of 185 measurements. Each measurement was taken in the field using a SatisGeo GS-512, with an acquisition time of 60 seconds (see Martinez et al., 2013 for the detailed procedure). The total gamma-ray signal the device collected is expressed in energy equivalent to ppm of uranium (ppm eU; Martinez et al., 2013).

Mass Magnetic Susceptibility (MS) was acquired at Vergol every 5 cm from beds VGL-B95 to VGL-V24. This represents a total of 790 samples. The bulk volumetric MS of each of the samples was measured in a Kappabridge KLY-3. Blank volumetric MS was subtracted from the measurements and included the volumetric MS of the holder and the environment. The volumetric MS were then corrected from the sample mass and the volume measured, accounting a constant measurement volume of 10 cm^3 (1×10^{-5} m^3). The mass MS values are given in m^3kg^{-1}.

Astrochronology was obtained from the detection of the Milankovitch cycles from the GRTC and MS signals. Prior to spectral analysis, the drift in the average of both signals was removed using best-fit linear smoothing curves. The drift in amplitude was then removed to the residual signal by calculating the instantaneous amplitude of the residual signal, calculating the long-term trend of this instantaneous amplitude using a LOcally WEighted Scatterplot Smoothing (LOWESS; Cleveland, 1979) with a coefficient of 0.5, and dividing the residual signal by the long-term trend of the instantaneous amplitude. The detrended signal was then standardised (average = 0; standard deviation = 1), to compare variables of different units.

The spectral analyses were performed using a 2π-Multi-Taper Method (2π-MTM; Thomson, 1982). Confidence levels were calculated using a robust red noise procedure applied on a moving median calculated over 20 % of the spectrum (Mann and Lees, 1996). Filters were calculated using Taner lowpass or bandpass filter (Hinnov et al., 2002). This filter minimizes changes in amplitude and phase between the original and filtered series at the band of interest.

New data are presented here. The results on GRTC were published in Martinez et al. (2013); the levels at which each value has been acquired were updated to the log presented for this work.

The GRTC values range from 5.3 to 11.6 ppm eU (Fig. 24), with an average value of 7.6 ppm eU. The signal shows a long-term trend to increasing GRTC values until interval VGL-V24-V30. This trend reflects the progressive enrichment in clay content in the succession. At marl–limestone alternation scale, the GRTC values are higher in marl layers than in their surrounding limestone beds. This reflects higher content in K, U and Th in clay than in limestone. The amplitude of the elementary sequences (limestone–marl couplet) increases from base to top of the succession, which reflects (i) the progressive change from limestone-dominated alternations to more mixed content between clay and $CaCO_3$, and (ii) the progressive increase in thickness of the marl layers. The gamma-ray signal is acquired over a radius of ca. 20–25 cm. Thus, the GRTC values of the marl layers smaller than this radius are likely underestimated, which contribute to decreased amplitude of the fluctuations of the GRTC signal marl–limestone alternation scale below bed VGL-B143.

The MS values range from 2.5×10^{-9} m^3kg^{-1} to 41.6×10^{-9} m^3kg^{-1}

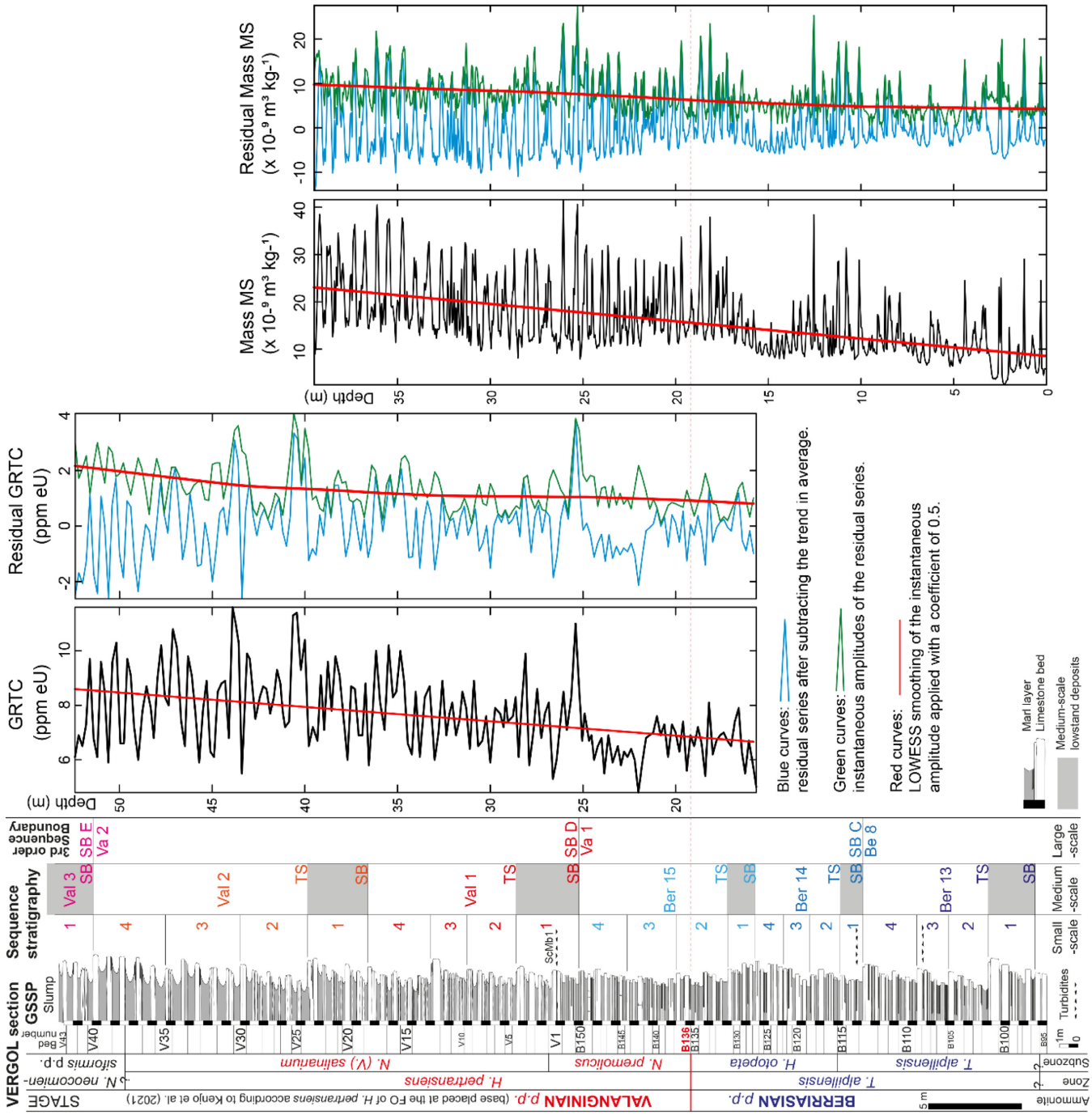

Figure 24. Gamma-Ray Total Count (GRTC, after Martinez et al., 2013) and Mass Magnetic Susceptibility (MS; new data from Martinez) curves of the Vergol section. For further explanations on the Vergol section, see Fig. 6 and its caption.

(Fig. 24), with an average value of 15.9×10^{-9} m^3kg^{-1}. The signal shows a long-term trend to increasing MS values, reflecting the progressive enrichment of clay in the succession. At marl–limestone alternation scale, the MS values in the marl layers are higher than in their surrounding limestone beds. This is a common feature in the marl–limestone alternations, as the content in paramagnetic clays is higher in marl layers than in limestone beds (e.g., Martinez et al., 2020). The amplitude of the elementary sequences increases from base to top of the succession, which reflects the progressive change from limestone-dominated marl–limestone alternations to mixed marl and limestone alternations.

The 2π-MTM spectrum of the GRTC signal shows spectral peaks above the 99% confidence level at 14 m, 3.3 m and from 0.80 to 0.67 m (Fig. 25A). Following Martinez et al. (2023), the peak at 3.3 m is attributed to the 100-kyr eccentricity cycle, while the band from 0.80 m to 0.67 m is attributed to the precession band. The precession band was filtered with a Taner bandpass filter, applying lower and higher frequency cuts of 1.1523 cycles.m^{-1} and 1.5912 cycles.m^{-1}, respectively. The spectrum of the instantaneous amplitude calculated from this filtered series shows a spectral peak at 8.6 m (Fig. 25B), attributed to the 405-kyr eccentricity cycle.

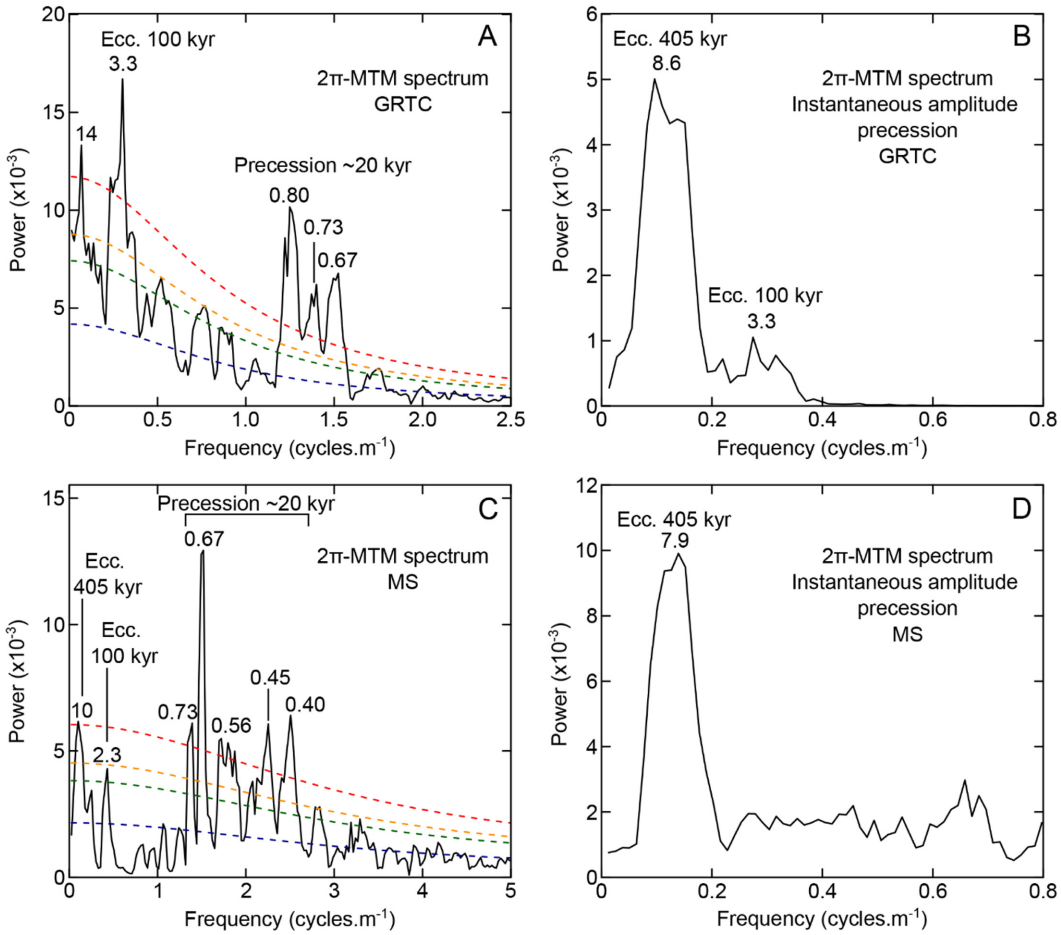

Figure 25. Spectral analysis of the Vergol section. A, the 2π-MTM spectrum of the Gamma-Ray Total Count (GRTC) signal. B, the 2π-MTM spectrum of the instantaneous amplitude filtered from the precession band of the GRTC signal. C, the 2π-MTM spectrum of the MS signal. D, the 2π-MTM spectrum of the instantaneous amplitude filtered from the precession band of the MS signal.

The 2π-MTM spectrum of the MS signal shows spectral peaks above the 99% confidence level at 10 m, and from 0.73 to 0.40 m (Fig. 25C). Another peak above the 95 % confidence level is observed at 2.3 m. The bands of 10 m, 2.3 m, and 0.73–0.40 m (average: 0.57 m), show a period ratio of 1:4.3:17.7, which is close to the ratio between 1:4.25:20 of the 405-kyr eccentricity, the 100-kyr eccentricity (mean period: 95.6 kyr), and the precession cycle. The precession band was filtered with a Taner bandpass filter, applying lower and higher frequency cuts of 1.3165 cycles.m^{-1} to 2.7089 cycles.m^{-1}, respectively. The spectrum of the instantaneous amplitude calculated from this filtered series shows a spectral peak at 7.9 m (Fig. 25D), attributed to the 405-kyr eccentricity cycle.

The filter of the 405-kyr eccentricity band from the MS signal and from the instantaneous amplitude of the precession band show consistent maxima above 35 m, 25 m, 18 m and 10 m, and used to bound the 405-kyr eccentricity cycles (Fig. 26). The maximum of the instantaneous amplitude of the precession band of the MS signal is preferred to bound the lower boundary of cycle T.A.-405-1 at 1.2 m, as this is consistent with the number of marl–limestone alternations. The filter of the 405-kyr band from the instantaneous amplitude of the precession band of the GRTC signal shows maxima at 18.20 m, 26.65 m, 34.75 m consistent with the maxima observed in the MS signal (Fig. 26). The upper boundary of cycle V2 is located consistently with Martinez et al. (2023) and with the number of marl–limestone alternations, in between the two last maxima of the filter.

A comparison with the sequential analysis sensu Gréselle and Pittet (2010) shows some discrepancies in the identification of the medium-scale sequences (400 kyr long-term eccentricity cycles). Their method is partly based on a visual identification and a counting of small-scale sequences (100 kyr short-term eccentricity cycles) that composed the medium-scale sequences; however, this approach partly depends on outcrop conditions and thus could be partly subjective. Nevertheless, a match can be made as follows: Ber 13 and TA-405-1; Ber 14 and TA-405-2; Ber 15 and B/V; Val 1 and V1; Val 2 and V2 (Fig. 26).

The sedimentation rate from the obtained age model (Table 1) ranges from a minimum of 17 m/Myr within cycle B/V to a maximum of 29 m/Myr within cycle V2. The average sedimentation rate of the whole studied succession is 23 m/Myr (Fig. 26).

The floating ages of the 405-kyr eccentricity cycles are anchored on a CA-ID-TIMS U-Pb age of 130.394 ± 0.16 Ma obtained from zircons coming from a tuff layer in the Neuquén basin (Argentina) near the base of the *Holcoptychites agrioensis* Andean ammonite Subzone (Aguirre-Urreta et al., 2017). The calendar age of the *Olcostephanus laticosta* Subzone was deduced with astrochronology anchored on this tuff layer (Aguirre-Urreta et al., 2019). The presence of the short-lived subgenus *Olcostephanus (Jeannoticeras)* within the *O. laticosta*

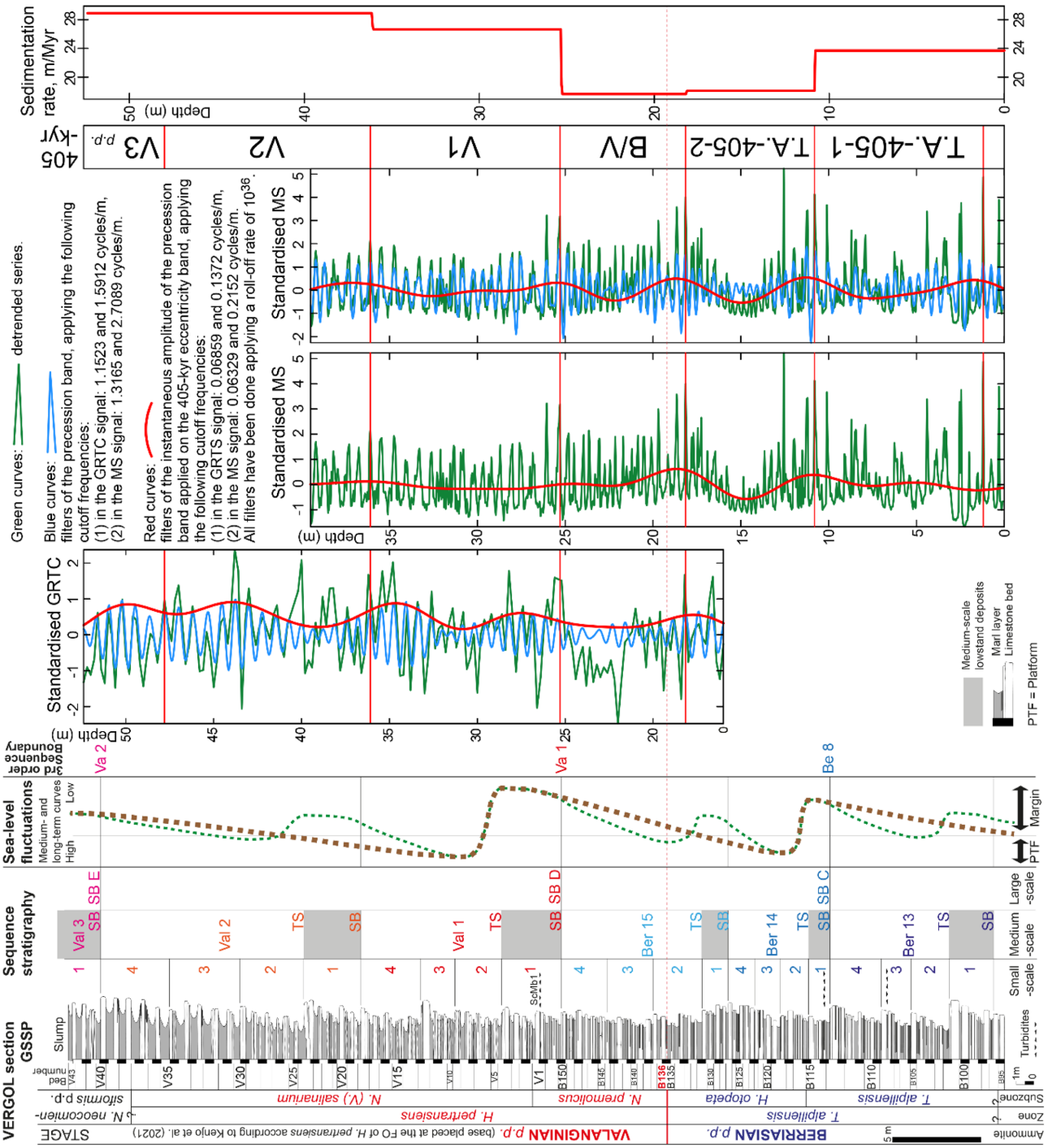

Figure 26. Astrochronology of the Vergol section from the standardised Gamma-Ray Total Count (GRTC) and Mass Magnetic Susceptibility (MS) signals, and the sedimentation rate curve. For further explanations on the Vergol section, see Fig. 6 and its caption.

Table 1. Age model of the Vergol section around the Berriasian/Valanginian boundary; the bases of the 405-kyr eccentricity cycles are measured from the base of the section (see Fig. 26)

Base cycle	Level (m)	Numerical age (Ma)
V3	47.80	135.89
V2	36.10	136.30
V1	25.30	136.70
B/V	18.15	137.11
T.A.-405-2	10.80	137.51
T.A.-405-1	1.20	137.92

Andean ammonite Subzone allows the correlation of this ammonite subzone to the *Olcostephanus (Jeannoticeras) jeannoti* Tethyan ammonite Subzone (Reboulet et al., 2014; Lehmann et al., 2015), then allowing the calendar ages of the 405-kyr eccentricity cycles of the Vocontian basin to be calculated (Martinez et al., 2023). The uncertainty of the correlation was assessed at one 100-kyr eccentricity cycle by comparison of the duration from the anchor point to the base of the Hauterivian Stage in the Neuquén and the Vocontian basins (page 12 *in* Martinez et al., 2023 and Fig. 27 here). The age model allows the base of the Valanginian Stage (= base of the *H. pertransiens* Zone) to be dated at

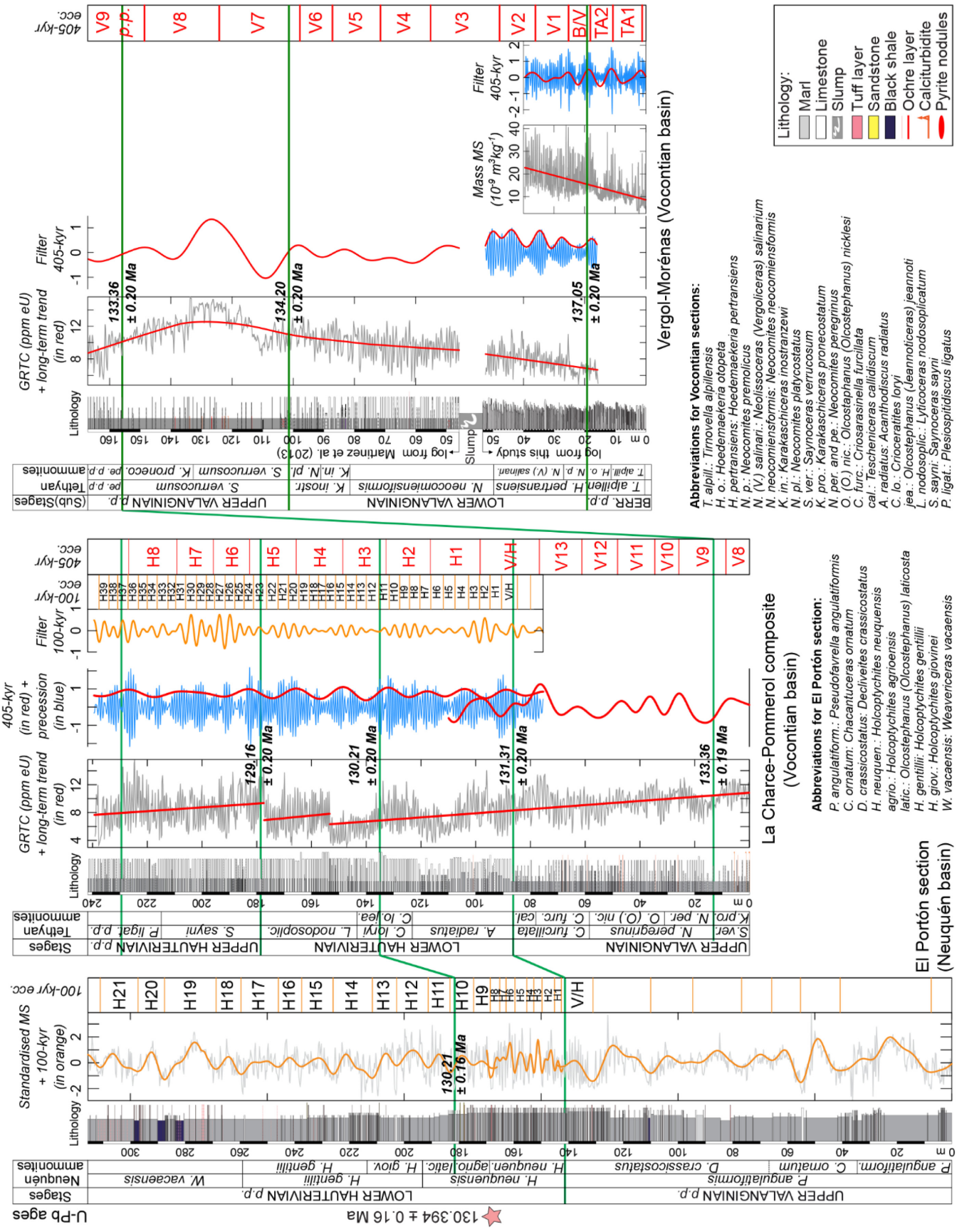

Figure 27. Correlation of astronomical age models of the El Portón (Neuquén basin), La Charce-Pommerol (Vocontian basin, Drôme Department) and Vergol-Morénas. Modified from Martinez et al. (2023). In the Vergol-Morénas section, the levels in metres above the slump are from Martinez et al. (2013), while below the slump, the levels are from this study.

Table 2. Ages of the base of the Valanginian Stage and ammonite (sub-)zones including their durations; the bases of the (sub-)zones are measured from the base of the section (see Fig. 8)

Base ammonite (sub-)zone	Base bed	Level (m)	Age (Ma)	Duration (kyr)
N. neocomiensiformis Zone	VGL-V38	49.76	135.82	-
N. (V.) salinarium Subzone	VGL-V2	26.91	136.64	820
H. pertransiens Zone *N. premolicus* Subzone	VGL-B136	19.23	137.05	410
H. otopeta Subzone	VGL-B116	11.33	137.48	430
T. alpillensis (Sub-)Zone	VGL-B96	0.38	137.96	480

137.05 Ma (± 0.2 Ma; Martinez et al., 2015, 2023; this work). The total uncertainty is the quadratic propagation of the uncertainties in the CA-ID-TIMS age in the Neuquén basin and the uncertainty in the correlation between the Neuquén and the Vocontian basins. The uncertainty in the age of a given level calibrated by astrochronology increases with the distance from the nearest anchor points (De Vleeschouwer and Parnell, 2014). It does, however, not propagate throughout the series unless there is miscounting of the number of repetitions of the 405-kyr eccentricity cycles within the studied series. This miscounting can happen if the record of the 405-kyr eccentricity cycle is unclear in the proxy studied and if entire 405-kyr eccentricity cycles are not preserved in the sedimentary record due to erosion or non-deposition. In these cases, those risks are limited as multiple sections for a given time intervals, well correlated by lithostratigraphy, chemostratigraphy and biostratigraphy were studied (Martinez et al., 2013, 2015, 2023). Recent LA-ICP-MS U-Pb ages were obtained on zircons from volcanic tuff layers in Japan (Tomaru et al., 2025). These ages were anchored with carbon isotope ratios to the Vocontian basin and currently give undistinguishable ages compared to the ages proposed in the astrochronology here regarding the uncertainty of the ages published in Tomaru et al. (2025). The ages of the base of (sub-)zones (and therefore their numerical durations) are proposed here (Table 2).

Magnetic stratigraphy and elemental geochemistry

This palaeomagnetic and rock magnetic study utilizes a total number of 114 samples collected from a 53.12 m thick interval of the upper Berriasian–lower Valanginian of the Vergol section. All the palaeomagnetic samples come from limestone beds from which they were collected using a drilling machine. Additionally, field measurements were made of 181 magnetic susceptibility (MS) and 165 gamma-ray spectrometry horizons; these were performed both in limestone beds and marl layers using ZH Instruments SM-30 magnetic susceptibility meter and Georadis GT-32 portable radioisotope assay analyzer, respectively. Geochemical composition of 114 limestone horizons was additionally evaluated using an Olympus DP-6000 portable x-ray fluorescence spectrometer. All palaeomagnetic experiments were carried in the Polish Geological Institute–NRI in Warsaw, according to the standard procedure described by Lodowski et al. (2022). New data are presented here.

Natural Remanent Magnetizations are in general low and very low (typically 0.5–1.5 × 10^{-4} A/m; 2–4 × 10^{-8} Am2/kg), as is the Magnetic Susceptibility signal (typically 0–4 × 10^{-5} SI; 0.5–2 × 10-8 m^3/kg), which point to the low contribution of a magnetic fraction. Palaeomagnetic investigations (both thermal demagnetization (TD) and alternating field demagnetization (AF) treatment) revealed the presence of the characteristic component of an exclusively normal polarity (Figure S3), which indicates that the upper Berriasian–lower Valanginian of the Vergol section has been remagnetized (see also Katz et al., 2000, Kechra et al., 2003). MS generally rises through the section; this applies also to Th and Ti contents, however correlation between MS and clastic proxies is only moderate, which implies a possible contribution from authigenic magnetic minerals (Fig. 28 and Figure S4). The dominant magnetic phase is magnetite (S ratio is usually near or above 0.75), however diagenetic (?) hematite also occurs, especially in samples coming from near the rock surface (Figure S4).

Geochemical investigations (field GRS and XRF measurements) performed in the Vergol section point to increasing contribution of clastic fraction in its lower part (upper Berriasian–lowermost Valanginian) and relatively stable values above (Fig. 28). The seafloor was well oxygenated (U/Th usually near 0.5); however the lowermost part of the section (*T. alpillensis* Subzone) might have been deposited under more hypoxic conditions (U/Th usually at 0.75–1; Fig. 29; see also Jones and Manning, 1994; Algeo and Liu, 2020). Importantly, this phenomenon correlates with enrichment of Zn at the base of the section (Fig. 29), which can evidence perturbations in the water column mixing (= relative stratification) during this time. Finally, palaeohumidity proxies (Th/K, Ti/K on Fig. 29; e.g., Schnyder et al., 2006; Grabowski et al., 2021a) point to less humid late Berriasian (especially during the *T. alpillensis* Subzone) in relation to the subsequent early Valanginian.

The Cañada Luenga Section (Cehegín, SE Spain): the Valanginian SABS

The Spanish section is included as a Standard Auxiliary Boundary Stratotype (SABS, see Head et al., 2023) to support the GSSP and extend its correlation potential. This proposal is justified by the fact that the Cañada Luenga section provides a robust magnetostratigraphic record of the Berriasian/Valanginian (B/V) boundary interval, together with a rich, diverse and well-preserved fossil content that ensures precise correlation with the Vergol section (see below). Previous works on the bio- and magnetostratigraphy of this section were published by Allemann et al. (1975), Company (1987), Ogg et al. (1988), Aguado (1994), Aguado et al. (2000), and Janssen (2003). On the basis of these works, an informal proposal to establish the Cañada Luenga section as the Valanginian GSSP was made (Company et al., 2023).

Geological and Geographical Location

Geologically, the Cañada Luenga section belongs to the Subbetic zone, a complex tectonostratigraphic domain characterized by the prevalence of pelagic and hemipelagic sediments deposited from the

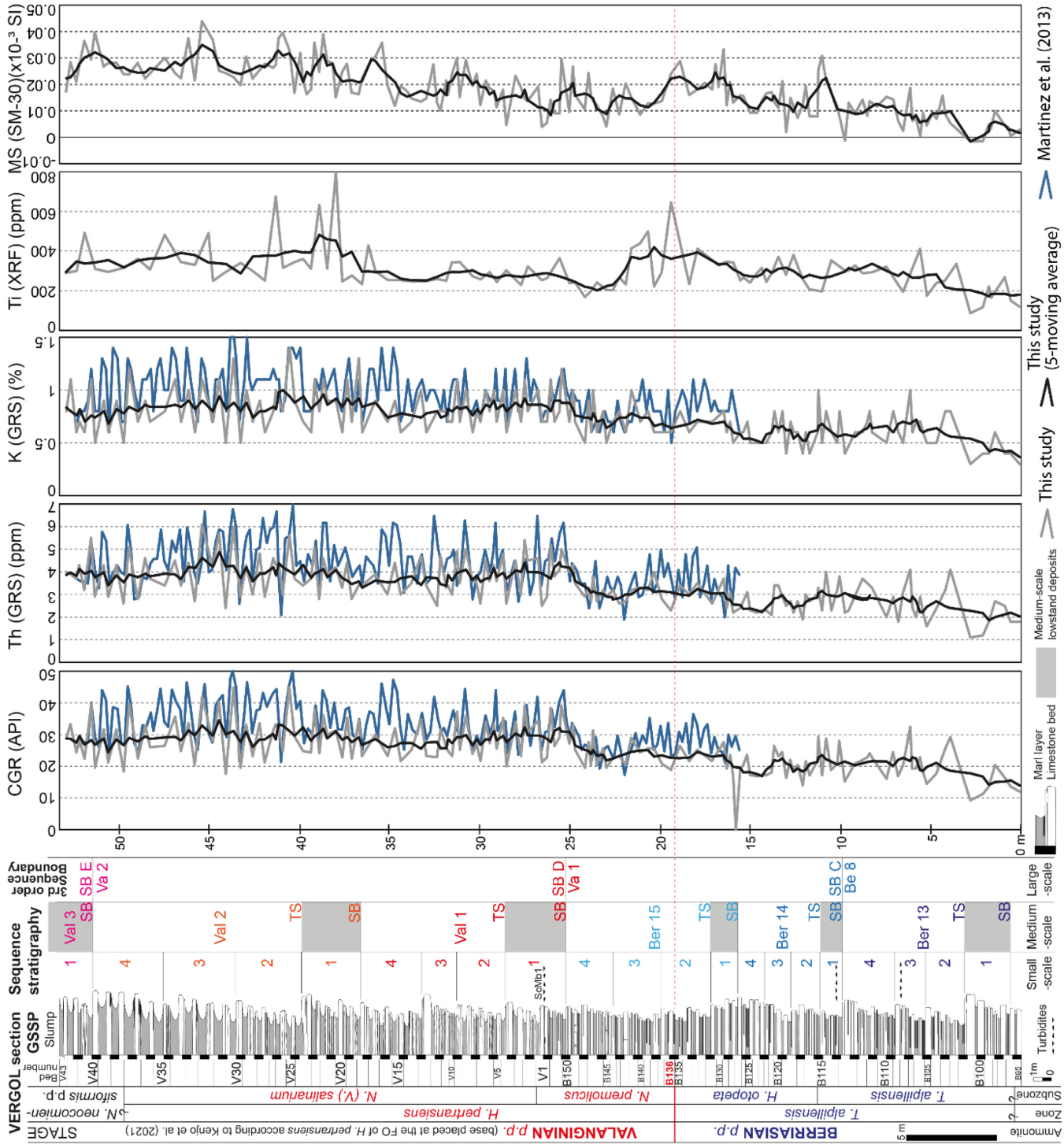

Figure 28. Clastic proxies in the Vergol section. Magnetic Susceptibility (MS) shown for comparison. CGR: Computer Gamma Ray. For further explanations on the Vergol section, see Fig. 6 and its caption.

Early Jurassic to the Early Miocene in the south Iberian palaeomargin. Extensional tectonics linked to the Atlantic seafloor spreading affected the Subbetic basin during the Jurassic and Early Cretaceous, resulting in active listric faults that led to block tilting and lateral changes in depth and subsidence rates (Vera et al., 2004). The Cañada Luenga succession was deposited on a pelagic swell bordered by troughs to the north and south (Rey, 1993; Gea, 2004). A palaeolatitude of 29°N (± 3.5°) was determined by Ogg et al. (1988) (Fig. 30).

The section is located in the Cañada Luenga ravine, 3.1 km SSW of Cehegín and some 750 m upstream from the confluence of the ravine with the River Quípar. The geographic coordinates of the middle part of the section are 38°03'55"N, 1°48'43"W (WGS84 reference frame; https://www.google.com/maps; Fig. 30). The Lower Cretaceous exposures along the Cañada Luenga ravine are listed in the geosite inventory (Arana et al., 2009) and in the Archaeological and Palaeontological Chart of the Region of Murcia. In addition, the Cehegín Town Council, in

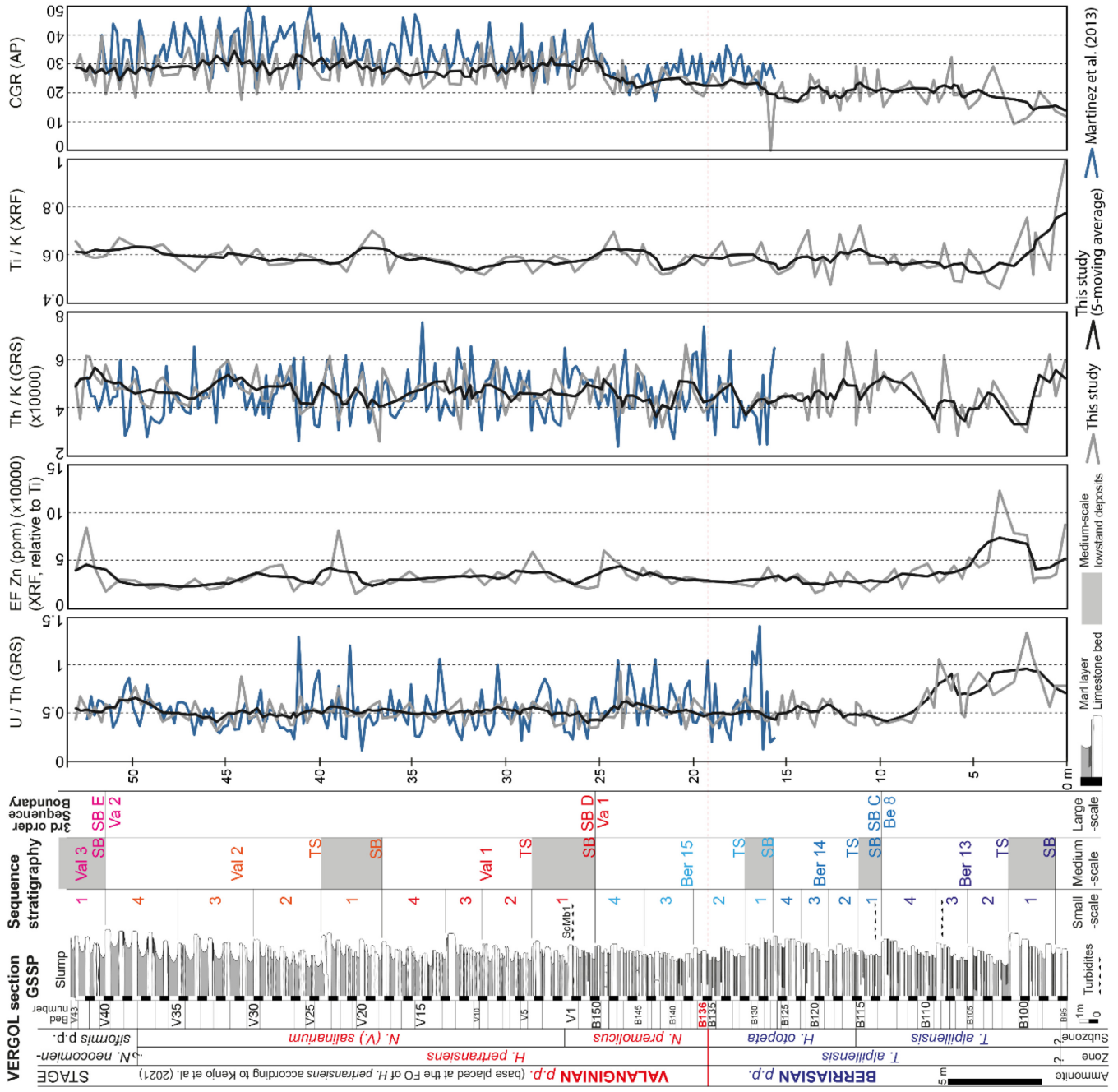

Figure 29. Selected palaeoenvironmental proxies in the Vergol section. Computer Gamma Ray (CGR) shown for comparison. For further explanations on the Vergol section, see Fig. 6 and its caption.

a plenary session held on January 28, 2022, unanimously approved to carry out the pertinent actions for the permanent protection of the Cañada Luenga section. In any case, the section lies along the bed of the ravine and is therefore located in the public domain managed by the Segura River Hydrographic Confederation.

Description of the Section

The entire Cañada Luenga section extends from the middle Berriasian to the lower Valanginian. For the present work we have analysed only the upper part of the section, an interval about 13 m thick embracing the levels around the B/V boundary (beds 0 to 20; Fig. 30).

The base of the section (beds 0 to 3, approximately 1.25 m thick), belonging to the lower part of the *Tirnovella alpillensis* Subzone, is made up of reddish to gray nodular calcilutites to calcirudites that correspond to the top of the Upper Ammonitico Rosso Formation (Rey, 1993; Gea, 2004). The microfacies are wackestones to crinoidal packstones, with calpionellids, calcareous dinoflagellates, benthic foraminifera, calcified radiolaria, and ostracods. The macrofossils are abundant, mostly ammonites, accompanied by belemnites, bivalves, pygopid brachiopods and irregular echinoids. The intense bioturbation, the presence of omission surfaces (marked by thin limonitic crusts), and the corrosion of the upper side of the fossils indicate small interruptions in the sedimentation of these materials, which have been usually interpreted

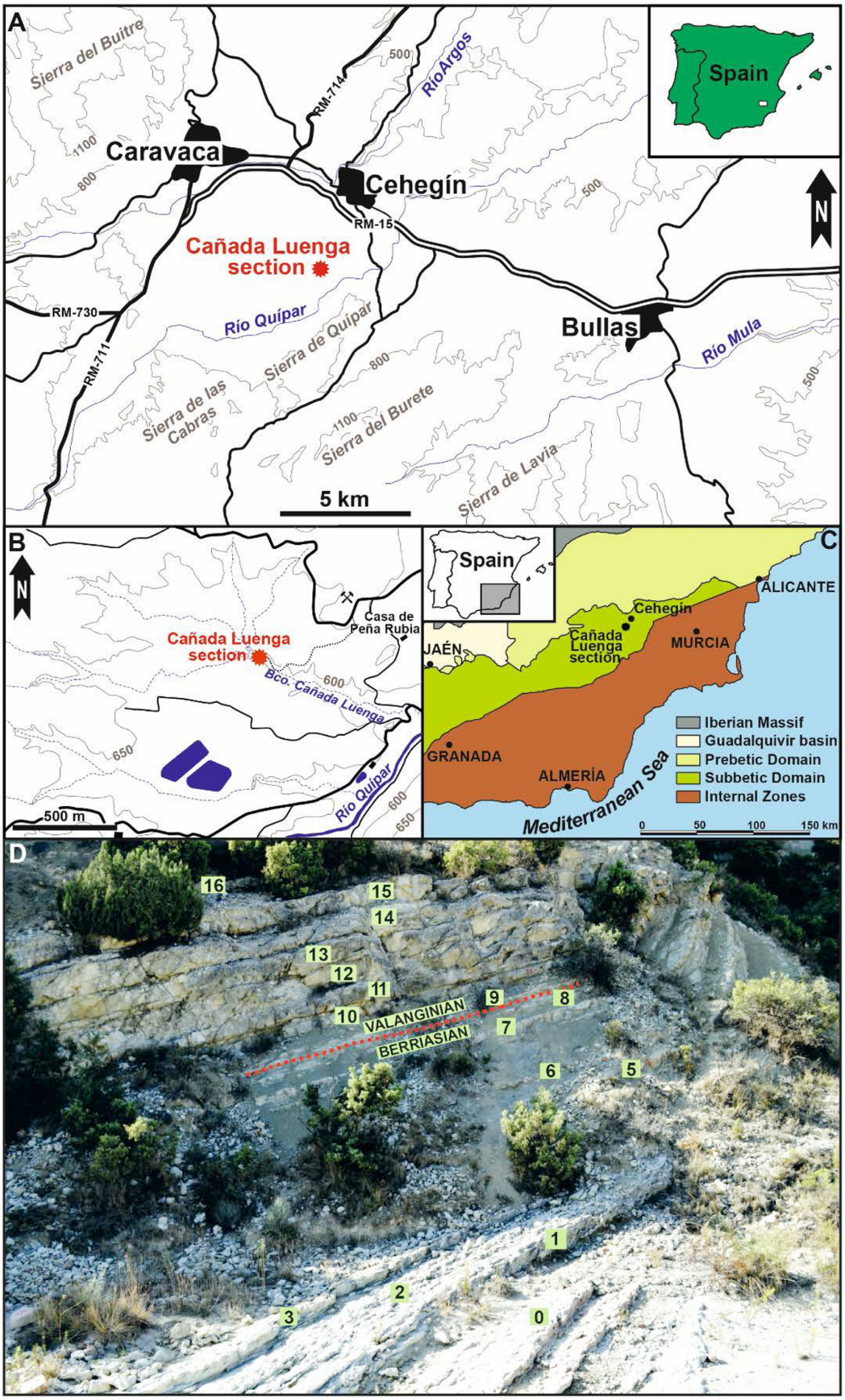

Figure 30. Cañada Luenga section. A, General geographic location; red star: GPS coordinates are 38º03'55''N, 1º48'43''W (WGS84 reference frame; https://www.google.com/maps). B, Detailed location and access. C, Location of the section in a simplified geologic map of the Betic Cordillera. D, General view of the succession.

as having been deposited on little subsident, relatively shallow pelagic swells (Cecca et al., 1992; Rey, 1993).

The remainder of the section consists of alternating light grey limestone and marly limestone beds (5 to 55 cm thick) and dark grey marlstone interbeds (2 to 110 cm thick) of the Miravetes Formation (Veen, 1969). Texturally, these sediments are mudstones with calpionellids, calcareous dinoflagellates, calcitised radiolarians and benthic foraminifera. The lime fraction is mostly made up of calcareous nannofossils remains, whereas clay minerals (mainly illite and kaolinite) are, by far, the main components of the detrital fraction (Fesneau, 2008). Pyrite, generally altered to limonite, is also common in these facies either as nodules or filling burrows and ammonite phragmocones. Macrofossil remains are common throughout this interval, with ammonites constituting the vast majority of these (more than 95%). The same benthic invertebrates present at the top of the Upper Ammonitico Rosso Formation (crinoid plates, irregular echinoids, brachiopods, and bivalves) are still relatively frequent in the lower levels of the Miravetes Formation, but decrease progressively upwards. The lithological and palaeontological characteristics of the marl–limestone rhythmites of the Miravetes Formation indicate a deposit in a distal, low-energy, relatively deep environment, considerably more subsident than that of the Upper Ammonitico Rosso Formation.

Biostratigraphy

Ammonites are the most abundant group of macrofossils in the Cañada Luenga section and also the most useful for biostratigraphically characterising the B/V boundary. Belemnites have been shown to have some biochronological value. Among microfossils, calpionellids, calcareous dinoflagellate cysts and calcareous nannofossils provide very valuable information, while benthic foraminifera and organic walled dinoflagellate cysts, also well represented, are potentially interesting (further explanations in Company et al., 2023). The material is housed at the palaeontological collections of the University of Granada (Spain). Main biostratigraphic events are represented in Fig. 31.

Ammonites

More than 600 ammonites have been collected in the successive bed-by-bed sampling carried out on the section. Most of these are well enough preserved to be identified at the species level. The analysis of their stratigraphic distribution (details in Aguado et al., 2000, and Company and Tavera, 2015) has enabled us to accurately characterize the uppermost Berriasian *Tirnovella alpillensis* Zone and the lowermost Valanginian *Hoedemaekeria pertransiens* Zone of the standard zonation (Szives et al., 2024).

The lowermost part of the section (beds 0 to 4) corresponds to the *T. alpillensis* Subzone (Fig. 31). The ammonite assemblage is composed of typical Berriasian neocomitids such as *T. alpillensis*, *Berriasella calisto*, *Fauriella boissieri* and *Erdenella paquieri*. Olcostephanids are also frequent, being mainly represented by *Spiticeras gevreyi*, which is replaced by *Spiticeras polytroptychum*, a transitional species to the genus *Olcostephanus*, in the uppermost part of the subzone. Bed 3 has yielded a rich population of a form very similar to the Andean *Groebericeras bifrons*. Some representatives of the genus *Kilianiceras* also occur in this interval.

The FO of *Hoedemaekeria otopeta* in bed 5 defines the base of the uppermost Berriasian subzone. The assemblage of this subzone largely coincides with that of the *T. alpillensis* Subzone. *Berriasella calisto*, *T. alpillensis* and *E. paquieri* are still present. *Spiticeras polytroptychum* reaches its acme in this interval and gives way to its descendant *Olcostephanus drumensis* in the uppermost part of the subzone (bed 8). The heteromorph genus *Leptoceras*, which has its first records in the underlying subzone, also shows its maximum frequency in these levels, shortly before disappearing.

The marker to define the base of the Valanginian is the FO of *H. pertransiens.* This event has been recorded in bed 9 in the Cañada Luenga section and coincides with a major renewal in the ammonite fauna. Most of the species present in lower levels disappear. Only *O. drumensis*, *Kilianella lucensis* (an uncommon species that had appeared in the middle part of the *H. otopeta* Subzone), and the last and rare representatives of *Kilianiceras*, together with other long-ranging species, pass into the *H. pertransiens* Zone. Besides the index species, other new taxa that appear at the base of the Valanginian are *Kilianella roubaudiana*, *Neocomites premolicus*, *Sarasinella eucyrta* and *Hoedemaekeria gratianopolitensis*.

The FO of *Neolissoceras* (*Vergoliceras*) *salinarium* marks the base of the upper subzone of the *H. pertransiens* Zone. This event takes place in bed 17 in the Cañada Luenga section. *Hoedemaekeria pertransiens* and *K. roubaudiana* continue to be present, although scarcely, throughout the *N.* (*V.*) *salinarium* Subzone, whereas *H. gratianopolitensis*, *N. premolicus* and *O. drumensis* disappear in its lower part (Company and Tavera, 2015). Some new neocomitid species, like *Kilianella drumensis*, appear in this interval.

Belemnites

Janssen (2003) provided a thorough account on the B/V boundary belemnites from Cañada Luenga and other sections in SE Spain. These data were later updated (Janssen, 2021), and have been revised again for this work. Typical latest Berriasian belemnites include *Berriasibelus* aff. *exstinctorius*, *Berriasibelus triquetrus*, *Gillieronibelus mayeri*, *Conobelus piradoensis*, *Duvalia miravetesensis*, and *Tithonobelus orbignyi*. *Castellanibelus orbignyanus* appears near the base of the Valanginian replacing another undescribed species of *Castellanibelus* (Fig. 31). Other typical earliest Valanginian species are *Hibolites* aff. *pistilliformis* and *B. exstinctorius*. The FO of *Duvalia superconstricta* is recorded at the base of the *N.* (*V.*) *salinarium* Subzone.

Calpionellids

A total of 21 thin sections from samples collected in the limestone beds have been studied. Calpionellids are abundant and very well preserved in all the samples.

The lower beds (0 to 5) of the section correspond to the *Calpionellopsis oblonga* Subzone. Together with the index species, *Tintinnopsella carpathica* is the dominant species in the assemblage. *Calpionellopsis simplex* and *Calpionellopsis* sp. A are also very abundant, while *Calpionella alpina*, *Calpionella minuta*, *Tintinnopsella longa* and *Lorenziella hungarica* are common. Rare to single occurrences of *Lorenziella plicata*, and several species of *Remaniella* have been also found in this interval. Sporadic records of species characteristic of lower strati-

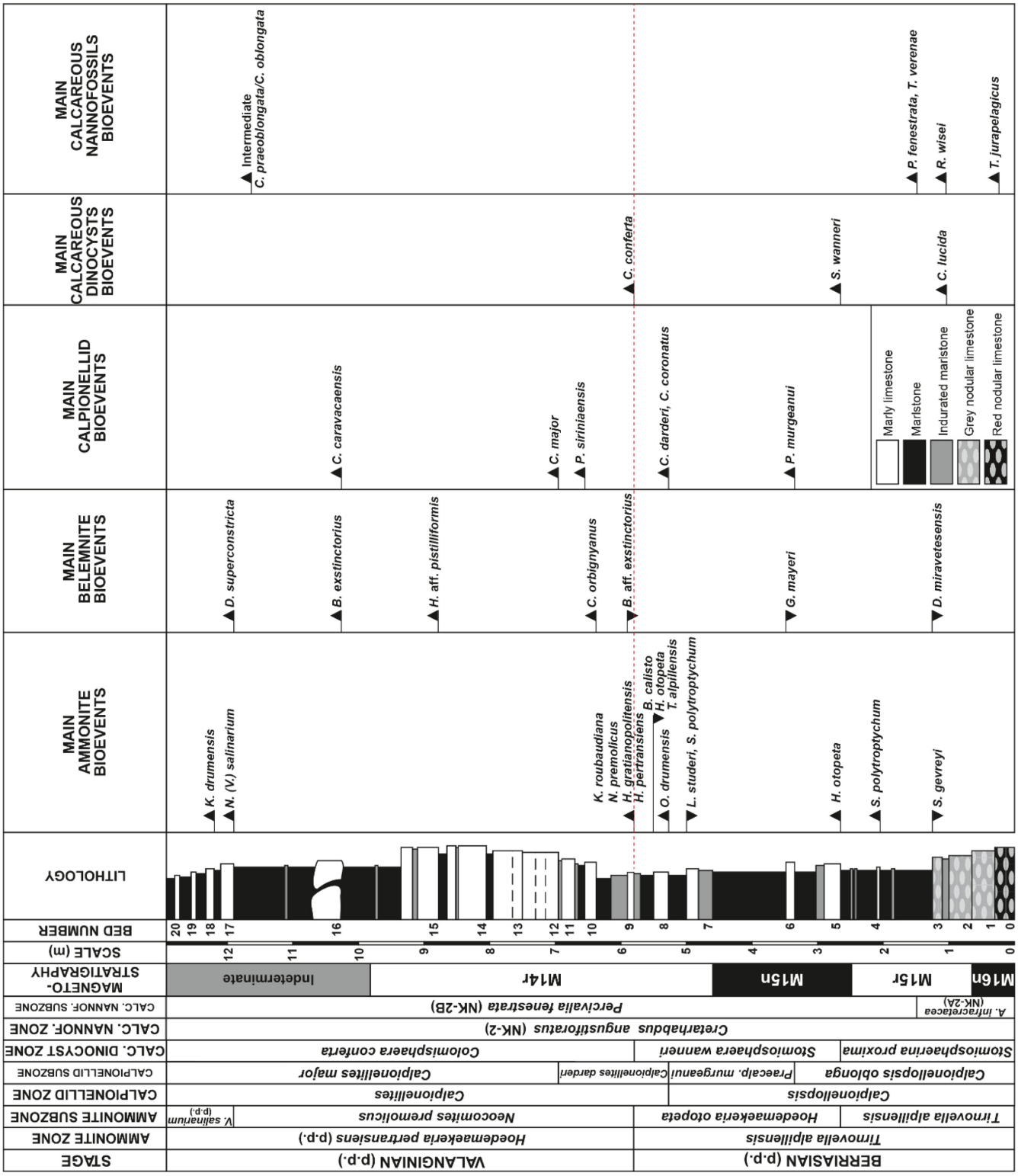

Figure 31. Cañada Luenga section. Main biostratigraphic markers.

graphic levels, such as *Crassicollaria parvula*, *Sturiella dolomitica* and *Borzaites atava*, are restricted to the basal levels (beds 0 to 3).

The FO of *Praecalpionellites murgeanui*, which marks the base of the upper subzone of the *Calpionellopsis* Zone, has been recorded in bed 6, corresponding to the lower part of the *H. otopeta* Subzone (Fig. 31). *Tintinnopsella carpathica* and *C. oblonga* are the dominant species. *Praecalpionellites murgeanui, C. minuta* and *T. longa* are abundant. *Calpionellopsis simplex, Calpionellopsis* sp. A, *L. plicata, Remaniella filipescui* and *R. cadischiana* are rare to common, whereas *Remaniella colomi, R. catalanoi, and R. borzai* are rare to very rare. *Remaniella colomi* disappears at the base of this subzone.

The base of the *Calpionellites darderi* Zone and Subzone is defined

by the FO of the index species. This event, together the FOs of *Calpionellites coronatus* and *Praecalpionellites hillebrandti* takes place in bed 8, just below the base of the *H. pertransiens* Zone. *Calpionellites darderi* is abundant to common but *T. carpathica* is the dominant taxon in the assemblage. Species that were already present in the *C. oblonga* Zone, *P. murgeanui*, *Tintinnopsella longa*, *C. alpina, L. hungarica, C. oblonga, Calpionellopsis* sp. A, continue to be common in the *C. darderi* Subzone. *Calpionella minuta*, *L. plicata*, *R. cadischiana*, *R. filipescui* and *R. catalanoi* are rare to very rare, the latter species disappearing in bed 11, at the top of this subzone. The FO of *Praecalpionellites siriniaensis* has been recorded in this same bed.

The upper levels of the section (beds 12 to 20) can be assigned to the *Calpionellites major* Subzone. The subzonal index is associated in this interval with other species of *Calpionellites* such as *C. darderi* and *C. coronatus*, already present in the underlying subzone, and *Calpionellites caravacaensis*, which first appears in bed 16. The frequency of these species of *Calpionellites* is variable throughout the interval, whereas *T. carpathica* is still the dominant element, and *T. longa*, *C. oblonga* and *L. hungarica* are abundant, particularly in the highest beds of the section. *Praecalpionellites murgeanui* and *L. plicata* are rare.

Calcareous dinoflagellate cysts

Calcareous dinocysts were studied in the same thin sections as the calpionellids. Significant events recorded in the Cañada Luenga section are: the FO of *Colomisphaera lucida* (bed 3), the FO of *Stomiosphaera wanneri* (bed 5), and the FO of *Colomisphaera conferta* (bed 9; Fig. 31). Therefore, the upper part of the *Stomiosphaerina proxima* Zone, the entire *Stomiosphaera wanneri* Zone and the lower part of the *Colomisphaera conferta* Zone of the zonal scheme proposed by Lakova et al. (1999) are represented in the section.

Calcareous nannofossils

For the present study a total of 40 samples, mainly from marly lithologies, were investigated for calcareous nannofossil content. Preservation fluctuates between moderate to poor. Nannofossil abundance varies from very abundant (more than 20 nannofossils / field of view) to very rare (1 nannofossil / 2 fields of view or less).

Calcareous nannofossil assemblages in the Cañada Luenga section are dominated by the representatives of the genus *Watznaueria* (*W. barnesiae*/*W. fossacincta*, *W. britannica*, *W. manivitiae*, and *W. cynthae*) followed by narrow canal *Nannoconus* (mainly *N. steinmannii* ssp. *steinmannii*, and *N. steinmannii* ssp. *minor*). Wide canal nannoconids, such as *N. kamptneri* and *N. globulus*, are rare. Other common taxa include *Cyclagelosphaera margerelii*, *Diazomatolithus lehmanii* and *Micrantholithus hoschulzii*. All these species are typical of low-latitude cosmopolitan and Tethyan assemblages. However, scattered records of very rare specimens of *Crucibiscutum salebrosum* and *Sollasites horticus* within the lowermost 1.8 m of the section could indicate a cool water influx.

The calcareous nannofossil subzones NK-2A (*pro parte*) and NK-2B (*pro parte*) of the zonation proposed by Bralower et al. (1989) were identified in the section (Fig. 31). The lowermost beds (0 to 3), with *C. angustiforatus*, and *Percivalia nebulosa* (= *Rhagodiscus nebulosus*) correspond to the NK-2A Subzone. The FO of *Percivalia fenestrata*, recorded at the base of the marly interbed 3-4 (middle part of the *T. alpillensis* Subzone), defines the lower boundary of the NK-2B Subzone, although it is difficult in practice to place this limit due to the presence of specimens showing morphologic characters intermediate between *P. nebulosa* and *P. fenestrata* (see Bralower et al., 1989; Aguado et al., 2000).

Typical specimens of *Calcicalathina oblongata*, whose FO marks the base of NK-3 Zone, were not recorded, and only some specimens showing intermediate characters between *Calcicalathina praeoblongata* (= *Calcicalathina erbae*) and *C. oblongata* were found near the top of the section.

Other stratigraphically significant calcareous nannofossil events recorded throughout the section were the FO of *Tubodiscus jurapelagicus* (top of bed 0), the FO of *Rucinolithus wisei* (interbed 2-3) and the FO of *Tubodiscus verenae* (base of interbed 3-4, together with the FO of *P. fenestrata*), all of them in agreement with the stratigraphic position indicated by Bralower et al. (1989) and Aguado et al. (2000).

Magnetostratigraphy

The magnetostratigraphy of the Cañada Luenga section and of another one located some 300 m upstream in the same ravine was studied by Ogg et al. (1988). Both sections (which correspond, respectively, to VCY and VCZ in Ogg et al., 1988) display identical magnetic polarity sequences which can be correlated with the interval between the upper part of the polarity Chron M16n and the lower part of the polarity Chron M14r (Figs. 31, 32).

According to the results provided by Aguado et al. (2000) and updated here, the base of the polarity Chron M15r falls within the *T. alpillensis* Subzone and in the uppermost part of the NK-2A Subzone. The base of polarity Chron M15n practically coincides with the base of the *H. otopeta* Subzone, and its top correlates with the middle part of the *P. murgeanui c*alpionellid Subzone and the upper part of the *H. otopeta* Subzone. The base of the Valanginian, marked by the FO of *H. pertransiens*, calibrates with the lower part of the polarity Chron M14r.

Chemostratigraphy

A high-resolution analysis of 60 bulk carbonate samples from limestone, marlstone and marly limestone beds was performed to study the carbon and oxygen isotope stratigraphy in the Cañada Luenga section (Fig. 32). The $\delta^{13}C$ values fluctuate between -0.24‰ and 1.34‰, and the $\delta^{18}O$ between -2.08‰ and -1.03‰. The carbon isotope curve shows fairly stable values, around 1‰ throughout the entire section, except for two well defined, W-shaped negative excursions, one in the uppermost part of the *T. alpillensis* Subzone (upper part of Chron M15r) and one in the upper part of the *N. premolicus* Subzone (Chron M14r). The high(er) amplitude of these both peaks might be partly linked to a diagenetic impact. However, this effect can be minimized in the current study. According to Cramer and Jarvis (2020), remineralization effects are most likely where sediments have low carbonate content and high organic content; this is not the case at Cañada Luenga. Moreover, it seems relevant to consider these both $\delta^{13}C$ values as geochemical events as they are also recorded in similar stratigraphic intervals

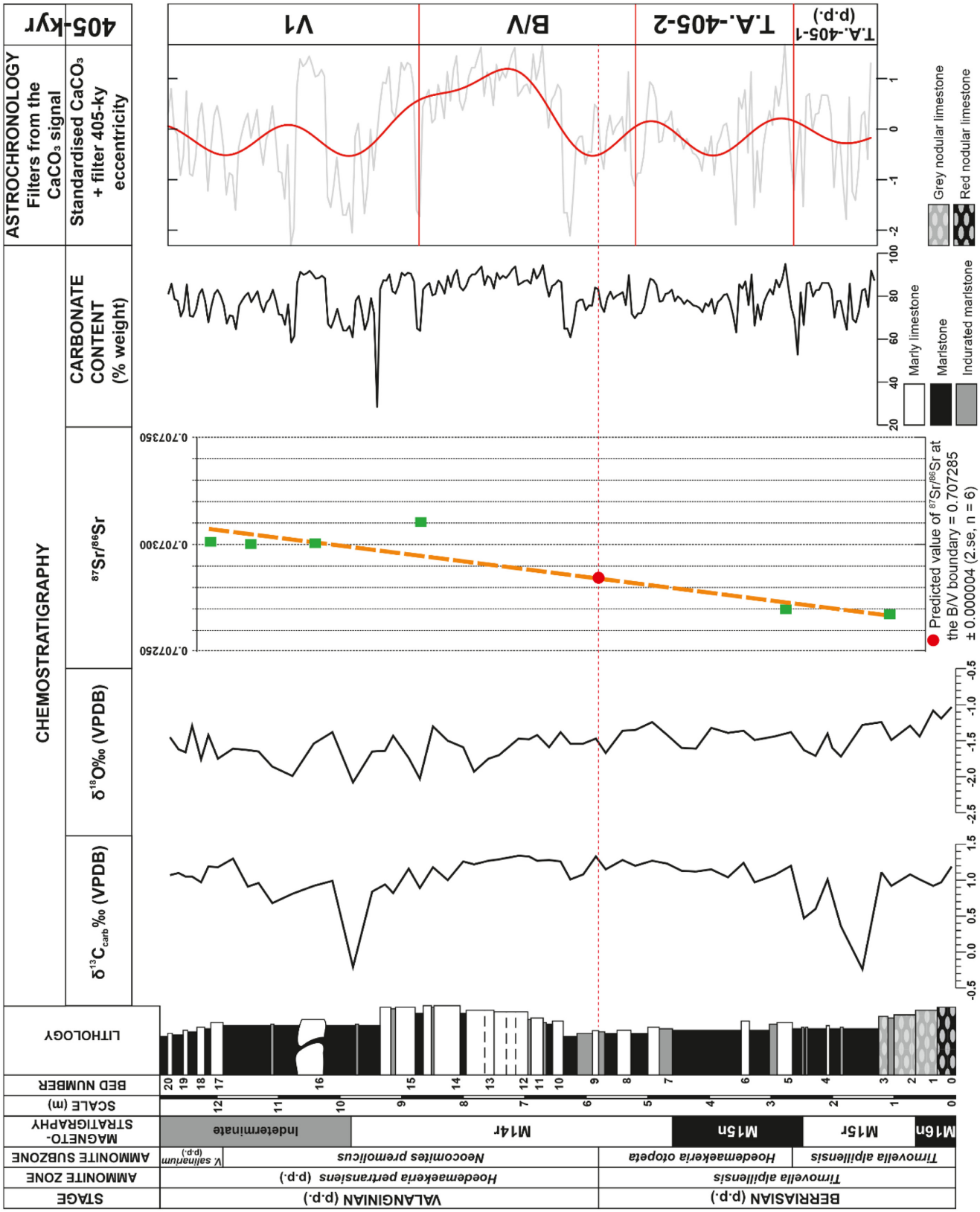

Figure 32. Cañada Luenga section. Magnetostratigraphy, chemostratigraphy and astrochronology.

of other sections such as Vergol and Montclus (France; see below). The $\delta^{18}O$ curve presents a slight negative trend from the base of the section to the middle part of the *N. premolicus* Subzone, where it undergoes abrupt oscillations and reaches minimum values; above this interval it recovers slightly towards more positive values.

No systematic analysis of $^{87}Sr/^{86}Sr$ has been conducted in the Cañada

Luenga section. However, McArthur et al. (2007) used some of the belemnites collected by Nico Janssen in this and other sections from SE Spain, together with others from SE France, to construct the Sr isotope curve around the B/V boundary. Data plotted in Fig. 32 are only those from the Cañada Luenga section. Fitted with a linear regression, the predicted value of $^{87}Sr/^{86}Sr$ at the B/V boundary is 0.707285 ± 0.000004 (2.se, $n = 6$).

Cyclostratigraphy and Astrochronology

The $CaCO_3$ content was measured every 5 cm in order to detect the sedimentary cycles through spectral analyses, determine their climatic origin, and provide an orbital time scale for the Cañada Luenga section. The sedimentation rates can be calculated using the cyclo-astrochonology.

The $CaCO_3$ signal is detrended and treated with spectral analyses following the same procedure as the gamma-ray and magnetic susceptibility signals from Vergol. The 2π-MTM spectrum of the $CaCO_3$ signal shows spectral peaks above the 95% confidence level at 5.1 m and 0.18 m. Other peaks at 1.2 m, 0.29 m and 0.18 m exceed the 90% confidence level. The ratio between the periods of 5.1:1.2:0.29:0.18 m is 1:4.25:17:28. The cycle of 5.1 m could thus relate to the 405-kyr eccentricity cycle, the peak of 1.2 m could relate to the 100-kyr eccentricity cycle and the periods from 0.29 m to 0.18 m to the precession cycles. The boundaries of the 405-kyr eccentricity are correlated from the Vergol section with biostratigraphy and carbon-isotope curves aided with the maximum of the filter of the 405-kyr band. The astrochronological interpretation, with the eccentricity (405-kyr) is presented in Fig. 32. The boundaries from the base of T.A.405-2 to the base of V1 are near maxima of the filter of the 405-kyr filter at Cañada Luenga. The top of V1 is near the top of the interval. A maximum of the filter of the 405-kyr filter does not correspond to a 405-kyr cycle boundary according to biostratigraphic correlation. This maximum is driven by the existence of limestone bed 16 within a thick marl interval. The presence of this bed only is enough to deviate the filter to higher values, so it is not sure whether it has an orbital origin. Three complete 405-kyr long-term eccentricity cycles are recognized across the interval covering the B/V boundary. The average sedimentation rate of the Cañada Luenga section is around 9 m/Myr (further explanation below).

Correlation of the Vergol (GSSP) with the Cañada Luenga (SABS) Sections

An attempt at correlation of the Vergol and Cañada Luenga sections is proposed here for the first time (Fig. 33) in order to show their suitability and complementarity as GSSP versus SABS, respectively. This integrated approach is mainly based on bio-and isotope stratigraphy. Cyclostratigraphy allows calculation of a sedimentation rate for some intervals. The zonal schemes are complemented by major bio-events which are put alongside the sections. The method of graphic correlations is also used in order to strengthen the characterization of the Berriasian/Valanginian (B/V) boundary, the correlation of some events between the two sections, and the comparison of the sedimentary record. A cross-plot is presented in Fig. 34. It is mainly based on First Occurrences (FO) and Last Occurrences (LO) of ammonoids and calpionellids; only one point on calcareous nannofossils is shared by the two sections (Fig. 34). These 3 groups have been selected as they were candidates for the primary marker due to their robust and proven biostratigraphic significance. The biostratigraphy of other groups is less known and probably more discrepant. The FO of *T. alpillensis* has been chosen as the reference "0 metre" (origin of the coordinates) for building the graph and comparing both sections. The reliability of this FO needed to be confirmed. However, the FO of the *Hoedemaekeria pertransiens* provides a possible alternative datum level as the origin of the coordinates; the results are identical for the calculation of the regression line and its correlation coefficient (NB: the use of the FO of *T. alpillensis* allows us to have positive values of both axes). As the Vergol section is more expanded, it is considered as the "standard reference section" (SRS) in the graphic correlations and so put on the x-axis, and the Cañada Luenga section (compared to the SRS) is put on the y-axis. The main results and interpretations can be summarised as follows.

Characterization of the Berriasian/Valanginian Boundary

The restricted interval around the B/V boundary, defined at the base of limestone bed VGL-B136 at Vergol that coincides with the FO of *H. pertransiens* (species recorded in bed CL9 at Cañada Luenga), is well characterized in both sections by ammonoid and calpionellid events such as the FOs of *H. gratianopolitensis*, *N. premolicus*, *C. darderi* and *Calpionellites coronatus*, and the LOs of *H. otopeta*, *T. alpillensis*, and *B. calisto*. According to the method of graphic correlation, the good correlation coefficient of the regression line ($y = 0.3992x - 1.4115$; $r^2 = 0.88$; green line in Fig. 34) shows that all considered biostratigraphic events (Fig. 33) are consistent and robust for the characterization of the studied interval; this strongly supports the boundary correlation between the two sections (NB: using a polynomial curve, this coefficient is higher, $r^2 = 0.93$).

In the Cañada Luenga section, the B/V boundary occurs in the lower part of polarity Chron M14r. According to the cyclo-astrochronology performed on the Vergol section and a radioisotopic age provided from the study of the Neuquén basin (Argentina, Aguirre-Urreta et al., 2017; this work, see above), the age model allows dating the base of the Valanginian Stage at 137.05 Ma (±0.2 Ma). In this section, the predicted value of $^{87}Sr/^{86}Sr$ at the B/V boundary is 0.707289 ± 0.000004 (2.se, $n = 12$), very close to the value measured on a belemnite found in the marly layer VGL-B134 (0.707293). At Cañada Luenga, a linear regression was used in order to estimate a strontium isotopic value on the B/V boundary; the predicted value of $^{87}Sr/^{86}Sr$ at the B/V boundary is 0.707285 ± 0.000004 (2.se, $n = 6$). However, this must be interpreted carefully as data are scarce, especially in the middle part of the section, and a linear fit may not be valid. The sequence stratigraphy established at Vergol shows that the B/V boundary is located between Sequence Boundaries SB Be8 and SB Va1.

Correlation of Some Events in the Upper Berriasian (p.p.)

A solid correlation can be drawn for the base of the *H. otopeta* Subzone using the FO of the index species (VGL-B116 and CL5). In both sections, the FOs of *P. fenestrata* and *P. murgeanui* are recorded below and above this line, respectively. As the base of polarity Chron M15n

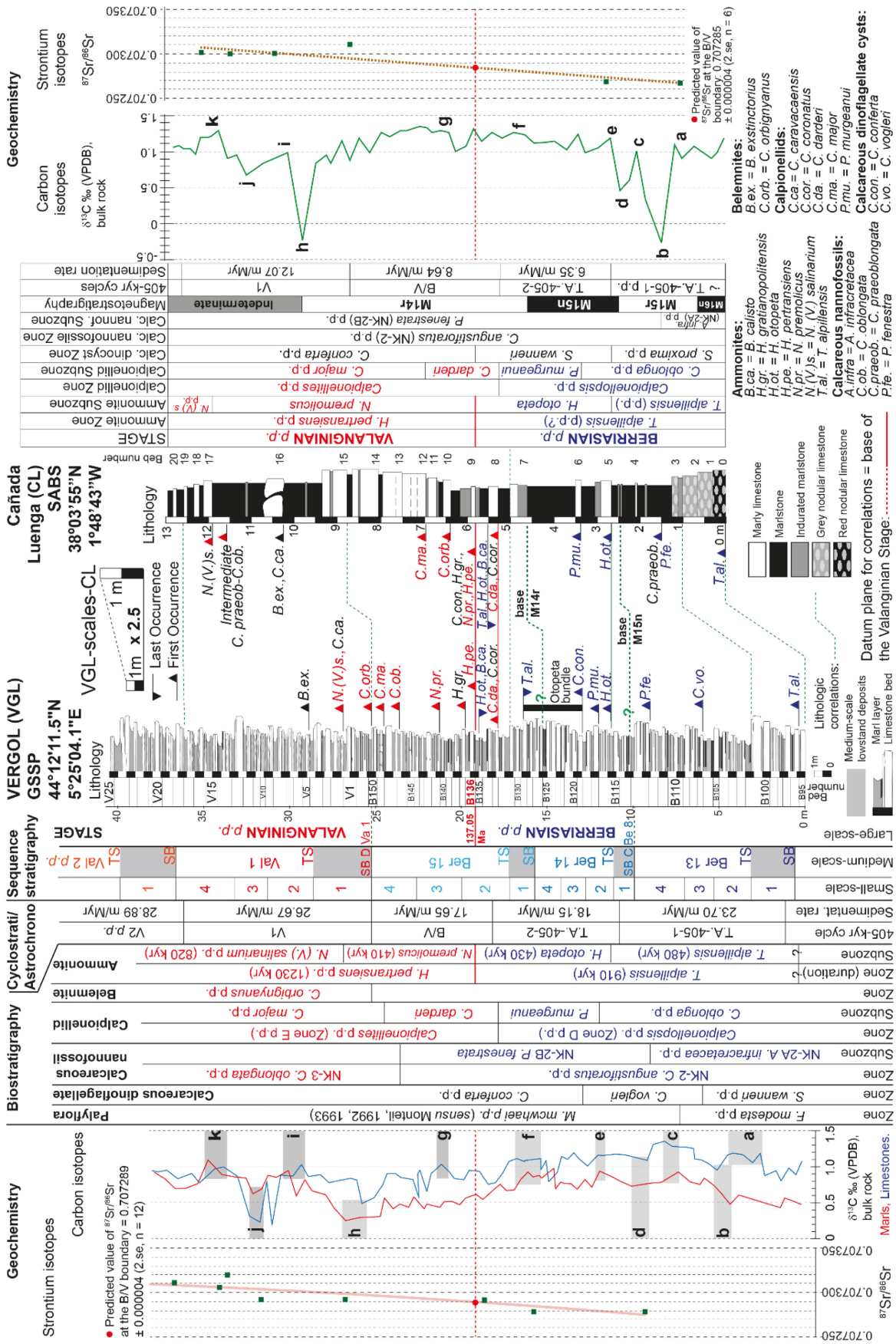

Figure 33. Correlations of the Vergol and Cañada Luenga sections using an integrated stratigraphy. See Kenjo et al. (2021, p. 23-24) and the current work (text and Fig. 34) for explanation on the ratio 2.5 between the scales of the two sections.

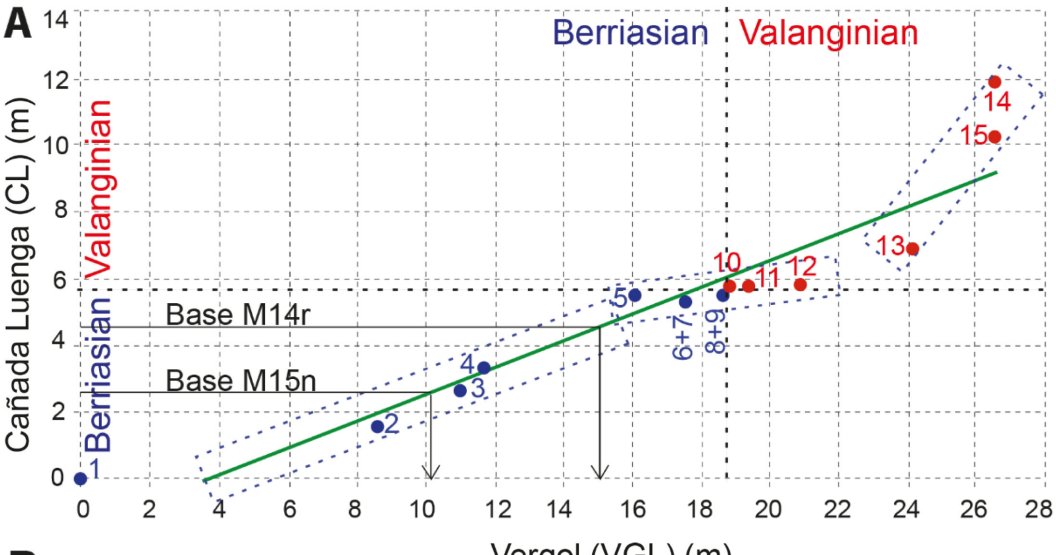

Species	Bed VGL-	Metre	Bed CL-	Metre
15 = FO *C. caravacaensis*	V2	26.53	16	10.25
14 = FO *N. (V.) salinarium*	V2	26.53	17	11.90
13 = FO *C. major*	B149	24.16	12	6.95
12 = FO *N. premolicus*	B141	20.89	9	5.80
11 = FO *H. gratianopolitensis*	B137	19.42	9	5.80
10 = FO *H. pertransiens*	B136	18.85	9	5.80
9 = LO *H. otopeta*	B135	18.66	8	5.50
8 = LO *B. calisto*	B135	18.66	8	5.50
7 = FO *C. coronatus*	B133	17.51	8	5.27
6 = FO *C. darderi*	B133	17.51	8	5.27
5 = LO *T. alpillensis*	B129	16.08	8	5.50
4 = FO *P. murgeanui*	B117	11.67	6	3.35
3 = FO *H. otopeta*	B116	10.95	5	2.65
2 = FO *P. fenestra*	B112	8.65	3-4	1.50
1= FO *T. alpillensis*	B96	0	0	0

Figure 34. A, graphic correlation: cross plot Vergol (VGL) versus Cañada Luenga (CL) sections. The slope of the regression line (green dash; $y = 0.3992x - 1.4115$; $r^2 = 0.88$) is around 0.4; this means that the Vergol section is 2.5 (= 1/0.4) times more expanded than the Cañada Luenga section. B, biostratigraphic events 1 to 15, table showing the location (in metres measured from the base of the beds VGL-B96 or CL0) of first (FO) and last (LO) occurrences of main taxa (ammonites, calpionellids and calcareous nannofossils).

practically coincides with the lower boundary of the *H. otopeta* Subzone at Cañada Luenga (CL5), this magnetic event should occur just below the bed VGL-B116 at Vergol. According to the Spanish section where the base of the polarity Chron M14r is located in the top third of the *P. murgeanui* Subzone (base of CL7), this magnetic event should occur in the top third part of the calcareous/Otopeta bundle of the Vergol section for which the calpionellid zonation is also well established. Using the graphic correlation, the regression line (Fig. 34) allows us to correlate approximatively the bases of M15n and M14r with beds VGL-B114 and VGL-B126, respectively (Fig. 33). The carbon-isotope stratigraphy may strengthen these suggestions taking into account that the small "peaks" "d" and "f" recorded at Vergol could be recognized just below and above the polarity Chron M15n at Cañada Luenga. However, as the carbon isotope curves are not characterized

by strong variations of $\delta^{13}C$, their correlation should be interpreted carefully. According to this integrated approach, the Sequence Boundary (SB) of medium-scale sequences Ber 14 (SB C = Be8) and Ber 15 of the Vergol section could be approximatively correlated just below beds CL5 and CL7, respectively.

Correlation of Some Events in the Lower Valanginian (p.p.)

At the Vergol and Cañada Luenga sections, above the B/V boundary, the carbon isotopic curve is characterized by a value decrease (from "g" to "h", located in the lower and upper parts of the *N. premolicus* Subzone, respectively) followed by an increase in values to reach the peaks "i" and "k", the latter recorded in the lower part of the *N.* (*V.*) *salinarium* Subzone (Fig. 33). The upper part of the medium-scale sequence Ber 15 (small-scale 4?) of the Vergol section may be correlated with beds CL12-13-14 as the FOs of *C. major* are observed in these intervals; the beginning of a stronger decrease in carbon isotope values is recorded in their top parts. Thus, the SB Va1 could be drawn at the base of bed CL15. The medium-scale lowstand deposits of the Vergol section could be correlated to the marly limestones CL15-16?; in this interval of both sections, the FOs of *Calpionellites caravacaensis* and *B. exstinctorius* are recorded.

Comparison of the Interval of the T. alpillensis – H. pertransiens (p.p.) *Zones*

The aim of this part is to compare the sedimentary record (sections more or less expanded). Four approaches are used here.

As previously stated, the bases of the *H. otopeta* Subzone and *H. pertransiens* Zone are interpreted as solid lines of correlation. Thus, the stratigraphic intervals dated from the *H. otopeta* Subzone are fully represented and their thickness can be compared: 8 m and 3.2 m for Vergol and Cañada Luenga sections, respectively. Therefore, as far as these intervals are concerned, the French section is 2.5 times (8/3.2) more expanded than the Spanish one (Kenjo et al., 2021). In Fig. 33, this ratio is used to compare the different scales of both sections.

The sedimentation rates can be calculated using the cyclo-astrochonology. Four 405-kyr long-term eccentricity cycles are identified on the Vergol and Cañada Luenga sections across the interval covering the B/V boundary (Fig. 33). As it is not complete in the Spanish section, the cycle TA-405-1 cannot be compared. As shown in Table 3, the average sedimentation rate of the Vergol section is 2.4 times higher than that of Cañada Luenga section.

The sedimentation rate can also be inferred using the correlation of the carbon isotope curves. Among the most relevant changes in the isotope changes recorded in both sections there are two negative shifts named "b" and "h". The thicknesses of the intervals between them are around 22 m and 8.50 m in the Vergol and Cañada Luenga sections, respectively. The ratio is 2.59 (22.50 m at VGL / 8.50 m at CL).

According to the graphic correlation (Fig. 34), the slope of the regression line ($y = 0.3992x - 1.4115$; $r^2 = 0.88$) is around 0.4. Thus, according to this method, the Vergol section is 2.5 (= 1/0.4) times more expanded than Cañada Luenga. In conclusion, the 4 approaches yield consistent results and show that the Vergol section is around 2.5 times more expanded than the Cañada Luenga section.

The plot distribution suggests some changes in the accumulation rate and can be commented as follows. For building the graph, the FO of *T. alpillensis* has been chosen as the reference "0 metre" (origin of the coordinates, cf. method of the graphic correlations). At Cañada Luenga, the FO of this index species is recorded at the base of the succession that is made up of reddish to gray nodular calcilutites to calcirudites from 0 to 1.25 m beds (beds 0 to 3; Upper Ammonitico Rosso Formation; Fig. 31). According to the description made previously, this interval is condensed (very low sedimentation rate, stratigraphic gaps). This explains the offset of point 1 (FO of *T. alpillensis*) with respect to the regression line (Fig. 34). Then, three sets of points (biostratigraphic events) can be recognized along this line. For the intermediate set (events 5 to 12; Fig. 34), the slope of the segment (linking these points) is lower than that of the entire regression line. This would suggest a stronger condensation at Cañada Luenga close to the B/V boundary, and so a lowered sedimentation rate. However, it would be not really appropriate to calculate a rate for this short interval (decimetric in thickness). Indeed, in this preliminary study, the cross-plot is based on FOs and LOs recorded in the Vergol and Cañada Luenga sections, and not on First Appearance Datums (FAD) and Last Appearance Datums (LAD) interpreted from a synthesis of biostratigraphic events observed in a larger number of sections. Even if a sedimentation rate was estimated using this approach, it would be irrelevant to compare it with the rate proposed by the cyclo-astrochonology (Table 3). Indeed, the eight events of the cross-plot are restricted to a 30 cm thick interval of the Cañada Luenga section (from event 5 at 5.5 m to event 12 at 5.8 m), while the 405-kyr cycle B/V covers an interval of 3.50 m thick (from 5.24 m to 8.74 m, Figs. 31, 32).

In the current work, the method of graphic correlations is used to establish a regression line based on fifteen biostratigraphic events, and its slope (0.4) provides a ratio (s-rVGL/s-rCL) showing that Vergol section is 2.5 times more expanded than Cañada Luenga section. This regression line allows to project the position of chrons M15n and M14r recorded at Cañada Luenga section (y-axis) onto the Vergol section (x-axis), in agreement with the correlations carried out under biostratigraphic control (see different zonal schemes on Fig. 33).

Table 3. Compared sedimentation rates of the Vergol (VGL) and Cañada Luenga (CL) sections and their ratios

Vergol (VGL) 405-kyr cycles and sedimentation rate (s-r)	Cañada Luenga (CL) 405-kyr cycles and sedimentation rate (s-r)	Ratio : s-r VGL / s-r CL
V1, s-r = 26.67 m/Myr	V1, s-r = 12.07 m/Myr	Ratio = 2.21
B/V, s-r = 17.65 m/Myr	B/V, s-r = 8.64 m/Myr	Ratio = 2.04
TA-405-2, s-r = 18.15 m/Myr	TA-405-2, s-r = 6.35 m/Myr	Ratio = 2.86
TA-405-1, s-r = 23.70 m/Myr	TA-405-1, not complete	-

Criteria for the Global Correlation of the Berriasian/Valanginian Boundary

The different types of stratigraphy are discussed in the following parts. Bio-chemical-physical criteria are reviewed for establishing global correlations with the boundary (interval), drawing on records from the GSSP and its auxiliary section for the magnetostratigraphy. As non-ambiguous markers (evolution being an irreversible process), fossils are used to calibrate chemical and physical binary markers. All these markers from the Berriasian/Valanginian boundary (B/V) interval have been studied in various land sections or ocean sites. In order to summurize this data set, a series of tables is presented.

Biostratigraphy

The latest Jurassic and earliest Cretaceous (Tithonian–Barremian) is an interval characterized by a well-marked evolution and development of endemic marine faunas and floras in different parts of the world. This provincialism makes supra-regional correlation of biostratigraphical zonations difficult between the Tethyan and Boreal realms. The late Berriasian and early Valanginian were times with relatively strong biogeographic restrictions (Mutterlose, 1992b; Möller et al., 2015; and references therein) when sea-level was particularly low (Haq et al., 1987; Haq, 2014), leading many marine basins to become isolated or even emerged. Considering ammonite faunas as an example, this situation gave rise to a high degree of endemism so that not only were the Boreal and Tethyan assemblages clearly different, but there was also faunal differentiation within each realm (Rawson, 1993, 1994; Lehmann et al., 2015), which considerably hampers interregional correlation. Besides the impact of physical barriers (cf. opening or closure of seaways), the biogeographic distribution could be also caused by environmental conditions, climate differences, oceanic circulation patterns and other factors as post-mortem transport.

Ammonites

In both the Vergol and Cañada Luenga sections, the ammonite fauna shows a typically Mediterranean character and consists of seven families, namely Neocomitidae, Olcostephanidae, Haploceratidae, Phylloceratidae, Lytoceratidae, Bochianitidae and Protancyloceratidae. The neocomitids and, to a lesser extent, the olcostephanids are the most relevant groups for biostratigraphy (Company and Tavera, 2015; Kenjo et al., 2021).

The uppermost beds of the Berriasian are mainly characterized by five species of neocomitids: *Berriasella calisto*, *Fauriella boissieri*, *Tirnovella alpillensis*, *Erdenella paquieri* and *Hoedemaekeria otopeta* (Figs. 8, 31). Except for the last of these, which seems to be restricted to the northern margin of the Mediterranean area, these species are distributed throughout the Mediterranean–Caucasian Subrealm (Westermann, 2000; Lehmann et al., 2015), and extend westwards to the Caribbean Province (Mexico). Some of them have also been reported from the Indo-Pacific (Spath, 1939; Collignon, 1962) and Andean (Rivera, 1951; Leanza and Wiedmann, 1989) subrealms, but these citations must be considered erroneous or highly doubtful.

The selected primary marker for the definition of the base of the Valanginian stage is the FO of *Hoedemaekeria pertransiens*. As stated above, *H. pertransiens* is a well-defined species, easily recognizable and frequent, especially in hemipelagic sections, as is the case of Vergol and Cañada Luenga. This frequency ensures the correct location of its FO and makes correlations more reliable. Its geographical distribution extends throughout the Mediterranean Province, having been reported from Morocco, Tunisia, Spain, France, Italy, Austria, Poland, Hungary, Romania, Bulgaria and Ukraine (Crimea; see references in Klein, 2005) and, recently, also in Mexico (Ovando-Figueroa et al., 2024a). By contrast, records of this species in Argentina (Leanza, 1945; Aguirre-Urreta, 1993), Peru (Rivera, 1951), Colombia (Huber and Wiedmann, 1986), Pakistan (Spath, 1939) and Sumatra (Baumberger, 1925) are definitely incorrect.

Closely related to *H. pertransiens* is *Hoedemaekeria gratianopolitensis*, which also appears at the base of the Valanginian (Aguado et al., 2000; Reboulet et al., 2022) and shows a similar geographical distribution. *Hoedemaekeria gratianopolitensis* has often been confused with *Thurmanniceras thurmanni*, a classic but usually misinterpreted species (see discussions in Bulot, 1995; Aguado et al., 2000; Kenjo, 2014) and which has occasionally been misreported from the Andean basins. Furthermore, a large number of species defined in the Boreal-Pacific, Indo-Pacific and Andean subrealms have been attributed to the genus *Thurmanniceras* (see Klein, 2005), but none of them seem to have a direct relationship with the Mediterranean forms and are therefore not suitable for correlation.

Neocomites premolicus (FO) is considered by the Valanginian Working Group (VWG) as a good secondary marker. This species is morphologically well characterized and easily recognizable in the field. According to Company and Tavera (2015) and Kenjo et al. (2021, and references therein), the FO of *N. premolicus* occurs in the basal part of the *H. pertransiens* Zone, and its short stratigraphic range is restricted to the lower part of the zone. Thus, *N. premolicus* is used as the index species of the first subzone of the *H. pertransiens* Zone. This species is frequent in basin environments. As it is also particularly common in neritic environments, in which *H. pertransiens* may be rare or even absent, the FO of *N. premolicus* can be used to recognize the B/V boundary (see discussions in Ettachfini, 2004; Company and Tavera, 2015; Reboulet et al., 2022). *Neocomites premolicus* has a relatively wide geographic distribution (see Klein, 2005, p. 307–308). The species has been recorded throughout the Mediterranean area, from Morocco to Bulgaria, also extending west to Mexico (Ovando-Figueroa et al., 2024b) and east as far as Japan (Ehiro et al., 2020). On the other hand, reports of this species in Madagascar (Barrabé, 1929), Antarctica (Covacevich, 1976) and California (Imlay and Jones, 1970) are most likely wrong.

The genus *Kilianella* is represented in the sections of Vergol and Cañada Luenga by three species: *Kilianella chamalocensis*, *Kilianella lucensis* and *Kilianella roubaudiana* (Figs. 8, 31). The first of these appears in the *T. alpillensis* Subzone and reaches the basal beds of the Valanginian, *K. lucensis* is present in the *H. otopeta* Subzone and in the lower part of the *H. pertransiens* Zone, and *K. roubaudiana* extends throughout the *H. pertransiens* and *Neocomites neocomiensiformis* zones (Aguado et al., 2000; Kenjo, 2014; Company and Tavera, 2015; Kenjo et al., 2021; Reboulet et al., 2022). The three species are typically Mediterranean, although *K. chamalocensis* has also been identified in Japan (Ehiro et al., 2020), and *K. roubaudiana* in Mexico (González-Arreola et al., 1995), Cuba (Myczyński, 1977) and Pakistan (Fatmi and Rawson, 1993). It should also be noted that other species closely

resembling *K. roubaudiana*, such as *Kilianella asiatica* and *Kilianella crassiplicata*, characterize respectively the lower Valanginian beds of the Indo-Pacific and Boreal-Pacific subrealms.

The genus *Sarasinella* also appears around the B/V boundary and, in its current conception, would be restricted to the *H. pertransiens* and *N. neocomiensiformis* zones, although similar morphologies reappeared iteratively throughout the late Valanginian and basal Hauterivian (Company, 1987; Ettachfini, 2004; Reboulet et al., 2022). Species such as *Sarasinella eucyrta*, *Sarasinella longi* or *Sarasinella trezanensis* appear only sporadically in pelagic settings, but are much more frequent in the basal beds of the Valanginian in the shelf environments of the Mediterranean area (Wippich, 2003; Ettachfini, 2004; Reboulet et al., 2022). Species very similar to these, such as *Sarasinella varians*, *Sarasinella subspinosa* and *Sarasinella uhligi* have been reported from the lower Valanginian of northern Indian subcontinent (Uhlig, 1910; Spath, 1939; Fatmi, 1977), while the actual status of many other species attributed to this genus in other parts of the world seems to be much more doubtful.

Among the olcostephanids, the most relevant species for the identification of the lower boundary of the Valanginian is *Olcostephanus drumensis*. Specimens strictly attributable to this species appear in the uppermost part of the *H. otopeta* Subzone and persist to the base of the *N.* (*V.*) *salinarium* Subzone. The geographical distribution of this species exceeds the Mediterranean–Caucasian Subrealm and extends towards Mexico (González-Arreola et al., 1995) and Pakistan (Fatmi and Rawson, 1993).

The presence of the Boreal genus *Platylenticeras*, which characterizes the lowermost Valanginian in NW Germany, has been well documented in many localities in SE France and other areas of the northern margin of the Mediterranean province (Spain, Switzerland, Czech Republic, Poland). In most cases, the specimens come from the lower part of the *N. neocomiensiformis* Zone and belong to offshoot species that are not known in Germany. However, the subspecies *Platylenticeras latum tenue* and *Platylenticeras heteropleurum occidentale* are common to both regions, having been recorded from the base of the *H. pertransiens* Zone in some French sections and allowing a direct correlation of this level with the German *Platylentyceras*-Schichten (Thieuloy, 1977; Kemper et al., 1981).

This correlation is further reinforced by the finding of some specimens of *Paratollia* also at the base of the *H. pertransiens* Zone in some French sections (Thieuloy, 1977). This genus defines the base of the Valanginian in England (Casey, 1973) and is also present in the *Platylenticeras* beds in Germany (Jeletzky and Kemper, 1988).

Another line of evidence for the correlation with the Boreal Realm is supported by the alleged close relationship (Thieuloy, 1977; Alsen and Rawson, 2005; Mitta, 2018) between *Delphinites (Delphinites) ritteri*, an extremely rare element of the ammonite assemblages of the base of the *H. pertransiens* Zone in SE France, and the species of *Delphinites (Pseudogarnieria)*, which characterize the base of the Valanginian in Russia and Greenland, and allow the correlation to be extended to the rest of the Boreal Realm (see discussion in Alsen, 2006).

Belemnites

The genus *Castellanibelus*, with type species *C. orbignyanus*, is well known from the Valanginian of SE France (Duval-Jouve, 1841; Orbigny, 1847; Combémorel, 1972; Picollier, 2022). Specific assignments and stratigraphic extent vary considerably (cf. Janssen, 2021; Picollier, 2022).

The palaeogeographic distribution of *Castellanibelus* is not well known but for their restricted occurrences in the Mediterranean Province of the Tethyan Realm. The genus occurs possibly as far west as Mexico, but firmly established occurrences, through published figured specimens, are only known from Spain (Janssen, 2003), Switzerland (Mayer-Eymar, 1887), Ukraine (Crimea; Kabanov, 1960; Krymgol'ts, 1997) and France (see above for references). In addition, the genus might occur in Hungary (Főzy et al., 2010) and the Czech Republic (Horák, 1988). While other figured and published specimens of *Castellanibelus*, among them figured specimens of *C. orbignyanus*, refer to the late early Barremian belemnite genus *Curtohibolites* (Switzerland, Ooster, 1857; Bulgaria, Stoyanova-Vergilova, 1963), the late Valanginian *Adiakritobelus*, the latest Jurassic to Berriasian–Valanginian belemnite genera *Conobelus* and/or *Berriasibelus* (Switzerland, Gilliéron, 1873; France, Toucas, 1890; Azerbaijan, Ali-Zade, 1972), or *Duvalia* (Hungary, Jekelius, 1915). In addition, some likely teratologic belemnite specimens have been figured as *Castellanibelus* (Serbia, Vašíček et al., 2009).

If we look at the distribution of this genus, just by looking at citations, it is additionally found in Algeria, Georgia, Morocco, Rumania, and Tunisia. All in all, this points to a distribution largely restricted to the western part of the Mediterranean Province. No further records are known outside this palaeogeographic area, let alone details regarding the stratigraphic distribution but for Spain and France.

Calpionellids

Calpionellid associations across the B/V boundary are generally not abundant (Allemann and Remane, 1979; Blanc, 1996; Vašíček et al., 1994, 1999; Petrova and Metodiev, 2012; Omaña et al., 2017) but they are well preserved and easily recognizable in oligotrophic environments (Pop, 1994; Vašíček et al., 1994; Grün and Blau, 1997; Andreini et al., 2007; Lakova and Petrova, 2013; Benzaggagh, 2020). In environments with increasing fertility, they are not so well preserved (for instances, see Omaña et al., 2017, Kietzmann et al., 2021). In this situation, *Calpionellites darderi* can be confused with other *Calpionellites* species, *Praecalpionellites murgeanui* and some species of *Remaniella*. The FO of *C. darderi* is considered by the VWG as a relevant secondary marker. Indeed, according to Blanc et al. (1994) and Aguado et al. (2000), the FOs of *C. darderi* and *H. pertransiens* lie very close to each other (see also Bulot et al., 1996; this work). *Calpionellites darderi* has a relatively long stratigraphic range (lower Valanginian). This species is recorded in Mexico, Argentina and Mediterranean area (see below).

Around the B/V boundary, three biostratigraphically significant events have been identified both in the Vergol and Cañada Luenga sections (Figs. 13, 31). They are the successive FOs of *P. murgeanui*, *C. darderi* and *Calpionellites major*. This homotaxial succession has been consistently recorded throughout the Tethyan Realm (Pop, 1986, 1994, 1997; Reháková, 1995; Blanc, 1996; Lakova et al., 1997, 1999; Reháková and Michalik, 1997a, b; Lukeneder and Reháková, 2004; Pszczółkowski and Myczyński, 2004, 2010; Andreini et al., 2007; Benzaggagh et al., 2012; Petrova and Metodiev, 2012; Lakova and Petrova, 2013;

Omaña et al., 2017; Benzaggagh, 2020). These calpionellid events have also been robustly correlated with ammonite successions (Le Hégarat and Remane, 1968; Allemann et al., 1975; Allemann and Remane, 1979; Company and Tavera, 1982; Vašíček et al, 1983, 1994, 1999; Pop, 1989; Blanc et al., 1994; Aguado et al., 2000; Lukeneder and Reháková, 2004, 2007; Pszczółkowski and Myczyński, 2004; Főzy et al, 2010; Petrova et al., 2011; Kietzmann et al., 2021; and this paper) and calibrated against the magnetostratigraphic scale (Channell and Grandesso, 1987; Channell et al., 1987; Ogg et al., 1988; Aguado et al., 2000; Grabowski et al., 2016, 2019a; Kietzmann et al., 2021; Lodowski et al., 2022).

The FO of *P. murgeanui* is recorded in the middle part of Chron M15n and correlates with the lower part of the *H. otopeta* Subzone. This event was used by Pop (1986) to define the base of the uppermost subzone of the *Calpionellopsis* Standard Zone. This *P. murgeanui* Subzone has been maintained in most of the subsequently proposed zonal schemes (Pop, 1994; Blanc, 1996; Grün and Blau, 1997; Lakova et al., 1997; Reháková and Michalík, 1997b; Ölveczká and Reháková, 2022). It has been recognized throughout the Mediterranean area, from Morocco to Greece and Romania, and also in Cuba.

The *Calpionellites* Zone, the highest of the Rome standard zonation agreed upon by Allemann et al. (1971), was originally defined as the interval between the FO of *C. darderi* and the disappearance of the calpionellids. Later, Borza (1984) reduced the extent of the zone to that of the total range of *C. darderi*, and Pop (1994) subdivided this short *Calpionellites* Zone into two subzones (the *C. darderi* Subzone below and the *C. major* Subzone above), using the FO of the latter species as the limit between both. This scheme has been adopted by practically all subsequent authors (Grün and Blau, 1997; Lakova et al., 1997; Reháková and Michalík 1997b; Andreini et al., 2007; Ölveczká and Reháková, 2022). Assemblages with *C. darderi* have been reported from throughout the Mediterranean-Caucasian Subrealm (from Morocco to Iran) and also from the Caribbean (Mexico and Cuba) and Andean (Argentina) basins. The FO of *C. darderi* correlates with the lower part of Chron M14r and the upper part of *H. otopeta* Subzone.

The FO of *C. major* is located within Chron M14r, in the lower to middle part of the *N. premolicus* Subzone. The FO of *Calpionellites caravacaensis* is recorded somewhat higher, near the boundary between the *N. premolicus* and the *N.* (*V.*) *salinarium* subzones, both in Vergol and in Cañada Luenga. These two species of *Calpionellites* with cylindrical loricae have been identified in assemblages throughout the western Tethys, from Mexico to Iran (Benzagagh et al., 2012; Jiménez-López et al., 2021).

Calcareous dinoflagellate cysts

The zonation based on calcareous dinoflagellate cysts is considered a useful tool for interregional correlation. Upper Berriasian and Valanginian deposits studied worldwide (summarized in Ivanova and Kietzmann, 2017) contain a cyst association consisting of *Stomiosphaera wanneri, Colomisphaera vogleri, Colomisphaera conferta, Colomisphaera heliosphaera, Cadosina minuta, Cadosina semiradiata semiradiata, Cadosina semiradiata fusca, Cadosina semiradiata cieszynica, Cadosina semiradiata olzae, Carpistomiosphaera valanginiana*, *Colomisphaera lucida, Cadosinopsis nowakii* and *Stomiosphaera echinata*. Apart from the last five mentioned cysts, the others were documented in the Vergol section (Fig. 13). Here, in accordance with similar profiles, most of the cysts mentioned above are rather rare to scarce, and only *C. minuta*, which forms clusters of several cysts, is more frequent. Thus, the *S. wanneri*, *C. vogleri* and *C. conferta* cyst zones (sensu Grabowski et al., 2016; Ivanova and Kietzmann, 2017; Kietzmann et al., 2023) could be considered as indicative of a late Berriasian to early Valanginian age of the deposits exposed in the Vergol section. A more precise determination of the Berriasian–Valanginian successional cyst events still needs to be verified in the future. The distributions of the above-mentioned taxa according to different authors are given in Figure S5.

Palynofloral zonations worldwide

Lower Cretaceous palynofloral zonal schemes world-wide were described and discussed by Williams and Bujak (1985) and Stover et al. (1996). The latter authors stated that (a) the major gaps in dinoflagellate cyst zonations are the Upper Triassic and Cretaceous; and (b) several works have been published for Boreal regions, but few for tropical or subtropical sections. The (sub-)zones are listed below following Williams and Bujak (1985). This list is far from comprehensive; it is meant to give some idea of the large variations in taxa used by various authors and the changes in dinocyst assemblages.

Arctic: Most taxa listed in the assemblages of the *Sentusidinium cuculliforme - Paragonyaulacysta borealis* (late Berriasian–early Valanginian) and *Tanyosphaeridium magneticum* zones (Valanginian; Davies and Norris, 1980; Davies, 1983) were not recorded at Vergol. Although Pocock (1976) compared his zones ("Small spinate dinoflagellate cysts" Zone, Berriasian; *Biorbifera johnewingii* Zone, lower Valanginian) with the standard European ammonite succession and with the Arctic Canadian ammonite-pelecypod zonation of Jeletsky (1970), the age-assignments are questionable - e.g., Habib and Drugg (1983) illustrated *Dapsilidinium deflandrei* ranging not older then the late Valanginian whereas Monteil (1992a, b) recorded it from the uppermost part of the lower Valanginian.

Boreal: Davey (1979) defined the *Pseudoceratium pelliferum* Zone (upper Ryazanian–lower Valanginian; N.B.: Ryazanian is here considered as a regional stage nearly equivalent to the middle–late Berriasian, according to the Geological Time Scale, Gale et al., 2020). He compared his zonation with Early Cretaceous assemblages from Speeton (England), the western North Atlantic, SE France, Switzerland and California. Despite this, the Ryazanian/Valanginian boundary interval is poorly covered in Davey's scheme partly because of low-resolution and because of range differences between his predominantly Boreal data and data from Tethys.

Duxbury (1977, 2001, 2018, 2023) defined a zonation based on interval (sub-)zones, including LKP5 (upper Berriasian) to LKP7 (lower Valanginian). Most taxa used to define these were not recorded at Vergol and others were much rarer (see Duxbury, 2024). Duxbury (2018, fig. 2) highlighted events that occur in Speeton unit D4 (lower Valanginian, *Paratollia* = *Platylenticeras* Zone) and some of these are shown in Fig. 35 (after Duxbury, 2024, text-fig. 14) as they occur at Speeton and at Vergol. If the events listed in Fig. 35 were isochronous between Speeton and Vergol, it might imply that the B/V boundary at Speeton is currently drawn too low (see Duxbury, 2024, p. 615 for further discussion).

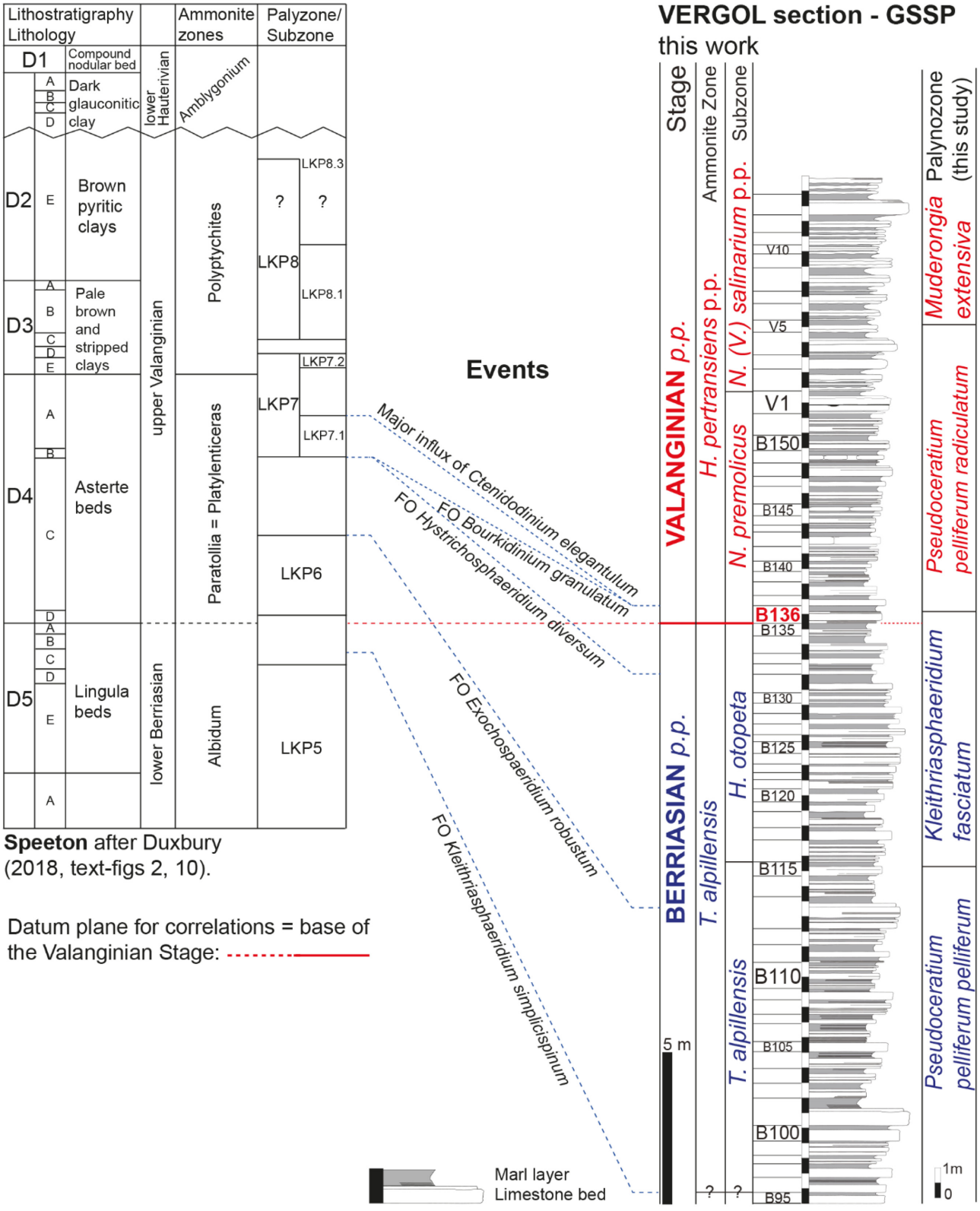

Figure 35. Some dinocyst events of the Vergol section correlated into the Speeton outcrop (England; after Duxbury, 2024, text-figure 14). If the correlation of events is further confirmed, this might imply that the Berriasian/Valanginian boundary in Speeton is currently drawn too low (see also Duxbury, 2024, p. 615).

According to Riley (1977) and Fisher and Riley (1980), their *Phoberocysta neocomica* Zone is subdivided into the *Dingodinium spinosum* (? upper Berriasian) and *Scriniodinium pharo* (lower Valanginian) subzones. This uses the LO of *D. spinosum* as a top Ryazanian marker. *Scriniodinium pharo* and *D. spinosum* were not recorded at Vergol. Riley (1977) used *Egmontodinium toryna* as an alternative for the top

of the Ryazanian (top *E. toryna* subzone). He emphasized that his zonation was valid for the Boreal Realm only.

Transitional: Williams et al. (1990) listed ten palynofloral zonation schemes for offshore Canada. The *Phoberocysta neocomica* Zone, as defined by Williams (1975), represents the entire Berriasian–Valanginian interval. The ranges of *Spiculodinium neptuni* and *P. neocomica* are restricted to this zone, and the range of *Biorbifera johnewingii* (index species of the subzone) is entirely within the lower part (Williams, 1975, fig. 5). All of these taxa range throughout the studied interval at Vergol.

Tethyan: See above "**Palynological events and zonations in the Tethys**" and Duxbury (2024).

Australasian: Berriasian–Valanginian dinocysts in Australasian biozonation schemes (Helby et al., 1987; Backhouse, 1987, 1988; Davey, 1988) are largely southern hemisphere-restricted and were largely absent from Vergol. Macrofaunal dating of sections analysed may be questionable in terms of chronostratigraphy and cannot be directly related to Tethyan ammonites. Helby et al.'s (1987) *Batioladinium reticulatum*, *E. toryna* and *Systematophora areolata* zones define their B/V boundary, which lies between the second and third of these zones. Their key species, *B. reticulatum* and *E. toryna,* occur at Vergol, but the first has a much younger range with its FO within Bed VGL-V48 (lower Valanginian; Duxbury, 2024). *Egmontodinium toryna* was very rare, occurring only in marl layers VGL-V5 and VGL-V26. The majority of accessory species named by Helby et al. were not recorded at Vergol.

Worldwide: All key taxa listed by Williams (1977) for the *Phoberocysta neocomica* Zone and its *Biorbifera johnewingii-Cribroperidinium orthoceras* Subzone (Berriasian–Valanginian) occur throughout the studied interval at Vergol.

Calcareous nannofossils

Since its definition (Worsley, 1971, emended by Thierstein, 1971), *Calcicalathina oblongata* has been reported to consistently occur in the lower part of the Valanginian in classical biozonation papers (Sissingh, 1977; Perch-Nielsen, 1985; Bralower et al., 1989; Bown et al., 1998). Even though the FO of *C. oblongata* is recorded later in the upper part of the *H. pertransiens* Zone in SE Spain (Cañada Luenga section; Aguado et al., 2000; this work), the FO of *C. oblongata* is considered by the VWG as a good secondary marker to approximate the base of the Valanginian considering that the discrepancy in the identification is probably related to different taxonomical concepts (see Kenjo et al., 2021, their appendix B, for further explanations on the taxonomy and identification of this taxa). *Calcicalathina oblongata* is characterized by a long stratigraphic range (lower Valanginian–lower Barremian). This taxon is relatively rare but recorded consistently in samples of hemipelagic and pelagic sections; it is very rare to absent in shelf facies. *Calcicalathina oblongata* has a wide geographic distribution in the Tethyan Realm, but this species is not record in Boreal Realm (see below).

Tethyan Realm: According to Mutterlose (1992b), two provinces can be recognized: a Mediterranean Province (southern and central Europe, the Mediterranean area, Mexico and Cuba) and an Indo-Pacific Province (the southern Oceans and Australia).

Perch-Nielsen (1985) presented a synthesis of the available standard biozonations for the Cretaceous and their correlations to historical stratotypes. She based her correlation for the Berriasian–Valanginian interval on the papers of Sissingh (1977), Roth (1978), and Perch-Nielsen (1979). Perch-Nielsen (1985) stated that the range of nannofossil species can be subject to controversy due to potentially different taxonomic concepts between authors, but also to uncertainties in sample position. Although ammonite zones are not shown in this synthetic scheme, *C. oblongata* is reported to consistently occur in the basal Valanginian. Considering the CC3 Zone of Thierstein (1971) emended by Sissingh (1977) (base placed at the FO of *C. oblongata*), Perch-Nielsen (1985, page 340) stated "… In the North Sea, the FO of *C. oblongata* can be substituted by the FO of *S. colligata* and/or the FO of *C. salebrosum*. In the Boreal region, CC3 can be subdivided by the range of *Micrantholithus speetonensis* into CC3a and CC3b (with *M. speetonensis*) and CC3c".

Bown et al. (1998, fig. 5.1) proposed a synthesis of Tethyan nannofossil biostratigraphy including the Tethyan NC zones (after Roth, 1978, 1983; Bralower, 1987), NK zones (after Bralower et al., 1989) and CC zones (after Sissingh, 1977, 1978; Perch-Nielsen, 1979, 1985; Applegate and Bergen, 1988). Nannofossil events were calibrated against ammonite zones, although ammonite zones are not available for the DSDP sites studied by some of the aforementioned authors (e.g., Bralower et al., 1989) and are not provided by some reference papers (e.g., Perch-Nielsen, 1985), and it remains unclear how Bown et al. (1998) established such cross correlations. In fact, as an example, in Bralower et al. (1989) ammonite zones are only available for the Berrias and Broyons sections, where *C. oblongata* was not recorded. A correlation with the Boreal realm and a calibration with the magnetostratigraphic scale were also provided by Bown et al. (1998). In this reference work (based upon numerous papers, see their Introduction and their part 5.2), the FO of *C. oblongata* is placed in their fig. 5.1 at the base of the Valanginian, "Pertransiens Zone". As the attribution of such event to the base of Valanginian seems to be a common record in the papers cited above, its attribution to the "Pertransiens Zone" might be an indirect, interpreted datum. This scheme was reported in the Geologic Time Scale 2012 and 2016 (Ogg et al., 2012, 2016). In GTS 2020 (Gale et al., 2020), the FO of *C. oblongata* is placed in the basal part of their "*Tirnovella pertransiens* Zone", and the base of polarity Chron M14r occurs in the top part of their "*Tirnovella alpillensis* Zone". Kenjo et al. (2021, p. 19, their figs. 10 and 11) showed that the appearance of *C. oblongata* is generally reported in the basal Valanginian, thus it is typical for the lower part of this stage. These authors also discussed the report by Aguado et al. (2000) of the FO of *C. oblongata* from the upper part of the *H. pertransiens* Zone in SE Spain.

In SE France (Vocontian basin), the FO of *C. oblongata* (that defined the base of the NK-3 Zone) is consistently recorded in the lowermost part of the Valanginian Stage as recorded at Vergol (Kenjo et al., 2021; this work, Fig. 13), Angles (Duchamp-Alphonse et al., 2007, fig. 2), Montclus (Morales et al., 2013, fig. 6) and Orpierre (Charbonnier et al., 2013, fig. 2). In these sections, the nannofossil biostratigraphy is calibrated with the calpionellid and/or ammonite zonations, and stable carbon isotopes data are also available.

In Italy, the nannofossil zonation of some sections is calibrated with the magnetostratigraphic scale and carbon isotopes are also provided. At Capriolo (Lombardian basin), the integrated stratigraphy includes a calpionellid zonal scheme (Channell et al., 1987, fig. 11). Accord-

ing to the latter authors, the FO of *C. oblongata*, recorded just above the FO of *Calpionellites darderi*, occurs in the magnetic Chron CM14r (see also Kuhn et al., 2005, figs. 3 and 8). At Fiume Bosso (Umbria Apennines), the appearance of *C. oblongata* occurs in the basal part of CM14r (Bralower et al., 1989, fig. 3). In the Fonte Giordano section (Umbria Apennines), the latter authors observed the bioevent in CM14n (see their fig. 4). The distribution of calcareous nannofossil marker species is also reported in the Pusiano section (Lombardian basin). The FO of *C. oblongata* is recorded in the basal part of the magnetic Chron CM13. In the Chiaserna Monte Acuto section (Umbria-Marche), the FO of *C. oblongata* is recorded at the base of the former "*Thurmanniceras otopeta* Zone" (Sprovieri et al., 2006, figs. 2, 5; but in fig. 6, this event is put in the upper part of their "*S. boissieri* Zone"), so in the upper part of the Berriasian Stage. However, due to a variable sedimentation rate in various localities and to a very different thickness of magnetic chrons, the attribution to a precise magnetic chron might be problematic in some sections.

In Turkey (NW Anatolia), the *C. oblongata* Zone was recognized, and its lower boundary occurs in the basal part of the Valanginian (Özkan, 1993, figs. 2, 3). In Romania, the FO of the marker is recorded in the upper Valanginian of three sections (Melinte and Mutterlose, 2001, figs. 3-6). Thus, as underlined by these authors, "a notable difference in the FO of this species is obvious" as elsewhere in the Tethys this FO is observed in the lower Valanginian. In both publications, the nannofossil biostragraphy is calibrated with the calpionellid and/or ammonite zonations.

In the Atlantic Ocean, *C. oblongata* was recorded in several sites and the NK/NC-3 Zone was reported according to some works such as Roth (1978, fig. 3, site 391 DSDP Leg 44, site 534 DSDP Leg 76; 1983, fig. 6, site 534 DSDP Leg 76), Watkins and Bowdler (1984, fig. 2, tab. 1, site 535 DSDP Leg 77), Covington and Wise (1987, tab. 1, site 603 DSDP Leg 93), Applegate and Bergen (1988, fig. 5, ODP Leg 103), Bralower et al. (1989, fig. 9, DSDP 534A; fig. 10, DSDP 391C), Bornemann et al. (2003, fig. 2, DSDP 105- 534A-367), and Bergen (1994, fig. 2, tab. 1, DSDP 534).

In the Southern Ocean, Mutterlose and Wise (1990; east Antarctica, Weddell Sea, site 692B ODP Leg 113) noted the absence of important Valanginian index taxa such as *C. oblongata*. A calcareous nannofossil zonal scheme for the Indo-Pacific Province was suggested by Mutterlose (1992a, NW Australia, sites 765-766 ODP Leg 123) and he proposed a correlation with the zonations of the Tethyan (mainly based on the Mediterranean Province) and Boreal Realm (see also Mutterlose, 1992b). In the Pacific Ocean, Lozar and Tremolada (2003, figs. 2, 3, 4) recognized the NK-3 Zone in site 1149 ODP Leg 185 and underlined the scarcity and sporadic occurrence of *C. oblongata*. According to Bown (2005, fig. 3), this Tethyan zonal marker is absent in site 1213 DSDP Leg 198 (NW Pacific Ocean, Shatsky Rise) and rare in site 1214. This author used *Rhagodiscus dekaenelii* as proxy marker to identify the NK-3 Zone.

In North America, according to Bralower (1990), *C. oblongata* was not recorded in the studied sections of the Sacramento Valley (California). Concerning South America, in the Neuquén basin (Argentina), Bown and Concheyro (2004) noted the absence of *C. oblongata* as well as other standard index species of both Tethyan and Boreal affinity. Aguirre-Urreta et al. (2005, fig. 9) proposed a calibration of Neuquén nannofossil events against the ammonite zonation, and a comparison with Tethyan nannofossil events that is calibrated against the West Mediterranean ammonite zones.

Boreal Realm (Germany, England, The Netherlands, Greenland, North Sea, Barents Sea): As summarized by Möller et al. (2015), two zonal schemes have been proposed for this realm: (a) the BC zonation (Boreal Cretaceous) of Bown et al. (1998) that is derived from the work of Perch-Nielsen (1979), Jakubowski (1987), Crux (1989) and Mutterlose (1991); for the Ryazanian–Hauterivian interval, this zonation is based on material from sections in NE England (Speeton), NW Germany (Lower Saxony basin), North Sea basin and the Barents Sea; and (b) the LK zonation (Lower Kreide) of Jeremiah (2001) that is based on boreholes and sections from the North Sea basin, The Netherlands, England and Germany. Pauly et al. (2012a, fig. 9) proposed a detailed biostratigraphic zonal scheme (calcareous nannofossils and ammonites) for the Ryazanian–Hauterivian stages of NE Greenland that is correlated with existing Boreal zonations (NW Europe). According to these authors, Tethyan taxa are rare or absent in the studied area (*C. oblongata* is missing, see Pauly et al., 2012b). According to Jeremiah (2001), in the southern North Sea basin and onshore UK sections, *C. oblongata* is absent from the Boreal nannofossil assemblages. However, farther north, this taxon occurs in the lower Hauterivian (cf. his fig. 21; see the LO of this taxon noted in fig. 9 of Pauly et al., 2012a). Möller et al. (2015) also provided results for the Ryazanian–Hauterivian interval of the Wollaston Forland (NE Greenland). They proposed a correlation with the zonal schemes (ammonites and calcareous nannofossils) of northern Germany and Speeton (NE England), including the Tethyan ammonite biostratigraphy. These authors also discussed the characterization of the Ryazanian/Valanginian boundary, particularly in terms of calcareous nannofossil events (cf. LO of *Sollasites arcuatus*, FO of *Triquetrorhabdulus shetlandensis*, and FO *Micrantholithus speetonensis*) that occurs in the Wollaston Forland and in some other classical boreal areas (NW Europe, North Sea).

Chemical and Physical Stratigraphy

Carbon isotope stratigraphy

The Valanginian stage records the first positive carbon-isotope excursion of the Lower Cretaceous, namely the Weissert OAE (Erba et al., 2004) starting in the uppermost early Valanginian (lower part of the *Karakaschiceras inostranzewi* Zone; McArthur et al., 2007). No such isotopic event was recognized through the upper Berriasian–lower Valanginian interval; only relative minor variations in the carbon isotopic curve are recorded (see Weissert et al., 1998, fig. 2; Föllmi et al., 2006, fig. 3; Price et al., 2016, fig. 6). According to Cramer and Jarvis (2020; GTS, fig. 11.12), the $\delta^{13}C_{carb}$ values fall towards an absolute Cretaceous minimum (lower than 1‰) in the top part of the Berriasian (LBeE = Late Berriasian Event); low values are also recorded in the basal part of the Valanginian.

In the Vergol (France) and Cañada Luenga (Spain) sections, two shifts toward low $\delta^{13}C_{carb}$ values are recorded just below (negative shift "b", blue arrow in Fig. 36; *T. alpillensis* (Sub-)Zone, Chron M15r) and just above (negative shift "h", red arrow in Fig. 36; *H. pertransiens* Zone, *N. premolicus* Subzone, upper part of Chron M14r) the B/V boundary. The interval between these two isotopic events is characterized by higher values, around +1‰. In order to complete the descrip-

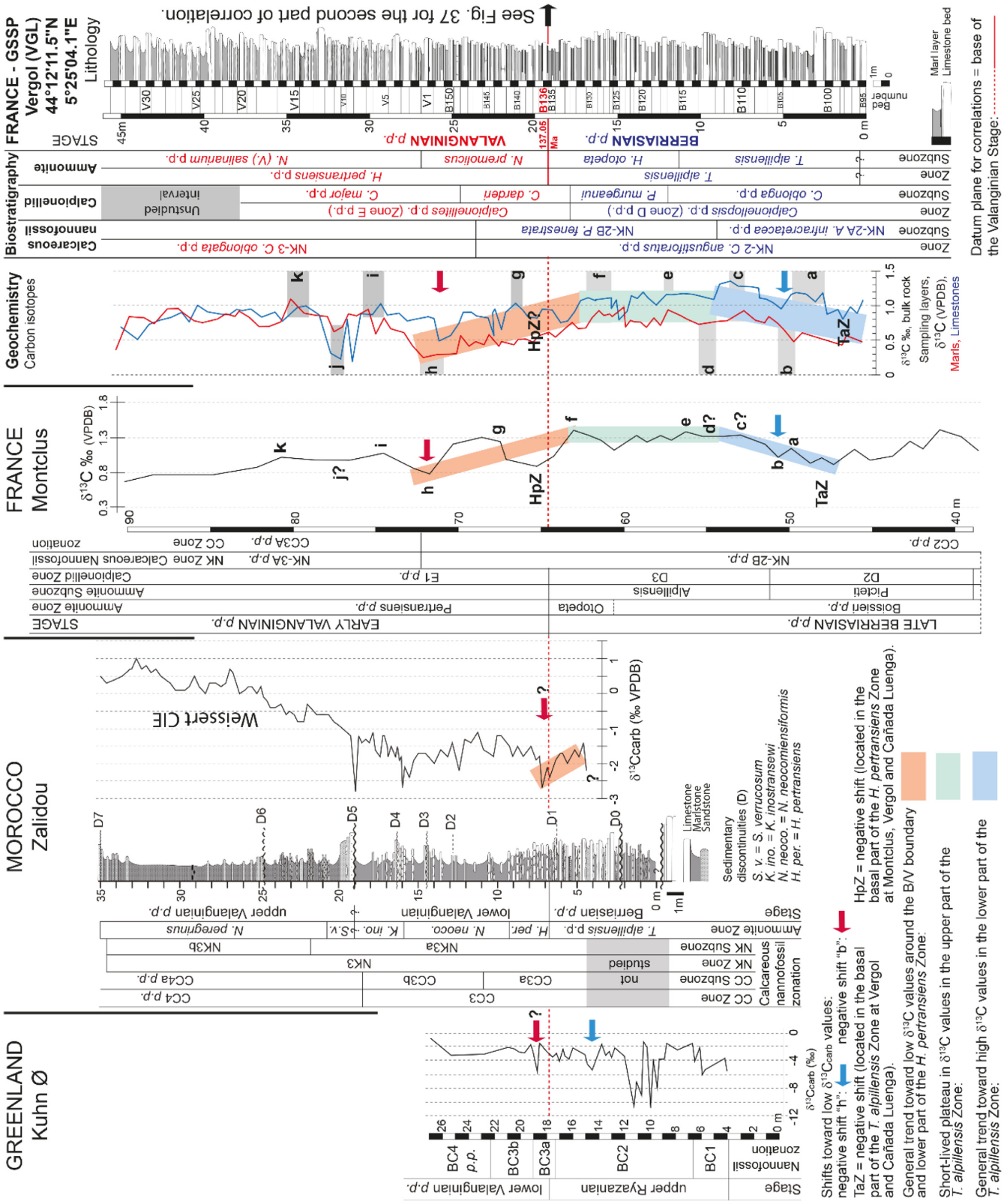

Figure 36. Carbon isotopic correlation of the Vergol section with other marine successions such as Montclus (France, after Morales et al., 2013), Zalidou (Morocco, after Reboulet et al., 2022) and Kuhn Ø (Greenland, after Pauly et al., 2013) calibrated by biostratigraphy. For correlation, the datum plane matches with the base of Valanginian characterized by biostratigraphic data. Carbon isotopic correlation with other sections, including Cañada Luenga, is continued in Fig. 37.

tion of the carbon isotopic curve of the Vergol section (see above), it is compared with another expanded section from the Vocontian basin, namely Montclus (carbon-isotope data in Morales et al., 2013). Previous peaks "a" to "k" identified at Vergol (and Cañada Luenga too) can

be recognized at Montclus and similar trends are recorded (Fig. 36). In the basal part of the Vergol section, the trend of the isotopic curve had to be interpreted carefully as no data are available below the *T. alpillensis* Zone. However, prior to small positive peak "a", lower $\delta^{13}C_{carb}$ values are recorded in the basal part of this zone (named "negative shift TaZ" in Fig. 36). This trend could be identified at Montclus, but just below the *T. alpillensis* Zone (N.B.: in this section, the zonal scheme was made by Le Hégarat (1973) and should be updated). At Cañada Luenga, this negative shift is not well marked and it is indicated with doubt (Fig. 37). At Vergol and Montclus, above an increase in values, a short-lived plateau in $\delta^{13}C_{carb}$ is recorded from peaks "d" to "f". Then, a general trend towards low $\delta^{13}C_{carb}$ values is observed in the interval around the B/V boundary, more precisely from peaks "f" to "h". In a more detailed description of the curves, it should be noted that, at Montclus, the boundary is characterized by a shift toward low $\delta^{13}C_{carb}$ values, named here "negative shift HpZ" (located between positive peaks "f" and "g"). This trend is less marked at Vergol and Cañada Luenga (Figs. 36, 37). In the framework of interregional correlations, it should be noted that small variations in the carbon isotopic curve may not be observed in more condensed sections (such as some sections in Italy or Hungary, see below) and/or in sections from which the sampling resolution is insufficient. Consequently, negative shifts (such as "b" and "h") of the carbon isotopic curve are indicated with a question mark on sections selected to illustrate the global correlation based on isotope stratigraphy.

In Morales et al. (2016), the Montclus section was correlated with three successions located in the Helvetic Alps (northern Tethyan carbonate platform). The authors noted an abrupt decrease in $\delta^{13}C_{carb}$ values (0.7‰) in the interval around the B/V boundary. In SE France, carbon-isotope stratigraphy was also provided for the Angles (Vocontian basin, Emmanuel and Renard, 1993; Duchamp-Alphonse et al., 2007), Orpierre (Vocontian basin, Charbonnier et al., 2013), and La Chambotte and Juracime (inner Jura Platfom, Morales et al., 2013) successions. Basinal sections were calibrated with the ammonite and/or calcareous nannofossil and/or calpionellid zonations. Reboulet et al. (2022) proposed a correlation between a French Valanginian composite basinal section (Angles-Vergol-La Charce) and some Moroccan successions characterized by carbon-isotope data. As invoked above for some successions, a shift toward low $\delta^{13}C_{carb}$ values (shift "h", red arrow in Fig. 36) is also recorded in the basal part of the Valanginian (*N. premolicus* Subzone) in the Zalidou, Aït Hamouch and Igouzoulen sections (Essaouira-Agadir basin).

In the Barlya section (Western Balkan, Bulgaria; Grabowski et al., 2016), the general trend of the carbon isotopic curve is similar to that observed at Vergol and Cañada Luenga: the negative shift "b" (blue arrow in Fig. 37) in the lower part of Chron M15r; a short-lived plateau in $\delta^{13}C_{carb}$ values occurring in Chron M15n and basal part of Chron M14r; and then, on the interval crossing the B/V boundary, a decrease in $\delta^{13}C_{carb}$ values to reach the negative shift "h" (red arrow) in Chron M14r. Grabowski et al. (2016) proposed to correlate the Barlya section with the Berrias section (Vocontian basin, carbon-isotope data in Emmanuel and Renard, 1993) where a shift toward low values also occurs in Chron M15r (Fig. 37). The uppermost part of the section must be interpreted carefully as recent work on magnetostratigraphy proposed a new scale without the record of chrons M15n and M14r (Wimbledon et al., 2024; see discussion below). According to this new result, the last shift toward higher values could correspond to the peak "c" or "e" observed at Cañada Luenga. Grabowski et al. (2021b) added a correlation with the Montclus section (Vocontian basin, carbon-isotope data in Morales et al., 2013); they noted a good coincidence of second-order variations between the $\delta^{13}C_{carb}$ of the three aforementioned sections.

In some sections of the Lombardian basin such as Capriolo, Polaveno (Fig. 37) and Pusiano, (northern Italy; Breggia, Switzerland), variations in $\delta^{13}C_{carb}$ are calibrated with the calcareous nannofossil zonation and magnetostratigraphy (Lini et al., 1992; Channell et al., 1987, 1993; Bersezio et al., 2002); calpionellid zonation is added for the Xausa section (Trento Plateau, northern Italy; Weissert and Channell, 1989), and Capriolo. For the Umbria-Marche basin (Chiaserna Monte Acuto section, central Italy), Sprovieri et al. (2006) provided a carbon-isotope composite record calibrated by calcareous nannofossil zonation. According to these all studies, from the upper part of the Berriasian up to the lower part of the Valanginian, the $\delta^{13}C_{carb}$ curve oscillates around an average value of 1.3‰ (Fig. 37; see also Weissert et al., 1998, fig. 2). Similar values with low variations in the $\delta^{13}C_{carb}$ curves are also recorded in the Lysonka section (western Carpathians, Poland, Grabowski et al., 2013) and Hárskút succession (Fig. 37; Bakony Mountains, Transdanubian Range, Hungary; Főzy et al., 2010; Lodowski et al., 2022). Concerning the latter section, the authors provided a high-resolution stratigraphic calibration using biostratigraphy and magnetostratigraphy. The Kryta Valley section (Tatra Mts, Western Carpathians, Poland) was calibrated using biostratigraphy (such as calpionellids and calcareous nannofossils), magnetic and stable-isotope stratigraphy (Grabowski et al., 2024). From the upper part of the Berriasian (M16n) up to the lower part of the Valanginian (M14n), the $\delta^{13}C_{carb}$ curve oscillates slightly around an average value of 0.7‰, and thus it is difficult to identify the negative shifts "b" and "h". Indeed, the latter (red arrow in Fig. 37) could be linked to the general trend toward low $\delta^{13}C$ values (observed after the short-lived plateau, see rectangles); however, this negative shift "h" is located in the basal part of Chron M14n at Kryta Valley, while this peak is dated from the top part of Chron M14r at Cañada Luenga. At Hlboča (Slovakia; Grabowski et al., 2010, fig. 11), $\delta^{13}C_{carb}$ values vary between 1.2 and 1.3‰ through chrons M17–M16; then, a decrease is recorded from the chrons M15 to M13 to reach 0.6‰.

Carbon-isotope data are also available for NE Mexico (Adatte et al., 2001), the Atlantic Ocean, such as Deep Sea Drilling Project (DSDP) site 535 (Gulf of Mexico; Robertson and Bliefnick, 1983), sites 534A and 603B (west Atlantic, Bornemann and Mutterlose, 2008). For hole 534A (Fig. 37), a minor shift toward low $\delta^{13}C_{carb}$ values is recorded in the basal part of Chron M15r; this could be interpreted as the negative shift "b". Another shift toward low $\delta^{13}C_{carb}$ values is observed in Chron M14r, very closely to the boundary NK-2/NK-3 calcareous nannofossil zones (the base of NK-3 Zone can be considered as a secondary marker to approximate the B/V boundary). Charbonnier et al. (2013) and Morales et al. (2013) correlated some typical French basinal sections (Angles, Orpierre and Montclus) with the site 534A. For the sites 416A (DSDP east Atlantic; Wortmann and Weissert, 2000) and 1149B (Ocean Drilling Project Leg 185, Pacific Ocean, Lozar and Tremolada, 2003), the resolution of the isotopic curves is low and the interval around the B/V boundary is probably not represented (see also Borneman and Mutterlose, 2008).

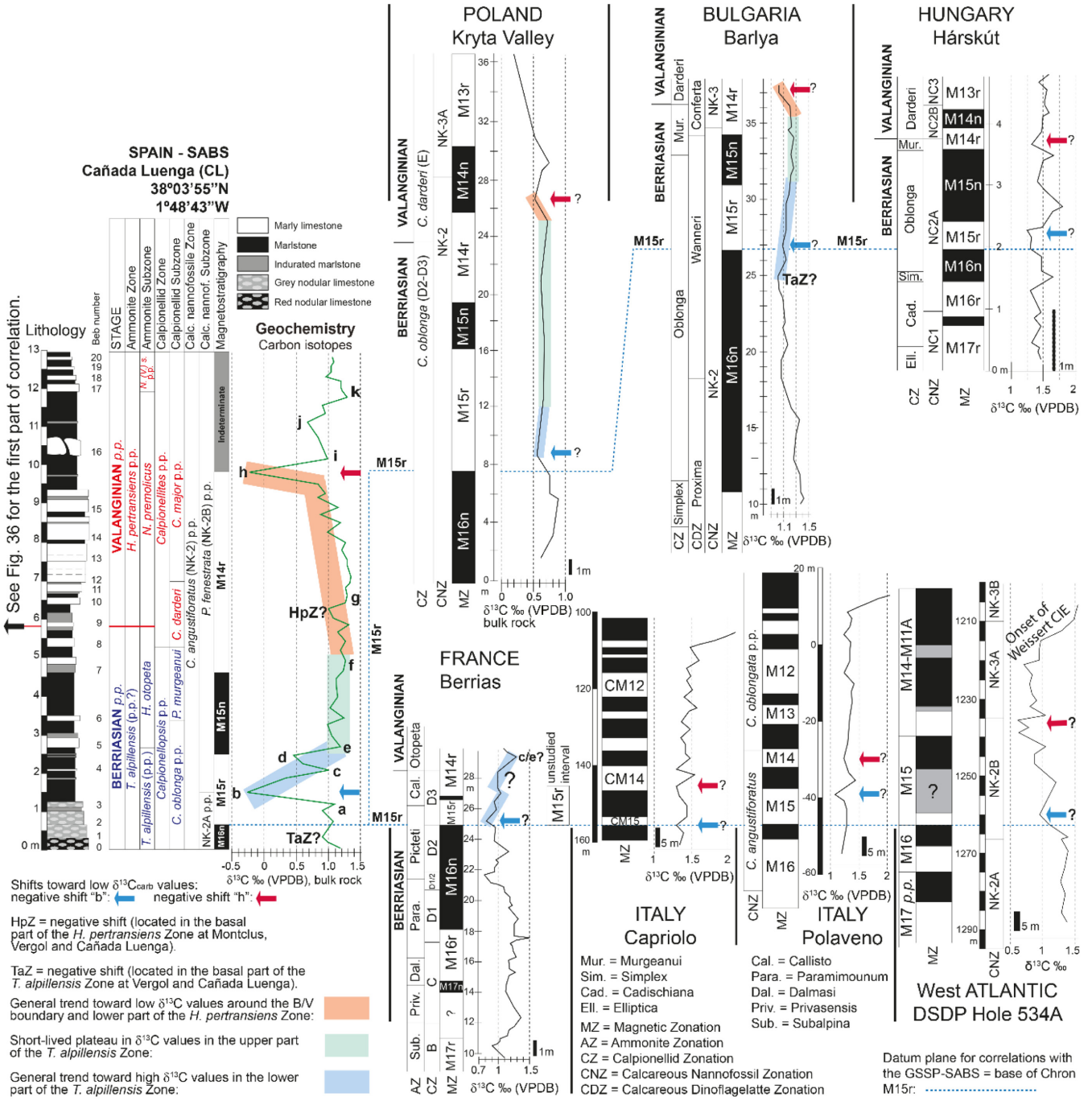

Figure 37. Carbon isotopic correlation of the Cañada Luenga section with other marine successions such as Berrias (France; section after Grabowski et al., 2016, 2021; on the right part, magnetic zonation after Wimbledon et al., 2024, see Fig. 38), Capriolo, Polaveno (Italy; sections after Channell et al., 1993 and Bersezio et al., 2002, respectively), Kryta Valley (Poland; section after Grabowski et al., 2024), Barlya (Bulgaria; section after Grabowski et al., 2021), Hárskút (Hungary; section after Lodowski et al., 2022), and Atlantic Ocean (DSDP Hole 534A after Bornemann and Mutterlose, 2008), calibrated by bio-magnetostratigraphy. The base of Chron M15r is used as the datum plane for correlation. Carbon isotopic correlation with other sections, including Vergol, is shown in Fig. 36.

Concerning the Boreal Realm, the Speeton section is characterized by carbon-isotope stratigraphy (McArthur et al., 2004). However, just two samples are available for the top part of the Berriasian stage, and the Berriasian–Valanginian interval is condensed or some strata are missing within the late Valanginian sequence. Mutterlose et al. (2014) compared these Boreal results with Tethyan data; the $\delta^{13}C$ values of the Boreal belemnites show the same long-term trend as the Tethyan ones, but they are in general by 1–2‰ more positive than the Tethyan data. Pauly et al. (2013) published the first carbon-isotope record ($\delta^{13}C_{carb}$ and $\delta^{13}C_{org}$) for the upper Ryazanian–Barremian interval of NE Greenland (Rødryggen and Kuhn Ø sections). They noted that $\delta^{13}C_{carb}$ values observed in their study are on average much lighter than contemporaneous values presented for the Tethyan bulk-rock carbonate (Weissert and Erba 2004) and belemnite guards (McArthur et al.,

2007). The minor negative shifts "b" and "h" are indicated with doubt on the Kuhn Ø section (Fig. 36).

Strontium isotope stratigraphy (SIS)

For Early Cretaceous time, the construction of $^{87}Sr/^{86}Sr$ trends (Figs. 22, 32, 33) is largely based on data coming from SE France and SE Spain, including the Vergol and Cañada Luenga sections, respectively (McArthur et al., 2007, 2020; Bodin et al., 2009, 2015; McArthur and Howarth, 2025).

Mutterlose et al. (2014) used SIS to resolve some of the difficulties of correlation between the Tethyan and Boreal realms in the Valanginian–Barremian interval. Their data were from Speeton (McArthur et al., 2004) and the Vocontian basin (McArthur et al., 2007; Bodin et al., 2009). According to Mutterlose et al. (2014; their fig. 3), the profile through the Boreal and the Tethyan realms show a good match. Nevertheless, these authors stated that "*the overlap of the two Sr-isotope curves highlights discrepancies between the Boreal and the Tethyan zonation schemes for the Valanginian/Hauterivian boundary and the lower/upper Barremian boundary*". Whether "discrepancies" is the appropriate term is moot: there seems to us to be no reason why Tethyan and Boreal zonal boundaries should coincide. Mutterlose et al. (2014) therefore both aided Tethyan–Boreal correlation and also highlighted minor zonal mismatches in existing correlations of that time. It is emphasised here that their fig. 3 repesents, in our view, a preliminary correlation of Tethyan and Boreal Realms and a correlation by SIS that can be substantially improved by further analysis of belemnites and brachiopods (which are readily available from multiple sites) to modern standards (to $\leq \pm 0.000004$ in $^{87}Sr/^{86}Sr$) at a greater sample density. This example therefore is for illustrative purposes only.

Möller et al. (2015, fig. 2) provided $^{87}Sr/^{86}Sr$-data for the upper Ryazanian and the Valanginian through the Rødryggen section (Wollaston Forland, NE Greenland). Data are for belemnite specimens. These authors noted a good match between the values of $^{87}Sr/^{86}Sr$ in Greenland and those from France, Spain and England (McArthur et al., 2004, 2007; Bodin et al., 2009). Of most importance, however, is that regression analysis of the $^{87}Sr/^{86}Sr$ data of Möller et al. (2015) predicts a value of 0.707293 ± 0.000003 (2.se., $n = 14$) for the Ryazanian/Valanginian boundary based on the ammonite zonal scheme of NE Greenland. This value is within uncertainty of the value of 0.707289 ± 0.000004 (2.se, $n = 12$) for the GSSP at Vergol. Further analysis could be made to test this point as material for analysis is not in short supply. Note that all samples of Möller et al. (2015) were > 0.15 m from the R/V boundary and that the boundary value was obtained by interpolation. These authors discussed the position of the Ryazanian/Valanginian boundary according to their data (cf. discrepancy of the ammonite and Sr-isotope based ages on one hand and the nannofossil findings on the other).

Magnetic stratigraphy

In the Cañada Luenga section, the base of the magnetic polarity Chron M14r occurs in the upper part of the *H. otopeta* Subzone, top part of the *P. murgeanui* calpionellid Subzone (Ogg et al., 1988; Aguado et al., 2000). Since then, in terms of magnetostratigraphy, the base of the Valanginian stage is consistently assigned to the lower part of Chron M14r (see the Geologic Time Scale, Ogg et al., 2012, 2016; Gale et al., 2020). The magnetic scale of the Cañada Luenga section can be drawn on the Vergol section according to a precise correlation based on an integrated calibration (see above; bio-chemio-cyclo-stratigraphy, Fig. 33; method of graphic correlations, Fig. 34). In terms of global correlations, this couple of sections will be correlated with (a) the Berrias section (SE France); (b) a set of sections along a European West–East transect; (c) sections and/or boreholes located in South America, Africa and Atlantic Ocean; and (d) two sections located in England and Colombia to establish correlations with continental successions.

Vergol-Cañada Luenga versus Berrias: At Berrias, the magnetostratigraphy was performed by Galbrun (1984, 1985; see also Galbrun and Rasplus, 1984, and Galbrun et al., 1986). According to Galbrun (1985, p. 134), "a correlation between BER.SZ.N.1 and Chron M15n seems improbable because of the short thickness of this polarity subzone". Ogg et al. (1988) did not correlate them either. However, subsequent authors such as Jan du Chène et al. (1993), and Blanc (1996) interpreted this small interval of normal polarity (layer 193/65 in Galbrun et al., 1986) as Chron M15n, and Grabowski et al. (2016, 2021b) followed that interpretation (Fig. 38). It should be noted that Galbrun (1985) included the top part of the section (beds 191 to 198) in his interval BER.Z.R.1 (see his fig. 5) that is correlated with Chron M15r. But it seems that he correlated the top of the BER.SZ.N.1 with the top of Chron M15n in his fig. 6 (see the dashed line). This could explain this interpretation made by some authors.

However, the presence and position of M15n in the Berrias section is difficult to accept from the point of view of ammonite and calpionellid stratigraphy in the Cañada Luenga section. According to Jan du Chêne et al. (1993), the base of their Chron M14r is reported in the upper part of the "Callisto Subzone" and so below the "Otopeta Subzone". For Blanc (1996, fig. 60), the base of this magnetic event (M14r) occurs in the "Otopeta Subzone" as the author lowered its base to nearly match with the base of Chron M15r. This is not in agreement with the current magneto-bio-stratigraphic calibration (see data on the Cañada Luenga section). Some discrepancies in the correlations based on the calpionellid zonation are also noted (Fig. 38). Indeed, at Cañada Luenga, the base of Chron M14r is recorded in the top part of the *P. murgeanui* Subzone. However, at Berrias, this magnetic event is stratigraphically lower, in a transitional interval covering the d3i and d3s calpionellid subzones, and the d3t subzone (= *P. murgeanui* Subzone) is not recorded (Blanc, 1996, figs. 56 and 60). This is further evidence that the interpretations of (the base of) M14r proposed by Jan du Chêne et al. (1993) and Blanc (1996) might be wrong. These issues might be partly due to the bad outcrop conditions for the top part of the section (cf. alluvial deposits of the river partly covering beds) that could be characterized by some condensed intervals and even stratigraphic gaps.

Recently, the magnetostratigraphy of the Berrias section was revised and calibrated with the biostratigraphy (Wimbledon et al., 2024). According to these authors, the top part of the section (including the layer 193) is characterized by Chron M15r and dated from the *C. oblonga* Subzone (Fig. 38). They did not recognize M15n and M14r. Therefore, the base of M15r was chosen as datum plane for the correlations of sections.

Vergol-Cañada Luenga versus a European W–E transect (France, Italy, Austria, Hungary, Poland, Bulgaria, Ukraine): Ogg et al.

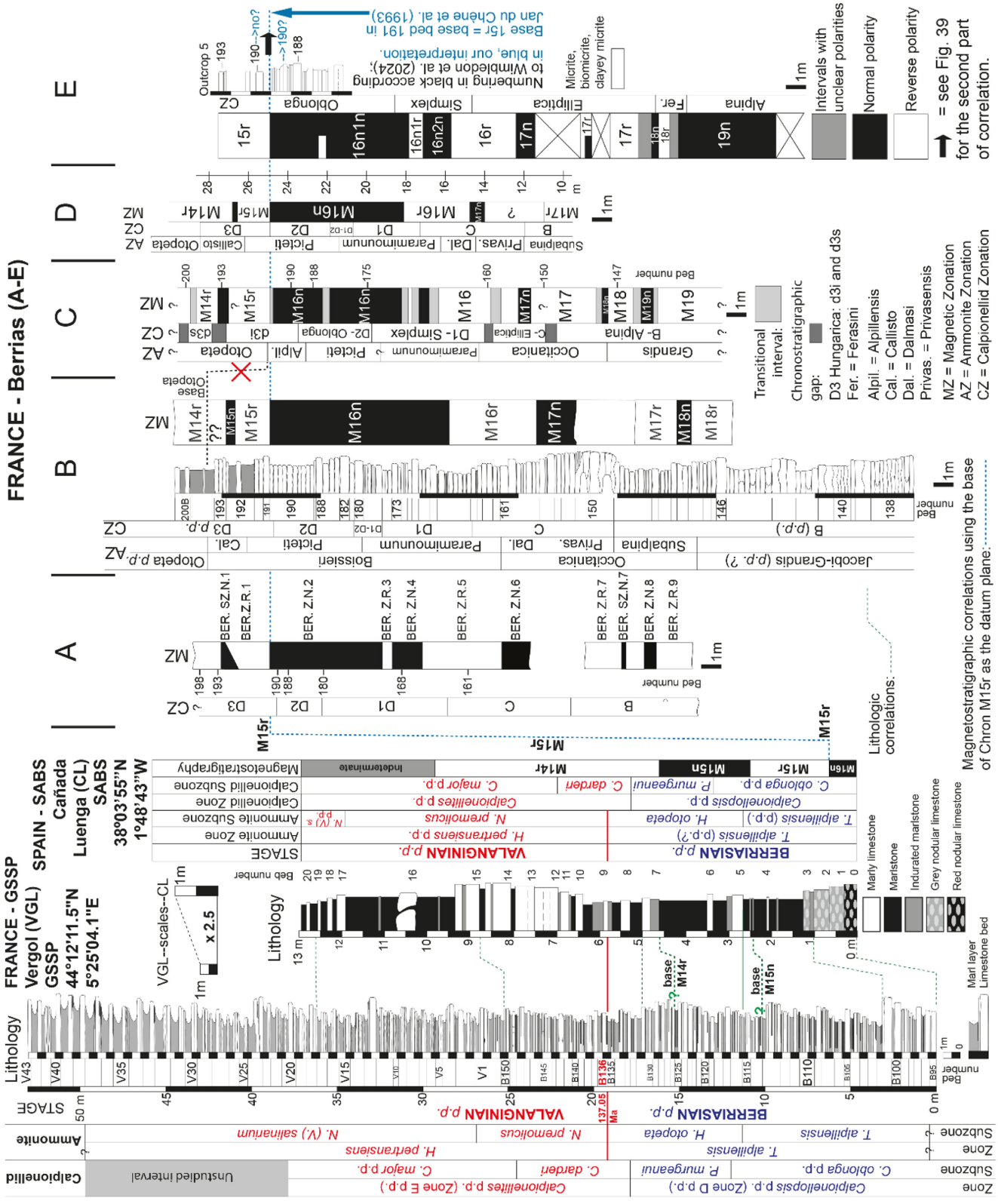

Figure 38. Magnetostratigraphic correlation of the Vergol-Cañada Luenga sections with the Berrias section: A, section after Galbrun (1984, 1985), Galbrun and Rasplus (1984), Galbrun et al. (1986); B, section after Jan du Chène et al. (1993); C, section after Blanc (1996); D, section after Grabowski et al. (2016, 2021b); E, section after Wimbledon et al. (2024). The base of Chron M15r is used as datum plane for correlation. Magnetostratigraphic correlation with other sections is continued in Fig. 39.

(1988) proposed a correlation of the Berrias section with others from Spain (Cehegín), central (Bosso) and northern (Capriolo and Xausa) Italy (Fig. 39). For the Italian sections, the base of Chron M14r is recorded in the upper part of the *Calpionellopsis* Zone (Zone D, i.e.

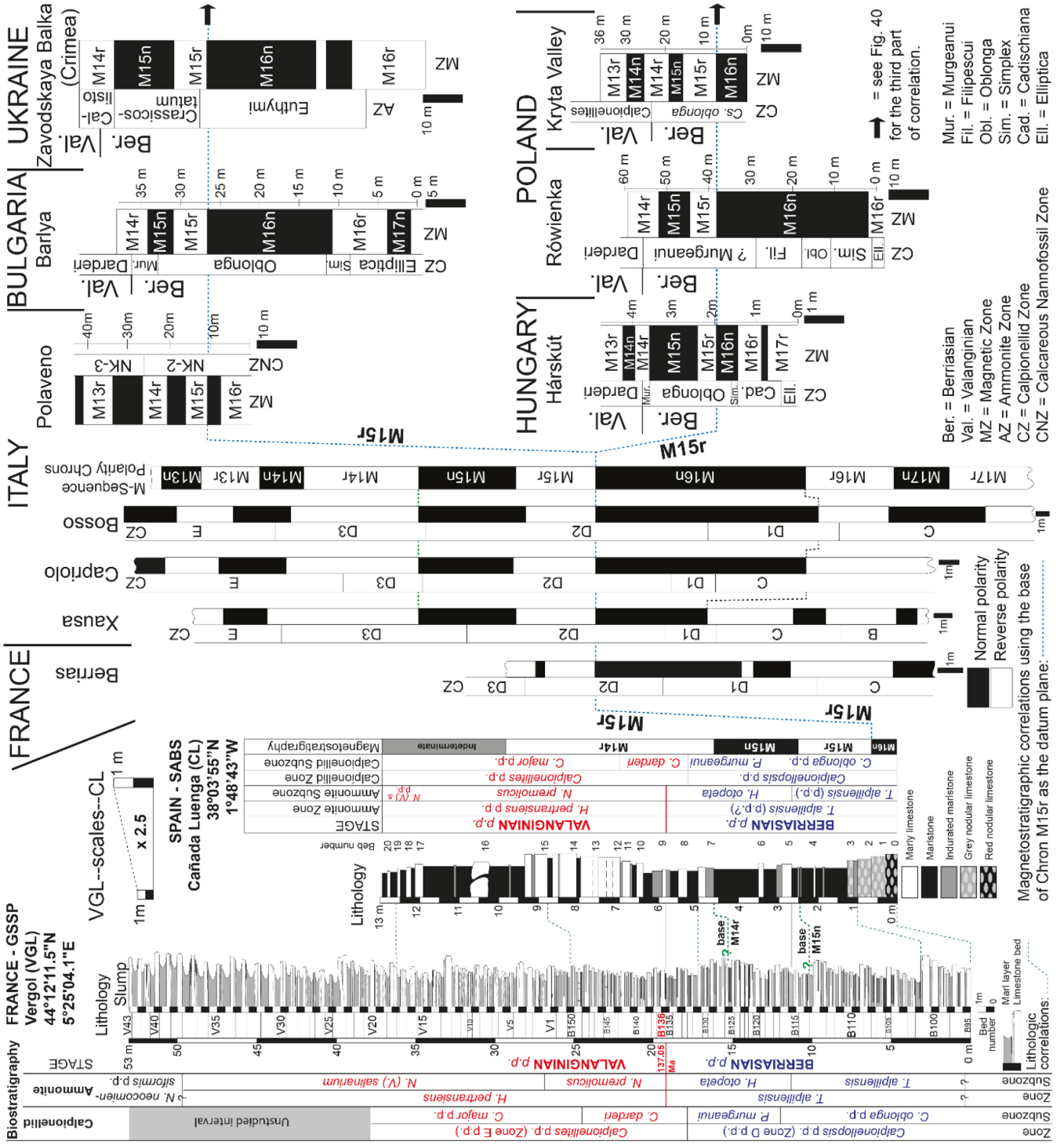

Figure 39. Magnetostratigraphic correlation of the Vergol-Cañada Luenga sections with other marine successions from France (Berrias section after Ogg et al., 1988), Italy (Xausa, Capriolo and Bosso sections after Ogg et al., 1988; Polaveno section after Bornemann and Mutterlose, 2008), Hungary (Hárskút section after Lodowski et al., 2022), Poland (Równienka section after Grabowski et al., 2019; Kryta Valley after Grabowski et al., 2024), Bulgaria (Barlya section after Grabowski et al., 2021), and Ukraine (Crimea, Zavodskaya Balka composite after Arkadiev et al., 2017). The base of Chron M15r is used as the datum plane for correlation. Magnetostratigraphic correlation with other sections is continued in Fig. 40.

H. otopeta Subzone) as observed at Cañada Luenga. The issue about the interpretation of M14r at Berrias clearly appears on this figure. It can be also noted in their work that the base of M15r occurs in the middle part of the Calpionellid D2 Subzone, while for Jan du Chêne et al. (1993) this magnetic event matches with the basal part of D3 Subzone. Channell et al. (1993) also provided an integrated study (magnetostratigraphic scale and carbon isotopic curve calibrated by a calcareous nannofossil zonation) on some Italian sections such as Capri-

olo (Fig. 39), Pusiano and Polaveno (see also Bornemann and Mutterlose, 2008; Fig. 39). Chron M14r is recorded in the central northern Calcareous Alps (Austria), however without detailed data (Krische et al., 2018). In agreement with data of the Cañada Luenga section (Aguado et al., 2000), the base of M14r is recorded in the top part of the *Calpionellopsis* Zone, *P. murgeanui* Subzone, of the Hárskút (Hungary, Lodowski et al., 2022; see also Főzy et al., 2010), Rówienka (Poland, Grabowski et al., 2019a) and Barlya (Bulgaria, Grabowski et al., 2016, 2021b; see also Lakova et al., 1999; Petrova et al., 2011) sections (Fig. 39). In the Kryta Valley section (Poland, Grabowski et al., 2024), the *P. murgeanui* Subzone is not recognized but the base of M14r is also recorded in the top part of the *Calpionellopsis* Zone. For

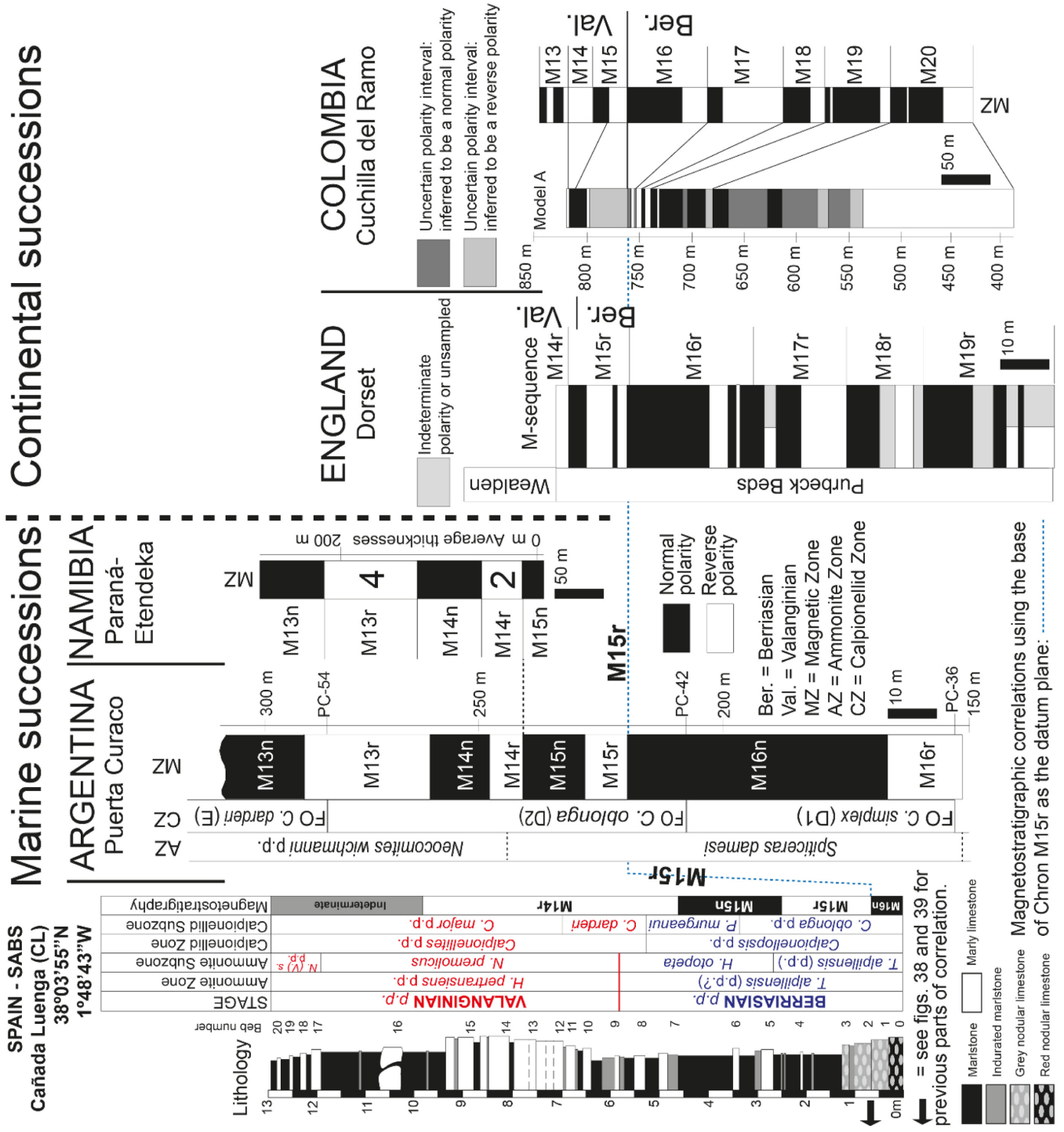

Figure 40. Magnetostratigraphic correlation of the Cañada Luenga section with other marine successions from Argentina (Puerta Curaco section after Kohan Martinez et al., 2017, including calpionellid-ammonite zonal schemes reported here from Kietzmann et al., 2021) and Namibia (Paraná–Etendeka composite section after Dodd et al., 2015); two continental successions located in England (Dorset composite section after Ogg et al., 1994) and Colombia (Cuchilla del Ramo section after Jiménez et al., 2021) are included. The base of Chron M15r is used as the datum plane for correlation. Magnetostratigraphic correlation with other sections is shown in Figs. 38 and 39.

the four sites, a calibration with nannofossil and/or ammonite zonations and/or a carbon isotopic curve is provided. For Ukraine (Crimea), Arkadiev et al. (2017, 2018) proposed a magnetic scale alongside the Zavodskaya Balka composite section in which the base of Chron M14r is dated from the top part of the Berriasian (Fig. 39).

Vergol-Cañada Luenga versus South America, Africa and Atlantic Ocean: In their cyclostratigraphic study performed on sequences of the Neuquén basin (Argentina), Kietzmann et al. (2015) interpreted that the top part of the Arroyo Loncoche section could correspond to the Chron M14r that is correlated with the base of the *Neocomites wichmanni* Zone (cf. Andean ammonite zonation). However, according to them, the succession above the M15n is an interval with no magnetic data. In the same basin, Kohan Martínez et al. (2017) studied the Puerta Curaco section characterized by a magnetostratigraphic scale (with unnamed chrons), but with no zonal scheme for dating. A few years later, this section was dated by the study of a calpionellid distribution and an ammonite zonation (Kietzmann et al., 2021). As the magnetostratigraphy is not reported in fig. 6 of the latter authors, we propose to report some calpionellid events in fig. 1 of Kohan Martínez et al. (2017). This allowed us to identify the magnetic chrons, mainly using the FOs of *C. simplex* and *C. oblonga* that are generally recorded in chrons M16r and M16n of the studied sections, respectively (Fig. 40). According to this pattern, the FO of *C. darderi* is observed in Chron M13r at Puerta Curaco; but it should be noted that this index species is represented by one sample and could occur earlier (in M14r as expected). However, our interpretation should be considered with caution. Dodd et al. (2015) reported an extensive magnetostratigraphic study for the Etendeka portion (in Namibia, Tafelkop section) of the Paraná–Etendeka LIP (Fig. 40). In the basal part of their composite magnetostratigraphy, Chron M14r is recorded. For the Atlantic Ocean, the DSDP holes 534A and 603B are characterized by a magnetostratigraphic scale (Ogg, 1983, 1987). According to Ogg (1987), "the Valanginian cannot be correlated between sites and do not match the M-sequence block model". However, in site 534A, the M14r seems to be recognized. These two boreholes were correlated with the Polaveno section (Bornemann and Mutterlose, 2008; see Fig. 37 for the correlation between the Polaveno section and DSDP hole 534A), showing in the three sites the trend in the carbon isotopic curve during the Valanginian.

Vergol-Cañada Luenga versus continental successions: A synthesis of Tethyan–Boreal correlations between marine and continental facies covering the Berriasian–Valanginian interval was made by Hoedemaker (1987). It should be noted that the B/V boundary is placed in his chart at the base of the *T. alpillensis* Zone, and the interpretation of his *T. pertransiens* Zone does not correspond to the current concept. The B/V boundary defined and largely characterized in marine successions can be correlated with the non-marine ones of the English Purbeck–Wealden stratotypes zoned by ostracods and palynomorphs (Allen and Wimbledon, 1991). Those authors proposed updated correlations between the north European Purbeck–Wealden onshore basins, and with global marine standards. Ogg et al. (1994), who provided a composite magnetic scale of the Portland and Purbeck Beds from the Dorset and Wilshire of southern England, noted that "the terrestrial to marginal-marine Purbeck Beds encompass polarity chrons M19r through M14r, implying deposition from latest Tithonian (Late Portlandian) to the beginning of the Valanginian stage" (Fig. 40). Another work allowing us a correlation with a non-marine succession is given by Jiménez et al. (2021) who provided a magnetostratigraphy of a thick continental succession (largely fluvial-facies sedimentary sequence) well exposed in the northern Andes (Colombia). According to their Model A (their fig. 11), the Chron M14 could be recorded in the top part of the Cuchilla del Ramo section (Fig. 40).

Synthesis

In order to summarize and complete previous parts on the global correlation, a compilation of marine successions is made for France and Spain (Table 4a), Europe (Table 4b), and South America and Africa (Table 4c). DSDP wells and continental successions are also reported (Table 4d). For each line (section/wells), a cross (or a circle) is put in the column (markers) when original/source data are available; main references are also indicated.

The Vergol section: Requirements for a GSSP and Series of Stratigraphic Markers

The Vergol Section and Requirements for a GSSP

Requirements and key features of the Vergol section for the GSSP of the Berriasian/Valanginian (B/V) boundary are presented in Table 5: geology and lithology (Table 5a), bio-chemical-physical stratigraphy (Table 5b), and accessibility, development and protection Table 5c).

Series of Stratigraphic Markers through the Vergol Section

The base of the Valanginian is defined at the base of limestone bed number VGL-B136. This level coincides with the First Occurrence (FO) of the ammonite species *Hoedemaekeria* (nov. gen.) *pertransiens* which marks the base of the *H. pertransiens* Zone.

Concerning the carbon isotope stratigraphy, a short-lived plateau in values (~1.1‰ in limestone; ~0.8‰ in marls) is recorded in the upper part of *T. alpillensis* Zone, and then a general trend toward low $\delta^{13}C$ values occurs across the B/V boundary to reach a negative shift in the lower part of the *H. pertransiens* Zone (~0.5‰ in limestone; ~0.3‰ in marls).

At the base of VGL-B136 (19.23 m), the predicted value of $^{87}Sr/^{86}Sr$ is 0.707289 (± 0.000004; 2.se, $n = 12$). The Valanginian GSSP is, for now, the only Cretaceous GSSP that has been profiled for $^{87}Sr/^{86}Sr$.

In addition to the primary marker, a series of secondary biostratigraphic events of inter-regional correlation value is provided in Table 6 in order to characterize the interval around the B/V boundary at the Vergol section.

Summary

The Global boundary Stratotype Section and Point (GSSP) for the base of the Valanginian Stage is the base of bed VGL-B136 at 19.23 metres in the Vergol Section (Montbrun-les-Bains, Drôme, France). This point is marked by the First Occurrence (FO) of the ammonite *Hoedemaekeria* (nov. gen.) *pertransiens* as primary marker. Additional

Table 4a. Lists of sections or wells representing marine palaeo-environments located in France and Spain (Table 4a), in other countries of Europe (Table 4b), and in South America and Africa (Table 4c); list of DSDP wells and continental successions (Table 4d). For each site, data available on biostratigraphy (A= ammonite, B = belemnite, C = calpionellid, N = calcareous nannofossil, CD = calcareous dinoflagellate, OD = organic dinoflagellate) and chemical-physical stratigraphy (C = carbon isotopes, Sr = strontium isotopes, Mag = magnetic scale) is indicated by a cross (x) or a circle (o). Main references are indicated; some of them can be consulted preferentially (* = see references therein)

Section	Location	Biostratigraphy					Chemical-physical stratigraphy			Reference
		A	B	C	N	CD=x OD=o	Isotope		Mag	
							C	Sr		
Vergol	France	x	x	x	x	x, o	x	x		McArthur et al. (2007) Gréselle et al. (2011) Martinez et al. (2013) Janssen (2021) Kenjo et al. (2021*) McArthur and Howarth (2025) Current work
Angles	France	x		x	x		x			Allemann and Remane (1979) Duchamp-Alphonse et al. (2007*)
Barret-le-Bas	France	x		x						Remane and Thieuloy (1973a) Allemann and Remane (1979) Thieuloy (1979) Blanc (1996)
Montclus	France	x		x	x		x			Morales et al. (2013, 2016*)
Orpierre	France			x	x		x			Charbonnier et al. (2013*)
Berrias	France	x		x	x	x, o	x		x	Galbrun et al. (1986) Emmanuel and Renard (1993) Jan du Chène et al. (1993*) Blanc (1996)
Ginestoux – Les Oliviers La Garenne	France	x		x						Le Hégarat and Remane (1968) Le Hégarat (1973)
La Faurie - Pusteau	France	x		x						Le Hégarat (1973) Remane and Thieuloy (1973b)
Majastres	France	x	x	x	x					Bulot (1995) Blanc (1996) Janssen (2021)
Cañada Luenga	Spain	x	x	x	x	x, o	x	x	x	Ogg et al. (1988) Aguado et al. (2000*) Janssen (2003, 2021) McArthur et al. (2007) Current work
Miravetes	Spain	x	x	x	x	o				Allemann et al. (1975) Hoedemaeker (1982) Hoedemaeker and Leereveld (1995) Janssen (1997, 2003) Leereveld (1997) Aguado et al. (2000*)

markers for correlation are provided. A Standard Auxiliary Boundary Stratotype (SABS) at Cañada Luenga section (Cehegin, SE Spain) demonstrates that this point corresponds to a level within magnetic Chron M14r.

Integrated Stratigraphy of the Berriasian/Valanginian Boundary of the Vergol Section

The Vergol section (Vocontian basin, SE France) is located in a parcel of land that belongs to the municipality of Montbrun-les-Bains (Departement of Drôme); as public property, the site is fully and permanently accessible. The outcrop conditions are highly suitable for accurate observations and high-resolution sampling.

The Berriasian/Valanginian (B/V) boundary was studied in a 53.12 m thick interval from beds VGL-B95 to VGL-V43 (Fig. 41). The succession is composed of a marl–limestone alternation, stacked hierarchically (see below), characterized by a continuous sedimentation (no gaps or condensation) and the absence of tectonic disturbance. This thick and expanded section has a very good sedimentary record; the average sedimentation rate is 23 m/Myr (see below).

The Vergol site is well correlated with other sections of SE France, from the Jura-Dauphinois to Provence platforms, *via* the Vocontian basin. This large transect allowed us to define a cyclostratigraphic framework, and four orders of depositional cycles were recognized (elementary and small/medium/large sequences). Coupled with a study on the depositional geometries, a reconstruction of sea-level fluctuations is proposed for the studied interval. It can be noted that the boundary level (VGL-B136) occurred during a sea-level highstand (Fig. 41). A correlation between the Vergol and Ait Hamouch (Morocco) sections shows that the major sequence boundaries Be8, Va1 and Va2 were recognized in

Table 4b. (continued)

Section	Location	Biostratigraphy					Chemical-physical stratigraphy			Reference
		A	B	C	N	CD=x OD=o	Isotope C	Isotope Sr	Mag	
(Fiume) Bosso	Italy			x	x				x	Channell and Grandesso (1987*) Ogg et al. (1988) Bralower et al. (1989)
Capriolo	Italy			x	x		x		x	Channell et al. (1987, 1993) Ogg et al. (1988)
Chiaserna Monte Acuto	Italy				x		x			Sprovieri et al. (2006)
Fonte Giordano	Italy				x				x	Bralower et al. (1989)
Polaveno	Italy				x		x		x	Bornemann and Mutterlose (2008)
Pusiano	Italy				x		x		x	Channell et al. (1993)
Xausa	Italy			x	x		x		x	Channell et al. (1987) Ogg et al. (1988) Weissert and Channell (1989)
Hollenstein an der Ybbs	Austria	x		x		x				Vašíček et al. (1999)
Klausriegler-Bach	Austria	x		x		x				Lukeneder and Reháková (2004)
Hochkogel	Austria	x		x		x				Lukeneder and Reháková (2007)
Hárskút	Hungary	x	x	x	x	x	x		x	Főzy et al. (2010) Price et al. (2016*) Lodowski et al. (2022)
Kapuśnica	Poland	x		x		x				Pszczółkowski and Myczyński (2004)
Kryta Valley	Poland			x	x	x	x		x	Grabowski et al. (2024)
Lysonka	Poland	x		x		x	x			Pszczółkowski and Myczyński (2004) Grabowski et al. (2013)
Rówienka	Poland			x			x		x	Grabowski et al. (2019a)
Strážovce	Slovakia	x	x	x	x	x				Vašíček et al. (1983)
Mráznické Lúcky	Slovakia			x		x				Vašíček et al. (1983)
Brodno	Slovakia			x		x				Vašíček et al. (1994)
Hlboč	Slovakia			x		x	x			Vašíček et al. (1994) Grabowski et al. (2010)
Barlya	Bulgaria	x		x	x	x	x		x	Lakova et al. (1999) Petrova et al. (2011) Grabowski et al. (2016, 2021*)
Zavodskaya Balka	Ukraine (Crimea)	x							x	Arkadiev et al. (2017, 2018)
Speeton	England	x			x	o	x	x		McArthur et al. (2004*) Mutterlose et al. (2014) Duxbury (2018)
Rødryggen	Greenland	x			x		x	x		Pauly et al. (2012a, b, 2013) Möller et al. (2015) McArthur and Howarth (2025)

Table 4c. (continued)

Section/well	Location	Biostratigraphy					Chemical-physical stratigraphy			Reference
		A	B	C	N	CD=x OD=o	Isotope C	Isotope Sr	Mag	
Puerta Curaco	Argentina	x		x					x	Kohan Martínez et al. (2017) Kietzmann et al. (2021)
Cuesta del Chihuido	Argentina	x		x		x				Kietzmann et al. (2021, 2023)
Narambuena block (wells 1-3)	Argentina			x		x				Kietzmann et al. (2021, 2023)
Zalidou, Aït Hamouch	Morocco	x			x			x		Reboulet et al. (2022*)
Tafelkop	Namibia								x	Dodd et al. (2015)

Table 4d. (continued)

Well/section	Location	Biostratigraphy					Chemical-physical stratigraphy			Reference
		A	B	C	N	CD=x OD=o	Isotope C	Isotope Sr	Mag	
DSDP 535	Gulf of Mexico				x		x		x	Bornemann and Mutterlose (2008*)
DSDP 534A DSDP 603B	West Atlantic				x		x		x	Bornemann and Mutterlose (2008*) Price et al. (2016*)
Dorset (continental succession)	England								x	Ogg et al. (1994*)
Cuchilla del Ramo (continental succession)	Colombia								x	Jiménez et al. (2021)

Table 5a. Key features of the Vergol section for geology and lithology (Table 5a), bio-chemical-physical stratigraphy (Table 5b), and accessibility, development and protection (Table 5c)

GEOLOGY and LITHOLOGY	Vergol section (Montbrun-les-Bains, France, Vocontian basin)
Exposure over an adequate thickness.	Yes. 53 m thick, from beds VGL-B95 to VGL-V43.
Continuous sedimentation. No gaps or condensation close to the boundary.	Yes. A basinal and expanded section without gaps or condensation.
Rate of sedimentation.	According to the astrochronology, the average sedimentation rate is around 23 m/Myr.
Absence of synsedimentary or tectonic disturbance.	Yes, both factors can be excluded. There is a slump, but 35 m above the B/V boundary.
Absence of metamorphism and strong diagenetic alteration.	Yes, both factors can be excluded. According to the clay mineralogy, the influence of diagenesis was not sufficient to profoundly modify the initial detrital composition of the clay assemblages.
Absence of vertical facies changes at/near the boundary.	Yes. From the base to the top of the section, there is a uniform lithology made by a monotonous marl-limestone alternation.
Favourable facies for long range correlations.	Yes. Located in open marine environment and characterized by a hemipelagic facies, the section is suitable for long distance correlations.

Table 5b. (continued)

BIO-CHEMICAL-PHYSICAL STRATIGRAPHY	Vergol section (Montbrun-les-Bains, France, Vocontian basin)
Biostratigraphy.	Abundant and diverse of generally well-preserved ammonoids, belemnites, calpionellids, nannofloras and dinoflagellates (and other palynomorphs). The section is also characterized by ichnofossils and microfacies study.
Chemostratigraphy.	Accurate carbon, oxygen and strontium isotope stratigraphy available. Carbonate, organic and phosphorus contents also analysed.
Sequence stratigraphy.	Cyclostratigraphic framework available. Four orders of depositional cycles are recognized. The major sequence boundaries are identified in the northern (France, including Vergol) and southern (Morocco) margins of the Tethys Ocean.
Astrochronology.	Available. Obtained from the detection of the Milankovitch cycles from the Gamma-Ray Total Count and Mass Magnetic Susceptibility signals. The age model, based on astrochronology performed on the Vergol section and anchored on a radioisotopic age from the Neuquén basin (Argentina), allows us to date the base of the Valanginian Stage (= base of the *H. pertransiens* ammonite Zone) at 137.05 Ma (± 0.2 Ma), and the base of ammonite (sub-)zones (and therefore their numerical durations).
Magnetostratigraphy.	No. Palaeomagnetic investigations (both thermal and alternating field demagnetization methods) reveal that the Vergol section is remagnetized. However, an integrated stratigraphy provides an accurate correlation with the Cañada Luenga SABS characterized by magnetic chrons.
Chronometry.	No. But see astrochronology for an age model.

Table 5c. (continued)

ACCESSIBILITY, DEVELOPMENT and PROTECTION	Vergol section (Montbrun-les-Bains, France, Vocontian basin)
GSSP indicated by a permanent marker.	A permanent marker will be placed.
Physical and logistical accessibility.	Section very close of the road (D159) with car park. Large area of exposure. Very good outcrop conditions highly suitable for accurate observations and high-resolution sampling.
Free access for research.	Open access from public. Section fully and permanently accessible for researchers as it is public property.
Permanent protection of the site.	Section located in the "Parc Naturel Régional des Baronnies Provençales". Substantial public support also provided by the Montbrun-les-Bains municipality and the Council of the Drôme Department. These institutions are engaged in the development and protection of the site (in preparation).

Table 6. Series of primary and secondary biological markers along the Vergol section. See also Fig. 4 for the indications of cumulative thicknesses (in meter, measured from the base of the section) of the Vergol section

Bed number M (Marl layer) L (Limestone layer)	Meter at the base (b) or top (t) of layer	Event LO (Last Occurrence) FO (First Occurrence)
VGL-V5 (L)	28.87 (b)	FO *Berriasibelus exstinctorius* (belemnite)
VGL-V4 (L)	28.11 (b)	FO *Micrantholithus speetonensis* (calcareous nannofossil)
VGL-V2 (L)	26.91 (b)	FO *Neolissoceras* (*Vergoliceras*) *salinarium* (ammonite) and *Calpionellites caravacaensis* (calpionellid)
VGL-B150 (M)	25.27 (b)	FO *Castellanibelus orbignyanus* (belemnite)
VGL-B149 (L)	24.54 (b)	FO *Calpionellites major* (calpionellid)
VGL-B146 (M)	23.57 (b)	FO *Calcicalathina oblongata* (calcareous nannofossil)
VGL-B142 (M)	22.08 (b)	occurrence *Thalassiphora*? *charollaisii* (organic dinoflagellate)
VGL-B141 (L)	21.27 (b)	FO *Neocomites premolicus* (ammonite)
VGL-B137 (L)	19.80 (b)	FO *Hoedemaekeria* (nov. gen.) *gratianopolitense* (ammonite)
VGL-B136 (L)	**19.23 (b)**	**FO *Hoedemaekeria* (nov. gen.) *pertransiens* (ammonite)**
VGL-B135 (L)	19.04 (t)	LO *Hoedemaekeria* (nov. gen.) *otopeta* and *Berriasella calisto* (ammonite)
VGL-B133 (L)	17.89 (b)	FO *Calpionellites darderi* and *C. coronatus* (calpionellid)
VGL-B129 (L)	16.46 (t)	LO *Tirnovella alpillensis* (ammonite)
VGL-B119 (L)	12.98 (b)	FO *Colomisphaera conferta* (calcareous dinoflagellate)
VGL-B117 (L)	12.05 (b)	FO *Praecalpionellites murgeanui* (calpionellid)
VGL-B116 (L)	11.33 (b)	FO *Hoedemaekeria* (nov. gen.) *otopeta* (ammonite)
VGL-B112 (M)	9.03 (b)	FO *Percivalia fenestrata* (calcareous nannofossil)
VGL-B110 (M)	7.28 (b)	FO *Muderongia mcwhaei* (organic dinoflagellate)
VGL-B107 (L)	5.97 (b)	FO *Colomisphaera vogleri* (calcareous dinoflagellate)
VGL-B96 (L)	0.38 (b)	FO *Tirnovella alpillensis* (ammonite)
VGL-B95 (L)	0 m (b)	Base of this bed = base of the section

the northern and southern margin of the Mesozoic Tethys Ocean, respectively.

Macro/microfossils are generally abundant, diverse and well preserved. Ammonites, belemnites, calpionellids, calcareous nannofossils and calcareous dinoflagellate cysts, palynomorphs (including organic-walled dinoflagellate cysts), ichnofossils and microfacies were studied with high-resolution sampling and analysis. At Vergol, the base of the Valanginian is defined at the base of limestone bed VGL-B136 (base of layer at 19.23 m) that coincides with the FO of *Hoedemaekeria pertransiens* which, as index species, also marks the base of the first Valanginian ammonite zone (Fig. 41). The ammonite data/results from two authors (J. Klein and S. Reboulet) are largely in agreement. The FO of *Castellanibelus orbignyanus* (belemnite) is recorded in marl layer VGL-B150 (base of layer at 25.27 m). The microfossil events that best approximate the B/V boundary are the FO of *Calpionellites darderi* (calpionellid) in limestone bed VGL-B133 (base of layer at 17.89 m) and the FO of *Calcicalathina oblongata* (calcareous nannofossil) in marl layer VGL-B146 (base of layer at 23.57 m). Other secondary biostratigraphic markers include the FO of *Colomisphaera conferta* (calcareous dinoflagellate) recorded in limestone bed VGL-B119 (base of layer at 12.98 m). Two organic-walled dinoflagellate cysts events might be of particular significance for regional value: an isolated occurrence of *Thalassiphora*? *charollaisii* in marl layer VGL-B142 (base of layer at 22.08 m) and the FO of *Muderongia mcwhaei* in marl layer VGL-B110 (base of layer at 7.28 m).

Concerning the carbon isotope stratigraphy, both marls and limestones displays the same long-term trend in $\delta^{13}C$ values in the interval around the B/V boundary: a short-lived plateau in values (~1.1‰ in limestone; ~0.8‰ in marls) in the upper part of the *Tirnovella alpillensis* ammonite Zone, and then a general trend toward low $\delta^{13}C$ values occurring across the B/V boundary to reach a negative shift in the lower part of the *H. pertransiens* ammonite Zone (~0.5‰ in limestone; ~0.3‰ in marls; Fig. 41). Strontium isotope stratigraphy (based on belemnites) is available for the Vergol section. According to the curve, the predicted value of $^{87}Sr/^{86}Sr$ at the B/V boundary is 0.707289 ± 0.000004 (2.se, n = 12).

Vergol is a suitable reference section to establish an astronomical time scale of the studied interval (detection of the Milankovitch cycles from the GRTC and MS signals). Five 405-kyr eccentricity cycles are identified; for each of these, a sedimentation rate is proposed (Fig. 41). For the B/V sequence covering the boundary, the value is 17 m/Myr. A rate increase is observed for the Valanginian sequences to reach 26.5 m/Myr for V1 and 29 m/Myr for V2. Comparatively, both Berriasian sequences are characterized by lower sedimentation rates, 23.5 m/Myr for T.A.-405-1 and 18 m/Myr for T.A.-405-2. This is in agreement with the study of ichnofossils as only these two Berriasian sequences are characterized by the presence of *Zoophycos*, considering that their installation and development are partly explained by a low(er) sedimentation rate.

The floating ages of the 405-kyr eccentricity cycles are anchored on a CA-ID-TIMS U-Pb age obtained from zircons coming from a tuff layer in the Neuquén basin (Argentina, lower Hauterivian). This radioisotopic age is tied to the ammonite zonation recognized in this basin which in turn is correlated with the Mediterranean standard

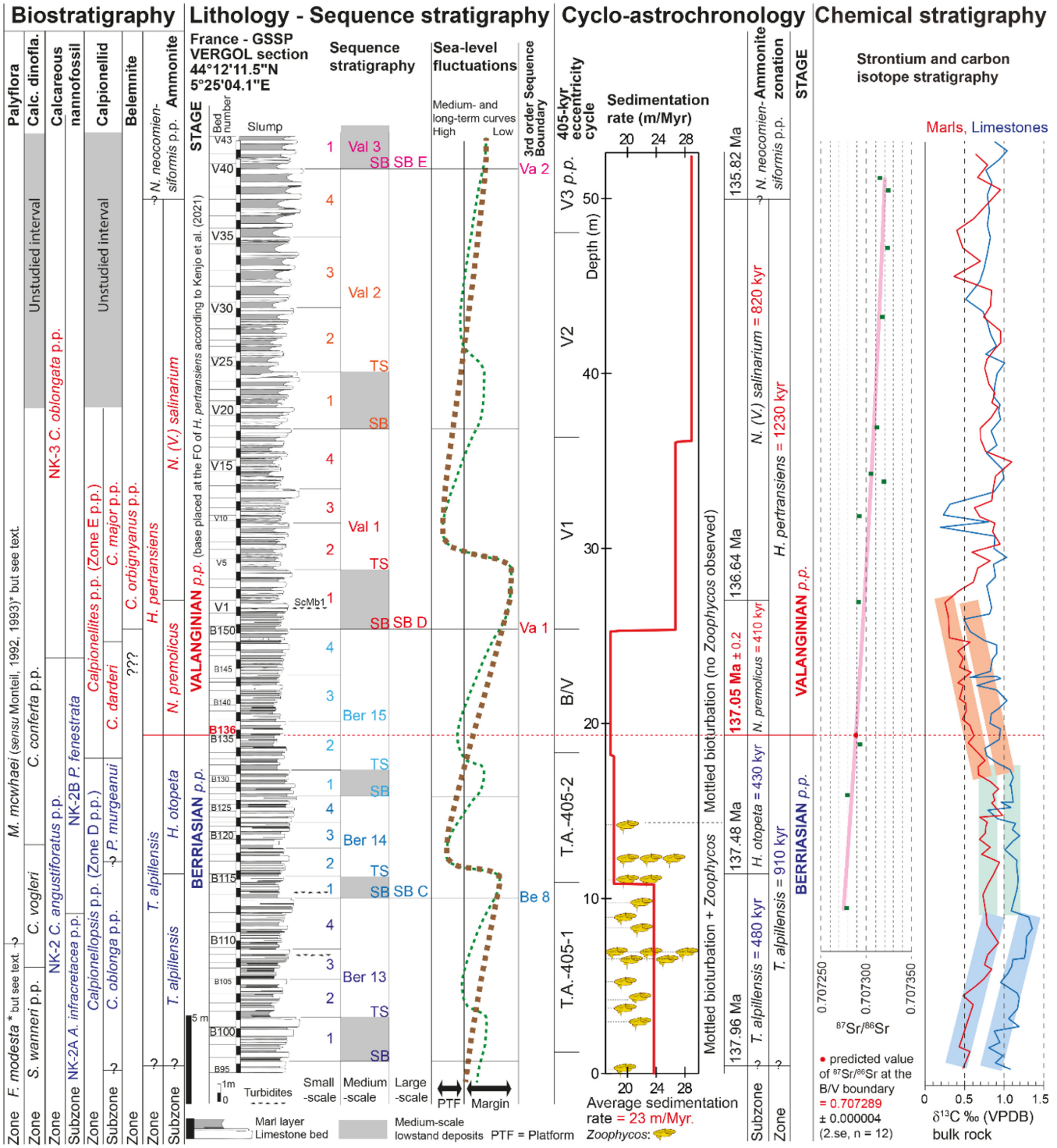

Figure 41. Integrated stratigraphy of the Vergol section: biostratigraphy including ichnofossils, sequence stratigraphy, cyclo-astrochronology and chemical stratigraphy (strontium and carbon isotopes).

zonation. The age model allows the base of the Valanginian Stage (= base of the *H. pertransiens* ammonite Zone) to be dated at 137.05 Ma (±0.2 Ma). The uncertainty here includes the uncertainty in the radio-isotopic age obtained in the lower Hauterivian of the Neuquén basin and the uncertainty in the correlations from the Neuquén basin to the Vocontian basin. Numerical ages and durations of ammonite (sub-) zones are also provided.

Concerning the magnetostratigraphy, it was not possible to characterize magnetic reversals through the Vergol section. The palaeomagnetic study indicates that the upper Berriasian–lower Valanginian succession of Vergol was remagnetized. However, the magnetic scale was established in the Cañada Luenga section that is very well-correlated with the Vergol section using a solid integrated stratigraphy.

The integrated stratigraphy (bio-chemical-physical investigations)

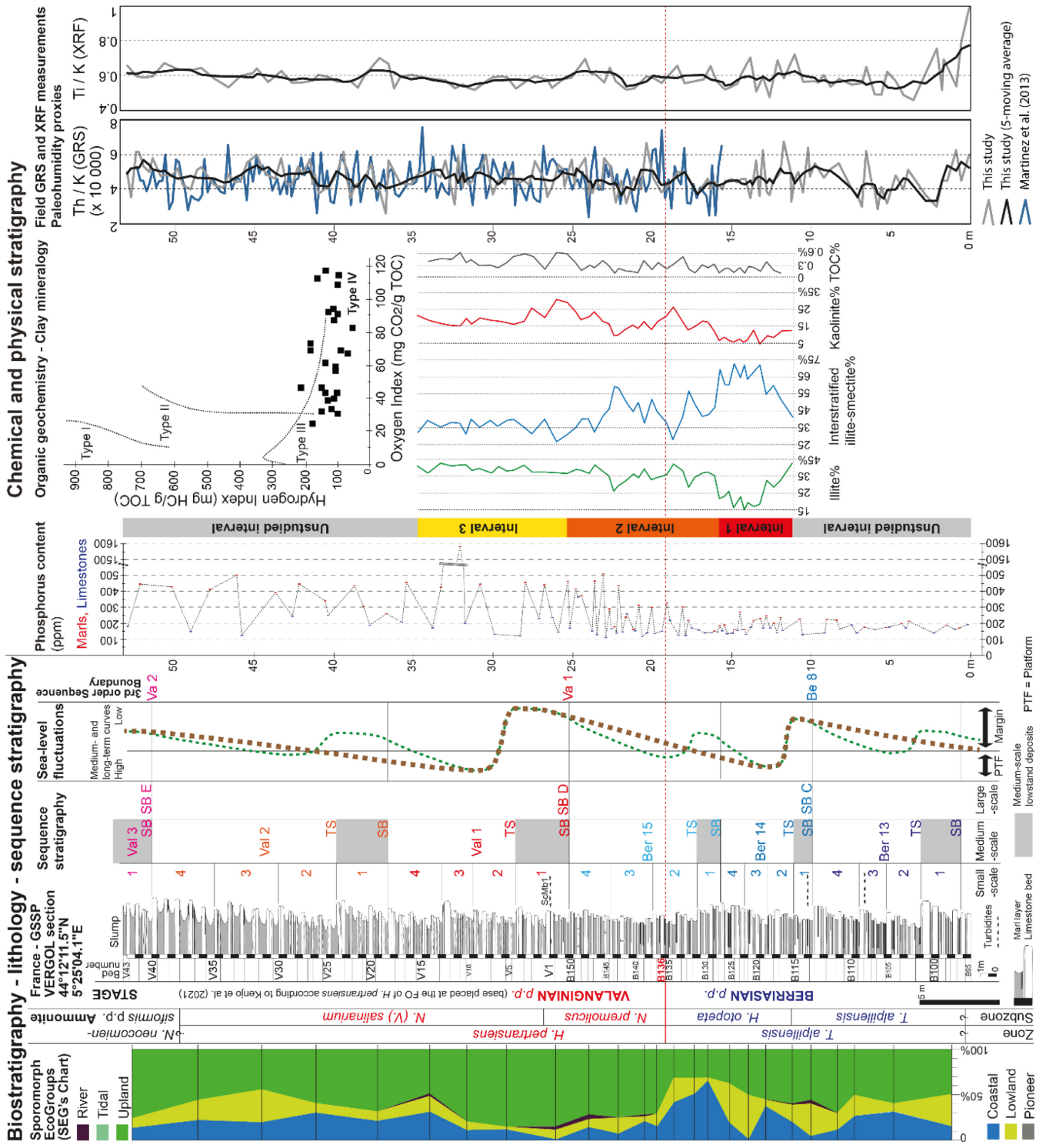

Figure 42. Integrated stratigraphy of the Vergol section: biostratigraphy including a Sporomorph EcoGroup (SEG) plot, sequence stratigraphy, chemical stratigraphy (phosphorus content, clay mineralogy and organic geochemistry) and physical stratigraphy (Field GRS and XRF measurements).

applied on the studied interval of the Vergol section allowed us to characterize sea-level and climatic fluctuations, and to give some information on water column and seafloor conditions. For example, this can be interpreted by modifications observed in the clay mineral assemblages, phosphorus contents, field GRS and XRF measurements, and Sporomorph EcoGroups (Fig. 42).

In conclusion, the base of the Valanginian is accurately dated by (bio-)stratigraphic events and the B/V boundary interval is also strongly characterized by major palaeoenvironmental changes well expressed at Vergol. This has strengthened the choice of the section as a GSSP.

Main Characteristics of the Cañada Luenga Section

The SABS section for the base of the Valanginian is located in the Cañada Luenga ravine, near Cehegín (Murcia, SE Spain). The analyzed interval (beds 0 to 20) is about 13 metres thick and includes the uppermost Berriasian *Tirnovella alpillensis* ammonite Zone and the lower part of the basal Valanginian *Hoedemaekeria pertransiens* ammonite Zone. The lowermost part of the section (beds 0 to 3, 1.2 m thick, corresponding to the lower part of the *T. alpillensis* ammonite Subzone) is made up of nodular limestone, with evident signs of condensation. The rest of the section consists of an alternation of marl and marly limestone beds, deposited in a distal marine environment, with an average sedimentation rate of 9 m/Myr.

The fossil record is abundant and well preserved. The analysis of the stratigraphic distribution of ammonites, belemnites, calpionellids, calcareous dinoflagellates and calcareous nannofossils allows the establishment of a very accurate correlation with the Vergol section. The FO of *H. pertransiens*, primary marker for the B/V boundary, is located in bed 9 of the section (Figs. 31, 32). The correlation with the Vergol section is also reinforced by non-biostratigraphic tools, such as the carbon isotope curve, strontium isotope record and cyclostratigraphic analysis.

The Cañada Luenga section provides a reliable magnetostratigraphic record for the B/V boundary interval, spanning from the upper part of the M16n polarity chron to the lower part of the M14r polarity Chron. The high-resolution correlation between the Cañada Luenga and Vergol sections, well-controlled by an integrated stratigraphy (Fig. 33; see also graphic correlation, Fig. 34), ensures precise calibration of the GSSP against the Geomagnetic Polarity Time Scale. Thus, the base of magnetic Chron M14r recognized at Cañada Luenga (bed CL7) should occur in the "Otopeta calcareous bundle" at Vergol, and may be placed approximatively at layer VGL-B126 (Fig. 33).

Acknowledgements

The final work on the Vergol section benefited from financial support of a project (2021-2023) funded by the Polish and French Ministries of foreign affairs (*Partenariat Hubert Curien*, cf. the current palaeomagnetic study that also includes the contribution of Chmielewski Andrezj, Iwanczuk Jolanta and Ploch Izabela from the Polish Geological Institute of Warsaw, colleagues who are hereby thanked), the CNRS SYSTER program (*WOAW SYSTER French project;* with the contribution of two students Léa Baubant and Durel Franchevel who are acknowledged), Project APVV-20-0079 (Slovakian National Grant Agency, thanks to Diana Ölveczká) and various grants from the Laboratoire de Géologie de Lyon. The International Subcommission on Cretaceous Stratigraphy is thanked for its support (*via* the former chair Maria Rose Petrizzo and the current chair Ian Jarvis) on the activities of the Valanginan Working Group and for the relevant comments made on the proposal by members (see the list in: http://cretaceous.stratigraphy.org/). We are also grateful to the Executive Committee and members of the International Commission on Stratigraphy who carefully scrutinized the formal proposal. Sincere thanks are also extended to the IUGS Executive Committee. The municipality of Montbrun-les-Bains, the Drôme Department and the "Parc Naturel Régional des Baronnies Provençales" are thanked for their support in the project of development and protection of the Vergol site. The authors are grateful to other members of the Valanginian Working Group, the members of the Subcommission on Cretaceous Stratigraphy and the International Commission on Stratigraphy for their contribution in the "selection process" of a GSSP/SABS for the Stage. We acknowledge Peter Rawson and Ian Jarvis (Chair, Cretaceous Subcommission) for correcting the English of the formal proposal and the current manuscript, respectively. We would like to thank Sophie Passot (Lyon) for her bibliographic assistance. We are grateful to the editorial team of Episodes, especially Maria Rose Petrizzo, Associate Editor, and Brad S. Singer and an anonymous reviewer for both corrections and comments which improved the quality of an earlier version of the manuscript.

References

Abbink, O.A., 1998, Palynological investigations in the Jurassic of the North Sea region. LPP Contributions Series, v. 8, 192 p.

Abbink, O.A., Konijnenburg-van Cittert van, J.H.A., and Visscher, H., 2004, A sporomorph ecogroup model for the Northwest European Jurassic–Lower Cretaceous: Concepts and framework. Netherlands Journal of Geosciences, v. 83, pp. 17–31.

Adatte, T., Stinnesbeck, W., Hubberten, H., Remane, J., and López-Oliva, J.G., 2001, Correlation of a Valanginian stable isotopic excursion in northeastern Mexico with the European Tethys. In: Bartolini, C., Buffler, R.T., and Cantú-Chapa, A. (Eds.), The Western Gulf of Mexico basin: Tectonics, sedimentary basins, and petroleum systems. American Association of Petroleum Geologists Memoir, v. 75, pp. 371–388. doi:10.1306/M75768C16

Aguado, R., 1994, Nannofósiles del Cretácico de la Cordillera Bética (sur de España). Bioestratigrafía. Universidad de Granada, Granada, 413 pp.

Aguado, R., Company, M., and Tavera, J.M., 2000, The Berriasian/Valanginian boundary in the Mediterranean region: New data from the Caravaca and Cehegín sections, SE Spain. Cretaceous Research, v. 21, p. 1–21. doi:10.1006/cres.2000.0198

Aguirre-Urreta, M.B., 1993, Neocomian ammonite biostratigraphy of the Andean basins of Argentina and Chile. Revista Española de Paleontología, v. 8, pp. 53–74.

Aguirre-Urreta, M.B., Rawson, P.F., Concheyro, G.A., Bown, P.R., and Ottone, E.G., 2005, Lower Cretaceous (Berriasian-Aptian) biostratigraphy of the Neuquén basin. In: Veiga, G.D., Spalleti, L.A., Howell, J.A., and Schwarz, E. (Eds), The Neuquén basin, Argentina: A case study in sequence stratigraphy and basin dynamics. Geological Society, Special Publications, v. 252, pp. 57–81. doi:10.1144/GSL.SP.2005.252.01.04

Aguirre-Urreta, B., Schmitz, M., Lescano, M., Tunik, M., Rawson, P. F., Concheyro, A., Buhler, M., and Ramos, V.A., 2017, A high precision U–Pb radioisotopic age for the Agrio Formation, Neuquén basin, Argentina: Implications for the chronology of the Hauterivian Stage. Cretaceous Research, v. 75, pp. 193–204. doi:10.1016/j.cretres.2017.03.027

Aguirre-Urreta, B., Martinez, M., Schmitz, M., Lescano, M., Omarini, J., Tunik, M., Kuhnert, H., Concheyro, A., Rawson, P.F., Ramos, V.A., Reboulet, S., Noclin, N., Frederichs, T., Nickl, A.-L., and Pälike, H., 2019, Interhemispheric radio-astrochronological calibration of the time scales from the Andean and the Tethyan areas in the Valanginian–Hauterivian (Early Cretaceous). Gondwana Research, v. 70, pp. 104–132. doi:10.1016/j.gr.2019.01.006

Algeo, T.J., and Liu, J., 2020, A re-assessment of elemental proxies for paleoredox analysis. Chemical Geology, v. 540, 119549. doi:10.1016/j.chemgeo.2020.119549

Ali-Zade, A.A., 1972, Cretaceous belemnites of Azerbaijan. Nedra, Mos-

cow, 279 p. [in Russian].

Allemann, F., and Remane, J., 1979, Les faunes de calpionelles du Berriasien supérieur/Valanginien. In: Busnardo, R., Thieuloy, J. P., and Moullade, M. (Eds.), Hypostratotype Mésogéen de l'Étage Valanginien (sud-est de la France). CNRS, Paris, pp. 99–109.

Allemann, F., Catalano, R., Fares, F., and Remane, J., 1971, Standard calpionellid zonation (upper Tithonian–Valanginian) of the Western Mediterranean Province. Proceedings of the 2nd Planktonic Conference, 1970, pp. 1337–1340.

Allemann, F., Grünn, W., and Wiedmann, J., 1975, The Berriasian of Caravaca (Prov. of Murcia) in the Subbetic zone of Spain and its importance for defining this stage and the Jurassic–Cretaceous boundary. Mémoires du Bureau de Recherches Géologiques et Minières, v. 86, pp. 14–22.

Allen P., and Wimbledon, W.A., 1991, Correlation of NW European Purbeck–Wealden (nonmarine Lower Cretaceous) as seen from the English type-areas. Cretaceous Research, v. 12, pp. 511–526. doi:10.1016/0195-6671(91)90005-W

Alsen, P., 2006, The Early Cretaceous (late Ryazanian–early Hauterivian) ammonite fauna of north-east Greenland: taxonomy, biostratigraphy, and biogeography. Fossils and Strata, v. 53, pp. 1–229. doi:10.18261/9781405180146-2006-01

Alsen, P., and Rawson, P.F., 2005, The early Valanginian (Early Cretaceous) ammonite *Delphinites* (*Pseudogarnieria*) from north-east Greenland. Bulletin of the Geological Society of Denmark, v. 52, pp. 201–212. doi:10.37570/bgsd-2005-52-15

Andreini, G., Caracuel, J.E., and Parisi, G., 2007, Calpionellid biostratigraphy of the upper Tithonian–upper Valanginian interval in Western Sicily (Italy). Swiss Journal of Geosciences, v. 100, pp. 179–198. doi:10.1007/s00015-007-1227-z

Applegate, J.L., and Bergen, J.A., 1988, Cretaceous calcareous nannofossil biostratigraphy of sediments recovered from the Galicia margin, ODP Leg 103. Proceedings of the Ocean Drilling Program, Scientific Results, v. 103, pp. 293–348. doi:10.2973/odp.proc.sr.103.144.1988

Arana, R., Guillén, F., Mancheño, M.A., Manteca, J.I., del Ramo, A., Rodríguez, T., Santisteban, C. de, and Romero, G., 2009, Actualización del inventario de lugares de interés geológico en la Región de Murcia. Consejería de Agricultura y Agua, Murcia, 254 p.

Arkadiev, V.V., Grishchenko, V.A., Guzhikov, A.Y., Manikin, P.E., Savelieva, Y.N., Feodorova, A.A., and Shurekova, O.V., 2017, Ammonites and magnetostratigraphy of the Berriasian–Valanginian boundary deposits from eastern Crimea. Geologica Carpathica, v. 68, pp. 505–516. doi:10.1515/geoca-2017-0033

Arkadiev, V., Guzhikov, A., Baraboshkin, E., Savelieva, J., Feodorova, A., Shurekova, O., Platonov, E., and Manikin, A., 2018, Biostratigraphy and magnetostratigraphy of the upper Tithonian–Berriasian of the Crimean Mountains. Cretaceous Research, v. 87, pp. 5–41. doi:10.1016/j.cretres.2017.07.011

Backhouse, J. 1987, Microplankton zonation of the Lower Cretaceous Warnbro Group, Perth basin, Western Australia. In: Jell, P.A. (Ed.), Studies in Australian Mesozoic palynology. Memoir of the Association of Australasian Palaeontologists, v. 4, pp. 205–226.

Backhouse, J., 1988, Late Jurassic and Early Cretaceous palynology of the Perth basin, Western Australia. Geological Survey of Western Australia, Bulletin, v. 135, pp. 1–233.

Barbier, R., and Thieuloy, J.P., 1965, Étage Berriasien. Mémoires du Bureau de Recherches Géologiques et Minières, v. 34, pp. 69–77.

Barrabé, L., 1929, Contribution a l'étude stratigraphique et pétrographique de la partie médiane du Pays Sakalave (Madagascar). Mémoires de la Société Géologique de France, nouvelle série, v. 12, pp. 1–270.

Baumberger, E., 1906, Fauna der untern Kreide im westschweizerischen Jura (zweiter Teil): Die Ammonitiden der untern Kreide im westschweizerischen Jura, mit einer kurzen Übersicht über die Stratigraphie der Haureviensedimente in diesem Gebiete. Abhandlungen der Schweizerischen Paläontologischen Gesellschaft, v. 32(3) (1905), pp. 1–8.

Baumberger, E., 1925, Die Kreidefossilien von Dusun Pobungo, Batu Kapur-Menkadai und Sungi Pobungo (Djambi, Sumatra). Verhandelingen van het Koninklijk Nederlandsch Geologisch-Mijnbouwkundig Genootschap, Geologische Serie, v. 8, pp. 17–48.

Behar, F., Beaumont, V., De, B., and Penteado, H.L., 2001, Rock-Eval Technology 6: Performances and developments. Oil & Gas Science and Technology, Revue de l'Institut Français du Pétrole, v. 56, pp. 111–134. doi:10.2516/ogst:2001013

Beltran, C., Rafélis de, M., Renard, M., Moullade, M., and Tronchetti, G., 2007, Environmental changes during marl–limestone formation: evidence from the Gargasian (Middle Aptian) of La Marcouline Quarry (Cassis, SE France). Carnets de Géologie [Notebooks on Geology], v. 7(A01), pp. 1–13. doi:10.4267/2042/6828

Benzaggagh, M., 2020, Discussion on the calpionellid biozones and proposal of a homogeneous calpionellid zonation for the Tethyan Realm. Cretaceous Research, v. 114, 104184. doi:10.1016/j.cretres.2019.07.014

Benzaggagh, M., Cecca, F., Schnyder, J., Seyed-Emami, K., and Majidifard, M.R., 2012, Calpionelles et microfaunes pélagiques du Jurassique supérieur–Crétacé inférieur dans les Formations Shal et Kolur (Montagnes du Talesh, chaîne de l'Elbourz, Nord-Ouest Iran). Répartition stratigraphique, espèces nouvelles, révision systématique et comparaisons régionales. Annales de Paléontologie, v. 98, pp. 253–301. doi:10.1016/j.annpal.2012.07.001

Bergen, J.A., 1994, Berriasian to early Aptian calcareous nannofossils from the Vocontian trough (SE France) and Deep Sea Drilling site 534: new nannofossil taxa and a summary of low-latitude biostratigraphic events. Journal of Nannoplankton Research, v. 16, pp. 59–69. doi:10.58998/jnr2015

Bersezio, R., Erba, E., Gorza, M. and Riva, A., 2002, Berriasian–Aptian black shales of the Maiolica Formation (Lombardian basin, southern Alps, northern Italy): local to global events. Palaeogeography, Palaeoclimatology, Palaeoecology, v. 180, pp. 253–275. doi:10.1016/S0031-0182(01)00416-3

Birkelund, T., Hancock, J.M., Hart, M.B., Rawson, P.F., Remane, J., Robaszynski, F., Schmid, F., and Surlyk, F., 1984, Cretaceous stage boundaries – Proposals. Bulletin of the Geological Society of Denmark, v. 33, pp. 3–20. doi:10.37570/bgsd-1984-33-01

Blanc, E. 1996, Transect plate-forme–bassin dans les séries carbonatées du Berriasien supérieur et du Valanginien inférieur (domaines jurassien et nord-vocontien); chronostratigraphie et transferts des sédiments. Géologie Alpine, Mémoire H.S., v. 25, pp. 1–312.

Blanc, E., Bulot, L.G., and Paicheler, J.-C., 1994, La coupe de référence de Montbrun-les-Bains (Drôme, SE France): un stratotype potentiel pour la limite Berriasien–Valanginien. Comptes Rendus de l'Académie des Sciences de Paris, v. 318, série II, pp. 101–108.

Bodin, S., Godet, A., Vermeulen, J., Linder, P., and Follmi, K.B., 2006, Biostratigraphy, sedimentology and sequence stratigraphy of the latest Hauterivian–early Barremian drowning episode of the Northern Tethyan margin (Altmann Member, Helvetic nappes, Switzerland). Eclogae Geologicae Helvetiae, v. 99, pp. 157–174. doi:10.1007/s00015-006-1188-7

Bodin, S., Fiet, N., Godet, A., Matera, V., Westermann, S., Clément A., Janssen, N.M.M., Stille P., and Föllmi, K.B., 2009, Early Cretaceous (late Berriasian to early Aptian) palaeoceanographic change along the northwestern Tethyan margin (Vocontian Trough, southeastern France): $\delta^{13}C$, $\delta^{18}O$ and Sr-isotope belemnite and whole-rock records. Cretaceous Research, v. 30, pp. 1247–1262. doi:10.1016/j.cretres.2009.06.006

Bodin, S., Meissner, P., Janssen, N.M.M., Steuber, S., and Mutterlose, J., 2015, Large igneous provinces and organic carbon burial: Controls on global temperature and continental weathering during the Early Cretaceous. Global and Planetary Change, v. 133, pp. 238–253. doi:10.1016/j.gloplacha.2015.09.001

Bornemann, A., and Mutterlose, J., 2008, Calcareous nannofossil and $\delta^{13}C$ records from the Early Cretaceous of the western Atlantic Ocean: Evidence for enhanced fertilization across the Berriasian–Valanginian

transition. Palaios, v. 23, pp. 821–832. doi:10.2110/palo.2007.p07-076r

Bornemann, A., Aschwer, U., and Mutterlose, J., 2003, The impact of calcareous nannofossils on the pelagic carbonate accumulation across the Jurassic–Cretaceous boundary. Palaeogeography, Palaeoclimatology, Palaeoecology, v. 199, pp. 187–228. doi:10.1016/S0031-0182(03)00507-8

Borza, K., 1969, Die Mikrofazies und Mikrofossilien des Oberjuras und der Unterkreide der Klippenzone der Westkarpaten. Vydav, Bratislava, 301 p.

Borza, K., 1984, The Upper Jurassic–Lower Cretaceous parabiostratigraphic scale on the basis of Tintinninae, Cadosinidae, Stomiosphaeridae, Calcisphaerulidae and other microfossils from the West Carpathians. Geologický Zborník – Geologica Carpathica, v. 35, pp. 539–550.

Bown, P.R., 2005, Early to mid-Cretaceous calcareous nannoplankton from the Northwest Pacific Ocean, Leg 198, Shatsky Rise. Proceedings of the Ocean Drilling Program, Scientific Results, v. 198, pp. 1–82. doi:10.2973/odp.proc.sr.198.103.2005

Bown, P.R., and Concheyro, A., 2004, Lower Cretaceous calcareous nannoplankton from the Neuquén basin, Argentina. Marine Micropaleontology, v. 52, pp. 51–84. doi:10.1016/j.marmicro.2004.04.006

Bown, P.R., Rutledge, D.C., Crux, J.A., and Gallagher, L.T., 1998, Lower Cretaceous. In: Bown, P.R. (Ed.), Calcareous nannofossil biostratigraphy. Chapman and Hall, London, pp. 86–131.

Bralower, T.J., 1987, Valanginian to Aptian calcareous nannofossil stratigraphy and correlation with the upper M-sequence magnetic anomalies. Marine Micropaleontology, v. 11, pp. 293–310. doi:10.1016/0377-8398(87)90003-X

Bralower, T.J., 1990, Lower Cretaceous calcareous nannofossil stratigraphy of the Great Valley Sequence, Sacramento Valley, California. Cretaceous Research, v. 11, pp. 101–123. doi:10.1016/S0195-6671(05)80029-1

Bralower, T.J., Monechi, S., and Thierstein, H.R., 1989, Calcareous nannofossil zonation of the Jurassic–Cretaceous boundary interval and correlation with the geomagnetic polarity timescale. Marine Micropaleontology, v. 14, pp. 153–235. doi:10.1016/0377-8398(89)90035-2

Bulot, L.G., 1990. Évolution des Olcostephaninae (Ammonitina, Cephalopoda) dans le contexte paléo-biogéographique du Crétacé inférieur (Valanginien-Hauterivien) du sud-est de la France. Unpublished D.S.E.R., Université de Bourgogne, Dijon, 178 p.

Bulot, L.G., 1995. Les formations à ammonites du Crétacé inférieur dans le sud-est de la France (Berriasien à Hauterivien): biostratigraphie, paléontologie et cycles sédimentaires. Unpublished PhD Thesis, Muséum National d'Histoire Naturelle, Paris, 375 p.

Bulot, L.G., and Thieuloy, J.-P., 1995, Les biohorizons du Valanginien du sud-est de la France: un outil fondamental pour les corrélations au sein de la Téthys occidentale. Géologie Alpine, Mém. H.S., v. 20 (1994), pp. 15–41.

Bulot, L. G., Blanc, E., Thieuloy, J.-P., and Remane, J., 1993. La limite Berriasien–Valanginien dans le sud-est de la France: données biostratigraphiques nouvelles. Comptes Rendus de l'Académie des Sciences de Paris, v. 316, série II, pp. 1771–1778.

Bulot, L.G. (compiler), Blanc, E., Company, M., Gardin, S., Hennig, S., Hoedemaeker, P.J., Leereveld, H., Magniez-Jannin, F., Mutterlose, J., Pop, G., and Rawson, P.F., 1996, The Valanginian Stage. Bulletin de l'Institut Royal des Sciences Naturelles de Belgique, Sciences de la Terre, v. 66-supp., pp. 11–18.

Busnardo, R., and Thieuloy, J.-P., 1979, Les zones d'ammonites du Valanginien (sud-est de la France). In: Busnardo, R., Thieuloy, J.-P., and Moullade, M. (Eds.), Hypostratotype mésogéen de l'étage Valanginien. CNRS, Paris, pp. 58–68.

Campiche, G., 1853, Énumération des terrains observés dans les environs de Ste Croix. Bulletin des Séances de la Société Vaudoise des Sciences Naturelles, v. 3, pp. 253–255.

Casey, R., 1973, The ammonite succession at the Jurassic–Cretaceous boundary in eastern England. In: Casey, R., and Rawson, P.F. (Eds.), The Boreal Lower Cretaceous. Geological Journal, Special Issue, v. 5, pp. 193–266.

Cecca, F., Fourcade, E., and Azéma, J., 1992, The disappearance of the "Ammonitico Rosso". Palaeogeography, Palaeoclimatology, Palaeoecology, v. 99, pp. 55–70. doi:10.1016/0031-0182(92)90007-R

Channell, J.E.T., and Grandesso, P., 1987, A revised correlation of Mesozoic polarity chrons and calpionellid zones. Earth and Planetary Science Letters, v. 85, pp. 222–240. doi:10.1016/0012-821X(87)90033-1

Channell, J.E.T., Bralower, T.J., and Grandesso, P., 1987, Biostratigraphic correlation of Mesozoic polarity chrons CM1 to CM23 at Capriolo and Xausa (Southern Alps, Italy). Earth and Planetary Science Letters, v. 85, pp. 203–221. doi:10.1016/0012-821X(87)90032-X

Channell, J.E.T., Erba, E. and Lini, A., 1993, Magnetostratigraphic calibration of the late Valanginian carbon isotope event in pelagic limestones from northern Italy and Switzerland. Earth and Planetary Science Letters, v. 118, pp. 145–166. doi:10.1016/0012-821X(93)90165-6

Charbonnier, G., Boulila, S., Gardin, S., Duchamp-Alphonse, S., Adatte, T., Spangenberg, J.E., Föllmi, K.B., Colin, C., and Galbrun, B., 2013, Astronomical calibration of the Valanginian "Weissert" episode: The Orpierre marl–limestone succession (Vocontian basin, southeastern France). Cretaceous Research, v. 45, pp. 25–42. doi:10.1016/j.cretres.2013.07.003

Charbonnier, G., Duchamp-Alphonse, S., Deconinck, J.F., Adatte, T., Spangenberg, J.E., Colin, C. and Föllmi, K.B., 2020, A global palaeoclimatic reconstruction for the Valanginian based on clay mineralogical and geochemical data. Earth-Science Reviews, v. 202, 103092. doi:10.1016/j.earscirev.2020.103092

Cleveland, W.S., 1979, Robust locally weighted regression and smoothing scatterplots. Journal of the American Statistical Association, v. 74, pp. 829–836. doi:10.1080/01621459.1979.10481038

Collignon, M., 1962, Atlas des fossiles caractéristiques de Madagascar (Ammonites). Fascicule 8: Berriasien, Valanginien, Hauterivien, Barrémien. Service Géologique, Tananarive, 96 p.

Combémorel, R., 1972, Position systématique de *Castellanibelus* nov. gen. et de trois espèces de bélemnites du Crétacé inférieur français. Géobios, v. 5, pp. 67–86. doi:10.1016/S0016-6995(72)80006-8

Company, M., 1982, Contribución a la bioestratigrafía del Valanginiense en las Cordilleras Béticas. Cuadernos de Geología Ibérica, v. 8, pp. 665–676.

Company, M., 1987, Los ammonites del Valanginiense del sector oriental de las Cordilleras Béticas (SE de España). Universidad de Granada, Granada, 294 p.

Company, M., and Tavera, J. M., 1982, Los ammonites del tránsito Berriasense–Valanginiense en la región de Cehegín (prov. de Murcia, SE de España). Cuadernos de Geología Ibérica, v. 8, pp. 651–664.

Company, M., and Tavera, J.M., 2013, Lower Valanginian ammonite biostratigraphy in the Betic Cordillera (southeastern Spain): New data. Abstracts of the 9th International Symposium on the Cretaceous System, 2013, pp. 118–119.

Company, M., and Tavera. J.M., 2015, Lower Valanginian ammonite biostratigraphy in the Subbetic domain (Betic Cordillera, southeastern Spain). Carnets de Géologie [Notebooks on Geology], v. 15, pp. 71–88. doi:10.4267/2042/56745

Company, M., Adatte, T., Aguado, R., Duxbury, S., Gea, G. de, Granier, B., Ivanova, D., Janssen, N.M.M., Lakova, I., Martinez, M., Reboulet, S., and Tavera, J.M., 2023, The Global boundary Stratotype Section and Point (GSSP) for the base of the Valanginian Stage (Lower Cretaceous): Cañada Luenga candidate section (Cehegín, SE Spain). Unpublished informal proposal, pp. 1–30.

Coquand, H., 1863, Du terrain jurassique de la Provence, et surtout des étages supérieurs de ce terrain. Bulletin de la Société Géologique de France, 2ème série, v. 20 (1862-63), pp. 553–570.

Coquand, H., 1866, Modifications à apporter dans le classement de la craie inférieure. Bulletin de la Société Géologique de France, 2ème série, v. 23 (1865-66), pp. 560–580.

Coquand, H., 1871, Sur le Klippenhalk des départements du Var et des Alpes-Maritimes. Bulletin de la Société Géologique de France, 2ème

série, v. 28 (1870-71), pp. 208–234.
Coquand, H., and Boutin, E., 1869, Sur les relations qui existent entre la formation jurassique et la formation crétacée des cantons de Ganges (Hérault), de Saint-Hippolyte et de Sumène (Gard). Bulletin de la Société Géologique de France, 2ème série, v. 26 (1868-69), pp. 834–854.
Cotillon, P., Ferry, S., Gaillard, C., Jautée, E., Latreille, G., and Rio, M., 1980, Fluctuation des paramètres du milieu marin dans le domaine vocontien (France sud-est) au Crétacé inférieur: mise en évidence par l'étude des formations marno-calcaires alternantes. Bulletin de la Société Géologique de France, 7ème série, v. 22, pp. 735–744. doi:10.2113/gssgfbull.S7-XXII.5.735
Covacevich, V., 1976, Fauna valanginiana de Península Byers, Isla Livingston, Antártica. Revista Geológica de Chile, v. 3, pp. 25–56.
Covington, J.M., and Wise, S.W., 1987, Calcareous nannofossil biostratigraphy of a Lower Cretaceous deep-sea fan complex: Deep Sea Drilling Project Leg 93 site 603, lower continental rise off cape Hatteras. Deep Sea Drilling Project, Initial Reports, v. 93, pp. 617–660. doi:10.2973/dsdp.proc.93.116.1987
Cramer, B.D., and Jarvis, I., 2020, Carbon isotope stratigraphy. In: Gradstein, F.M., Ogg, J.G., Schmitz, M.D., and Ogg, G.M. (Eds.), Geologic Time Scale 2020, Elsevier, pp. 309–343. doi:10.1016/B978-0-12-824360-2.00011-5
Crux, J.A., 1989, Biostratigraphy and palaeogeographical application of Lower Cretaceous nannofossils from north-western Europe. In: Crux, J.A., and Heck, S.E. van (Eds.), Nannofossils and their applications. Ellis Howrwood, Chichester, pp. 143–211.
Davey, R.J., 1979, The stratigraphic distribution of dinocysts in the Portlandian (latest Jurassic) to Barremian (Early Cretaceous) of northwest Europe. American Association of Stratigraphic Palynologists, Contributions Series, v. 2, pp. 49–81.
Davey, R.J., 1988, Palynological zonation of the Lower Cretaceous, Upper and uppermost Middle Jurassic in the northwestern Papuan basin of Papua New Guinea. Memoir of the Geological Survey of Papua New Guinea, v. 13, pp. 1–77.
Davies, E.H., 1983, The dinoflagellate Oppel-zonation of the Jurassic–Lower Cretaceous sequence in the Sverdrup basin, Arctic Canada. Geological Survey of Canada Bulletin, v. 359, pp. 1–59. doi:10.4095/119736
Davies, E.H., and Norris, G., 1980, Latitudinal variations in encystment modes and species diversity in Jurassic dinoflagellates. In: D.W. Strangway (Ed.), The continental crust and its mineral deposits. Geological Association Canada, Special Paper, v. 20, pp. 361–373.
De Vleeschouwer, D., and Parnell, A.C., 2014. Reducing time-scale uncertainty for the Devonian by integrating astrochronology and Bayesian statistics. Geology, v. 42, pp. 491–494. doi:10.1130/G35618.1
Deconinck, J.F., Beaudoin, B., Chamley, H., Joseph, P., and Raoult, J.F., 1985, Contrôles tectonique, eustatique et climatique de la sédimentation argileuse du domaine subalpin français au Malm-Crétacé. Revue de Géologie Dynamique et de Géographie Physique, v. 26, pp. 311–320.
Desor, E., 1854, Quelques mots sur l'étage inférieur du groupe Néocomien (étage Valanginien). Bulletin de la Société des Sciences Naturelles de Neuchâtel, v. 3, pp. 172–180.
Desor, E., and Gressly, A., 1859, Études géologiques sur le Jura neuchâtelois. Mémoires de la Société des Sciences Naturelles de Neuchâtel, v. 4, pp. 1–153.
Dodd, S.C., Mac Niocaill, C., and Muxworthy, A.R., 2015, Long duration (>4Ma) and steady-state volcanic activity in the early Cretaceous Paraná–Etendeka Large Igneous Province: New palaeomagnetic data from Namibia. Earth and Planetary Science Letters, v. 414, pp. 16–29. doi:10.1016/j.epsl.2015.01.009
Duchamp-Alphonse, S., Gardin, S., Fiet, N., Bartolini, A., Blamart, D., and Pagel, M., 2007, Fertilization of the northwestern Tethys (Vocontian basin, SE France) during the Valanginian carbon isotope perturbation: Evidence from calcareous nannofossils and trace element data. Palaeogeography, Palaeoclimatology, Palaeoecology, v. 243, pp. 132–151. doi:10.1016/j.palaeo.2006.07.010
Dunham, R.J., 1962, Classification of carbonate rocks according to depositional texture. In: Ham, W.E.(Ed.): Classification of carbonate rocks. American Association of Petroleum Geologists Memoir, v. 1, pp. 108–121.
Duval-Jouve, J., 1841, Bélemnites des terrains crétacés inférieurs des environs de Castellane (Basses-Alpes), considérées géologiquement et zoologiquement, avec la description de ces terrains. Fortin, Masson et Cie., Paris, 80 p.
Duxbury, S., 1977, A palynostratigraphy of the Berriasian to Barremian of the Speeton Clay of Speeton, England. Palaeontographica B, v. 160, pp. 17–67.
Duxbury, S., 2001, A palynological zonation scheme for the Lower Cretaceous – United Kingdom sector, central North Sea. Neues Jahrbuch für Geologie und Paläontologie, Abhandlungen, v. 219, pp. 95–137. doi:10.1127/njgpa/219/2001/95
Duxbury, S., 2018, Berriasian to lower Hauterivian palynostratigraphy, U.K. onshore and Outer Moray Firth. Micropaleontology, v. 64, pp. 171–252. doi:10.47894/mpal.64.3.01
Duxbury, S., 2023, Organic-walled marine microplankton from the Hauterivian and early Barremian of the North Sea Region – biostratigraphy and taxonomy. Micropaleontology, v. 69, pp. 113–258. doi:10.47894/mpal.69.2.01
Duxbury, S., 2024, Palynology of the late Berriasian to early Hauterivian of the Tethyan Realm in SE France: biostratigraphy and taxonomy of the Vergol (Montbrun-les-Bains) and La Charce (Serre de l'Âne) sections, Vocontian basin. Micropaleontology, v. 70, pp. 543–677. doi:10.47894/mpal.70.6.01
Eaton, A.D., Clesceri, L.S., and Greenberg, A.E., 1995, Standard methods for the examination of water and waste water (19th ed.). American Public Health Association, Washington DC, pp. 4.113–4.114.
Ehiro, M., Company, M., Takaizumi, Y., and Hanamatsu, S., 2020, Geological age of the Ayukawa Formation (Oshika Group) in the south Kitakami belt, northeast Japan based on the ammonoids. Journal of the Geological Society of Japan, v. 126, pp. 563–574. doi:10.5575/geosoc.2020.0025
Elbra, T., Schnabl, P., Čižková, K., Pruner, P., Kdýr, Š., Grabowski, J., Reháková, D., Svobodová, A., Frau, C., and Wimbledon, W.A.P., 2018. Palaeo- and rock-magnetic investigations across Jurassic–Cretaceous boundary at St Bertrand's Spring, Drôme, France: applications to magnetostratigraphy. Studia Geophysica et Geodetica, v. 62, pp. 323–338. doi:10.1007/s11200-016-8119-5
Emmanuel, L., and Renard, M., 1993, Carbonate geochemistry (Mn, $\delta^{13}C$, $\delta^{18}O$) of the late Tithonian–Berriasian pelagic limestones of the Vocontian trough (SE France). Bulletin des Centres des Recherches Exploration-Production Elf Aquitaine, v. 17, pp. 205–221.
Erba, E., Bartolini, A. and Larson, R.L., 2004, Valanginian Weissert oceanic anoxic event. Geology, v. 32, pp. 149–152. doi:10.1130/G20008.1
Espitalié, J., 1986, Use of Tmax as a maturation index for different types of organic matter. Comparison with vitrinite reflectance. In: Burrus, J. (Ed.), Thermal modelling in sedimentary basins. Technip, Paris, pp. 475–496.
Espitalié, J., La Porte, J.L., Madec, M., Marquis, F., Le Plat, P., Paulet, J., and Boutefeu, A., 1977, Rapid method for source rocks characterization and for determination of petroleum potential and degree of evolution. Oil & Gas Science and Technology, Revue de l'Institut Français du Pétrole, v. 32, pp. 23–42.
Espitalié, J., Deroo, G., and Marquis, F., 1985-86, La pyrolyse Rock Eval et ses applications. Oil & Gas Science and Technology, Revue de l'Institut Français du Pétrole, v. 40, pp. 563–579 (part 1); v. 40, pp. 755–784 (part 2); v. 41, pp. 73–89 (part 3).
Ettachfini, M., 1991, Le Valanginien de l'Atlas atlantique (Maroc): stratigraphie et ammonitofaune. Strata, série 2, v. 15, pp. 1–177.
Ettachfini, M., 2004, Les ammonites néocomiennes dans l'Atlas atlantique (Maroc): biostratigraphie, paléontologie, paléobiogéographie et paléoécologie. Strata, série 2, v. 43, pp. 1–224.

Fatmi, A.N., 1977, Neocomian ammonites from northern areas of Pakistan. Bulletin of the British Museum (Natural History), Geology, v. 28, pp. 255–296. doi:10.5962/p.313893

Fatmi., A.N., and Rawson, P.F., 1993, The first Early Cretaceous ammonite faunas from Baluchistan. Cretaceous Research, v. 14, pp. 91–100. doi:10.1006/cres.1993.1007

Ferry, S., 1991, Une alternative au modèle de stratigraphie séquentielle d'Exxon : la modulation tectono−climatique des cycles orbitaux. In: Cotillon, P., and Ferry, S., (Eds.), Mesozoic Eustacy Record on Western Tethyan Margins. Géologie Alpine hors série, v. 18: pp. 47–99.

Fesneau, C., 2008, Enregistrement des changements climatiques dans le domaine téthysien au Valanginien. Unpublished PhD thesis, Université de Bourgogne, Dijon, 340 p.

Fisher, M.J., and Riley, L.A., 1980, The stratigraphic distribution of dinoflagellate cysts at the boreal Jurassic/Cretaceous boundary. Proceedings of the 4th lnternational Palynology Conference, 1977, v. 2, pp. 313–29.

Flandrin, J., Gottis, M., Viallix, J.R., Golenko, N., Riche, P., Parant, J., Rebilly, G., Bejanin, J., Issenmann O., Teisserenc, P., Mollier, M, Cochet, E., Riche, P., and Rivier, F., 1964, Carte géologique détaillée de la France (1/50 000), feuille Séderon [916]. 1 notice explicative (6 p.). Service de la carte géologique de la France, Paris.

Flügel, E., 2004, Microfacies of carbonate rocks. Springer, Berlin, 976 p. doi:10.1007/978-3-662-08726-8

Föllmi, K.B., Godet, A., Bodin, S. and Linder, P., 2006, Interactions between environmental change and shallow water carbonate buildup along the northern Tethyan margin and their impact on the Early Cretaceous carbon isotope record. Paleoceanography, v. 21, PA4211. doi:10.1029/2006PA001313

Főzy, I., Janssen, N.M.M., Price, G.D., Knauer, J., and Pálfy, J., 2010, Integrated isotope and biostratigraphy of a Lower Cretaceous section from the Bakony Mountains (Transdanubian Range, Hungary): A new Tethyan record of the Weissert event. Cretaceous Research, v. 31, pp. 525–545. doi:10.1016/j.cretres.2010.07.003

Galbrun, B., 1984, Magnétostratigraphie de la limite Jurassique–Crétacé. Proposition d'une échelle de polarité à partir du stratotype du Berriasien (Berrias, Ardèche, France) et de la Sierra de Lugar (province de Murcie, Espagne). Unpublished PhD thesis, Université Pierre et Marie Curie, Paris, 94 p.

Galbrun, B., 1985, Magnetostratigraphy of the Berriasian stratotype section (Berrias, France). Earth and Planetary Science Letters, v. 74, pp. 130–136. doi:10.1016/0012-821X(85)90172-4

Galbrun, B., and Rasplus L., 1984, Magnétostratigraphie du stratotype du Berriasien. Premiers résultats. Comptes Rendus de l'Académie des Sciences de Paris, v. 298, série II, pp. 219–222.

Galbrun, B., Rasplus, L., and Le Hégarat, G., 1986, Données nouvelles sur le stratotype du Berriasien: corrélations entre magnétostratigraphie et biostratigraphie. Bulletin de la Société Géologique de France, 8ème série, v. 2, pp. 575–584. doi:10.2113/gssgfbull.II.4.575

Gale, A.S., Mutterlose, J., and Batenburg, S., with contributions by, Gradstein, F.M., Agterberg, F.P., Ogg, J.G., and Petrizzo, M.R., 2020. The Cretaceous Period. In: Gradstein, Ogg, J.G., Schmitz, M.D., and Ogg, G.M. (Eds.), Geologic Time Scale 2020. Elsevier, pp. 1023–1086. doi:10.1016/B978-0-12-824360-2.00027-9

Gayte, D., 1984, Le Valanginien et l'Hauterivien de la bordure cévénole méridionale. Biostratigraphie, paléontologie, sédimentologie. Unpublished Thèse Doct. 3ème Cycle, Université Claude Bernard, Lyon. 147 p.

Gea, G.A. de, 2004, Bioestratigrafía y eventos del Cretácico Inferior en las Zonas Externas de la Cordillera Bética. Universidad de Jaén, Jaén, 658 p.

Gilliéron, V., 1873, Aperçu géologique sur les Alpes de Fribourg en général et description spéciale du Monsalvens en particulier. Matériaux pour la Carte Géologique de la Suisse, v. 12, pp. 1–273.

Godet, A., Bodin, S., Adatte, T., and Föllmi, K.B., 2008, Platform-induced clay-mineral fractionation along anorthern Tethyan basin-platform transect: Implications for the interpretation of Early Cretaceous climate change (late Hauterivian–early Aptian). Cretaceous Research, v. 29, pp. 830–847. doi:10.1016/j.cretres.2008.05.028

González-Arreola, C., Olóriz, F., and Villaseñor, A.B., 1995, Nuevos datos sobre el Valanginiano en el nor-noreste de México. Géologie Alpine, Mém. H.S., v. 20 (1994), pp. 191–203.

Grabowski, J., Michalík, J., Pszczółkowski, A., Lintnerová, O., 2010. Magneto-, and isotope stratigraphy around the Jurassic/Cretaceous boundary in the Vysoká Unit (Malé Karpaty Mountains, Slovakia): correlations and tectonic implications. Geologica Carpathica, v. 61, pp. 309–326. doi:10.2478/v10096-010-0018-z

Grabowski, J., Krzemiński, L., Schnyder, J., Sobień, K., Hejnar, J., Koptiková, L., Pszczółkowski, A., and Schnabl, P., 2013, Integrated magnetic susceptibility and geochemical record of $\delta^{13}C$ anomalies in the Berriasian and Valanginian sections from the Tethyan Domain (Western Carpathians, Poland). Proceedings STRATI 2013, pp. 847–851. doi:10.1007/978-3-319-04364-7_159

Grabowski, J., Lakova, I., Petrova, S., Stoykova, K., Ivanova, D., Wójcik-Tabol, P., Sobień, K., and Schnabl, P., 2016, Paleomagnetism and integrated stratigraphy of the upper Berriasian hemipelagic succession in the Barlya section Western Balkan, Bulgaria: Implications for lithogenic input and paleoredox variations. Palaeogeography, Palaeoclimatology, Palaeoecology, v. 461, pp. 156–177. doi:10.1016/j.palaeo.2016.08.018

Grabowski, J., Lodowski, D.G., Schnyder, J., Sobień. K., Chadimová, L., Pszczółkowski, A., Krzemiński, L., and Schnabl, P., 2019a, Magnetic stratigraphy, stable isotopes and chemostratigraphy in the upper Berriasian of Rówienka section (Western Tatra Mts., Fatric succession, Poland): Towards a consistent model of late Berriasian paleoenvironmental changes in the Western Tethys. Proceedings of the International Meeting around the Jurassic–Cretaceous Boundary, 2018, pp. 30–33.

Grabowski, J., Bakhmutov, V., Kdýr, Š., Krobicki, M., Pruner, P., Reháková, D., Schnabl, P., Stoykova, K., and Wierzbowski, H., 2019b, Integrated stratigraphy and palaeoenvironmental interpretation of the upper Kimmeridgian to lower Berriasian pelagic sequences of the Velykyi Kamianets section (Pieniny Klipen Belt, Ukraine). Palaeogeography, Palaeoclimatology, Palaeoecology, v. 532, 109216. doi:10.1016/j.palaeo.2019.05.038

Grabowski, J., Chmielewski, A., Ploch, I., Rogov, M., Smoleń, J., Wójcik-Tabol, P., Leszczyński, K., and Maj-Szeliga, K., 2021a, Paleoclimatic changes and inter-regional correlations in the Jurassic/Cretaceous boundary interval of the Polish basin: Portable XRF and magnetic susceptibility study. Newsletters on Stratigraphy, v. 54, pp. 123–158. doi:10.1127/nos/2020/0600

Grabowski, J., Stoykova, K., Wierzbowski, H., and Wójcik-Tabol, P., 2021b, Upper Berriasian chemostratigraphy, clay minerals and calcareous nannofossils of the Barlya section (Western Balkan, Bulgaria): Implications for palaeoclimate and productivity changes, and stratigraphic correlations across the Alpine Tethys. Palaeogeography, Palaeoclimatology, Palaeoecology, v. 567, 110252. doi:10.1016/j.palaeo.2021.110252

Grabowski, J., Pszczółkowski, A., Stoykova, K., Martinez, M., Iwańczuk, J., Krzemiński, L., Sidorczuk, M., 2024, Integrated stratigraphy of the Valanginian Carbon-Isotope-Excursion (Weissert event) from the Kryta Valley section, Western Carpathians (Poland): Correlation with the Vocontian basin and palaeoenvironmental implications. Newsletters on Stratigraphy, v. 58, pp. 1–46. doi:10.1127/nos/2024/0849

Granier, B., 2024, *Octahedronoides tethysianus* n.gen., n.sp., enigmatic clusters of microspheres at the Jurassic–Cretaceous transition. Carnets Geol., v. 24, pp. 127–133. doi:10.2110/carnets.2024.2407

Gréselle, B., 2007, Impact des variations paléoclimatiques sur la sédimentation carbonatée au Valanginien. Unpublished PhD thesis, Université Claude Bernard, Lyon 1, 337 p.

Gréselle, B., and Pittet, B., 2010, Sea-level reconstructions from the Peri-Vocontian zone (SE France) point to Valanginian glacio-eustasy. Sedimentology, v. 57, pp. 1640–1684. doi:10.1111/j.1365-3091.2010.01159.x

Gréselle, B., Pittet, B., Mattioli, E., Joachimski, M., Barbarin, N., Riquier, L., Reboulet, S., and Pucéat, E., 2011. The Valanginian isotope event: A complex suite of palaeoenvironmental perturbations. Palaeogeogra-

phy, Palaeoclimatology, Palaeoecology, v. 306, pp. 41–57. doi:10.1016/j.palaeo.2011.03.027

Grün, B., and Blau, J., 1997, New aspects of calpionellid biochronology: Proposal for a revised calpionellid zonal and subzonal division. Revue de Paléobiologie, v. 16, pp. 197–214.

Habib, D., 1975, Neocomian dinoflagellate zonation in the western North Atlantic. Micropaleontology, v. 21, pp. 373–392. doi:10.2307/1485290

Habib, D., 1977, Comparison of Lower and Middle Cretaceous palynostratigraphic zonations in the western North Atlantic. In: F.W. Swain (Ed.), Stratigraphic micropaleontology of Atlantic basin and borderlands. Elsevier, Amsterdam, pp. 341–367. doi:10.1016/S0920-5446(08)70359-5

Habib, D., 1978, Palynostratigraphy of the Lower Cretaceous section at Deep Sea Drilling Project site 391, Blake-Bahama basin, and its correlation in the North Atlantic. Deep Sea Drilling Project, Initial Reports, v. 44, pp. 887–897. doi:10.2973/dsdp.proc.44.139.1978

Habib, D., and Drugg, W.S., 1983, Dinoflagellate age of Middle Jurassic–Early Cretaceous sediments in the Blake-Bahama basin. Deep Sea Drilling Project, Initial Reports, v. 76, pp. 623–638. doi:10.2973/dsdp.proc.76.126.1983

Haq, B.U., 2014, Cretaceous eustasy revisited. Global and Planetary Change, v. 113, pp. 44–58. doi:10.1016/j.gloplacha.2013.12.007

Haq, B.U., Hardenbol, J., and Vail, P.R., 1987, Chronology of fluctuating sea levels since the Triassic. Science, v. 235, pp. 1156–1167. doi:10.1126/science.235.4793.1156

Hardenbol, J., Thierry, J., Farley, M.B., Jacquin, T., Graciansky, P.C. de, and Vail, P.R., 1998, Cretaceous sequence chronostratigraphy. In: Graciansky, P.C. de, Hardenbol, J., Jacquin, T., and Vail, P.R. (eds), Mesozoic and Cenozoic sequence stratigraphy of European basins. SEPM Special Publication, v. 60, chart 4.

Head, M.J., Aubry, M.P., Piller, W.E., and Walker, M., 2023, Standard Auxiliary Boundary Stratotype (SABS) approved to support the Global boundary Stratotype Section and Point (GSSP). Episodes, v. 46, pp. 99−100. doi:10.18814/epiiugs/2022/022044

Helby, R., Morgan, R. and Partridge, A.D., 1987, A palynological zonation of the Australian Mesozoic. Memoir of the Association of Australasian Palaeontologists, v. 4, pp. 1–94.

Hinnov, L.A., Schulz, M., and Yiou, P., 2002, Interhemispheric space-time attributes of the Dansgaard-Oeschger oscillations between 100 and 0 ka. Quaternary Science Reviews, v. 21, pp. 1213–1228. doi:10.1016/S0277-3791(01)00140-8

Hoedemaeker, P.J., 1982, Ammonite biostratigraphy of the uppermost Tithonian, Berriasian, and lower Valanginian along the Río Argos (Caravaca, SE Spain). Scripta Geologica, v. 65, pp. 1–81.

Hoedemaeker, P.J., 1983, Reconsideration of the stratigraphic position of the boundary between the Berriasian and the Nemausian (=Valanginian sensu stricto). Zitteliana, v. 10, pp. 447–457.

Hoedemaeker, P.J., 1984, Proposals for the stratigraphic positions of the Berriasian–Valanginian and the Valanginian–Hauterivian boundaries. Bulletin of the Geological Society of Denmark, v. 33, pp. 139–146. doi:10.37570/bgsd-1984-33-12

Hoedemaeker, P.J., 1987, Correlation possibilities around the Jurassic/Cretaceous boundary. Scripta Geologica, v. 84, pp. 1–55.

Hoedemaeker, P.J., 1995, The Berriasian stage: A review. Géologie Alpine, Mém. H.S., v. 20 (1994), pp. 5–14.

Hoedemaeker, P.J., and Leereveld, H., 1995, Biostratigraphy and sequence stratigraphy of the Berriasian–lowest Aptian (Lower Cretaceous) of the Rio Argos succession, Caravaca, SE Spain. Cretaceous Research, v. 16, pp. 195–230. doi:10.1006/cres.1995.1016

Hoedemaeker, P.J., Reboulet, S., Aguirre-Urreta, M.B., Alsen, P., Aoutem, M., Atrops, F., Barragán, R., Company, M., González-Arreola, C., Klein, J., Lukeneder, A., Ploch, I., Raisossadat S.N., Rawson, P.F., Ropolo, P., Vašíček, Z., Vermeulen, J., and Wippich, M.G.E., 2003, Report on the 1st International Workshop of the IUGS Lower Cretaceous Ammonite Working Group, the 'Kilian Group' (Lyon, 11 July 2002). Cretaceous Research, v. 24, 89–94. doi:10.1016/S0195-6671(03)00018-1

Horák, J., 1988, Die Belemniten aus der Unterkreide-Ablagerungen im Steinbruch Kotouc bei Stramberk (Silesische Einheit, CSSR). Acta Musei Moraviae, Scientiae Naturales, v. 72, pp. 59–70.

Huber, K., and Wiedmann, J., 1986, Sobre el límite Jurásico–Cretácico en los alrededores de Villa de Leiva, Depto. de Boyacá, Colombia. Geología Colombiana, v. 15, pp. 81–92.

Imlay, R.W., and Jones, D.L., 1970, Ammonites from the *Buchia* Zones in northwestern California and southwestern Oregon. Geological Survey Professional Paper, v. 647-B, pp. 1–60.

Irwin, H., Curtis, C., and Coleman, M., 1977, Isotopic evidence for source of diagenetic carbonates formed during burial of organic-rich sediments. Nature, v. 269, pp. 209–213. doi:10.1038/269209a0

Ivanova, D., 2001, *Cadosinopsis nowaki* – a new calcareous dinocyst zone (upper Valanginian–lower Hauterivian) in West Bulgaria. Comptes Rendus de l'Académie Bulgare des Sciences, v. 54, pp. 55–58.

Ivanova, D., and Kietzmann, D.A., 2017, Calcareous dinoflagellate cysts from the Tithonian–Valanginian Vaca Muerta Formation in the southern Mendoza area of the Neuquén basin, Argentina. Journal of South American Earth Sciences, v. 77, pp. 150–169. doi:10.1016/j.jsames.2017.05.004

Jakubowski, M, 1987, A proposed Lower Cretaceous calcareous nannofossil zonation scheme for the Moray Firth area of the North Sea. Abhandlungen der Geologischen Bundesanstalt, v. 39, pp. 99–119.

Jan du Chêne, R., Busnardo, R., Charollais, J., Clavel, B., Deconinck, J.F., Emmanuel, L., Gardin, S., Gorin, G., Manivit, H., Monteil, E., Raynaud, J.F., Renard, M., Steffen, D., Steinhauser, N., Strasser, A., Strohmenger, C., and Vail, P.R., 1993, Sequence stratigraphic interpretation of the upper Tithonian–Berriasian reference sections in South East France: A multidisciplinary approach. Bulletin des Centres de Recherches Exploration-Production Elf Aquitaine, v. 17, pp. 151–181.

Janssen, N.M.M., 1997, Mediterranean Neocomian belemnites, part 1: Río Argos sequence (province of Murcia, Spain): the Berriasian–Valanginian and the Hauterivian–Barremian boundaries. Scripta Geologica, v. 114, pp. 1–55.

Janssen, N.M.M., 2003, Mediterranean Neocomian belemnites, part 2: the Berriasian–Valanginian boundary in southeast Spain (Río Argos, Cañada Lengua and Tornajo). Scripta Geologica, v. 126, pp. 121–183.

Janssen N.M.M., 2021, Mediterranean Neocomian belemnites, part 5: Valanginian temporal distribution and zonation (and some lithological remarks). Carnets Geol., v. 21, pp. 67–125. doi:10.2110/carnets.2021.2104

Janssen, N.M.M., and Clément, A, 2002, Extinction and renewal patterns among Tethyan belemnites in the Verrucosum Subzone (Valanginian) of southeast France. Cretaceous Research, v. 23, pp. 509–522. doi:10.1006/cres.2002.1019

Jekelius, E., 1915, Die mesozoischen Faunen der Berge von Brassó. II. Die Neokomfauna von Brassó. Mitteilungen aus dem Jahrbuch der Königlichen Ungarischen Geologischen Reichsanstalt, v. 23, pp. 114–135.

Jeletsky, J. A., 1970, Cretaceous macrofaunas. In: R.J.W., Douglas (Ed.), Geology and economic minerals of Canada. Geological Survey of Canada, Economic Geology Report 1, pp. 649–62.

Jeletzky, J.A., and Kemper, E., 1988, Comparative paleontology and stratigraphy of Valanginian Polyptychitinae and Simbirskitinae in Svendrup basin (Arctic Canada) and Lower Saxony basin (northwest Germany). Geological Survey of Canada Bulletin, v. 337, pp. 1–355.

Jeremiah, J., 2001, A Lower Cretaceous nannofossil zonation for the North Sea basin. Journal of Micropalaeontology, v. 20, pp. 45–80. doi:10.1144/jm.20.1.45

Jiménez, G., García-Delgado, H., and Geisssman, J.W., 2021, Magnetostratigraphy and magnetic properties of the Jurassic to Lower Cretaceous Girón Group (northern Andes, Colombia). Geosphere, v. 17, pp. 2172–2196. doi:10.1130/GES02186.1

Jiménez-López, J.C., López-Martínez, R.A., Barragán, R., and Buitrón-Sánchez, B.E., 2021, Calpionélidos de la transición Berriasiano–Valanginiano en la Sección Padhi, centro-este de Hidalgo, México: sistemática y bioestratigrafía. Revista Mexicana de Biodiversidad, v. 92, e923376. doi:10.22201/ib.20078706e.2021.92.3376

Jones, B., and Manning, D.A.C., 1994, Comparison of geochemical indices used for the interpretation of palaeoredox conditions in ancient mudstones. Chemical Geology, v. 111, pp. 111–129. doi:10.1016/0009-2541(94)90085-X

Kabanov, G.K, 1960, Belemnites. In: Drushchits, V.V., and Kudryavtsev, M.P. (Eds.), Atlas of the Lower Cretaceous fauna of the Northern Caucasus and Crimea. GONTI, Moscow, pp. 356-369 [in Russian].

Katz, B., Elmore, R. D., Cogoini, M., and Ferry, S., 1998, Widespread chemical remagnetization: Orogenic fluids or burial diagenesis of clays? Geology, v. 26, pp. 603–606. doi:10.1130/0091-7613(1998) 026%3C0603:Wcrofo%3E2.3.Co;2

Katz, B., Elmore, R.D., Cogoini, M., Engel, M.H., and Ferry, S., 2000, Associations between burial diagenesis of smectite, chemical remagnetization, and magnetite authigenesis in the Vocontian trough, SE France. Journal of Geophysical Research, v. 105, pp. 851–868. doi:10.1029/1999JB900309

Kechra, F., Vandamme, D., and Rochette, P., 2003, Tertiary remagnetization of normal polarity in Mesozoic marly limestones from SE France. Tectonophysics, v. 362, pp. 219–238. doi:10.1016/S0040-1951(02)00639-X

Kemper, E., Rawson, P.F., and Thieuloy, J.P., 1981, Ammonites of Tethyan ancestry in the early Lower Cretaceous of north-west Europe. Palaeontology, v. 24, pp. 251–311.

Kenjo, S., 2014, Biostratigraphie intégrée à nannofossiles calcaires et ammonoïdes: développement et implications pour la définition et la valorisation des stratotypes d'unité et de limite. L'exemple des étages Berriasien et Valanginien et de leur limite (~140 Millions d'années). Unpublished PhD Thesis, Université Claude Bernard, Lyon, 226 p.

Kenjo, S., Reboulet, S. Mattioli, E., and Ma'louleh, K., 2021, The Berriasian–Valanginian boundary in the Mediterranean Province of the Tethyan Realm: Ammonite and calcareous nannofossil biostratigraphy of the Vergol section (Montbrun-les-Bains, SE France), candidate for the Valanginian GSSP. Cretaceous Research, v. 121, 104738. doi:10.1016/j.cretres.2020.104738

Kietzmann, D.A., Palma, R.M., and Iglesia Llanos, M.P., 2015, Cyclostratigraphy of an orbitally-driven Tithonian–Valanginian carbonate ramp succession, southern Mendoza, Argentina: Implications for the Jurassic–Cretaceous boundary in the Neuquén basin. Sedimentary Geology, v. 315, pp. 29–46. doi:10.1016/j.sedgeo.2014.10.002

Kietzmann, D.A., Iglesia Llanos, M.P., González Tomassini, F., Lanusse Noguera, I., Vallejo, D., and Reijenstein, H., 2021, Upper Jurassic–Lower Cretaceous calpionellid zones in the Neuquén basin (Southern Andes, Argentina): Correlation with ammonite zones and biostratigraphic synthesis. Cretaceous Research, v. 127, 104950. doi:10.1016/j.cretres.2021.104950

Kietzmann, D.A., Iglesia Llanos, M.P., and Iovino, F., 2023, Tithonian–Berriasian calcisphere (calcareous dinoflagellate cysts) zones in the Neuquén basin, Argentina: Correlation between Southern Andes and Tethyan regions. Newsletters on Stratigraphy, v. 56, pp. 157–185. doi:10.1127/nos/2022/0729

Kilian, W., 1887, Système Crétacé. Annuaire Géologique Universel, v. 3, pp. 299–356.

Kilian, W., 1889, Description géologique de la Montagne de Lure (Basses-Alpes). Masson. Paris, 458 p.

Kilian, W., 1896, Notice stratigraphique sur les environs de Sisteron et contributions à la connaissance des terrains secondaires du sud-est de la France. Bulletin de la Société Géologique de France, 3ème série, v. 23 (1895), pp. 659–803.

Kilian, W., 1907, Erste Abteilung: Unterkreide (Palaeocretacicum). Erste Lieferung: Allgemeines über Palaeocretacicum; Unterkreide im südostlichen Frankreich, Einleitung. In: Lethaea Geognostica. II Teil, Das Mesozoicum. 3 Band, Kreide. Schweizerbart, Stuttgart, pp. 1–168.

Kilian, W., 1910, Erste Abteilung: Unterkreide (Palaeocretacicum). Zweite Lieferung: Das bathyale Palaeocretacicum im südostlichen Frankreich; Valendis-Stufe; Hauterive-Stufe; Barreme-Stufe; Apt- Stufe. In: Lethaea Geognostica. II Teil, Das Mesozoicum. 3 Band, Kreide. Schweizerbart, Stuttgart, pp. 169–288.

Klein, J., 2005, Lower Cretaceous Ammonites I. Perisphinctaceae 1: Himalayitidae, Olcostephanidae, Holcodiscidae, Neocomitidae, Oosterelliidae. In: Riegraf, W. (Ed.), Fossilium Catalogus I: Animalia, Pars 139. Backhuys, Leiden, 484 p.

Klein, J., Busnardo, R., Company, M., Delanoy, G., Kakabadze, M., Reboulet, S., Ropolo, P., Vašíček, Z., and Vermeulen, J., 2007, Lower Cretaceous Ammonites III. Bochianitoidea, Protancyloceratoidea, Ancyloceratoidea, Ptychoceratoidea. In: Riegraf, W. (Ed.), Fossilium Catalogus I: Animalia, Pars 144. Backhuys, Leiden, 381 p.

Klein, J., Hoffmann, R., Joly, B., Shigeta, Y., and Vašíček, Z., 2009, Lower Cretaceous Ammonites IV. Boreophylloceratoidea, Phylloceratoidea, Lytoceratoidea, Tetragonitoidea, Haploceratoidea including the Upper Cretaceous representatives. In: Riegraf, W. (Ed.), Fossilium Catalogus I: Animalia, Pars 146. Backhuys, Leiden, 416 pp.

Kohan Martinez, M., Iglesia Llanos, M.P., Kietzmann, D.A., and Luppo, T., 2017, Preliminary magnetostratigraphy and rock magnetic analysis of the Vaca Muerta Formation (Upper Jurassic-Lower Cretaceous) in the Puerta Curaco section, Argentina. Latinmag Letters, v. 7, PM03.

Kowal-Kasprzyk, J., 2016, Micropaleontological characteristics of Mesozoic limestone rocks from the Silesian mantle between Sola and Dunajec. Unpublished PhD Thesis, Universytet Jagielloński w Krakowie, 310 p. [in Polish, with English abstract].

Krische, O., Grabowski, J., Bujtor, L., and Gawlick, H.-J., 2018, Latest Jurassic to Early Cretaceous evolution in the central Northern Calcareous Alps. Field Trip Post-Ex-2, 21st International Congress of the Carpathian Balkan Geological Association (CBGA 2018), Berichte der Geologischen Bundesanstalt, v. 126, pp. 223–258.

Krymgol'ts, G.Y., 1997, Belemnites. Subclass Endocochlia, inner-shelled. In: Arkadiev, V.V., and Bogdanova, T.N. (Eds.), Atlas of the Cretaceous fauna of south-west Crimea. Pangeya, Saint Petersburg, pp. 146–155 [in Russian].

Kuhn, O., Weissert, H., Föllmi, K.B., and Hennig, S., 2005, Altered carbon cycling and trace-metal enrichment during the late Valanginian and early Hauterivian. Eclogae Geologicae Helvetiae, v. 98, pp. 333–344. doi:10.1007/s00015-005-1172-7

Kujau, A., Heimhofer, U., Hochuli, P.A., Pauly, S., Morales, C., Adatte T., Föllmi, K.B., Ploch, and I., Mutterlose, J., 2013, Reconstructing Valanginian (Early Cretaceous) mid-latitude vegetation and climate dynamics based on spore–pollen assemblages, Review of Palaeobotany and Palynology, v. 197, pp. 50–69. doi:10.1016/j.revpalbo.2013.05.003

Lafargue, E., Marquis, F., and Pillot, D., 1998, Rock-Eval 6 applications in hydrocarbon exploration, production and soil contamination studies. Oil & gas science and technology, Revue Institut Française du Pétrole, v. 53, pp. 421–437. doi:10.2516/ogst:1998036

Lakova, I., and Petrova, S., 2013, Towards a standard Tithonian to Valanginian calpionellid zonation of the Tethyan Realm. Acta Geologica Polonica, v. 63, pp. 201–221. doi:10.2478/agp-2013-0008

Lakova, I., Stoykova, K., and Ivanova, D., 1997, Tithonian to Valanginian bioevents and integrated zonation of calpionellids, calcareous nannofossils and calcareous dinocysts from the Western Balcanides, Bulgaria. Mineralia Slovaca, v. 29, pp. 301–303.

Lakova, I., Stoykova, K., and Ivanova, D., 1999, Calpionellid, nannofossil and calcareous dinocyst bioevents and integrated biochronology of the Tithonian to Valanginian in the Western Balkanides, Bulgaria. Geologica Carpathica, v. 50, pp. 151–168.

Leanza, A.F., 1945, Ammonites del Jurásico superior y del Cretáceo inferior de la Sierra Azul, en la parte meridional de la provincia de Mendoza. Anales del Museo de La Plata, Paleontología (nueva serie), v. 1, pp. 1–99.

Leanza, H.A., and Wiedmann, J., 1989, Nuevos ammonites del Berriasiano/Valanginiano (Cretácico inferior) de Neuquén, Argentina. In: Wiedmann (Ed.), Cretaceous of the Western Tethys. Schweizerbart, Stuttgart, pp. 793–810.

Leereveld, H., 1997, Upper Tithonian–Valanginian (Upper Jurassic–Lower Cretaceous dinoflagellate cyst stratigraphy of the western Mediterranean.

Cretaceous Research, v. 18, pp. 385–420. doi:10.1006/cres.1997.0070

Le Hégarat, G., 1973, Le Berriasien du sud-est de la France. Documents des Laboratoires de Géologie de la Faculté des Sciences de Lyon, v. 43, pp. 1–576.

Le Hégarat, G., and Remane, J., 1968, Tithonique supérieur et Berriasien de l'Ardèche et de l'Hérault; corrélation des ammonites et des calpionelles. Géobios, v. 1, pp. 7–69. doi:10.1016/S0016-6995(68)80001-4

Lehmann, J., Ifrim, C., Bulot, L., and Frau, C., 2015, Paleobiogeography of Early Cretaceous ammonoids. In: Klug, C., Korn, D., De Baets, K., Kruta, I., and Mapes, R.H. (Eds.), Ammonoid paleobiology: From macroevolution to paleogeography. Topics in Paleobiology, v. 44, pp. 229–257. doi:10.1007/978-94-017-9633-0_9

Levert, J., and Ferry, S., 1988, Diagenèse argileuse complexe dans le Mésozoïque subalpin révélée par cartographie des proportions relatives d'argiles selon des niveaux isochrones. Bulletin de la Société Géologique de France, 8ème série, v. 4, pp. 1029–1038. doi:10.2113/gssgfbull.IV.6.1029

Lini, A., Weissert, H., and Erba, E., 1992, The Valanginian carbon isotope event: a first episode of greenhouse climate conditions during the Cretaceous. Terra Nova, v. 4, pp. 374–384. doi:10.1111/j.1365-3121.1992.tb00826.x

Lister, J.K., and Batten, D.J., 1988, Stratigraphic and palaeoenvironmental distribution of Early Cretaceous dinoflagellate cysts in the Hurlands Farm Borehole, West Sussex, England. Palaeontographica B, v. 210, pp. 9–89.

Lodowski, D.G., Pszczółkowski, A., Szives, O., Főzy, I., and Grabowski, J., 2022, Jurassic–Cretaceous transition in the Transdanubian Range (Hungary): Integrated stratigraphy and paleomagnetic study of the Hárskút and Lókút sections. Newsletters on Stratigraphy, v. 55, pp. 99–135. doi:10.1127/nos/2021/0656

Lory, C., 1860-64, Description géologique du Dauphiné (Isère, Drôme, Hautes-Alpes) pour servir à l'explication de la carte géologique de cette province. Savy, Paris, 748 p.

Lory, P., 1898, Sur le Crétacé inférieur du Dévolvy et des régions voisines. Bulletin de la Société Géologique de France, 3ème série, v. 26, pp. 132–138.

Lozar, F., and Tremolada, F., 2003, Calcareous nannofossil biostratigraphy of Cretaceous sediments recovered at ODP site 1149 (Leg 185, Nadezhda basin, western Pacific). Proceedings of the Ocean Drilling Program, Scientific Results, v. 185, pp. 1–21. doi:10.2973/odp.proc.sr.185.010.2003

Lukeneder, A., and Reháková, D., 2004, Lower Cretaceous section of the Ternberg Nappe (Northern Calcareous Alps, Upper Austria): Facies-changes, biostratigraphy and paleoecology. Geologica Carpathica, v. 55, pp. 227–237.

Lukeneder, A., and Reháková, D., 2007, Chronostratigraphic significance of an early Valanginian (Cretaceous) calpionellid association (Hochkogel section, Upper Austria, Northern Calcareous Alps). Geological Quarterly, v. 51, pp. 27–38.

Mann, M.E., Lees, J.M., 1996, Robust estimation of background noise and signal detection in climatic time series. Climatic Change, v. 33, pp. 409–445. doi:10.1007/BF00142586

Martinez, M., Deconinck, J.F., Pellenard, P., Reboulet, S., and Riquier, L., 2013, Astrochronology of the Valanginian Stage from reference sections (Vocontian basin, France) and palaeoenvironmental implications for the Weissert Event. Palaeogeography, Palaeoclimatology, Palaeoecology, v. 376, pp. 91–102. doi:10.1016/j.palaeo.2013.02.021

Martinez, M., Deconinck, J.F., Pellenard, P., Riquier, L., Company, M., Reboulet, S., and Moiroud, M., 2015, Astrochronology of the Valanginian–Hauterivian stages (Early Cretaceous): Chronological relationships between the Paraná–Etendeka Large Igneous Province and the Weissert and the Faraoni events. Global and Planetary Change, v. 131, pp. 158–173. doi:10.1016/j.gloplacha.2015.06.001

Martinez, M., Guillois, L., Boulvais, P., and Deconinck, J.F., 2020, Inverted responses of the carbon cycle to orbital forcing in Mesozoic peripl-atform marginal basins: Implications for astrochronology. Paleoceanography and Paleoclimatology, v. 35, e2019PA003705. doi:10.1029/2019PA003705

Martinez, M., Aguirre-Urreta, B., Dera, G., Lescano, M., Omarini, J., Tunik, M., O'Dogherty, L., Aguado, R., Company, M., and Bodin, S., 2023, Synchrony of carbon cycle fluctuations, volcanism and orbital forcing during the Early Cretaceous. Earth-Science Reviews, v. 239, 104356. doi:10.1016/j.earscirev.2023.104356

Mayer-Eymar, K., 1887, Systematisches Verzeichnis der Kreide- und Tertiärversteinerungen der Umgegend von Thun nebst Beschreibung der neuen Arten. Beiträge zur Geologischen Karte der Schweiz, v. 24, pp. 1–128.

Mazenot, G., 1939, Les Palæohoplitidae tithoniques et berriasiens du sud-est de la France. Mémoires de la Société Géologique de France, nouvelle série, v. 41, pp. 1–303.

McArthur J.M. and Howarth R.J., 2025. Strontium isotope stratigraphy of the Cretaceous. In: Hart, M. B., Batenburg, S. J., Huber, B. T., Price, G. D., Thibault, N., Wagreich, M. and Walaszczyk, I. (eds). Cretaceous Project 200 Volume 1: the Cretaceous World. Geological Society, Special Publications, v. 544, pp. 343–366. First published online January 15, 2024, doi:10.1144/SP544-2023-85

McArthur, J.M., Mutterlose, J., Price, G.D., Rawson, P.F., Ruffell, A., and Thirlwall, M.F., 2004, Belemnites of Valanginian, Hauterivian and Barremian age: Sr-isotope stratigraphy, composition ($^{87}Sr/^{86}Sr$, $\delta^{13}C$, $\delta^{18}O$, Na, Sr, Mg), and palaeo-oceanography. Palaeogeography, Palaeoclimatology, Palaeoecology, v. 202, pp. 253–272. doi:10.1016/S0031-0182(03)00638-2

McArthur, J.M., Janssen, N.M.M., Reboulet, S., Leng, M.J., Thirlwall, M.F., and Schootbrugge, B. van de, 2007, Palaeotemperatures, polar ice-volume, and isotope stratigraphy (Mg/Ca, $\delta^{18}O$, $\delta^{13}C$, $^{87}Sr/^{86}Sr$): The Early Cretaceous (Berriasian, Valanginian, Hauterivian). Palaeogeography, Palaeoclimatology, Palaeoecology, v. 248, 391–430. doi:10.1016/j.palaeo.2006.12.015

McArthur, J.M., Howarth, R.J., Shields G.A., and Zhou, Y., 2020, Strontium isotope stratigraphy. In: Gradstein, F.M., Ogg, J.G., Schmitz, M.D., and Ogg, G.M. (Eds), A Geologic Time Scale 2020. Elsevier, Amsterdam, pp. 211–238. doi:10.1016/B978-0-12-824360-2.00007-3

McArthur, J.M., Millar, I.L., Drury, A.J., and Wagner, D., 2025. Strontium-isotope stratigraphy: methodology, standard values (SRM987, EN-1, E&A), a new Neogene curve of $^{87}Sr/^{86}Sr$ against time, its implications for astrochronology ([I]ODP Sites 1146, 1264, U1337, and U1338), and its application to ODP Site 758 (Indian summer monsoon) and IODP Site 1120 (a new age-model). Palaeogeography, Palaeoclimatology, Palaeoecology, v. 669, 112907. doi:10.1016/j.palaeo.2025.112907

Melinte, M., and Mutterlose, J., 2001, A Valanginian (Early Cretaceous) 'boreal nannoplankton excursion' in sections from Romania. Marine Micropaleontology, v. 43, pp. 1–25. doi:10.1016/S0377-8398(01)00022-6

Mercuzot, M., Pellenard, P., Durlet, C., Bougeault, C., Meister, C., Dommergues, J.L., Thibault, N., Baudin, F., Mathieu, O., Bruneau, L., Huret, E., and El Hmidi, K., 2020, Carbon-isotope events during the Pliensbachian (Lower Jurassic) on the African and European margins of the NW Tethyan Realm. Newsletters on Stratigraphy, v. 53, pp. 41–69. doi:10.1127/nos/2019/0502

Michalík, J., Grabowski, J., Lintnerová, O., Reháková, D., Kdýr, Š., and Schnabl, P., 2021, Jurassic–Cretaceous boundary record in Carpathian sedimentary sequences. Cretaceous Research, v. 118, 104659. doi:10.1016/j.cretres.2020.104659

Mitta, V.V., 2018, The genus *Delphinites* Sayn (Ammonoidea: Neocomitidae) in the Lower Valanginian of the Russian Platform. Paleontological Journal, v. 52, pp. 1504–1516. doi:10.1134/S0031030118130105

Molčan Matejová, M., Reháková, D., Aubrecht, R., Ledvényiová, L., and Měchová, L., 2022, Unusual microfacies character of the Pieniny Limestone in the Orava sector of the Pieniny Klippen Belt. Acta Geologica Slovaca, v. 14, pp. 73–86.

Möller, C., Mutterlose, J., and Alsen, P., 2015, Integrated stratigraphy of Lower Cretaceous sediments (Ryazanian–Hauterivian) from north-

east Greenland. Palaeogeography, Palaeoclimatology, Palaeoecology, v. 437, pp. 85–97. doi:10.1016/j.palaeo.2015.07.014

Monteil, E., 1985, Les dinokystes du Valanginien du bassin du sud-est (Ardèche, France). Unpublished Thèse Doct. 3ème Cycle, Université Pierre et Marie Curie, Paris, 314 p.

Monteil, E., 1990, Revision and emendation of dinocyst genus *Amphorula* Dodekova 1969. The concept of morphostratigraphy. Bulletin des Centres de Recherches Exploration-Production Elf-Aquitaine, v. 14, pp. 597–609.

Monteil, E., 1992a, Quelques nouvelles espèces-index de kystes de dinoflagellés (Tithonique-Valanginien) du sud-est de la France et de l'ouest de la Suisse. Revue de Paléobiologie, v. 11, pp. 273–297.

Monteil, E., 1992b, Kystes de dinoflagelles index (Tithonique–Valanginien) du sud-est de la France: proposition d'une nouvelle zonation palynologique. Revue de Paleobiologie, v. 11, pp. 299–306.

Monteil, E., 1993, Dinoflagellate cyst biozonation of the Tithonian and Berriasian of southeast France: Correlation with the sequence stratigraphy. Bulletin des Centres de Recherches Exploration-Production Elf Aquitaine, v. 17, pp. 249–275.

Moore, D.M., and Reynolds, R.C., 1997, X-ray diffraction and the identification and analysis of clay minerals. Oxford University Press, New York, 378 p.

Morales, C., Gardin, S., Schnyder, J., Spangenberg, J.E., Arnaud-Vanneau, A., Arnaud, H., Adatte, T., and Föllmi, K.B., 2013, Berriasian and early Valanginian environmental change along a transect from the Jura platform to the Vocontian basin. Sedimentology, v. 60, pp. 36–63. doi:10.1111/sed.12019

Morales, C., Spangenberg, J.E., Arnaud-Vanneau, A., Adatte, T., and Föllmi, K.B., 2016, Evolution of the northern Tethyan Helvetic platform during the late Berriasian and early Valanginian. The Depositional Record, v. 2, pp. 47–73. doi:10.1002/dep2.13

Mutterlose, J., 1991, Das Verteilungs- und Migrationsmuster des kalkigen Nannoplanktons in der borealen Unterkreide (Valangin–Apt) NW-Deutschlands. Palaeontographica B, v. 221, pp. 27–152.

Mutterlose, J., 1992a, Lower Cretaceous nannofossil biostratigraphy off northwestern Australia (Leg 123). Proceedings of the Ocean Drilling Program, Scientific Results, v. 123, pp. 343–368. doi:10.2973/odp.proc.sr.123.124.1992

Mutterlose, J., 1992b, Biostratigraphy and palaeobiogeography of Early Cretaceous calcareous nannofossils. Cretaceous Research, v. 13, pp. 167–189. doi:10.1016/0195-6671(92)90034-N

Mutterlose, J., and Wise, S.W., 1990, Lower Cretaceous nannofossil biostratigraphy of ODP Leg 113 holes 692B and 693A, continental slope off East Antarctica, Weddell Sea. Proceedings of the Ocean Drilling Program, Scientific Results, v. 113, pp. 325–351. doi:10.2973/odp.proc.sr.113.143.1990

Mutterlose, J., Bodin, S., and Fähnrich, L., 2014, Strontium-isotope stratigraphy of the Early Cretaceous (Valanginian–Barremian): Implications for Boreal–Tethys correlation and paleoclimate. Cretaceous Research, v. 50, pp. 252–263. doi:10.1016/j.cretres.2014.03.027

Myczyński, R., 1977, Lower Cretaceous ammonites from Sierra del Rosario (western Cuba). Acta Palaeontologica Polonica, v. 22, pp. 139–173.

Nasiri, Y., Reza, M.H., Mahboubi, A., Olivero, D., and Mosaddegh, H., 2020, *Zoophycos* ichnogenus distribution and paleoenvironmental analysis: examples from the Mississippian Mobarak formation (Alborz basin, Iran). Historical Biology, v. 32, pp. 848–867. doi:10.1080/08912963.2018.1540614

Ogg, J.G., 1983, Magnetostratigraphy of the Upper Jurassic and lowest Cretaceous sediments, Deep Sea Drilling Project site 534, western North Atlantic. Deep Sea Drilling Project, Initial Reports, v. 76, pp. 685–697. doi:10.2973/dsdp.proc.76.131.1983

Ogg, J.G., 1987, Early Cretaceous magnetic polarity time scale and the magnetostratigraphy of Deep Sea Drilling Project sites 603 and 534, western Central Atlantic. Deep Sea Drilling Project, Initial Reports, v. 93, pp. 849–879. doi:10.2973/dsdp.proc.93.131.1987

Ogg, J.G., 2020, Geomagnetic Polarity Time Scale. In: Gradstein, F.M., Ogg, J.G., Schmitz, M.D., and Ogg, G.M. (Eds.), Geologic Time Scale 2020. Elsevier, Amsterdam, pp. 159–192. doi:10.1016/B978-0-12-824360-2.00005-X

Ogg, J.G., Steiner, M.B., Company, M., and Tavera, J.M., 1988, Magnetostratigraphy across the Berriasian–Valanginian stage boundary (Early Cretaceous), at Cehegín (Murcia Province, southern Spain). Earth and Planetary Science Letters, v. 87, pp. 205–215. doi:10.1016/0012-821X(88)90075-1

Ogg, J.G., Hasenyager, R.W., and Wimbledon, W.A., 1994, Jurassic–Cretaceous boundary: Portland–Purbeck magnetostratigraphy and possible correlation to the Tethyan faunal realm. Geobios, M.S., v. 17, pp. 519–527. doi:10.1016/S0016-6995(94)80217-3

Ogg, J.G., Hinnov, L.A., and Huang, C., 2012, Cretaceous. In: Gradstein, F.M., Ogg, J.G., Schmitz, M., and Ogg, G. (Eds.), The Geologic Time Scale 2012. Elsevier, Amsterdam, pp. 793–853. doi:10.1016/B978-0-444-59425-9.00027-5

Ogg, J.G., Ogg, G.M., and Gradstein, F.M., 2016. A concise Geologic Time Scale 2016. Elsevier, Amsterdam, 234 p.

Olivero, D., 1996, *Zoophycos* distribution and sequence stratigraphy. Examples from the Jurassic and Cretaceous deposits in south-eastern France. Palaeogeography, Palaeoclimatology, Palaeoecology, v. 123, pp. 273–287. doi:10.1016/0031-0182(95)00120-4

Olivero, D., 2003, Early Jurassic to Late Cretaceous evolution of *Zoophycos* in the French Subalpine basin (southeastern France). Palaeogeography, Palaeoclimatology, Palaeoecology, v. 192, pp. 59–78. doi:10.1016/S0031-0182(02)00679-X

Olivero, D., and Gaillard, C., 2007, A constructional model for *Zoophycos*. In: Miller, W. (Ed.). Trace fossils: Concepts, problems, prospects. Elsevier, Amsterdam, pp. 466–477. doi:10.1016/B978-044452949-7/50154-6

Olszewska, B., 2005, Microfossils of the Cieszyn Beds (Silesian Unit, Polish Outer Carpathians) – a thin section study. Polish Geological Institute Special Papers, v. 19, pp. 1–58.

Olszewska, B., 2010, Microfossils of the Upper Jurassic–Lower Cretaceous formations of the Lublin Upland (SE Poland) based on thin section studies. Polish Geological Institute Special Papers, v. 26, pp. 1–56.

Ölveczká, D., and Reháková, D., 2022, Upper Tithonian *Crassicollaria* Zone: New data on the calpionellid distribution and subzonal division of the Pieniny Klippen Belt in Western Carpathians. Acta Geologica Slovaca, v. 14, pp. 37–56.

Omaña, L., González-Arreola, C., and Núñez-Useche, F., 2017, The Berriasian–Valanginian boundary interval based on calpionellids from the Taraises Formation, Cuencamé de Ceniceros, Durango, NW Mexico: Biostratigraphic, paleoecologic and paleobiogeographic significance. Journal of South American Earth Sciences, v. 80, pp. 589–600. doi:10.1016/j.jsames.2017.10.011

Ooster, W.A., 1857, Catalogue des céphalopodes fossiles des Alpes suisses avec la description et les figures des espèces remarquables. Céphalopodes acétabulifères: Décapodes. Nouveaux Mémoires de la Société Helvétique des Sciences Naturelles, v. 17, pp. 5–34.

Orbigny, A. d', 1847, Paléontologie française. Description zoologique et géologique de tous les animaux mollusques et rayonnés fossiles de France. Terrains Crétacés, Supplément. Bertrand, Paris, 28 p.

Ovando-Figueroa, J.R., Moreno-Bedmar, J.A., Company, M., Barragán, R., Ramírez-Peña, C.F., and Chávez-Cabello, G., 2024a, Lower Valanginian ammonite biostratigraphy of the Cañón de la Vaca section, Taraises Formation, Coahuila state, northern Mexico. Journal of South American Earth Sciences, v. 144, 104994. doi:10.1016/j.jsames.2024.104994

Ovando-Figueroa, J.R., Moreno-Bedmar, J.A., Company, M., and Jacobo-Delgado, J.A., 2024b, Taxonomic review of Berriasian and Valanginian ammonites from Zacatecas State (north-central Mexico) studied by Burckhardt in 1906. Cretaceous Research, v. 154, 105743. doi:10.1016/j.cretres.2023.105743

Özkan, S., 1993, Calcareous nannofossils from the Late Jurassic–Early

Cretaceous of Northwest Anatolia, Turkey. Geological Journal, v. 28, pp. 295–307. doi:10.1002/gj.3350280308

Paquier, V.L., 1900, Recherches géologiques dans le Diois et les Baronnies orientales. Allier, Grenoble, 402 p.

Pauly, S., Mutterlose, J., and Alsen, P., 2012a, Lower Cretaceous (upper Ryazanian–Hauterivian) chronostratigraphy of high latitudes (northeast Greenland). Cretaceous Research, v. 34, pp. 308–326. doi:10.1016/j.cretres.2011.11.011

Pauly, S., Mutterlose, J., and Alsen, P., 2012b, Early Cretaceous palaeoceanography of the Greenland-Norwegian seaway evidenced by calcareous nannofossils. Marine Micropaleontology, v. 90–91, pp. 72–85. doi:10.1016/j.marmicro.2012.04.004

Pauly, S., Mutterlose, J., and Alsen, P., 2013, Depositional environments of Lower Cretaceous (Ryazanian–Barremian) sediments from Wollaston Forland and Kuhn Ø, north-east Greenland. Bulletin of the Geological Society of Denmark, v. 61, pp. 19–36. doi:10.37570/bgsd-2013-61-02

Perch-Nielsen, K., 1979, Calcareous nannofossils from the Cretaceous between the North Sea and the Mediterranean. Aspekte der Kreide Europas, IUGS Series A 6, pp. 223–272.

Perch-Nielsen, K., 1985, Mesozoic calcareous nannofossils. In: Bolli, H.M., Saunders, J.B., and Perch-Nielsen, K. (Eds.), Plankton stratigraphy. Cambridge University Press, Cambridge, pp. 329–426.

Petrova, S., and Metodiev, L., 2012, Berriasian and Valanginian calpionellids from the Ticha Formation of the East Fore-Balkan (Bulgaria). Proceedings of the Bulgarian Geological Society National Conference "Geosciences 2012", pp. 95–96.

Petrova, S., Lakova, I., and Ivanova, D., 2011, Berriasian–Valanginian boundary in Bulgaria. Review of the Bulgarian Geological Society, v. 72, pp. 91–97.

Picollier, M.C., 2022, Biometry and biostratigraphy of the Early Cretaceous belemnite genus *Castellanibelus* from the southeast of France. Comptes Rendus Géoscience, Sciences de la Planète, v. 354, Special Issue S3, pp. 27–43. doi:10.5802/crgeos.166

Pictet, F.J., and Campiche, G., 1860, Description des fossiles du terrain Crétacé des environs de Sainte-Croix, première partie. Matériaux pour la Paléontologie Suisse, seconde série, pp. 209–380.

Pocock, S.A.J., 1976, A preliminary dinoflagellate zonation of the uppermost Jurassic and lower part of the Cretaceous, Canadian Arctic, and possible correlation in the Western Canada basin. Geoscience and Man, v. 15, pp. 101–114. doi:10.1080/00721395.1976.9989778

Pop, G., 1974, Les zones de calpionellides tithoniques-valanginiennes du sillon de Reşiţa (Carpates Méridionales) (Carpathes méridionales). Revue Roumaine de Géologie Géophysique et Géographie, Série Géologie, v. 18, pp. 109–125.

Pop, G., 1986, Les zones de calpionelles tithoniques-néocomiennes de la région de Sviniţa (Carpathes méridionales). Dări de Seamă ale Şedinţelor, Institutul de Geologie şi Geofizică, v. 70-71/4 (1983-84), pp. 87–108.

Pop, G., 1989, Age and Facies of the Calpionellid formations from the South Carpathians. In: Wiedmann (Ed.), Cretaceous of the Western Tethys. Schweizerbart, Stuttgart, pp. 525–542.

Pop, G., 1994, Calpionellid evolutive events and their use in biostratigraphy. Romanian Journal of Stratigraphy, v. 76, pp. 7–24.

Pop, G., 1997, Tithonian to Hauterivian praecalpionellids and calpionellids: bioevents and biozones. Mineralia Slovaca, v. 29, pp. 304–305.

Price, G.D., Főzy, I., and Pálfy, J., 2016, Carbon cycle history through the Jurassic–Cretaceous boundary: A new global $\delta^{13}C$ stack. Palaeogeography, Palaeoclimatology, Palaeoecology, v. 451, pp. 46–61. doi:10.1016/j.palaeo.2016.03.016

Pross, J., and Brinkhuis, H., 2005, Organic-walled dinoflagellate cysts as paleoenvironmental indicators in the Paleogene; a synopsis of concepts. Paläontologische Zeitschrift, v. 79, pp. 53–59. doi:10.1007/BF03021753

Pszczółkowski, A., and Myczyński, R., 2004, Ammonite-supported microfossil and nannoconid stratigraphy of the Tithonian–Hauterivian limestones in selected sections of the Branisko Succession, Pieniny Klippen Belt (Poland). Studia Geologica Polonica, v. 123, pp. 133–197.

Pszczółkowski, A., and Myczyński, R., 2010, Tithonian–early Valanginian evolution of deposition along the proto-Caribbean margin of North America recorded in Guaniguanico successions (western Cuba). Journal of South American Earth Sciences, v. 29, pp. 225–253. doi:10.1016/j.jsames.2009.07.004

Rawson, P.F., 1983, The Valanginian to Aptian stages – current definitions and outstanding problems. Zitteliana, v. 10, pp. 493–500.

Rawson, P.F., 1993, The influence of sea-level changes on the migration and evolution of early Cretaceous (pre-Aptian) ammonites. In: House, M.R. (Ed.), The Ammonoidea: Environment, ecology and evolutionary change. Systematics Association Special Volume 47, pp. 227–242.

Rawson, P.F., 1994. Sea level changes and their influence on ammonite biogeography in the European Early Cretaceous. In: Proceedings of the 3rd Pergola International Symposium, Palaeopelagos Special Publication, v. 1., pp 317–326.

Reboulet, S., Hoedemaeker, P.J. (reporters), Aguirre-Urreta, M.B., Alsen, P., Atrops, F., Baraboshkin, E.J., Company, M., Delanoy, G., Dutour, Y., Klein, J., Latil, J.L., Lukeneder, A., Mitta, V.V., Mourgues, F.A., Ploch, I., Raisossadat, S.N., Ropolo, P., Sandoval, J., Tavera, J.M., Vašíček, Z., and Vermeulen, J., 2006, Report on the 2nd International Meeting of the IUGS Lower Cretaceous Ammonite Working Group, the "Kilian Group" (Neuchâtel, Switzerland, 8 September 2005). Cretaceous Research, v. 27, pp. 712–715. doi:10.1016/j.cretres.2006.03.006

Reboulet, S., Klein, J. (reporters), Barragán, R., Company, M., González-Arreola, C., Lukeneder, A., Raisossadat, S.N., Sandoval, J., Szives, O., Tavera, J.M., Vašíček, Z., and Vermeulen, J., 2009, Report on the 3rd International Meeting of the IUGS Lower Cretaceous Ammonite Working Group, the "Kilian Group" (Vienna, Austria, 15th April 2008). Cretaceous Research, v. 30, pp. 496–502. doi:10.1016/j.cretres.2008.12.009

Reboulet, S., Rawson, P.F., Moreno-Bedmar, J.A., Aguirre-Urreta, M.B., Barragán, R., Bogomolov, Y., Company, M., González-Arreola, C., Idakieva Stoyanova, V., Lukeneder, A., Matrion, B., Mitta, V.V., Randrianaly, H., Vašíček, Z., Baraboshkin, E.J., Bert, D., Bersac, S., Bogdanova, T.N., Bulot, L.G., Latil, J.L., Mikhailova, I.A., Ropolo, P., and Szives, O., 2011, Report on the 4th International Meeting of the IUGS Lower Cretaceous Ammonite Working Group, the "Kilian Group" (Dijon, France, 30th August 2010). Cretaceous Research, v. 32, pp. 786–793. doi:10.1016/j.cretres.2011.05.007

Reboulet, S., Szives, O., Aguirre-Urreta, M.B., Barragán, R., Company, M., Idakieva, V., Ivanov, M., Kakabadze, M.V., Moreno-Bedmar, J.A., Sandoval, J., Baraboshkin, E.J., Çağlar, M.K., Főzy, I., González-Arreola, C., Kenjo, S., Lukeneder, A., Raisossadat S.N., Rawson, P.F., and Tavera, J.M., 2014, Report on the 5th International Meeting of the IUGS Lower Cretaceous Ammonite Working Group, the Kilian Group (Ankara, Turkey, 31st August 2013). Cretaceous Research, v. 50, pp. 126–137. doi:10.1016/j.cretres.2014.04.001

Reboulet, S., Szives, O., Aguirre-Urreta, M.B., Barragán, R., Company, M., Frau, C., Kakabadze, M.V., Klein, J., Moreno-Bedmar, J.A., Lukeneder, A., Pictet, A., Ploch, I., Raisossadat S.N., Vašíček, Z., Baraboshkin, E.J., and Mitta V.V., 2018, Report on the 6th International Meeting of the IUGS Lower Cretaceous Ammonite Working Group, the Kilian Group (Vienna, Austria, 20th August 2017). Cretaceous Research, v. 91, pp. 100–110. doi:10.1016/j.cretres.2018.05.008

Reboulet, S., Jaillard, E., Shmeit, M., Giraud, F., Masrour, M., and Spangenberg, J.E., 2022, Biostratigraphy, carbon isotope and sequence stratigraphy of South Tethyan Valanginian successions in the Essaouira-Agadir basin (Morocco). Cretaceous Research, v. 140, 105341. doi:10.1016/j.cretres.2022.105341

Reboulet, S., Adatte, T., Baudin, F., Company, M., Deconinck, J.F., Duxbury, S., Grabowski, J., Granier, B., Janssen, N.M.M., Klein, J., Leng, M.G., Lodowski, D.G., Martinez, M., Mattioli, E., McArthur, J.M., Olivero, D., and Reháková, D., 2023, The Global boundary Stratotype Section and Point (GSSP) for the base of the Valanginian Stage (Lower Cretaceous): the informal proposal of the Vergol candidate section

(Drôme, southeast France). Unpublished informal proposal, pp. 1–75.
Reháková, D., 1995, Nové poznatky o distribúcii kalpionelíd vo vrchnojurských a spodnokriedových súvrstviach Západných Karpát. Mineralia Slovaca, v. 27, pp. 308–318.
Reháková, D., 2000a, Calcareous dinoflagellate and calpionellid bioevents versus sea-level fluctuations recorded in the West-Carpathian (Late Jurasic/Early Cretaceous) pelagic environments. Geologica Carpathica, v. 51, pp. 229–243.
Reháková, D., 2000b, Evolution and distribution of the Late Jurassic and Early Cretaceous calcareous dinoflagellates recorded in the Western Carpathian pelagic carbonate facies. Mineralia Slovaca, v. 32, pp. 79–88.
Reháková, D., 2019. Plankton evolution and biostratigraphy during Late Jurassic and Early Cretaceous. Proceedings of the Geologica Carpathica 70 Conference, 2019, pp. 137–140.
Reháková, D., and Michalík, J., 1997a, Calpionellid associations versus Late Jurassic and Early Cretaceous sea-level fluctuations. Mineralia Slovaca, v. 29, pp. 306–307.
Reháková, D., and Michalík, J., 1997b, Evolution and distribution of calpionellids – the most characteristic constituents of Lower Cretaceous Tethyan microplankton. Cretaceous Research, v. 18, pp. 493–504. doi:10.1006/cres.1997.0067
Remane, J., 1971, Les Calpionelles, protozoaires planctoniques des mers mésogéennes de l'époque secondaire. Annales Guébhard, v. 47, pp. 369–393.
Remane, J., and Thieuloy, J.P., 1973a, Coupe A III-2: Barret-le-Bas, Les Sausses. Documents des Laboratoires de Géologie de la Faculté des Sciences de Lyon, v. H.S. 1, pp. 90–95.
Remane, J., and Thieuloy, J.P., 1973b, Coupe A IV-1: La Faurie-Pusteau. Documents des Laboratoires de Géologie de la Faculté des Sciences de Lyon, v. H.S. 1, pp. 101–105.
Remane, J., Bakalova-Ivanova, D., Borza, K., Knauer, J., Nagy, I., Pop, G., and Tardi-Filacz, E., 1986, Agreement on the subdivision of the standard calpionellid zones defined at the II planktonic conference, Roma 1970. Acta Geologica Hungarica, v. 29, pp. 5–14.
Remane, J., Bassett, M.G., Cowie, J.W., Gohrbandt, K.H., Lane, H.R., Michelsen, O, and Naiwen, W., 1996, Revised guidelines for the establishment of global chronostratigraphic standards by the International Commission on Stratigraphy (ICS). Episodes, v. 19, pp. 77–81. doi:10.18814/epiiugs/1996/v19i3/007
Renevier, E., 1897, Seconde édition du tableau des terrains sédimentaires formés pendant les époques de la phase organique du globe terrestre. Compte-Rendu du 6ème Congrès Géologique International, 1894, pp. 523–695.
Rey, J., 1993, Análisis de la cuenca subbética durante el Jurásico y el Cretácico en la transversal Caravaca-Vélez Rubio. Universidad de Granada, Granada, 460 p.
Ricken, W., 1993, Sedimentation as a three-component system: Organic carbon, carbonate, noncarbonate. Lecture Notes in Earth Sciences, v. 51, pp. 1–211.
Riley, L.A., 1977, Stage nomenclature at the Jurassic–Cretaceous boundary, North Sea basin. Proceedings of the Mesozoic Northern North Sea Symposium, 1977, v. 4, pp. 1–11.
Rivera, R., 1951, La fauna de los Estratos Puente Inga, Lima. Boletín de la Sociedad Geológica del Perú, v. 22, pp. 1–53.
Robertson, A.H.F., and Bliefnick, D.M., 1983, Sedimentology and origin of Lower Cretaceous pelagic carbonates and redeposited clastics, Blake-Bahama formation, Deep Sea Drilling Project site 534, western Equatorial Atlantic. Deep Sea Drilling Project, Initial Reports, v. 76, pp. 795–828. doi:10.2973/dsdp.proc.76.140.1983
Roth, P.H., 1978, Cretaceous nannoplankton biostratigraphy and oceanography of the northwestern Atlantic Ocean. Deep Sea Drilling Project, Initial Reports, v. 44, pp. 731–759. doi:10.2973/dsdp.proc.44.134.1978
Roth, P.H., 1983, Jurassic and Lower Cretaceous calcareous nannofossils in the western North Atlantic (site 534): Biostratigraphy, preservation, and some observations on biogeography and paleoceanography. Deep Sea Drilling Project, Initial Reports, v. 76, pp. 587–621. doi:10.2973/dsdp.proc.76.125.1983
Savostin, L., Sibuet, J.C., Zonenshain, L.P., Le Pichon, X., and Roulet, M.J., 1986, Kinematic evolution of the Tethys belt from the Atlantic Ocean to the Pamirs since the Triassic. Tectonophysics, v. 123, pp. 1–35. doi:10.1016/0040-1951(86)90192-7
Sayn, G., 1907, Les ammonites pyriteuses des marnes valanginiennes du sud-est de la France. Mémoires de la Société Géologique de France, Paléontologie, v. 15, pp. 29–68.
Schnyder, J., Ruffell, A., Deconinck, J.F., and Baudin, F., 2006, Conjuctive use of spectral gamma-ray logs and clay mineralogy in defining Late Jurassic–Early Cretaceous palaeoclimate change (Dorset, U.K.). Palaeogeography, Palaeoclimatology, Palaeoecology, v. 229, pp. 303–320. doi:10.1016/j.palaeo.2005.06.027
Sissingh, W., 1977, Biostratigraphy of Cretaceous calcareous nannoplankton. Geologie en Mijnbouw, v. 56, pp. 37–65.
Sissingh, W., 1978, Microfossil biostratigraphy and stage-stratotypes of the Cretaceous. Geologie en Mijnbouw, v. 57, pp. 433–440.
Spath, L.F., 1939, The Cephalopoda of the Neocomian Belemnite Beds of the Salt Range. Palaeontologia Indica, new series, v. 25, pp. 1–154.
Sprovieri, M., Coccioni, R., Lirer, F., Pelosi, N., and Lozar, F., 2006, Orbital tuning of a Lower Cretaceous composite record (Maiolica Formation, central Italy). Paleoceanography, v. 21, PA4212. doi:10.1029/2005PA001224
Stover, L.E., Brinkhuis, H., Damassa, S.P., Verteuil, L. de, Helby, R.J., Monteil, E., Partridge, A.D., Powell, A.J., Riding, J.B., Smelror, M., and Williams, G.L., 1996, Mesozoic–Tertiary dinoflagellates, acritarchs and prasinophytes. In: Jansonius, J., and McGregor, D.C. (Eds.), Palynology: Principles and applications. American Association of Stratigraphic Palynologists Foundation, v. 2, pp. 641–750.
Stoyanova-Vergilova, M., 1963, *Curtohibolites* gen. nov. (Belemnitida) of the Lower Cretaceous of Bulgaria. Travaux sur la Géologie de Bulgarie (Paléontologie), v. 5, pp. 211–227 [in Bulgarian].
Strasser, A., Pittet, B., Hillgärtner, H., and Pasquier, J.B., 1999, Depositional sequences in shallow carbonate-dominated sedimentary systems: Concepts for a high-resolution analysis. Sedimentary Geology, v. 128, pp. 201–221. doi:10.1016/S0037-0738(99)00070-6
Szives, O., Moreno-Bedmar, J.A., Aguirre-Urreta, M.B., Company, M., Frau, C., López-Horgue, M., Pictet, A., Ploch, I., Salazar, C., Barragán, R., Latil, J.L., Lehmann, J., Robert, E., and Reboulet, S., 2024, Report on the 7th International Meeting of the IUGS Lower Cretaceous Ammonite Working Group, the Kilian Group (Warsaw, Poland, 21st August 2022): State of the art on the current Standard Ammonite Zonation of the Western Tethyan Mediterranean Province. Cretaceous Research, v. 153, 105716. doi:10.1016/j.cretres.2023.105716
Tavera, J. M., 1985, Los ammonites del Tithónico superior–Berriasense de la Zona Subbética (Cordilleras Béticas). Universidad de Granada, Granada, 381 p.
Thierstein, H.R., 1971, Tentative Lower Cretaceous calcareous nannoplankton zonation. Eclogae Geologicae Hevetiae, v. 64, pp. 459–488. doi:10.5169/seals-163990
Thieuloy, J.P., 1977, Les ammonites boréales des formations néocomiennes du sud-est français (Province Subméditerranéenne). Géobios, v. 10, pp. 395–461. doi:10.1016/S0016-6995(77)80026-0
Thieuloy, J.P., 1979, Les ammonites. Description des espèces indices et de quelques autres formes fondamentales. In: Busnardo, R., Thieuloy, J. P., and Moullade, M. (Eds.), Hypostratotype mésogéen de l'étage Valanginien (sud-est de la France). CNRS, Paris, pp. 37–57.
Thomson, D.J., 1982, Spectrum estimation and harmonic analysis. Proceedings of the IEEE, v. 70, pp. 1055–1096. doi:10.1109/PROC.1982.12433
Tissot, B.P., and Welte, D.H., 1984, Petroleum formation and occurrence (2nd ed.). Springer, Berlin, 699 p. doi:10.1007/978-3-642-87813-8
Tomaru, T., Takashima, R., Orihashi, Y., Yamanaka, T., Ando, H., Asahara, Y., Nishi, H., Kuroyanagi, A., and Otsubo, T., 2025, First evidence of

the Lower Cretaceous Weissert Event in the Northwestern Panthalassa: carbon isotope stratigraphy and U–Pb radiometric ages of the Somanakamura Group in Northeastern Japan. Newsletters on Stratigraphy, v. 58, pp. 219–238. doi:10.1127/nos/2025/0868

Toucas, A., 1890, Étude de la faune des couches tithoniques de l'Ardèche. Bulletin de la Société Géologique de France, 3ème série, v. 18, pp. 560–629.

Trejo, M., 1980, Distribución estratigráfica de los Tintínidos mesozoicos mexicanos. Revista del Instituto Mexicano del Petróleo, v. 12, pp. 4–13.

Tyson, R.H., 1995, Sedimentary organic matter. Organic facies and palynofacies. Chapman & Hall, London, 615 p.

Uhlig, V., 1910, The fauna of the Spiti Shales. Palaeontologia Indica, series 15, v. 4, pp. 133–395.

Vašíček, Z., Michalík, J., and Borza, K., 1983, To the "Neocomian" biostratigraphy in the Krížna-Nappe of the Strážovské Vrchy Mountains (northwestern Central Carpathians). Zitteliana, v. 10, pp. 467–483.

Vašíček, Z., Michalík, J., and Reháková, D., 1994, Early Cretaceous stratigraphy, paleogeography and life in Western Carpatians. Beringeria, v. 10, pp. 1–169.

Vašíček, Z., Reháková, D., and Faupl, P., 1999, Zur Biostratigraphie der Schrambachschichten der Oisbergmulde bei Hollenstein a. d. Ybbs (Lunzer Decke, Kalkalpen, Niederösterreich). Abhandlungen der Geologischen Bundesanstalt, v. 56, pp. 625–650.

Vašíček, Z., Rabrenovič, D., Radulovič, V., and Radulovič, B., 2009, Late Valanginian–Hauterivian cephalopod fauna from the Stara Planina Mountain (eastern Serbia). Neues Jahrbuch für Geologie und Paläontologie, Abhandlungen, v. 251, pp. 129–145. doi:10.1127/0077-7749/2009/0251-0129

Veen, G.W. van, 1969, Geological investigations in the region west of Caravaca, south-eastern Spain. Unpublished PhD thesis, University of Amsterdam, 143 p.

Vera, J.A., Arias, C., García-Hernández, M., López-Garrido, A.C., Martín-Algarra, A., Martín-Chivelet, J., Molina, J.M., Rivas, P., Ruiz-Ortiz, P.A., Sanz de Galdeano, C., and Vilas, L., 2004, Las Zonas Externas Béticas y el Paleomargen Sudibérico. In: Vera, J.A. (Ed.), Geología de España. Sociedad Geológica de España e Instituto Geológico y Minero de España, Madrid, pp. 354–361.

Watkins, D.K., and Bowdler, J.L., 1984, Cretaceous calcareous nannofossils from Deep Sea Drilling Project Leg 77, southeast Gulf of Mexico. Deep Sea Drilling Project, Initial Reports, v. 77, pp. 649–674. doi:10.2973/dsdp.proc.77.127.1984

Weissert, H., 1989, C-isotope stratigraphy, a monitor of paleoenvironmental change: A case study from the Early Cretaceous. Survey in Geophysics, v. 10, pp. 1–61. doi:10.1007/BF01901664

Weissert, H., and Channell, J.E.T., 1989, Tethyan carbonate carbon isotope stratigraphy across the Jurassic–Cretaceous boundary: An indicator of decelerated carbon cycling. Paleoceanography, v. 4, pp. 483–494. doi:10.1029/PA004i004p00483

Weissert, H., and Erba, E., 2004, Volcanism, CO_2 and palaeoclimate: a Late Jurassic–Early Cretaceous carbon and oxygen isotope record. Journal of the Geological Society, v. 161, pp. 695–702. doi:10.1144/0016-764903-087

Weissert, H., Lini, A., Föllmi, K.B. and Kuhn, O., 1998, Correlation of Early Cretaceous carbon isotope stratigraphy and platform drowning events: a possible link? Palaeogeography, Palaeoclimatology, Palaeoecology, v. 137, pp.189–203. doi:10.1016/S0031-0182(97)00109-0

Westermann, G.E.G., 2000, Marine faunal realms of the Mesozoic: review and revision under the new guidelines for biogeographic classification and nomenclature. Palaeogeography, Palaeoclimatology, Palaeoecology, v. 163, pp. 49–68. doi:10.1016/S0031-0182(00)00142-5

Williams, G.L., 1975, Dinoflagellate and spore stratigraphy of the Mesozoic–Cenozoic, offshore eastern Canada. Geological Survey of Canada Paper, v. 74-30, pp. 107–161.

Williams, G.L., 1977, Dinocysts: their paleontology, biostratigraphy and paleoecology. In: Ramsay, A.T.S. (Ed.), Oceanic micropalaeontology. Academic Press, London, pp. 1231–1325.

Williams, G.L., and Bujak, J.P., 1985, Mesozoic and Cenozoic dinoflagellates. In: Bolli H.M., Saunders, J.B., and Perch-Nielsen, K. (Eds.), Plankton stratigraphy. Cambridge University Press, Cambridge, pp. 847–964.

Williams, G.L., Ascoli, P., Barss, M.S., Bujak, J.P., Davies, E.H., Fensome, R.A., and Williamson, M.A., 1990, Biostratigraphy and related studies. In: Keen, M.J., and Williams, G.L. (Eds.), Geology of the continental margin of eastern Canada. Geological Survey of Canada, Geology of Canada Series, v. 2, pp. 87–137. doi:10.1130/DNAG-GNA-I1.87

Wilpshaar, M., and Leereveld, H., 1994, Palaeoenvironmental change in the Early Cretaceous Vocontian basin (SE France) reflected by dinoflagellate cysts. Review of Palaeobotany and Palynology, v. 84, pp. 121–128. doi:10.1016/0034-6667(94)90046-9

Wilson, J.L., 1975, Carbonate facies in geologic history. Springer, Berlin, 471 p. doi:10.1007/978-1-4612-6383-8

Wimbledon, W.A.P., Reháková, D., Svobodová, A., Elbra, T., Schnabl, P., Pruner, P., Šifnerová, K., Kdýr, Š., Dzyuba, O., Schnyder, J., Galbrun, B., Košťák, M., Vaňková, L., Copestake, P., Hunt, C.O., Riccardi, A., Poulton, T. P., Bulot, L.G., Frau, C., and Lena, L. de, 2020, The proposal of a GSSP for the Berriasian Stage (Cretaceous System): Part 1. Volumina Jurassica 2020, v. 18, pp. 53–106. doi:10.7306/vj.18.5

Wimbledon, W.A.P., Elbra, T., Pruner, P., Schnabl, P., Kdýr, Š., Šifnerová, K., Frau, C., Bulot, L.G., Ölveczká, D., Svobodová, A., Mikuláš, R., and Reháková, D., 2024, A re-description of the historical stratotype for the Berriasian Stage (Cretaceous System): Biostratigraphy and magnetostratigraphy. Cretaceous Research, v. 160, 105892. doi:10.1016/j.cretres.2024.105892

Wippich, M.G.E., 2003, Valanginian (Early Cretaceous) ammonite faunas from the western High Atlas, Morocco, and the recognition of western Mediterranean 'standard' zones. Cretaceous Research, v. 24, pp. 357–374. doi:10.1016/S0195-6671(03)00049-1

Worsley, T.R., 1971, Calcareous nannofossil zonation of Upper Jurassic and Lower Cretaceous sediments from the Western Atlantic. Proceedings of the 2nd Planktonic Conference, 1970, v. 2, pp. 1301–1321.

Wortmann, U.G., and Weissert, H., 2000, Tying platform drowning to perturbations of the global carbon cycle with a delta $\delta^{13}C_{Org}$-curve from the Valanginian of DSDP site 416. Terra Nova, v. 12, pp. 289–294. doi:10.1046/j.1365-3121.2000.00312.x

Stéphane Reboulet lecturer (since 1996) at the University of Lyon (France), teaches Palaeontology and Geology at the Lyon Observatory. His research interests in the Lyon Geology Laboratory include the taxonomy, evolution, biostratigraphy and palaeoecology of early Cretaceous ammonites from the Mediterranean Province. He is chair (since 2005) of the Lower Cretaceous Ammonite Working Group (the Kilian Group; https://cretaceous.stratigraphy.org/wgs/kilian), and co-chair (since 2016) of the Valanginian Working Group (https://cretaceous.stratigraphy.org/wgs/valanginian) of the International Subcommission on Cretaceous Stratigraphy. He was involved in the development of the Hauterivian Proposal (GSSP ratified in 2019) and the Golden Spike ceremony (2024, including the Albian GSSP).

Miguel Company is co-chair of the Valanginian Working Group of the International Subcommission on Cretaceous Stratigraphy. Now retired, he was until 2023 'Profesor Titular' (senior lecturer) at the Univesity of Granada (Spain), teaching general and applied palaeontology. His research interests focus on taxonomy, evolution, palaeoecology, palaeobiogeography and biostratigraphy of Early Cretaceous ammonites from the Tethyan Realm. He has also been chair of the Barremian Working Group, leading the development of the GSSP proposal for this stage (ratified in March 2023) and the Golden Spike ceremony (November 2024).

François Baudin is currently professor of Sedimentology and Petroleum Geology at Sorbonne University, Paris (France). He got his PhD at Pierre and Marie Curie University (1989) and "Habilitation à Diriger des Recherches" at the same place (1998). His researches are focused to the processes that control the preservation and distribution of organic matter in sedimentary rocks as well as recent sediments and soils. He has published more than 200 articles in international journals and several textbooks. François Baudin is active in some scientific societies including the Geological Society of France, which he has chaired from 2020 to 2022.

Jean-François Deconinck is Professor Emeritus at the University of Burgundy Europe. A specialist in clay sedimentation, he has worked mainly in Jurassic and Cretaceous formations where he focuses on reconstructing depositional environments. He uses clay minerals in particular as tools for reconstructing ancient climates.

Ginés Alfonso de Gea is senior lecturer in the Department of Geology at the University of Jaén (Spain). He teaches geology, stratigraphic, micropalaeontology, rock sedimentary and geologic maps. His research is focussed on stratigraphy, biostratigraphy (using nannofossils and planktonic foraminifera), sedimentology and geochemistry of the Cretaceous of the Betic Cordillera. Currently, his research focuses on the analysis of palaeogeographic and palaeoenvironmental changes during the Cretaceous, with special interest in the multidisciplinary study of Oceanic Anoxic Events.

Now retired, Jaap Klein was managing director science communication at the University of Amsterdam (The Netherlands), and from 1990 honorary researcher at the Naturalis Biodiversity Center, Department of Marine Zoology. He is the author of Fossilium Catalogus I: Animalia Lower Cretaceous Ammonites in 11 volumes.

Damian Gerard Lodowski holds the position of the assistant professor in the Polish Geological Institute, National Research Institute. In 2017-2023 he did his PhD entitled "Tracing the latest Jurassic-earliest Cretaceous paleoenvironmental changes in circum Carpathian region in light of sedimentologic, paleomagnetic and geochemical data". Currently he is primarily focused on the topic of the J/K oceanographic perturbations, their controlling factors and geographic distribution. Member of the Coniacian working group.

Davide Olivero is "Maétre de Conférences" (lecturer) at the Lyon Observatory at the University of Lyon (France). At the beginning of his career he worked on the Middle Jurassic ammonites of the French Subalpine basin. Now his research focuses on the ichnology and palaeoecology, especially in the Mesozoic and Cenozoic successions of southeastern France. He was formerly involved in the proposal of the Bathonian GSSP, ratified in 2008.

Daniela Reháková is university teacher in the Department of Geology and Palaeontology, Faculty of Natural Sciences, Comenius University in Bratislava. She teaches systematic, palaeontology of invertebrates, palaeoecology, biostratigraphy and sequence stratigraphy. She is the (co-)author of more than 300 scientific contributions in morphometry, biostratigraphy and evolution of Late Jurassic to Early Cretaceous calpionellids and calcareous dinoflagellates, and carbonate microfacies and paleoenvironmental modelings.

Appendix 1. Taxonomic note on the new genus *Hoedemaekeria* (Ammonite)

Company M. and Reboulet S. are contributors of this taxonomic note. Thus, considering taxonomic rules, they should be considered as co-authors of this new genus.

Order Ammonitida Haeckel, 1866
Suborder Ammonitina Haeckel, 1866
Superfamily Perisphinctoidea Steinmann, 1890
Family Neocomitidae Salfeld, 1921
Genus *Hoedemaekeria* nov. gen.
ZooBank registration number: 37B95C43-797A-4C5F-93B7-5602790-B8CAE
Type species: *Thurmannia pertransiens* Sayn, 1907, p. 43.

Specific content. *Hoedemaekeria pertransiens* (Sayn, 1907), *Hoedemaekeria gratianopolitensis* (Sayn, 1907) and *Hoedemaekeria otopeta* (Thieuloy, 1979).

Etimology. The new genus is dedicated to our Dutch colleague Philip J. Hoedemaeker, who was the first to question the attribution of its type species to the genus *Thurmanniceras,* in which it had traditionally been included (see Klein, 2005, pp. 279-280). The generic name is to be treated as feminine.

Diagnosis. Discoidal, subinvolute to subevolute neocomitids, with compressed, rectangular to subtrapezoidal whorl section, gently convex flanks and flattened venter. Marked sexual dimorphism, with small to moderate sized microconchs (45-70 mm in diameter) showing lappeted apertures, and large to very large macroconchs (120-250 mm in diameter) with simple apertures.

Both dimorphs show a similar ontogenetic development. In the early whorls, the section is equidimensional to weakly compressed. The ribs are rigid, slightly prorsiradiate, simple or bifurcated towards the middle of the flank, and end in an oblique, small ventrolateral thickening, leaving a narrow smooth ventral band. Numerous oblique constrictions regularly appear throughout this stage.

Gradually the shell acquires its characteristic morphology, the whorl expansion rate increasing and the section compressing. The ribs become sinuous, arise singly or in pairs from small periumbilical bullae and most of them bifurcate in the upper third of the flank. The constrictions tend to disappear and, in some species, also a more or less pronounced attenuation of the ribbing on the flank occurs.

In the body chamber, which occupies about half a whorl, noticeable changes occur in the structure of the shell. The microconchs develop an elliptical section, with a gently convex venter, accompanied by a moderate umbilical egression. In the macroconchs, the relative whorl width increases, and the ribs tend to cross the broadly rounded ventral region. Strongly thickened, even tuberculated, ribs may also appear near the aperture in the macroconchs.

Remarks. As mentioned above, the species included in the new genus have traditionally been assigned to the genus *Thurmanniceras* (see lists of synonymy in Klein, 2005). The type species of this genus (*T. thurmanni*) was defined by Pictet and Campiche (1860) on heterogeneous and poorly preserved material, which, together with a strongly idealized original iconography, considerably hampered the subsequent interpretation of the genus.

The lectotype of *T. thurmanni* (in Pictet and Campiche, 1860, pl. 34, fig. 1a, b; designated by Baumberger 1906), of which we have examined casts and photographs, is a fragment corresponding to half a whorl with a diameter close to 118 mm. At this stage, the whorl section is ovate, with moderately convex flanks, truncated venter, and sharp ventrolateral shoulders. The ornamentation consists of weakly falcoid ribs, which arise singly in a barely perceptible umbilical thickening and divide towards the middle of the flank into two ribs that exhibit a small, but distinct, ventrolateral tubercle, and cross the venter without hardly losing relief. Some additional bifurcated and intercalatory ribs also occur sporadically in the upper part of the flank.

From our perspective, the differences in shell shape and ornamentation pattern are sufficiently diagnostic to justify the exclusion of *H. pertransiens* and its close relatives from the genus *Thurmanniceras*, whose content would be restricted to the type species.

Stratigraphic and geographic distribution. Uppermost Berriasian (*Tirnovella alpillensis* Zone, *H. otopeta* Subzone) and lowermost Valanginian (*H. pertransiens* Zone) from the Western Tethys (Mediterranean Province and Mexico; see "**Criteria for the Global Correlation of the Berriasian/Valanginian Boundary**", part "*Ammonites*").

Appendix 2. Taxonomic index

Alphabetic list of the taxa mentioned in the text and figures.

Leptoceras Uhlig, 1883
Leptoceras studeri (Ooster, 1860)
Lytoceras Suess, 1865
Lytoceras honnoratianum (Orbigny, 1841)
Lytoceras quadrisulcatum (Orbigny, 1841)
Lytoceratidae Neumayr, 1875
Neocomites neocomiensiformis (Uhlig, 1902)
Neocomites premolicus Sayn, 1907
Neocomites wichmanni Leanza, 1945
Neocomitidae Salfeld, 1921
Neolissoceras (Neolissoceras) Spath, 1923
Neolissoceras (Neolissoceras) grasianum (Orbigny, 1841)
Neolissoceras (Vergoliceras) Atrops & Reboulet, 1996
Neolissoceras (Vergoliceras) extracornutum (Cecca, 1995)
Neolissoceras (Vergoliceras) salinarium (Uhlig, 1888)
Olcostephanidae Pavlow, 1892
Olcostephanus Neumayr, 1975
Olcostephanus laticosta (Gerth, 1925)
Olcostephanus drumensis Kilian, 1910
Olcostephanus (Jeannoticeras) Thieuloy, 1965
Olcostephanus (Jeannoticeras) jeannoti (Orbigny, 1841)
Paratollia Casey, 1973
Phylloceras (Hypophylloceras) tethys (Orbigny, 1841)
Phylloceratidae Zittel, 1884
Platylenticeras Hyatt, 1900
Platylenticeras heteropleurum occidentale (Sayn, 1901)
Platylenticeras latum tenue Koenen, 1915
Protancyloceras Spath, 1924
Protancyloceras punicum Arnould-Saget, 1953
Protancyloceratidae Breistroffer, 1947
Ptychophylloceras (Semisulcatoceras) semisulcatum (Orbigny, 1841)
Sarasinella Uhlig, 1905
Sarasinella ambigua (Uhlig, 1902)
Sarasinella eucyrta (Sayn, 1907)
Sarasinella longi (Sayn, 1907)
Sarasinella subspinosa (Uhlig, 1910)
Sarasinella trezanensis (Sayn, 1907)
Sarasinella uhligi Spath, 1939
Sarasinella varians (Uhlig, 1910)
Spiticeras Uhlig, 1903
Spiticeras gevreyi Djanélidzé, 1922
Spiticeras multiforme Djanélidzé, 1922
Spiticeras polytroptychum (Uhlig, 1888)
Thurmanniceras Cossmann, 1901
Thurmanniceras thurmanni (Pictet & Campiche, 1860)
Tirnovella alpillensis (Mazenot, 1939)

Belemnites
Adiakritobelus Janssen & Főzy, 2004
Berriasibelus Delattre, 1952
Berriasibelus conicus (Blainville, 1827)
Berriasibelus exstinctorius (Raspail, 1829)
Berriasibelus aff. *exstinctorius* (Raspail, 1829) sensu Janssen, 2021
Berriasibelus incertus (Weis, 1991)
Berriasibelus kabanovi (Weis, 1991)
Berriasibelus triquetrus (Weiss, 1991)
Castellanibelus Combémorel, 1972
Castellanibelus orbignyanus (Duval-Jouve, 1841)
Castellanibelus sp. E (sensu Janssen, 2021)
Conobelus piradoensis Janssen, 2003
Curtohibolites Stoyanova-Vergilova, 1963
Duvalia Bayle, 1878
Duvalia lata constricta Stoyanova-Vergilova, 1965
Duvalia lata lata (Blainville, 1827)
Duvalia miravetesensis Janssen, 2003
Duvalia superconstricta Janssen, 2018
Duvalia tornajoensis Janssen, 2003
Gillieronibelus mayeri (Gilliéron, 1873)
Hibolites (sensu Blainville, 1827, non *Hibolithes* Denys de Montfort, 1808)
Hibolites aff. *pistilliformis* (Blainville, 1827) sensu Janssen, 2021
Mirabelobelus Janssen & Clément, 2002
Mirabelobelus blanvillei Janssen & Clément, 2002
Pseudobelus Blainville, 1827
Pseudobelus bipartitus Blainville, 1827
Tithonobelus Janssen, 2022
Tithonobelus orbignyi (Janssen & Clément, 2002)

Calpionellids
Borzaites atava (Grün & Blau, 1996)
Calpionella alpina Lorenz, 1902
Calpionella elliptica Cadish, 1932
Calpionella minuta Houša, 1990
Calpionellites Colom, 1948
Calpionellites allemanni Řehánek, 1988
Calpionellites caravacaensis Allemann in Allemann & Trejo, 1975
Calpionellites coronatus Trejo in Allemann & Trejo, 1975
Calpionellites darderi (Colom, 1934)
Calpionellites major Colom, 1948
Calpionellites uncinatus Cita & Pasquaré, 1959
Calpionellopsis Colom, 1948
Calpionellopsis oblonga (Cadish, 1932)
Calpionellopsis simplex (Colom, 1939)
Crassicollaria parvula Remane, 1962
Lorenziella hungarica Knauer & Nagy, 1964
Lorenziella plicata Remane in Le Hégarat & Remane, 1968
Praecalpionellites Pop, 1986
Praecalpionellites hillebrandti Grün & Blau, 1999
Praecalpionellites murgeanui (Pop, 1974)
Praecalpionellites siriniaensis Pop, 1986
Remaniella Catalano, 1965
Remaniella borzai Pop, 1994
Remaniella cadischiana (Colom, 1948)
Remaniella catalanoi Pop, 1996
Remaniella colomi Pop, 1996
Remaniella filipescui Pop, 1994
Sturiella dolomitica (Grün & Blau, 1996)
Tintinnopsella carpathica (Murgeanu & Filipescu, 1933)
Tintinnopsella dacica Filipescu & Dragastan, 1970
Tintinnopsella doliphormis (Colom, 1939)
Tintinnopsella longa (Colom, 1939)
Tintinnopsella subacuta (Colom, 1948)

Calcareous dinoflagellate cysts

Cadosina minuta Borza, 1980 – note: This taxon should be transferred to the Acritarchs (Granier, 2024). This author introduces a new genus and a new species, namely *Octahedronoides tethysianus*. According to Daniela Reháková and Stan Duxbury, further investigations are needed before making any changes.

Cadosina semiradiata fusca Wanner, 1940
Cadosina semiradiata cieszynica (Nowak, 1968)
Cadosina semiradiata olzae (Nowak, 1966)
Cadosina semiradiata semiradiata Wanner, 1940
Cadosinopsis nowakii Borza, 1984
Carpistomiosphaera valanginiana Borza, 1986
Colomisphaera carpathica (Borza, 1964)
Colomisphaera conferta Řehánek, 1985
Colomisphaera fortis Řehánek, 1982
Colomisphaera heliosphaera (Vogler, 1941)
Colomisphaera lapidosa (Vogler, 1941)
Colomisphaera lucida Borza, 1986
Colomisphaera vogleri (Borza,1969)
Parastomiosphaera malmica Borza, 1964
Stomiosphaera echinata Nowak, 1968
Stomiosphaera moluccana Wanner, 1940
Stomiosphaera wanneri Borza, 1969
Stomiosphaerina proxima Řehánek, 1987

Organic-walled dinoflagellate cysts

Aprobolocysta humilis Duxbury, 2024
Aprobolocysta pustulosa Smith & Harding, 2004
Batioladinium reticulatum Stover & Helby, 1987
Bicornus obscurus Duxbury 2024
Biorbifera johnewingii Habib, 1972
Bourkidinium granulatum Morgan, 1975
Cauca maculosa Duxbury, 2018
Chlamydophorella Cookson & Eisenack, 1958
Chlamydophorella caminus Duxbury, 2024
Circulodinium hirtellum Alberti, 1961
Cribroperidinium Neale & Sarjeant, 1962
Cribroperidinium orthoceras (Eisenack, 1958) Davey 1969
Ctenidodinium elegantulum Millioud, 1969
Cymososphaeridium validum Davey, 1982
Dapsilidinium deflandrei (Valensi, 1947) Lentin & Williams, 1981
Dapsilidinium warrenii (Habib, 1976) Lentin & Williams, 1981
Diacanthum hollisteri Habib, 1972
Dingodinium spinosum (Duxbury, 1977) Davey, 1979
Downiesphaeridium flexuosum (Davey et al. 1966) Islam 1993
Druggidium apicopaucicum Habib, 1973
Egmontodinium toryna (Cookson & Eisenack, 1960) Davey, 1979
Exiguisphaera asketa Duxbury, 2018
Exiguisphaera phragma Duxbury, 1979
Exochosphaeridium robustum Backhouse, 1988
Foucheria modesta Monteil, 1992
Heslertonia inferior Duxbury, 2024
Hystrichodinium pulchrum Deflandre, 1935
Hystrichodinium voigtii (Alberti, 1961) Davey, 1974
Hystrichosphaeridium diversum Duxbury, 2018
Hystrichosphaerina schindewolfii Alberti, 1961
Impletosphaeridium tribuliferum (Sarjeant 1962) Islam 1993
Kleithriasphaeridium fasciatum (Davey & Williams, 1966) Davey, 1974
Kleithriasphaeridium simplicispinum (Davey &Williams, 1966) Davey, 1974
Muderongia Cookson & Eisenack, 1958
Muderongia dedecosa (Gocht, 1957) Duxbury, 2023
Muderongia extensiva Duxbury, 1977
Muderongia mcwhaei Cookson & Eisenack, 1958
Muderongia simplex Alberti, 1961
Paragonyaulacysta borealis Brideaux & Fisher, 1976
Perisseiasphaeridium cretaceum Duxbury, 2018
Phoberocysta Millioud, 1969
Phoberocysta latissima Duxbury, 2024
Phoberocysta neocomica (Gocht, 1957) Millioud, 1969
Prolixosphaeridium prolatum Duxbury, 2024
Protoellipsodinium seghire subsp. *medaaure* Below, 1981
Protoellipsodinium touile mugatae Below, 1981
Pseudoceratium pelliferum subsp. *pelliferum* Gocht, 1957
Pseudoceratium pelliferum subsp. *radiculatum* (Gocht, 1957) Duxbury, 2024
Scriniodinium pharo (Duxbury) Davey, 1982
Sentusidinium cuculliforme Davies, 1983*Spiculodinium? inordinatum* Duxbury, 2024
Spiniferites Mantell, 1850
Systematophora areolata Klement in Davey, 1982
Systematophora sp. A Monteil, 1993
Systematophora? daveyi Riding & Thomas, 1988
Systematophora? scoriacea (Raynaud, 1978) Monteil, 1992
Tanyosphaeridium hirsutum Duxbury 2024
Tanyosphaeridium magneticum Davies, 1983
Tanyosphaeridium cf. *variecalamum* Davey & Williams, 1966
Thalassiphora? charollaisii Monteil, in press
Vexillocysta spinosa Duxbury, 2018
Wallodinium lunum (Cookson & Eisenack, 1960) Lentin & Williams, 1973
Wrevittia helicoidea (Eisenack & Cookson, 1960) Helenes & Lucas-Clark, 1997

Miospores

Appendicisporites Weyland & Krieger, 1953
Callialasporites dampieri (Balme, 1957) Dev, 1961
Callialasporites trilobatus (Balme, 1957) Dev, 1961
Cicatricosisporites Potonié & Gelletich, 1933
Classopollis torosus Burger, 1965
Concavissimisporites variverrucatus Brenner 1963
Cyathidites Couper, 1953
Foveosporites subtriangularis Kemp, 1970
Gleichenidites senonicus Ross, 1949
Lycopodiumsporites austroclavatidites (Cookson, 1953) Potonié, 1956
Monosulcites Cookson ex Cooper, 1953
Pilosisporites trichopapillosus (Thiergart, 1949) Delcuort & Spru mont, 1955
Sestrosporites pseudoalveolatus (Couper, 1958) Dettmann, 1963
Staplinisporites caminus (Balme, 1957) Pocock, 1962
Trilobosporites bernissartensis (Delcuort & Sprumont 1955) Potonié, 1956
Vitreisporites pallidus (Reissinger, 1950) Nilsson, 1958

Acritarchs

Cyclopsiella Drugg & Loeblich, 1967
Halophoridia caperata (Srivastava 1984) Duxbury, 2024
Micrhystridium Deflandre, 1939
Pterospermella Eisenack, 1972
Rhombodella cf. *vesca* Duxbury, 1980
Tasmanites Newton, 1875

Calcareous nannofossils

Anfractus harrisonii (Medd, 1979)
Assipetra infracretacea (Thierstein, 1973) Roth, 1973
Axopodorhabdus dietzmannii Reinhardt, 1965
Biscutum constans (Górka, 1957) Black in Black & Barnes, 1959
Biscutum ellipticum (Gorka, 1957) Grün in Grün & Allemann, 1975.
Calcicalathina Thierstein, 1971
Calcicalathina erbae Bergen, 2000
Calcicalathina oblongata (Worsley, 1971) Thierstein, 1971
Calcicalathina praeoblongata Aguado in Aguado et al., 2000
Conusphaera mexicana subsp. mexicana (Trejo, 1969)
Conusphaera mexicana subsp. *minor* Bown & Cooper, 1989
Conusphaera rothii (Thierstein, 1971) Jakubowski, 1986
Cretarhabdus angustiforatus (Black, 1971) Bukry 1973, emended Bralower et al., 1989
Cretarhabdus conicus Bramlette & Martini, 1964
Cretarhabdus inaequalis Crux, 1987
Cretarhabdus aff. *striatus* (Stradner, 1963) Black, 1973
Crucibiscutum salebrosum (Black, 1971) Jakubowski, 1986
Cruciellipsis cuvillieri (Manivit, 1966) Thierstein, 1971
Cyclagelosphaera margerelii Noël, 1965
Diadorhombus rectus Worsley, 1971
Diazomatolithus lehmanii Noël, 1965
Diazomatolithus subbeticus Grün, 1975
Discorhabdus ignotus (Górka, 1957) Perch-Nielsen, 1968
Discorhabdus rotatorius (Bukry, 1969) Thierstein, 1973
Eiffellithus windii Applegate & Bergen, 1988
Ethmorhabdus hauterivianus (Black, 1971) Applegate et al. in Covington & Wise, 1987
Haqius circumradiatus (Stover, 1966) Roth, 1978.
Haqius ellipticus (Grün in Grün & Allemann, 1975), Bown, 2005
Helenea chiastia Worsley, 1971
Helenea quadrata (Worsley, 1971) Rutledge & Bown in Bown et al., 1998
Kokia curvata Perch-Nielsen, 1988
Manivitella pemmatoidea (Deflandre in Manivit, 1965) Thierstein, 1971
Micrantholithus hoschulzii (Reinhardt, 1966) Thierstein, 1971
Micrantholithus obtusus Stradner, 1963
Micrantholithus speetonensis Perch-Nielsen, 1979
Nannoconus bermudezii Brönnimann, 1955
Nannoconus broennimanni Trejo, 1959
Nannoconus bucheri Brönnimann, 1955
Nannoconus colomi Kamptner, 1938
Nannoconus dolomiticus Cita & Pasquaré, 1959
Nannoconus globulus subsp. *globulus* Brönnimann, 1955
Nannoconus globulus subsp. *minor* (Brönnimann, 1955) Bralower in Bralower et al., 1989
Nannoconus inornatus Rutledge & Bown, 1996
Nannoconus Kamptner, 1931
Nannoconus kamptneri subsp. *kamptneri* Brönnimann, 1955
Nannoconus kamptneri subsp. *minor* (Brönnimann, 1955) Bralower in Bralower et al., 1989
Nannoconus oviformis Perch-Nielsen, 1988
Nannoconus quadratus (Noël 1959) Deres & Achéritéguy 1980
Nannoconus steinmannii subsp. *minor* (Kamptner, 1931) Deres & Achéritéguy, 1980
Nannoconus steinmannii subsp. *steinmannii* Kamptner, 1931
Nannoconus wintereri Bralower & Thierstein, 1989
Percivalia fenestrata (Worsley, 1971) Wise, 1983
Percivalia nebulosa (Bralower in Bralower et al., 1989) Aguado in Aguado et al. 2000
Polycostella senaria Thierstein, 1971
Retecapsa octofenestrata Bralower *in* Bralower et al., 1989
Retecapsa surirella (Deflandre & Fert, 1954) Grün in Grün & Allemann, 1975
Rhagodiscus asper (Stradner, 1963) Reinhardt, 1967
Rhagodiscus dekaenelii Bergen, 1994
Rhagodiscus gallagheri (Rutledge & Bown, 1996)
Rhagodiscus nebulosus Bralower in Bralower et al., 1989
Rhagodiscus pseudoangustus (Crux, 1987)
Rotelapillus laffittei (Noël, 1957) Noël, 1973
Rucinolithus wisei Thierstein, 1971
Sollasites arcuatus Black, 1971
Sollasites horticus (Stradner et al. in Stradner & Adamiker, 1966) Cepek & Hay, 1969
Speetonia colligata Black, 1971
Staurolithites crux (Deflandre & Fert, 1954) Caratini, 1963
Staurolithites laffittei Caratini, 1963
Staurolithites mutterlosei Crux, 1989
Triquetrorhabdulus shetlandensis Perch-Nielsen, 1988
Tubodiscus frankiae Bown, 2005
Tubodiscus jurapelagicus (Worsley, 1971) Roth, 1973
Tubodiscus verenae Thierstein, 1973
Umbria granulosa Bralower & Thierstein in Bralower et al., 1989
Watznaueria Reinhardt, 1964
Watznaueria barnesiae (Black in Black & Barnes, 1959) Perch-Nielsen, 1968
Watznaueria biporta (Bukry, 1969)
Watznaueria britannica (Stradner, 1963) Reinhardt, 1964
Watznaueria communis Reinhardt, 1964
Watznaueria cynthae Worsley, 1971
Watznaueria fossacincta (Black, 1971) Bown in Bown & Cooper, 1989.
Watznaueria manivitae Bukry 1973
Watznaueria ovata Bukry, 1969
Zeugrhabdotus diplogrammus (Deflandre in Deflandre & Fert, 1954) Burnett in Gale et al., 1996
Zeugrhabdotus elegans (Gartner 1968) Burnett in Gale et al., 1996
Zeugrhabdotus embergeri (Noël, 1958) Perch-Nielsen, 1984
Zeugrhabdotus erectus (Deflandre *in* Deflandre & Fert, 1954) Reinhardt, 1965
Zeugrhabdotus fissus Grün & Zweili, 1980
Zeugrhabdotus trivectis Bergen, 1994
Zygolithus xenotus Stover, 1966

Ichnofossils

Zoophycos Massalongo, 1855